Title

MICROSCALE RESOLUTION OF INTERFACIAL MASS-TRANSFER RATES IN ELECTRODE PROCESSES

Authors

Whitney, G.M.
Tobias, C.W.

Publication Date

1987-06-01

Lawrence Berkeley Laboratory
UNIVERSITY OF CALIFORNIA

Materials & Chemical Sciences Division

MICROSCALE RESOLUTION OF INTERFACIAL MASS-TRANSFER RATES IN ELECTRODE PROCESSES

G.M. Whitney* and C.W. Tobias
(*Ph.D. Thesis)

June 1987

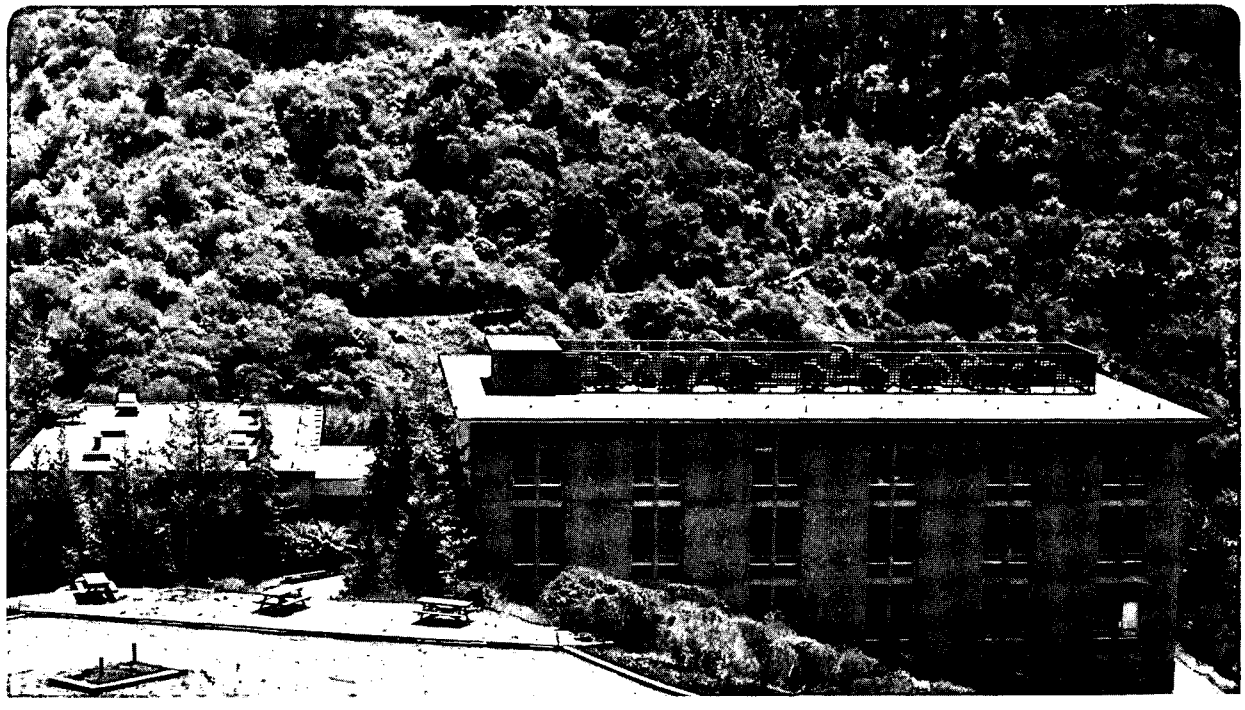

Prepared for the U.S. Department of Energy under Contract DE-AC03-76SF00098

DISCLAIMER

LBL-23596

Microscale Resolution of Interfacial Mass-Transfer Rates in Electrode Processes

Gina Marie Whitney

(Ph.D. Dissertation)

with

Charles W. Tobias

Department of Chemical Engineering
and Lawrence Berkeley Laboratory
University of California
Berkeley, California 94720

June 1987

This work was supported by the Assistant Secretary of Conservation and Renewable Energy, Office of Energy Systems Research, Energy Storage Division of the U.S. Department of Energy under Contract No. DE-AC03-76SF00098.

Microscale Resolution of Interfacial Mass-Transfer Rates in Electrode Processes

Gina Marie Whitney

Microscale Resolution of Interfacial Mass-Transfer Rates in Electrode Processes

Gina Marie Whitney

Department of Chemical Engineering
and Lawrence Berkeley Laboratory
University of California
Berkeley, California 94720

ABSTRACT

Results of four interrelated studies concerning the nature of electrolytic gas evolution are reported.

1. Configurations of axisymmetric bubbles formed on curved surfaces are evaluated. Numerical results are summarized by an equation that relates the maximum stable size of a bubble formed on a curved surface to the equilibrium contact angle, a characteristic length of the system, and the radius of curvature of the solid support.

2. Mass-transfer enhancement by a stream of bubbles rising near a mass-transfer surface is resolved spatially and temporally using a micro-mosaic electrode. Bubbles are generated electrolytically, inside or outside of the mass-transfer boundary layer. Enhancement resulting from bubbles rising within the mass-transfer boundary layer is strong and localized, in agreement with trends predicted by a surface-renewal model. Mass transfer resulting from bubbles rising outside the boundary layer receives steady, laminar enhancement, correlating well with predictions based on an approximation involving the bubble stream entraining a cylinder of liquid.

3. The onset of buoyancy-induced convection is investigated for a case in which the density profile develops in a semi-infinite fluid, due to a step change in surface concentration at a rigid, conducting boundary. The limiting current technique at a micro-mosaic electrode is used to effect the concentration change and to monitor the resulting mass transfer. Concentration and density profiles before the onset of convection are obtained numerically. The critical Rayleigh number based on the penetration depth of the concentration profile is approximately 900, and that based on the position and magnitude of the density profile is 1750.

4. Observations of galvanostatic growth and disengagement of hydrogen bubbles at a 127-μm-diameter micro-electrode embedded in a large, coplanar, horizontal electrode in 1.0-M sulfuric acid are reported. Time scales for the collapse of the contact area and for bubble disengagement are obtained using high-speed cinematography. Observations of hydrogen evolution in free convection along vertical platinum electrodes in 0.5-M sulfuric acid are also reported.

Acknowledgment

It has been a joy and a privilege to work with Charles Tobias. I want to thank him for sharing his insights and his humor, and most of all for his unwavering faith in me. Working with him has been a labor of love and of a desire to live up to that faith.

I have also been lucky to interact with John Newman on both a personal and a professional level. He has never hesitated to help me in any matter. His evening seminar has provided the opportunity to learn about all aspects of electrochemistry.

The third floor of Gilman is a special community, in which we rely on each other for support and advice. There are several people in particular who have always been happy to listen to an idea and to add valuable insight. Mark Verbrugge's intellectual curiosity has been an inspiration. John Dukovic, Vicki Edwards, Dennis Dees and Mike Matlosz have helped me on numerous occasions. Karrie Hansen, Dawn Bernardi, Corinne Coughanowr, Tarric El-Sayed, and Sholeh Hessami have been supportive friends who have helped enhance life at Berkeley.

Dennis Dees and the late Larry Galovich performed a series of small miracles in the design and operation of the micro-mosaic electrode. I have benefited greatly from the technical expertise they contributed to this project. Fred Wolfe helped on the design of the new micro-mosaic cell, and George Weber constructed this cell with meticulous care. Mark Prausnitz conducted some of the experiments in Chapter 5 and helped with my first micro-mosaic experiments.

Ed Middlesworth at Hewlett Packard Laboratories agreed to construct a new set of micro-mosaic electrodes, and H.K. Hu, David Liu, Paul Merchant and Joyce

Sum donated their time to make them. Adam Heller, D.D. Bacon, R.T. Kræetsch, R.G. Vadimsky and Y.H. Wong are responsible for the many micro-mosaic electrodes produced at AT&T Bell Laboratories. Katalin Voros and Marylin Kushner in the U. C. Microfabrication Laboratory helped me make measurements and photographs of the micro-mosaic electrodes. Marge Hutchinson and Bill Johnston in the Computer Science Research Department at Lawrence Berkeley Laboratory produced the video tape of the micro-mosaic experimental data.

Several teachers over the years have been especially important to me by teaching that there are many ways to attack a problem and by allowing their own curiosity and excitement to enter the classroom. They are John Angus, G.R. McMillan, Chris Hill and S. Machlup. I remain indebted to Sr. Joan Acker for first getting me involved in scientific research.

I want to thank Scott Lynn and Ralph Greif for their careful and timely reviews of this manuscript. Mark Verbrugge and John Dukovic also read major portions and improved the quality of writing significantly.

Mort Denn has been a tremendous influence for me as a fine scientist and a warm human being. He has been a source of love and encouragement.

Finally, my parents, Warren and Rose, and my brothers, Warren and Paul, are truly engineers in every sense. This dissertation is dedicated to them.

I would like to acknowledge fellowship support from the National Science Foundation and the Exxon Education Foundation. This work was supported by the Assistant Secretary of Conservation and Renewable Energy, Office of Energy Systems Research, Energy Storage Division of the U.S. Department of Energy under Contract No. DE-AC03-76SF00098.

Contents

Chapter 1. Introduction

This dissertation gives account of a series of studies conducted on the nature of electrolytic gas evolution. Each chapter describes a different phase of investigation and is intended to stand alone with its own abstract, nomenclature and bibliography.

The major portion of this dissertation concerns certain fundamental aspects of electrolytic gas evolution, a component of numerous important industrial processes. Chlorine is produced as a gas by the electrolysis of brine at vertically-oriented expanded-mesh electrodes. High-purity hydrogen and oxygen are produced by the electrolysis of water. In the reduction of aluminum from Al_2O_3 dissolved in molten cryolite, the anodic reaction is the oxidation of carbon to gaseous CO_2 at horizontal anodes facing downward. In numerous other electrolytic synthesis processes, and in electroplating, one of the reaction products is a gas.

The total electrical energy consumption by the chlorine and aluminum industries alone accounted in 1985 for 4% of the total U.S. electrical energy use. Yet many fundamental aspects of the complex processes that occur during electrolytic gas evolution are poorly understood. Relevant research issues may be listed as follows:

(1) nucleation;

(2) physics of bubble shape and stability;

(3) bubble growth by diffusion and coalescence; and detachment and rise from electrode

(4) ohmic effects;

(5) mass-transfer effects, both macroscopic and microscopic.

The physical phenomena in the area of bubble nucleation in gas evolution are essentially identical to those in nucleate boiling. Cole (1974) has written an excellent review on the subject of boiling nucleation; much of his monograph is also relevant to the subject of electrolytic gas evolution.

The second topic involves the balance of buoyancy and surface-tension forces, which determine the maximum-size bubble that can adhere to a solid support, and has been the subject of numerous investigations over the last one hundred years. In Chapter 2 of this thesis, the classic work on bubble shape and size by Bashforth and Adams (1883), Wark (1933), Fritz (1935), and Padday (1969), among others, is extended to account for the effect of the curvature of the solid support on the maximum stable bubble size. This topic becomes relevant today, simply because gas is rarely evolved on a flat, horizontal surface, and there has been no quantification of the effects of electrode morphology, such as protrusions or indentations, on the maximum equilibrium bubble size. Chapter 2 treats the problem of a bubble adhering to an axisymmetric curved surface, such as a hemispherical protrusion on an electrode.

The third topic includes bubble growth, disengagement, and coalescence, all dynamic processes that may occur simultaneously. In recent years, a number of

optical observations of bubble behavior have been recorded. Some of the theoretical work consists of simplified treatments of the complex phenomena, such as Scriven's (1959) classic treatment of the growth of a hemispherical bubble by diffusion from a super-saturated solution or Cheh and Tobias' (1968) work on bubble growth in a non-uniform concentration gradient. This area of study of gas evolution is one of the most complex, comprising fluid mechanics, mass transfer, and surface tension forces, as well as the electrical nature of the problem. Chapter 5 of this thesis is a collection of experimental observations of bubble growth and detachment from planar horizontal and vertical electrodes. The goal of these experiments has been to observe both single- and multiple-bubble behavior from the side (i.e., parallel to the electrode surface), rather than from either the front of the bubble layer, or from beneath, through a transparent electrode. First, examination of individual bubble growth has been performed by growing bubbles at a small electrode encased in another material, so that only one bubble evolution site was available, and an unobstructed view of the bubble base could be obtained. Photographs of hydrogen evolution in sulfuric acid at vertical platinum electrodes were also obtained by evolving the gas on narrow strip electrodes, on which only a few columns of bubbles could be formed, and a profile view of attached bubbles could be obtained.

The subject of ohmic effects due to the presence of bubbles in solution is one area that is well in hand. Sides and Tobias (1982) have shown that the effective conductivity of a dispersion can be treated quantitatively by applying the Bruggeman effective medium theory. The motion of the bubbles has little effect on the ohmic penalty they inflict. The incremental resistance caused by bubbles still

attached to the electrode has also been evaluated by the same authors, and later, by Dukovic and Tobias (1987).

In contrast to ohmic effects, mass-transfer processes at gas-evolving electrodes are not well characterized. Theoretical treatments have been aimed at obtaining a form of the applicable correlation for the mass-transfer coefficient as a function of gas-evolution rate and are based on a simplified view of the events taking place at the electrode surface. Experimental measurements have consisted of quantifying this relationship for different electrode geometries, gases, and electrolytes. Only recently have the first microscopic investigations been conducted (Dees and Tobias, 1987). The major difference between the popular theories of gas-evolution mass transfer is whether mass-transfer enhancement is the result of point disturbances of the boundary layer or of macroscopic flow generated by the ascending gas. The results of an experimental investigation into the mechanism of mass-transfer enhancement by bubble streams at vertical micro-sectioned electrodes are presented in Chapter 3.

Chapter 4 is an experimental investigation into the onset of convection resulting from an unstable density gradient at a horizontal surface. The limiting-current technique at a sectioned electrode is used to generate the density gradient and to monitor the mass-transfer rate; a change in the mass-transfer rate from the convection-free base case is used as the criterion for determining when convection has commenced. The micro-mosaic electrode is used to resolve the spatial distribution of the ensuing convection and to determine the size scale at which averaging over the electrode surface degrades the accurate determination of convection onset.

References

Bashforth, F., and Adams, J., 1883, *An Attempt to Test the Theory of Capillary Action*, University Press, Cambridge.

Cheh, H.Y., and Tobias, C.W., 1968, "On the Dynamics of Hemispherical Phase Growth in Non-Uniform Concentration Fields," *International Journal of Heat and Mass Transfer*, Vol. 11, pp. 709-719.

Cole, R., 1974, "Boiling Nucleation," *Advances in Heat Transfer*, Vol. 10, pp. 85-166.

Dees, D.W., and Tobias, C.W., 1987, "Mass Transfer at Gas Evolving Surfaces: a Microscopic Study," *Journal of the Electrochemical Society*, Vol. 134, 1702-1713.

Dukovic, J., and Tobias, C.W., 1987, "The Influence of Attached Bubbles on Potential Drop and Current Distribution at Gas-Evolving Electrodes," *Journal of the Electrochemical Society*, Vol. 134, pp. 331-343.

Fritz, V.W., 1935, "Berechnung des Maximalvolumens von Dampfblasen," *Physikalische Zeitschrift*, Vol. 36, pp. 379-384.

Padday, J.F., 1969, "Theory of Surface Tension," in *Surface and Colloid Science*, E. Matifević, Ed., pp. 39-249.

Scriven, L.E., 1959, "On the Dynamics of Phase Growth," *Chemical Engineering Science*, Vol. 10, pp. 1-13.

Sides, P.J., and Tobias, C.W., 1982, "Resistance of a Planar Array of Spheres: Gas Bubbles on an Electrode," *Journal of the Electrochemical Society*, Vol. 129, pp. 2715-2720.

Wark, I.W., 1933, "The Physical Chemistry of Flotation. I. The Significance of Contact Angle in Flotation," *Journal of Physical Chemistry*, pp. 623-644.

Chapter 2. The Shape and Stability of Axisymmetric Gas Bubbles Attached to a Curved Surface

1. Abstract

The equation of Bashforth and Adams is used to calculate the configurations of axisymmetric bubbles formed on a curved surface, such as on a hemispherical solid. A stability analysis is performed to determine which configurations are stable to a disturbance in shape. Numerical results are summarized by a correlation that relates the maximum size of a bubble formed on a curved surface to the equilibrium contact angle, a characteristic length of the system, and the radius of curvature of the solid support.

2. Introduction

The shape and size of electrolytically-generated gas bubbles is of interest in so far as they affect the ohmic cell resistance and mass transfer to and from gas-evolving electrodes. In nucleate boiling, the shape and size of bubbles affects the rate at which heat can be transferred to solution. Also, generation of small bubbles of uniform size is of technological interest, for example in mineral flotation. Equilibrium shapes of attached bubbles and drops have been the subject of numerous studies over the past two hundred years, involving such luminaries as Laplace, Gauss, Poisson, Gibbs, and Rayleigh, to name a few.

In spite of the massive amount of high quality work in this area, virtually no attention has been given to drops and bubbles attached to other than planar horizontal surfaces. Also, much of the past effort was directed to the elucidation of conditions that prevail in the case of large pendant drops as opposed to small emergent gas bubbles on electrode surfaces.

The principles that govern the shape of an interface between two phases have been long established. There is a balance between buoyancy forces, which tend to deform the interface, and surface-tension forces, which act to resist deformation. Young (1804) and Laplace (1805) independently proposed that the pressure difference Δp across an interface is related to the deformation of the interface by

$$\frac{\Delta p}{\gamma} = \frac{1}{R_1} + \frac{1}{R_2} \tag{1}$$

where γ is the surface tension and R_1 and R_2 are the two principal radii of curvature. Eq. (1) has become known as the Laplace equation. Young also proposed that the angle of contact formed between a solid and the surface of a fluid

exposed to air is a characteristic value for any combination of solid and fluid. Young's equation relates the contact angle θ to the surface tension of the liquid γ_{lg}, the surface tension of the solid γ_{sg}, and the tension of the interface between the solid and the liquid γ_{sl}:

$$\gamma_{lg} \cos \theta = \gamma_{sg} - \gamma_{sl} \quad . \tag{2}$$

As described by Padday (1969) in his excellent description of the development of this area, Gauss (1830), Poisson (1831), Rayleigh (1902), and Gibbs (1906) have all contributed to the early development of this field, and all work in this area is based on the principles they set forth. Padday (1969) also discusses the concepts of the forces of attraction and repulsion that give rise to the surface tension. For purposes of the present work, we shall accept the surface tension of a fluid as a thermodynamic quantity that equals the free energy associated with the formation of a unit area of interfacial surface.

Bashforth and Adams (1883) tested Eq. (1) by calculating shapes of axisymmetric sessile drops. They substituted an expression for the hydrostatic pressure as a function of position z from the apex of the drop, where the two principal radii of curvature are the same, defined as R_0. As a consequence, Eq. (1) assumes the form:

$$2 + \frac{\Delta\rho g R_0^2}{\gamma} \frac{z}{R_0} = \frac{1}{R_1/R_0} + \frac{1}{R_2/R_0} \quad , \tag{3}$$

which is commonly referred to as the equation of Bashforth and Adams. $\Delta\rho$ is the density of the included phase minus the density of the surrounding phase, and is positive for sessile drops and captive bubbles, and negative for pendant drops and emergent bubbles. Normally, $\Delta\rho$ is written as ρ since the density of one phase is

usually much greater than that of the other. R_1 is the radius of curvature in the plane of axial symmetry, given by

$$R_1 = \frac{\left[1 + \left(\frac{dz}{dx}\right)^2\right]^{3/2}}{\frac{d^2z}{dx^2}} \tag{4}$$

where x is the radial coordinate. R_2 is the radius of curvature in the plane normal to the plane of symmetry given by

$$R_2 = \frac{x\left[1 + \left(\frac{dz}{dx}\right)^2\right]^{1/2}}{\frac{dz}{dx}} \quad , \tag{5}$$

The geometry is shown in Figure 1. The dimensionless group

$$\beta \equiv \frac{\Delta\rho g R_0^2}{\gamma} \quad , \tag{6}$$

appearing as a parameter in Eq. (3), is characteristic of the shape of the bubble. In recent literature, this group is called the Bond number.

Bashforth and Adams compared calculated sessile drop shapes to experiment and published extensive tables of accurate values of profile shapes. The tables have been extended by Blaisdell (1940) to cover larger values of β and by Fordham (1948) and Mills (1953) to cover pendant drops ($\beta < 0$). Padday (1969) published these tables together, and later (1972) extended the range of the tables considerably, making them available on microfiche cards.

The determination of the largest equilibrium bubble volume on a flat surface has been addressed by Wark (1933) and by Fritz (1935). The equation of Bashforth and Adams is integrated numerically from the top of the bubble, generating values

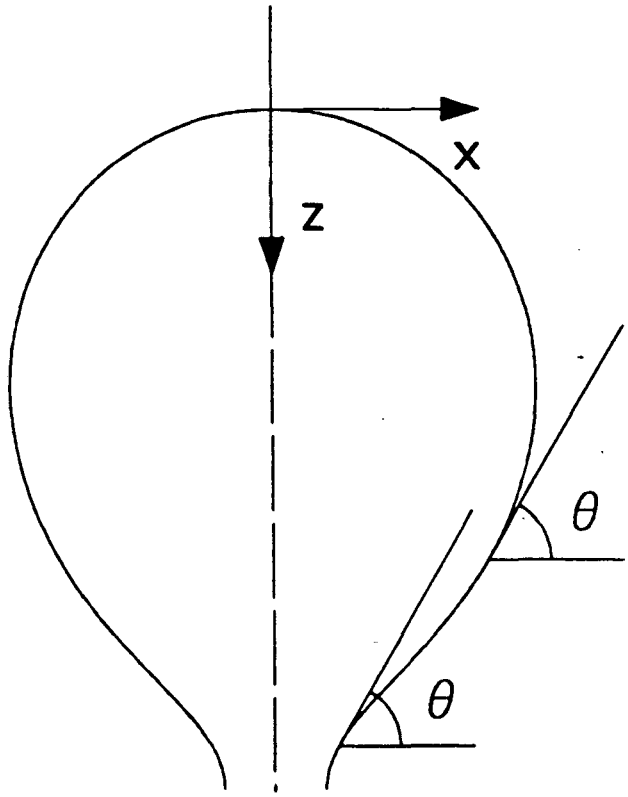

Figure 1. Coordinate system for calculation of axisymmetric bubble configurations. Two endpoints for $\theta = 60^\circ$ are shown.

for the coordinates of the bubble surface, until the interface meets the horizontal with the specified contact angle. Wark used the tables of Bashforth and Adams to construct graphical relations between bubble volume, radius of contact and contact angle. He found that there are two points in the bubble profile at which one can impose the contact angle condition and questioned the stability of the lower, or re-entrant, occurrence. He found that for any contact angle there exists a maximum equilibrium bubble volume. The physical explanation is that, for a volume greater than this maximum, the buoyancy forces are too great to be balanced by the surface tension forces of adhesion. Equivalently, there is too high a pressure gradient in solution to allow the bubble to remain sufficiently close to spherical in shape to meet the specified contact angle. Wark presented graphically the relationship between maximum bubble volume and contact angle, and included curves for both upper and lower occurrences of the contact angle. Kabanow and Frumkin (1933) found that their experimentally measured bubble volumes at departure fell on Wark's curve for the re-entrant contact angles.

Fritz (1935) has shown that a linear relationship exists between the group $\frac{V_{max,\,flat}^{1/3}}{R_0}\sqrt{-\beta}$ and contact angle for θ less than 120°. Cheh (1967) expressed Fritz' result by the simple relation

$$V_{max,\,flat} = \left(\frac{3}{\pi}\right)^3 \left(\frac{\gamma}{\rho g}\right)^{3/2} \theta^3 \quad (\theta \text{ in radians}) \quad . \tag{7}$$

Consider now a bubble attached to a solid support that curves away from the bubble, such as a wire, or a protrusion from a flat surface. If the bubble is to meet the solid support with the same angle of contact through the liquid phase as that

for a flat surface, the bubble interface must meet the horizontal at a sharper (smaller) angle. Thus, *for a given contact angle, a bubble adhering to a support that curves away from the bubble will be smaller and closer to spherical in shape than one on a flat support.*

The question of *stability* of the calculated bubble configurations must be addressed before the results for maximum bubble size can be correlated. Pitts (1974) derived the equations for the stability of axisymmetric pendant drops. He presents calculations of stability for *drop* contact angles of 20 and 50°, which correspond to *bubble* contact angles of 160 and 130°, respectively. (By convention, the contact angle is measured through the liquid phase.) Since we are concerned with bubble contact angles less than 90° (aqueous solutions generally wet metal surfaces), we conduct calculations of stability with respect to a perturbation in bubble shape for small contact angles and for bubbles adhering to curved surfaces.

The motivation for this investigation of bubble sizes on curved surfaces is that, in practice, gas is rarely evolved on flat, horizontal surfaces. The objective of this work then is to quantify the relationship between the maximum stable equilibrium bubble size and the properties of the system, the angle of contact, and the curvature of the surface. The method of calculation of bubble shape and size is described in Section 3. The question of stability of the calculated bubble configurations and the results for bubbles on a flat surface are presented in Section 4. The extension to axisymmetric curved surfaces is presented in Section 5.

3. The Calculation of Bubble Size

Consider first the general problem of the shape of a bubble. The equation of Bashforth and Adams (Eq. (3)) can be integrated numerically from the top of the bubble, where $R_1 = R_2 = R_0$, to give the coordinates describing the bubble interface. Equations (3), (4), and (5) are first transformed to a simple set of ordinary, coupled differential equations with s, the arc length along the interface, as the independent variable, and x and z as dependent variables. Using x^*, z^*, and s^* to designate variables made dimensionless with R_0, Eq. (3) becomes

$$2 + \frac{\Delta\rho g R_0^2}{\gamma} z^* = \frac{\dfrac{d^2 z^*}{ds^{*2}}}{\dfrac{dx^*}{ds^*}} + \frac{\dfrac{dz^*}{ds^*}}{x^*} \quad . \tag{8}$$

Eq. (8) is rearranged to obtain a set of differential equations for z' ($\equiv dz^*/ds^*$) and z^*:

$$\frac{dz'}{ds^*} = \left(2 + \frac{\Delta\rho g R_0^2}{\gamma} z^* - \frac{z'}{x^*}\right)(1 - z'^{\,2})^{1/2} \quad . \tag{9}$$

$$\frac{dz^*}{ds^*} = z' \quad . \tag{10}$$

x^* is obtained from integration of the geometric relation

$$\frac{dx^*}{ds^*} = (1 - z'^{\,2})^{1/2} \quad , \tag{11}$$

and the dimensionless volume V^* is given by

$$\frac{dV^*}{ds^*} = \pi \frac{dz^*}{ds^*} x^{*2} \quad . \tag{12}$$

Eqs. (9)-(12) are integrated numerically from the top of the bubble ($s^* = 0$), where

$x^* = z^* = V^* = 0$, $\frac{dx^*}{ds^*} = 1$ and $\frac{dz^*}{ds^*} = 0$, using a fourth-order Runge-Kutta-Gill integration scheme. The end condition is the specification of the contact angle at which the gas-liquid interface must meet the solid support.

$$\frac{dz^*}{ds^*} = \sin\theta \quad . \tag{13}$$

How far a bubble surface can be distorted from spherical is given by the Bond number β (Eq. (6)), which is a measure of the ratio of buoyancy forces, which act to deform the bubble surface from spherical, to the surface tension forces resisting deformation. This group appears as a parameter in the equation that describes the shape of the bubble (Eq. (8)). (It is negative for the emergent bubble and pendant drop problems, and positive for the captive bubble and sessile drop problems.) Because it includes R_0, the scaling of the dimensionless distance variables in Eq. (8), the Bond number is characteristic of both bubble *shape* and *size*. A small Bond number ($|\beta| < 0.1$) is indicative of a small bubble that is nearly spherical (small R_0, large γ). A large Bond number ($|\beta| > 0.3$) is characteristic of a large "floppy" bubble. Figure 2 shows calculated bubble shapes for three Bond numbers, -0.1, -0.2, and -0.3, using values characteristic of water at 25 ° C ($\gamma = 72.8$ dynes/cm, $\Delta\rho = -0.997$ g/cm ^{3}). The calculation of each bubble was terminated when the angle through the liquid phase reached 90 °.

The group

$$L_c \equiv \left(\frac{\gamma}{\Delta\rho g}\right)^{1/2} \tag{14}$$

is a characteristic length of the system that could alternatively have been used in the scaling of Eq. (3). Had we used this scaling, we would still obtain a parameter,

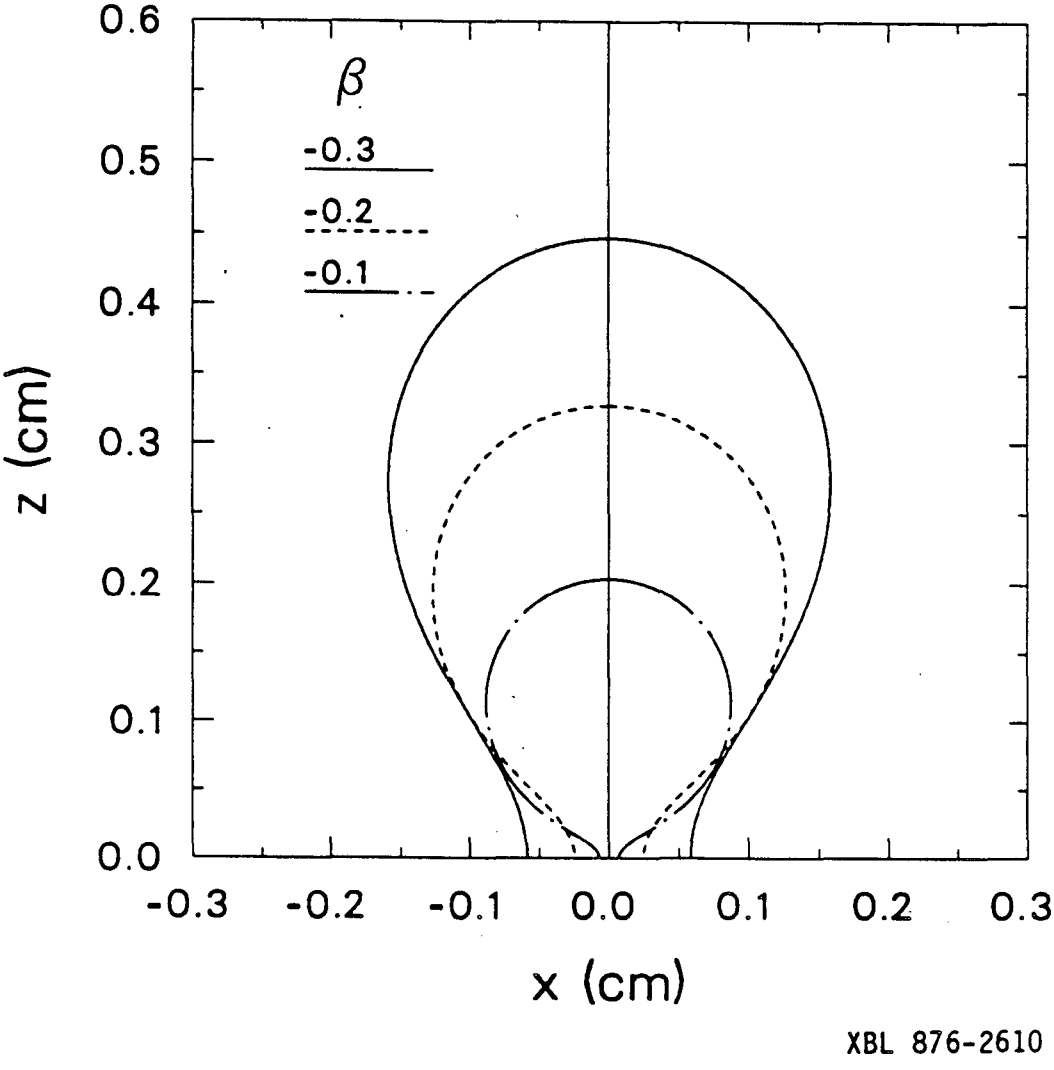

Figure 2. Calculated bubble configurations in water at 25 °C ($\gamma = 72.8$ dynes/cm, $\Delta\rho = -0.997$ g/cm^3) for three Bond numbers. The bubbles shown meet the horizontal at an angle of 90°.

often referred to as the capillary datum, which can be related to the Bond number and represents the pressure across the interface at some reference point. All lengths in the system do scale by L_c, in any case, and we expect the maximum bubble volume to be proportional to L_c to the third power, in agreement with the result of Fritz (1935).

For each chosen value of the Bond number, there are two points at which the end condition can be met. Figure 1 shows a bubble calculation for $\beta = -0.2$ with two 60° contact angles indicated. The stability of the lower occurrence of the contact angle, which has been questioned by Wark (1933), will be discussed in the following section. By varying the Bond number, and repeating the calculation, we obtain a family of solutions (two for each Bond number) for a given contact angle. At some point we reach a Bond number for which the buoyancy forces are too great to allow the bubble interface to meet the contact angle condition. Each time a solution is generated, we obtain a bubble volume, radius of contact, bubble height, and maximum radius. A plot of the family of bubble volumes versus radii of contact for a contact angle of 60° is shown in Figure 3. The lower (solid) curve represents the upper occurrences of the contact angle condition; the upper (dashed) curve represents the lower, or re-entrant, occurrences, for which the stability is in question. The point of maximum volume on the curve is very close to the meeting of the two curves, which represents the maximum value of β for which a solution can be obtained. A similar plot of families of solutions is shown in Figure 4 for contact angles from 30 to 90°. At contact angles greater than 60°, the point of maximum volume for a given contact angle lies on the re-entrant portion of the curve.

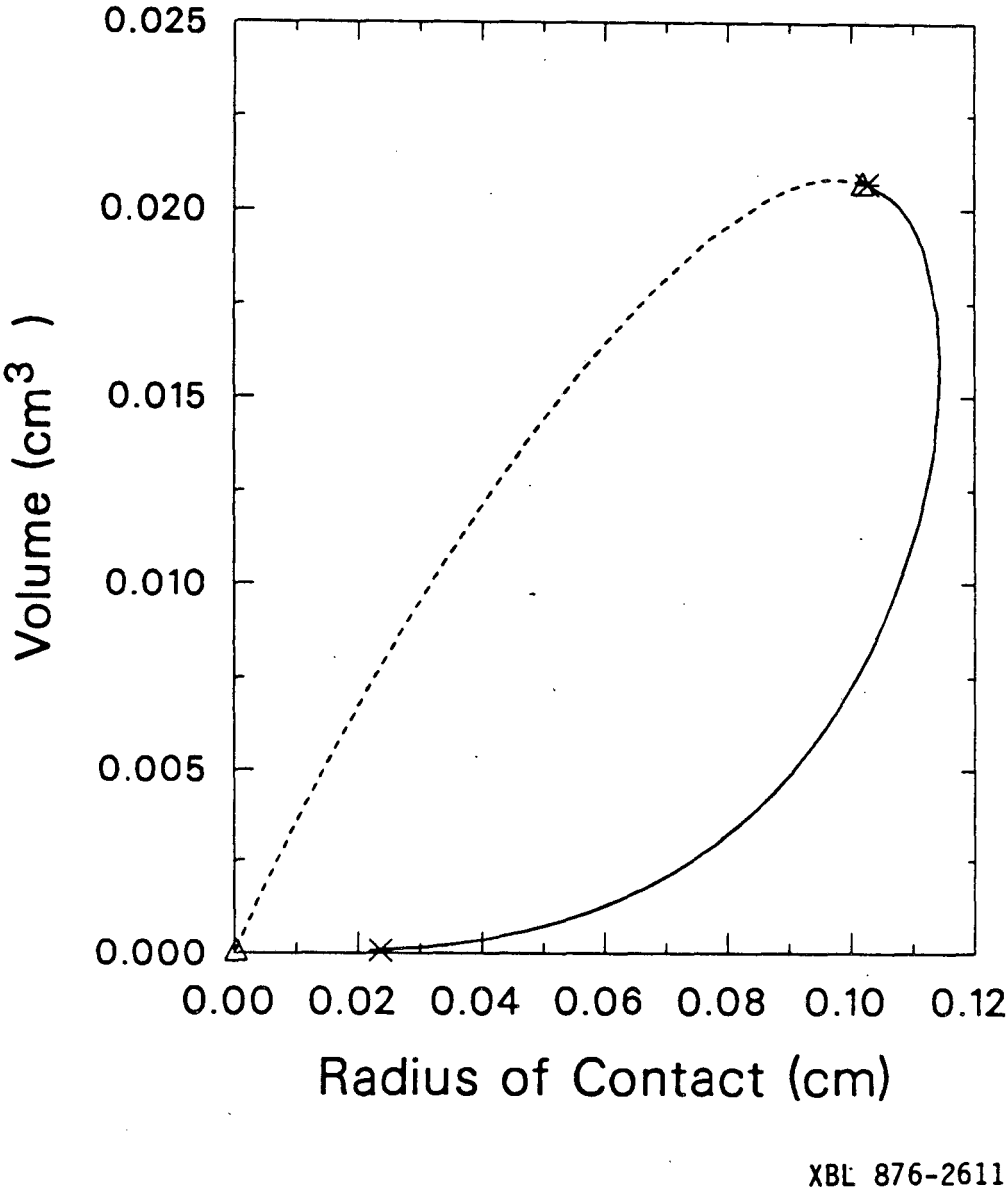

Figure 3. Family of solutions of volumes and radii of contact for a contact angle of 60°. Solid curve corresponds to first meeting of the contact angle condition (uppermost, in Figure 1); dashed curve corresponds to lower, or re-entrant, contact angles.

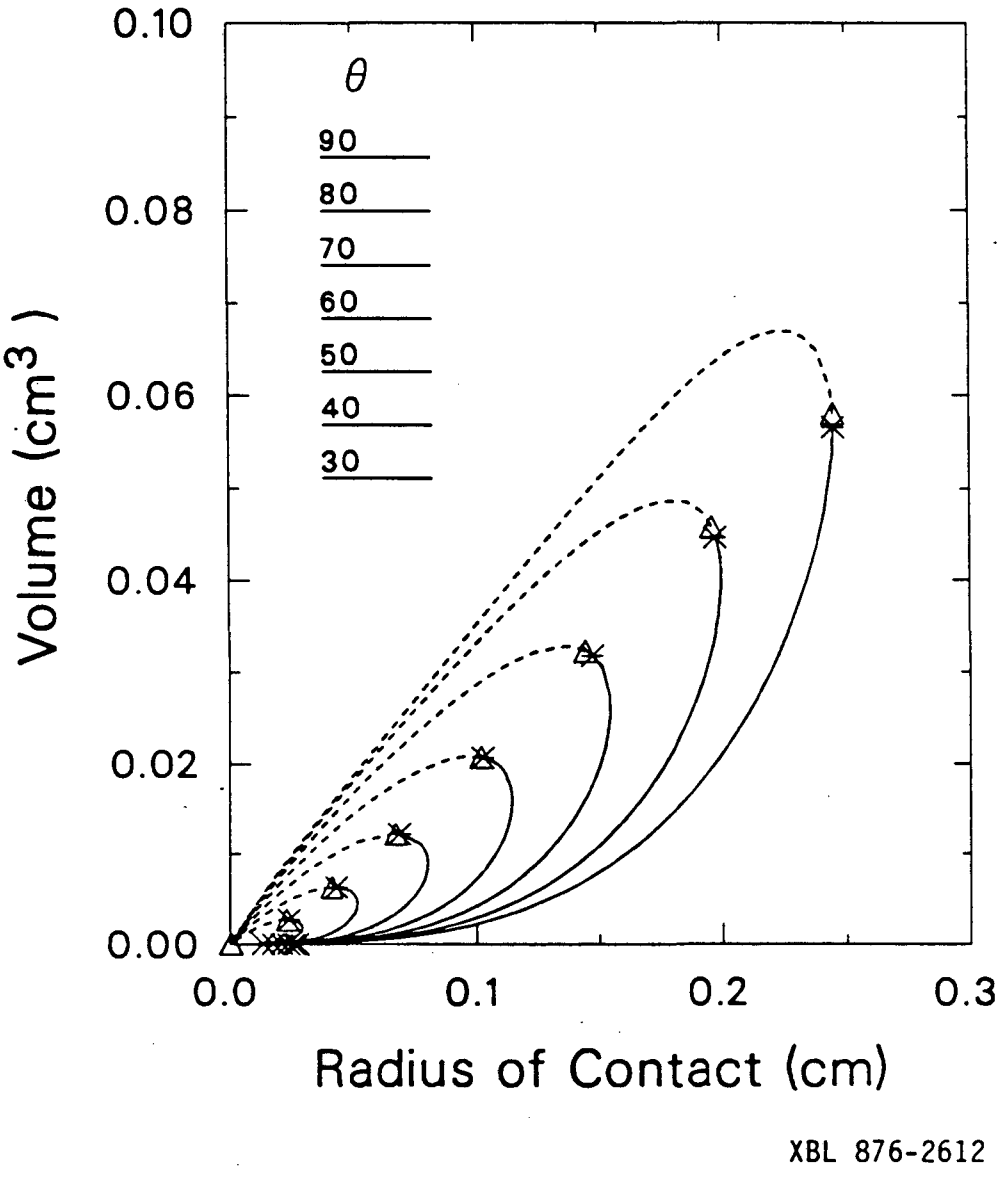

Figure 4. Families of solutions of volumes and radii of contact for a contact angles of 30 to 90°. Solid curves represent first meeting of the contact angle condition; dashed curves correspond to re-entrant contact angles.

4. The Stability of Calculated Configurations

The equations for stability of an axisymmetric pendant drop to an axisymmetric disturbance that extends over the profile of the drop have been derived by Pitts (1974) using the calculus of variations. Our treatment here follows that of Pitts directly, with only minor differences, and will be given in outline form only.

The total energy of a bubble adhering to a support that is at height h below the apex of the bubble is written

$$E = \int_0^h \left[2\pi\gamma x \frac{ds}{dy} - \pi\rho g (h - y) x^2 \right] dy + \pi\gamma {r_c}^2 \cos\theta \quad . \tag{15}$$

The first term is the surface energy required for the creation of an area of interface having profile length ds. The second term is the potential energy gained by raising a volume slice to a height $h - y$ above the plane of the support. The last term is the energy required to replace a surface of contact of area $\pi {r_c}^2$ between the solid and liquid with a surface of contact between gas and liquid. The only difference between our equations and those of Pitts is that, for a bubble, this last term is a positive contribution for contact angles θ less than 90°; for a drop this term is energy gained.

The drop volume is given by

$$V = \pi \int_0^h x^2 dy \quad . \tag{16}$$

The equilibrium profile is obtained by finding the function $x(y)$ that minimizes the energy E for a given volume V.

Pitts non-dimensionalizes equations (15) and (16) using $L_c = \left(\frac{\gamma}{\rho g}\right)^{1/2}$ as the scale of distance:

$$\kappa \equiv \frac{h}{L_c} \quad , \quad \lambda \equiv \frac{r_c}{L_c} \quad , \quad \xi \equiv \frac{x}{L_c} \quad , \quad \varsigma \equiv \frac{y}{L_c} \quad , \tag{17}$$

and

$$E_0 \equiv \frac{E\,\rho g}{\pi\gamma^2} \quad \text{and} \quad v \equiv \frac{V}{\pi {L_c}^3} \quad . \tag{18}$$

Eqs. (15) and (16) become

$$E_0 = -v\,\kappa + \int_0^{\kappa} \left[2\xi(1 + \xi'^{\,2})^{1/2} + \xi^2\varsigma\right] d\varsigma + \lambda^2\cos\theta \quad , \tag{19}$$

$$v = \int_0^{\kappa} \xi^2 d\varsigma \quad , \tag{20}$$

where $'$ denotes differentiation with respect to ς.

The calculus of variations is used to find the equilibrium profile by searching for the function $\xi(\varsigma)$ that minimizes E_0 for a given v. Thus we seek the vanishing of the first variation of $E_0 - \mu v$, where μ is an arbitrary multiplier. We substitute the functions

$$\xi(\varsigma) = \bar{\xi}(\varsigma) + \epsilon\eta(\varsigma) \quad , \tag{21-a}$$

$$\xi'(\varsigma) = \bar{\xi}'(\varsigma) + \epsilon\eta'(\varsigma) \quad , \tag{21-b}$$

where $\bar{\xi}$ is the equilibrium profile and ϵ is an arbitrary (small) constant, into Eq. (19) and (20) for the energy and volume, and take the derivatives with respect to ϵ. At the minimum in energy for a given volume,

$$\frac{\partial(E_0 - \mu v)}{\partial \epsilon} = 0 \quad . \tag{22}$$

Taking the first variation gives the Euler-Lagrange equation

$$\varsigma - \mu = \frac{-1}{\varsigma(1+\xi'^{\,2})^{1/2}} + \frac{\xi'\,'}{(1+\xi'^{\,2})^{3/2}} \quad . \tag{23}$$

Rearranging, and comparing to Eq. (3), we see that

$$\mu = \frac{2}{\sqrt{-\beta}} = \frac{2}{R_0/L_c} \quad , \tag{24}$$

is the sum of curvatures at the origin and is necessarily positive.

We can write Eq. (23) in the equivalent form

$$\xi\xi'\,(\mu - \varsigma) = \frac{d}{d\varsigma}\left[\frac{\xi}{(1+\xi'^{\,2})^{1/2}}\right] \quad , \tag{25}$$

and integrate over the height of the bubble

$$\int_0^\kappa \xi\xi'\,\mu d\varsigma - \int_0^\kappa \xi\xi'\,\varsigma d\varsigma = \frac{\xi}{(1+\xi'^{\,2})^{1/2}}\Bigg]_0^\kappa \quad . \tag{26}$$

Integrating the second term by parts and using the contact angle condition,

$$\xi'\,(\kappa) = -\cot\theta \quad , \tag{27}$$

and Eq. (20) for volume, gives

$$v = 2\lambda\sin\theta + (\kappa - \mu)\lambda^2 \quad . \tag{28}$$

Next we require that any calculated equilibrium be stable to a perturbation in shape. We solve for the change in energy δE_0 due to an axisymmetric perturbation in shape by substituting Eqs. (21) for the disturbed profile function, $\kappa + \delta\kappa$ for κ, and $\lambda + \delta\lambda$ for λ into Eq. (19) to obtain a form for $E_0 + \delta E_0$. We subtract E_0 to obtain

$$\delta E_0 = \delta\lambda^2 \cos\theta + 2\delta\lambda\delta\kappa\ [\lambda(\kappa - \mu) + \csc\theta]$$
$$+ (1/2)\ \delta\kappa^2\ [\lambda^2 + 2\csc\theta\cot\theta + 2\lambda(\kappa - \mu)\cot\theta]$$
$$+ \epsilon^2 \int_{\xi_0}^{\kappa + \delta\kappa} [\eta^2(\varsigma - \mu) + \frac{2\eta\eta'\ \xi'}{(1 + \xi'^{\ 2})^{1/2}} + \frac{\xi\eta'^{\ 2}}{(1 + \xi'^{\ 2})^{3/2}}] d\varsigma \qquad (29)$$

If an equilibrium configuration is stable, then δE_0 will be greater than zero, for all values of $\delta\lambda$ and $\delta\kappa$. The second variational problem then is to find $\eta(\varsigma)$ that minimizes δE_0, again subject to the constant volume condition, which becomes

$$-\int_{\kappa}^{\kappa + \delta\kappa} \xi^2 d\varsigma = 2\epsilon \int_{\varsigma_0}^{\kappa + \delta\kappa} \eta\xi d\varsigma + \epsilon^2 \int_{\varsigma_0}^{\kappa + \delta\kappa} \eta^2 d\varsigma \quad , \qquad (30)$$

where ς_0 is a point near the origin which is later set to 0. Following the same procedure as before, Eq. (30) is multiplied by an arbitrary constant and added to the integral in Eq. (29). The minimum in this integral is found by substituting $\eta = \overline{\eta} + \epsilon_2\nu$ and taking the derivative with respect to ϵ_2. We then have the expression for η that minimizes δE_0. After considerable manipulation, Pitts finds that at the minimum in δE_0,

$$\delta E_0 = 3\delta\lambda^2[\lambda(\kappa - \mu) + \sin\theta]\frac{\partial v}{\partial \mu}\left(\frac{\partial N}{\partial \mu}\right)^{-1} \quad , \qquad (31)$$

where

$$N \equiv -3v\cot\theta - \lambda^3 \quad . \qquad (32)$$

Defining

$$R \equiv \lambda(\kappa - \mu) + \sin\theta \quad , \qquad (33)$$

the equation for δE_0 at the minimum is

$$\delta E_0 = 3\delta\lambda^2 R\frac{\partial v}{\partial \mu}\left(\frac{\partial N}{\partial \mu}\right)^{-1} \quad , \tag{34}$$

where v is given by Eq. (28). Eq. (34) is derived considering that $\delta\lambda$ and $\delta\kappa$ do not both vanish. If the radius of contact and the height are both fixed ($\delta\lambda = \delta\kappa = 0$), we obtain an additional equation that must be satisfied for the configuration to be stable. The conjugate point condition can be written

$$M(\kappa) \equiv \frac{1}{2}\left(- \frac{\partial v}{\partial \mu}\cot\theta - \lambda^2\frac{\partial \lambda}{\partial \mu}\right) = \frac{1}{6}\frac{\partial N}{\partial \mu} \quad . \tag{35}$$

If $\frac{\partial N}{\partial \mu}$ goes through zero, the drop is unstable to the conjugate point condition.

Figure 5 shows R , v , N, and μ as functions of κ for a series of bubble configurations with a contact angle of 80°. Here too, solid curves are for the uppermost occurrences of the contact angle, and dashed curves represent re-entrant contact angles. At the point of changeover on the curves (maximum β), R , $\frac{\partial N}{\partial \kappa}$, and $\frac{\partial \mu}{\partial \kappa}$ all pass through zero, as shown by Pitts is necessarily the case. Along the portion A-B on the solid curves, R and $\frac{\partial N}{\partial \kappa}$ are negative and $\frac{\partial v}{\partial \kappa}$ is positive; hence δE_0 is positive and these bubble configurations are stable according to Eq. (34). From point B to point C, R , $\frac{\partial N}{\partial \kappa}$, and $\frac{\partial v}{\partial \kappa}$ are all positive and these configurations are also stable. At point C, $\frac{\partial v}{\partial \kappa}$ changes sign, so configurations between C and D are unstable. At point D, $\frac{\partial v}{\partial \kappa}$ again changes sign, but so does $\frac{\partial N}{\partial \kappa}$, making configurations between D and E unstable.

The characteristics of the curves are similar for smaller contact angles. As

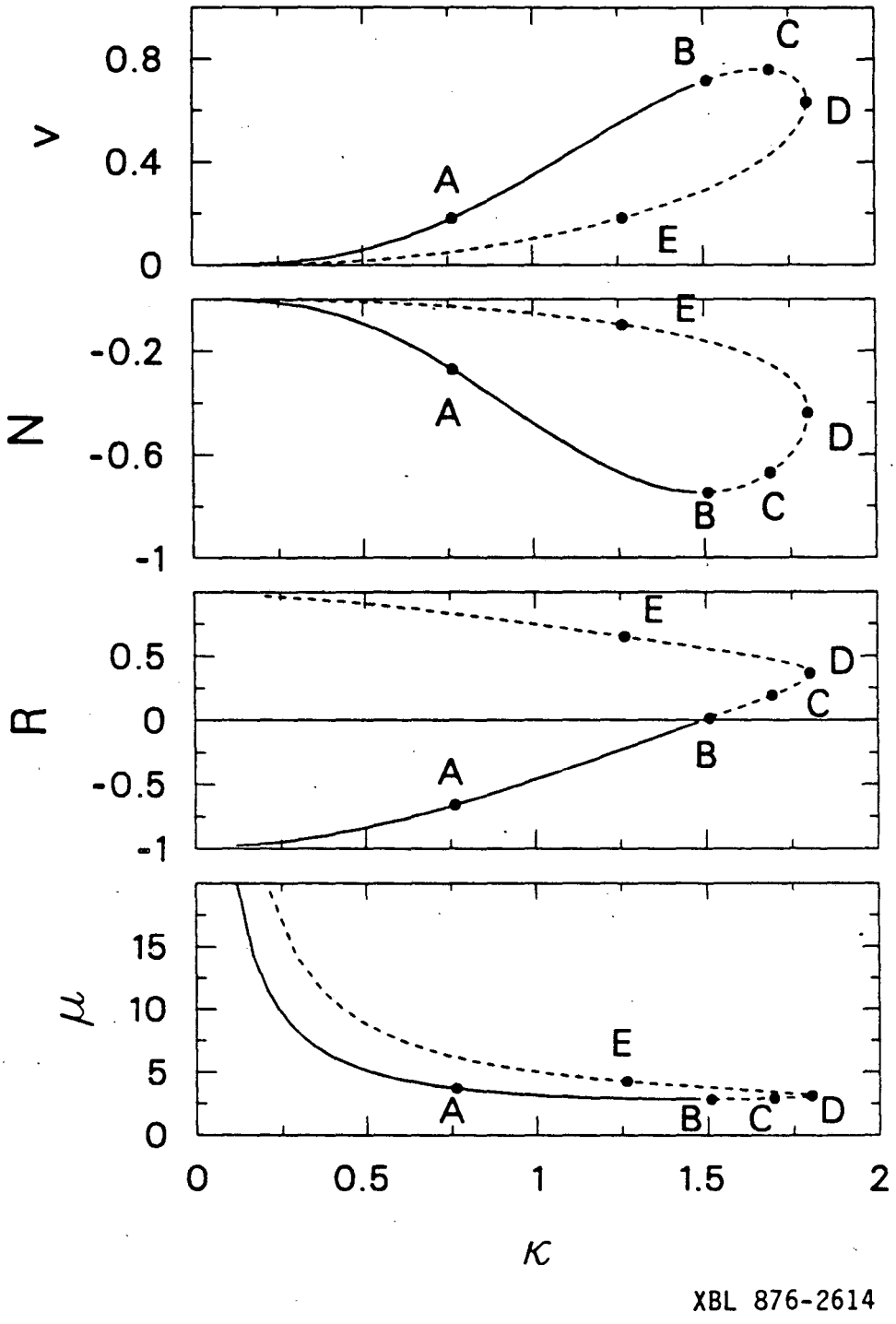

Figure 5. Relevant parameters in the determination of the stability of equilibrium bubble configurations for $\theta = 80°$. Solid curves represent first meeting of the contact angle condition; dashed curves correspond to re-entrant contact angles.

the contact angle decreases, the point of maximum β (point B) moves closer to the point of maximum volume (point C), and the envelopes decrease in size. An example is shown in figure 6 for a contact angle of 40°.

The calculated configurations are always stable to the conjugate point condition (Eq. (35)). Thus, the equilibrium bubble configuration are all stable up to the point of maximum volume. Re-entrant contact angles are more often than not unstable; however, for purposes of the calculation of the maximum bubble volume on a flat surface (as addressed by Wark (1933)), the bubble of maximum volume for a given contact angle is stable to an axisymmetric disturbance in shape.

The maximum bubble volume is given as a function of contact angle in Figure 7 for $L_c = 0.273$ cm. A least-squares fit of these data gives the correlation

$$\frac{V_{max,\,flat}}{\pi L_c^{\,3}} = 0.285\,\theta^{2.96} \quad (\theta \text{ in radians})\,. \tag{36}$$

which has a maximum error of 3% at $\theta = 9°$, and an average error of magnitude 0.7% from 9 to 90°. Our correlation is a minor improvement over that of Fritz (1935) and Cheh (1967), which has an average error of magnitude 4%.

5. The Size of a Bubble on a Curved Support

The calculation of the bubble interface for a bubble on a curved surface is identical to that for a horizontal support. The difference appears in the end point condition, the specified angle of contact measured through the liquid phase. The thermodynamic contact angle is the same as that used previously for a flat surface because Young's equation (Eq. (2)) can be derived independently of the orientation

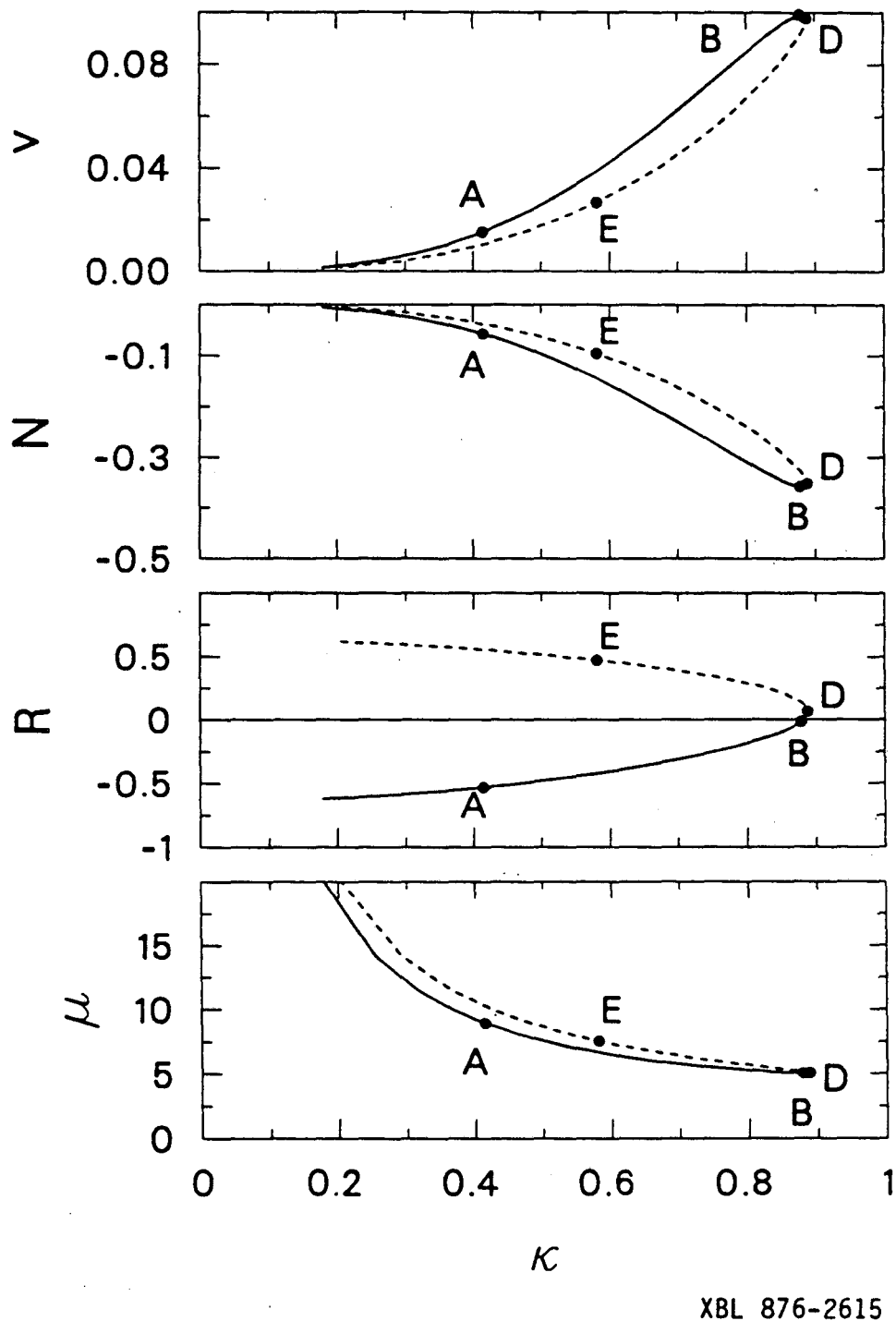

Figure 6. Relevant parameters in the determination of the stability of equilibrium bubble configurations for $\theta = 40^\circ$.

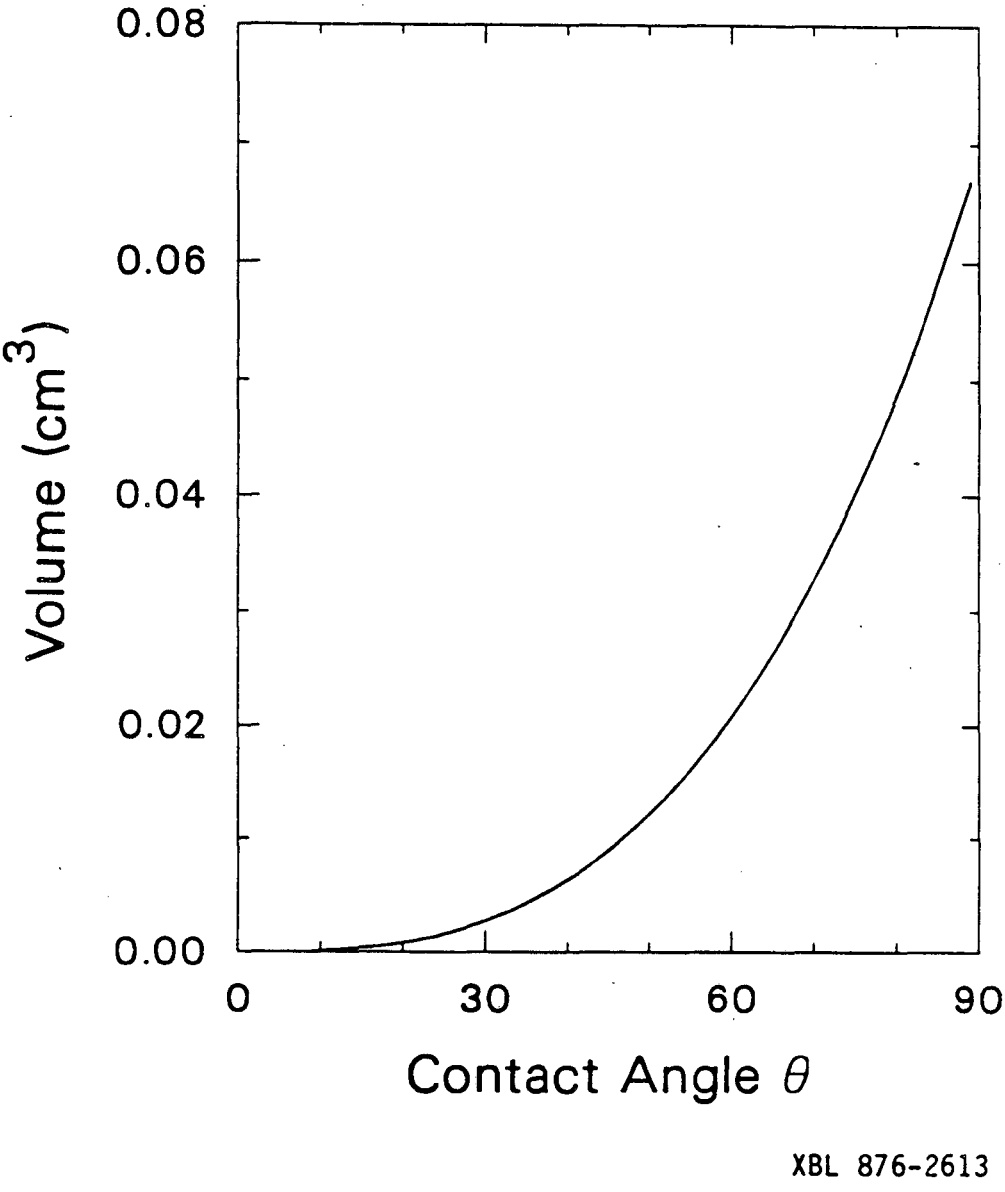

Figure 7. The maximum stable equilibrium bubble volume as a function of contact angle for parameters characteristic of water at 25 °C (L_c = 0.273 cm).

of the surface. If one assumes that this equilibrium angle is maintained, a geometric relation obtains between the thermodynamic contact angle θ, the radius of contact r_c, the radius of curvature of the surface r_w, and the contact angle θ_h measured from the bubble interface to the horizontal. This geometric relation is demonstrated in Figure 8 and is given by

$$r_c = r_w \sin(\theta - \theta_h) \quad . \tag{37}$$

To apply Eq. (37), we return to the families of solutions generated for a given value of θ_h, as described in Section 3. We plot the calculated values of volume as a function of r_c for values of θ_h (which is equal to θ for a flat surface), as in Figure 4. We then choose the radius of curvature of the surface r_w and a contact angle θ. For any value of θ_h, we calculate r_c according to Eq. (37) and generate a new family of solutions. This procedure is demonstrated graphically in Figure 9, which shows two solutions for $r_w = 0.1$ cm and $\theta = 60^\circ$ (circles) and $\theta = 90^\circ$ (squares). The point of maximum volume for a given θ and r_w falls on a dashed curve, which corresponds to one of the configurations determined to be unstable. It becomes obvious that the maximum *stable* volume for a given θ and r_w will be found when the curve generated for $V(r_c, \theta, r_w)$ intersects one of the curves for $V(\theta_h, r_c)$ at the point of the maximum volume on the $V(\theta_h, r_c)$ curve. This simplifies the procedure considerably, as now we have only to find the intersection of the curve for $r_c(\theta_h)$ at the maximum volume with the curve for the geometric relationship (Eq. (37)) $r_c(\theta_h)$ for a given θ, r_w. The curve of r_c vs θ_h at the maximum volume is given in Figure 10.

We choose values for r_w and θ and calculate r_c as a function of θ_h from Eq.

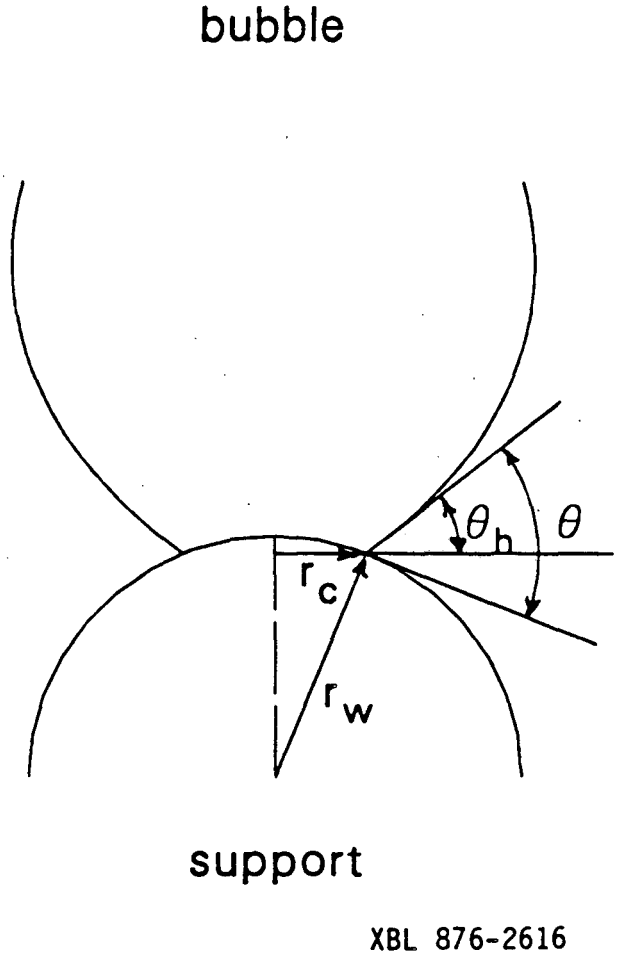

Figure 8. Geometric relation between r_w, r_c, θ and θ_h at the point of adherence.

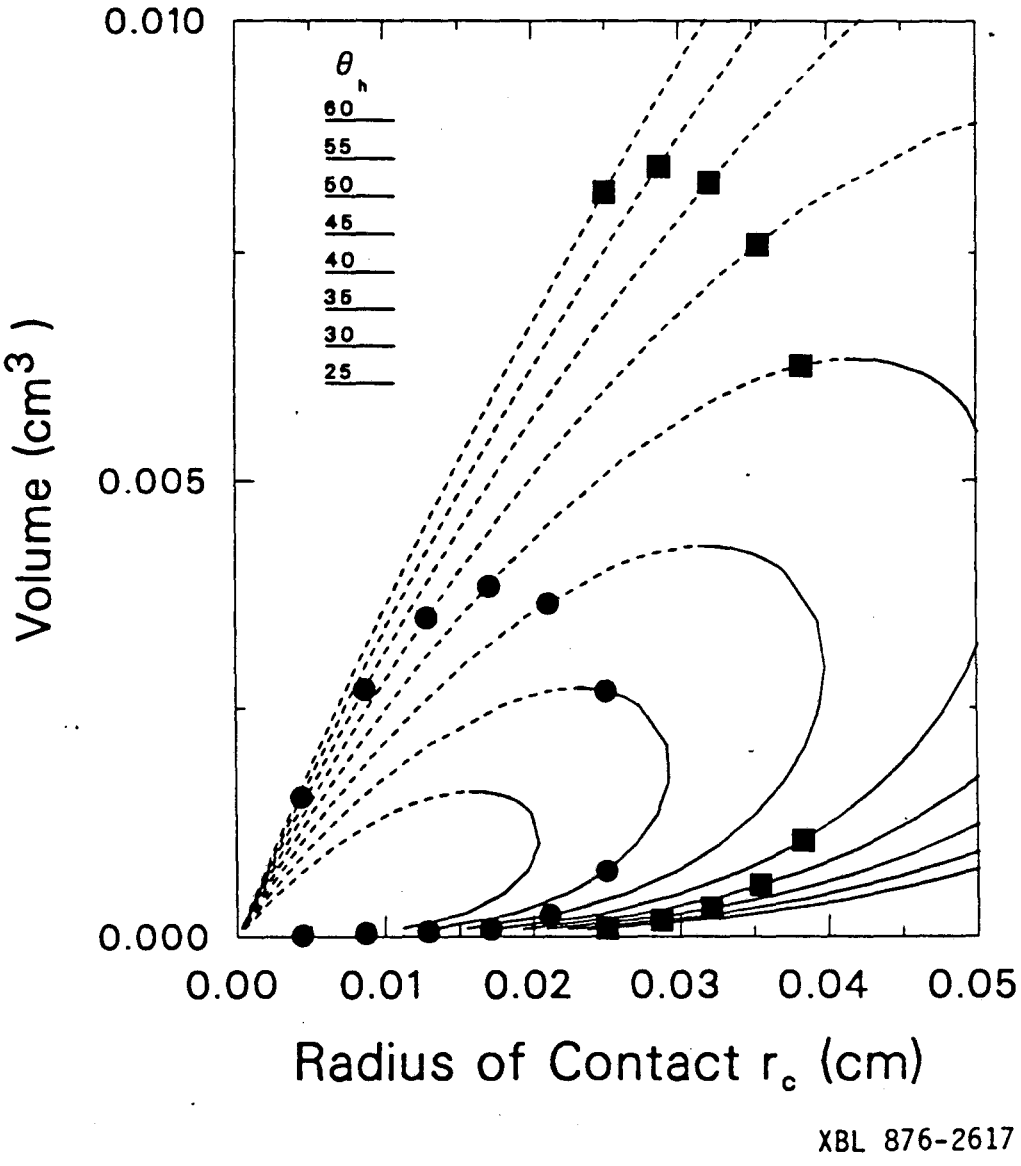

Figure 9. Graphical solution of the problem of a bubble on a curved surface. Curves are for $V(\theta_h, r_c)$. Symbols represent points where Eq. (37) is satisfied for contact angles of 60° (•) and 90° (■).

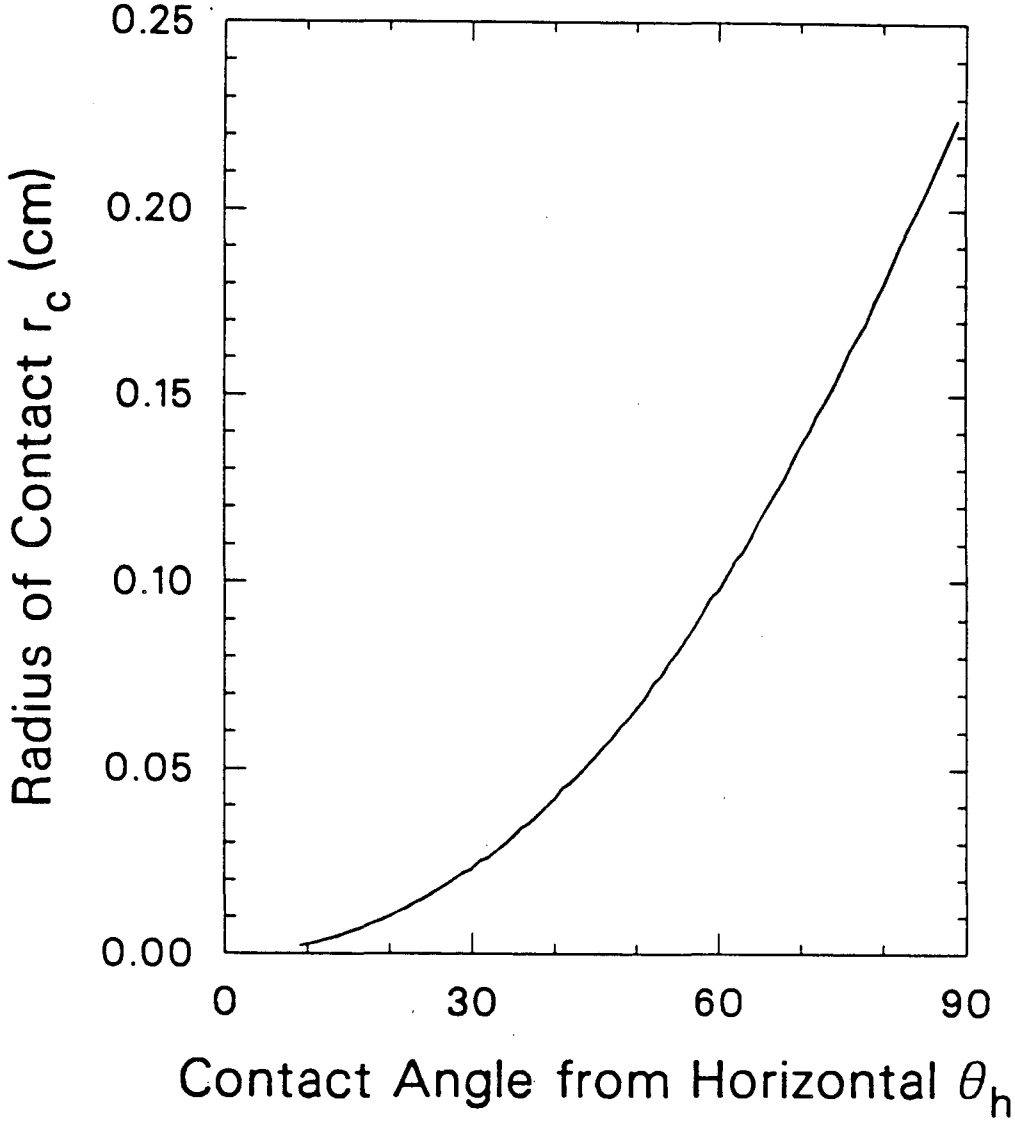

Figure 10. The relationship between r_c and θ_h corresponding to configurations at the point of maximum volume.

(37). The point where this curve crosses the curve of $r_c\,(\,\theta_h\,)$ in Figure 10 is found by numerical interpolation. This procedure is demonstrated graphically in Figure 11 for $r_w = 0.1$ cm for five values of θ from 30 to 90°. The corresponding volumes are also numerically interpolated. Figure 12 shows the bubble configurations of maximum volume for $\theta = 60°$ on a flat surface and on a hemispherical surface of curvature $r_w = 0.1$ cm .

The above procedure was repeated for contact angles from 10 to 90° and r_w from 0.01 to 1.0 cm. Figure 13 shows the maximum stable equilibrium bubble volume as a function of contact angle θ and radius of curvature of the surface r_w. The corresponding reduction in volume as a result of the curvature of the surface is shown in Figure 14, which shows the ratio of the maximum volume on a curved surface to that on a flat surface as a function of θ and r_w.

The goal of this work has been to obtain a simple correlation for the volume reduction resulting from the curvature of the surface. From Figure 14, we expect

$$\frac{V_{max,r_w}}{V_{max,flat}} \rightarrow 0 \text{ as } r_w \rightarrow 0$$

$$\rightarrow 1 \text{ as } r_w \rightarrow \infty$$

$$\rightarrow 1 \text{ as } \theta \rightarrow 0 \quad .$$

Several forms for the correlation were tested, some based on physical arguments, others based on manipulation of the equations and the graphical results, and still others more empirical. The best fit was obtained with the empirical correlation

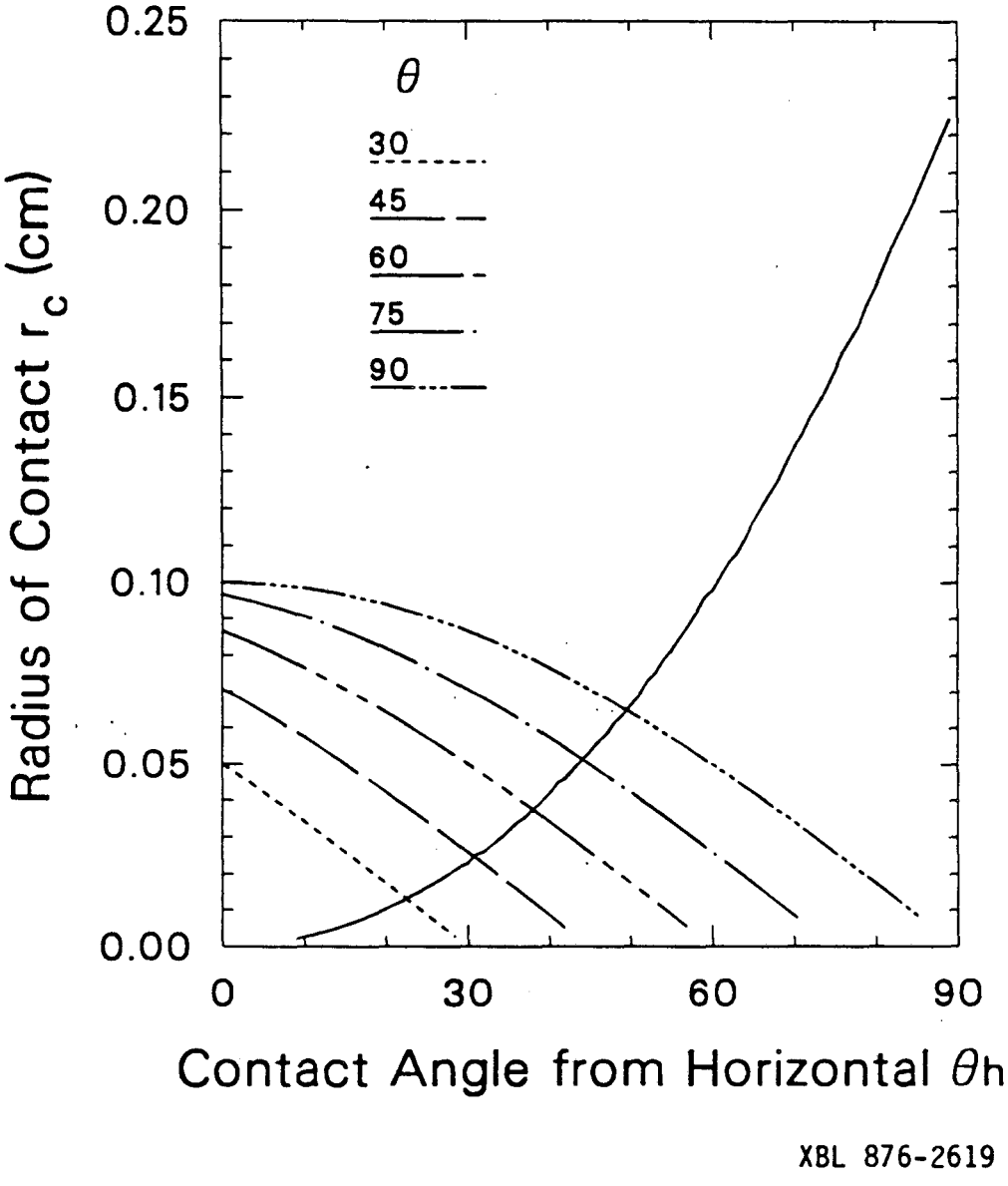

Figure 11. Graphical solution of the problem of a bubble on a curved surface for $r_w = 0.1$ cm and five values of θ. Points of intersection are points where Eq. (37) is satisfied.

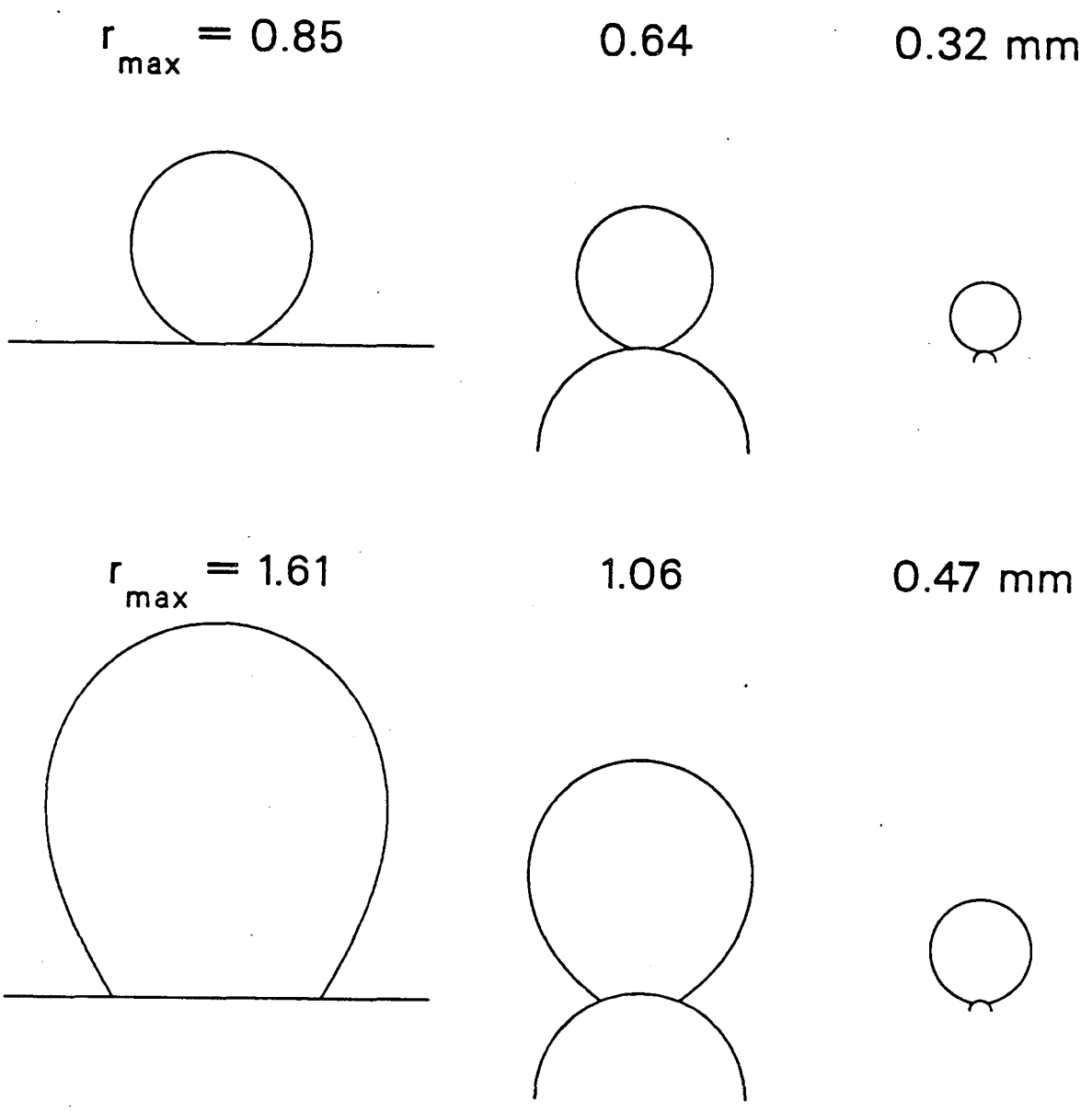

Figure 12. Largest stable equilibrium bubble configurations with a contact angle of 30° (top row) and 60° (bottom row) on a flat surface (left), on a surface of curvature $r_w = 1.0$ mm (middle) and $r_w = 0.1$ mm (right).

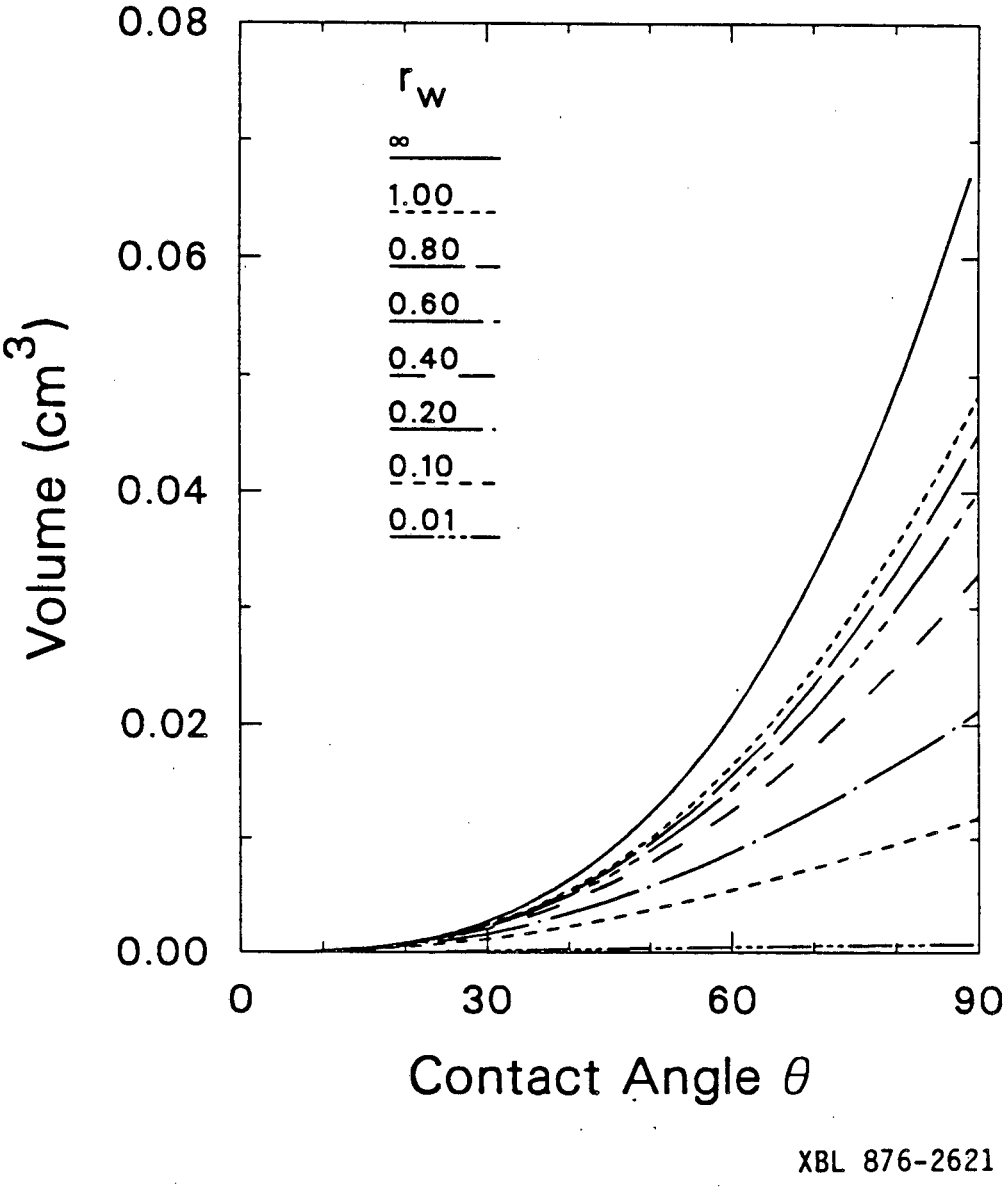

Figure 13. Maximum stable equilibrium bubble volume as a function of contact angle θ and radius of curvature of the surface r_w.

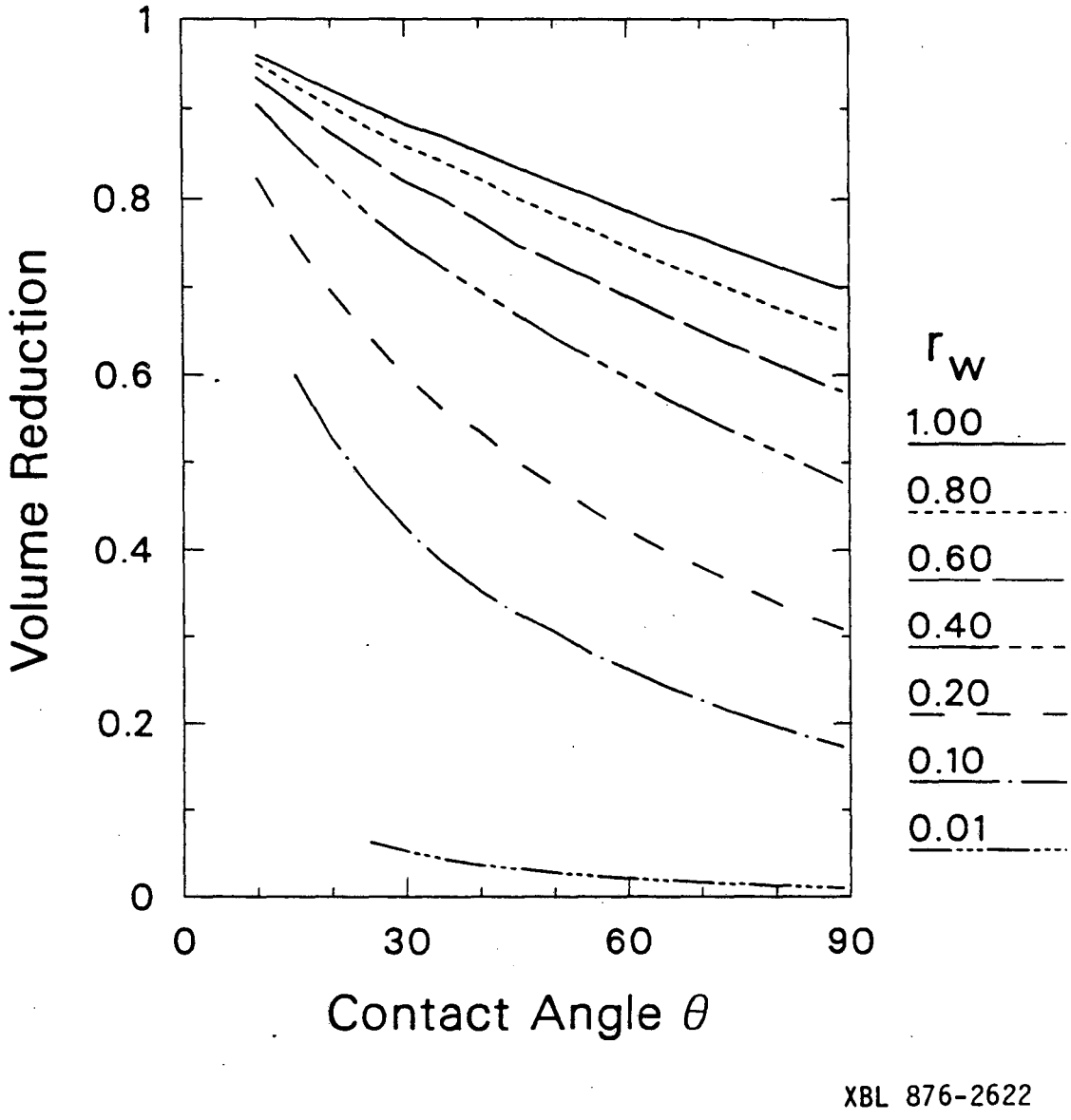

Figure 14. Reduction in the maximum stable equilibrium bubble volume as a function of contact angle θ and radius of curvature of the surface r_w.

$$\frac{V_{max,\,r_w}}{V_{max,\,flat}} = \left(\frac{r_w}{r_w + L_c} \right)^{0.95\,\theta} \quad (\theta \text{ in radians}) \quad . \tag{38}$$

A nonlinear least-squares fit was used to determine if any significant improvement could be gained by writing the correlation as

$$\frac{V_{max,\,r_w}}{V_{max,\,flat}} = a \left(\frac{r_w}{r_w + b\ L_c} \right)^{c\,\theta} \quad . \tag{39}$$

and solving for the three coefficients by minimizing the sum of squares between the fit and the determined values. The improvement in the fit does not justify using all three coefficients. The average magnitude of the error in the volume reduction using Eq. (38) is 0.02; this value was reduced only to 0.017 by using three coefficients. A demonstration of the fit of Eq. (38) for the volume reduction is shown in Figure 15. The individual points are the calculated values and the solid curves show the fit according to Eq. (38). The fit of maximum bubble volumes using γ and ρ for water at 25 °C is shown in Figure 16.

6. Conclusions

The volume of the largest stable equilibrium bubble that can adhere to a flat horizontal surface is a function of the characteristic length of the system,

$$L_c \equiv \left(\frac{\gamma}{\rho g} \right)^{1/2}$$

and the equilibrium contact angle and is given by

$$\frac{V_{max,\,flat}}{\pi {L_c}^3} = 0.285\ \theta^{2.96} \quad (\theta \text{ in radians}) \quad .$$

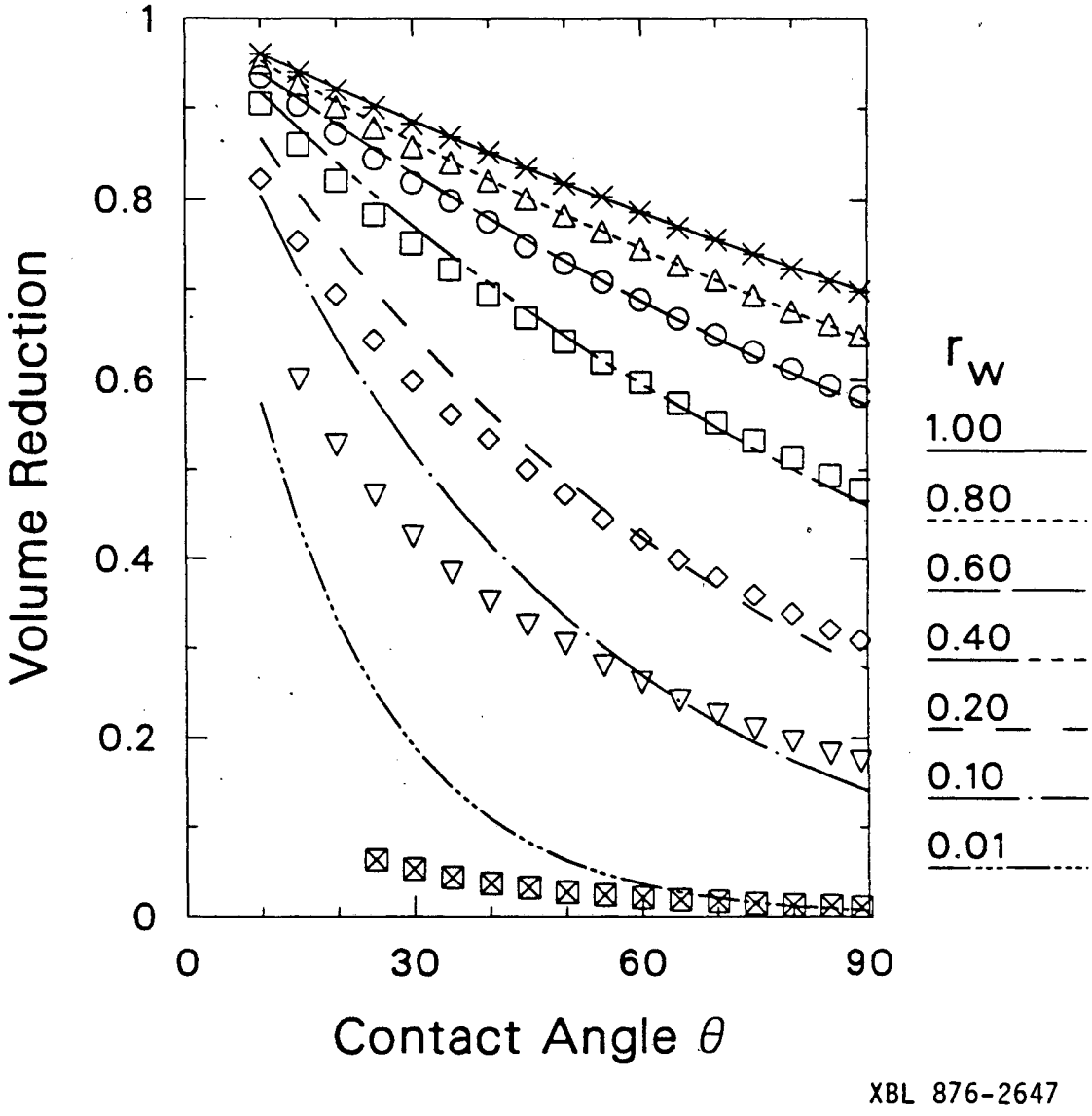

Figure 15. Reduction in the maximum stable equilibrium bubble volume as a function of contact angle θ and radius of curvature of the surface r_w. Individual points are the calculated values; solid curves show the fit according to Eq. (38).

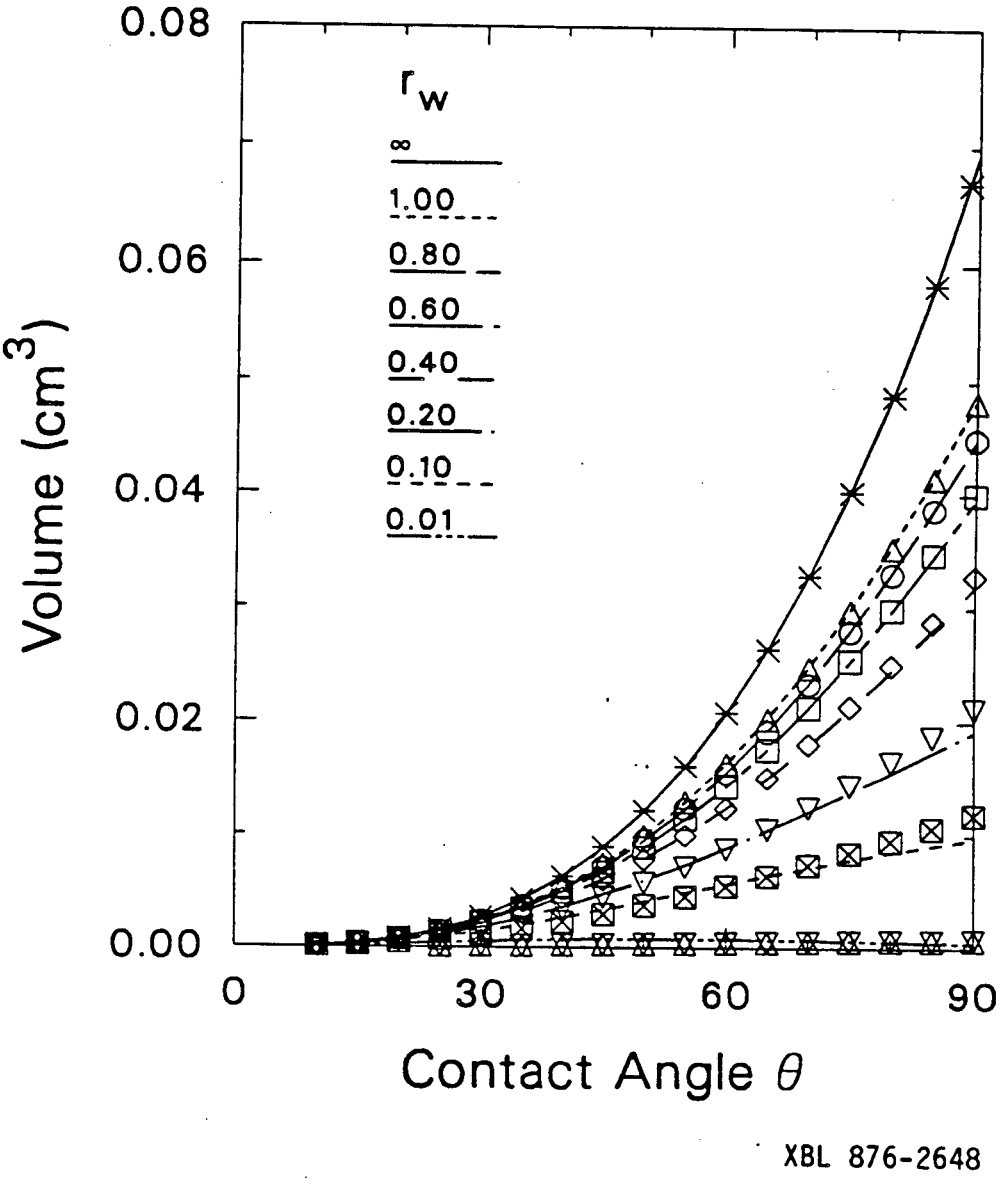

Figure 16. The maximum stable equilibrium bubble volume as a function of contact angle θ and radius of curvature of the surface r_w. Individual points are the calculated values; solid curves show the fit according to Eqs. (38) and (36).

The bubble configurations of maximum volume for contact angles greater than 60° have re-entrant contact angles. A stability analysis that accounts for axisymmetric disturbances in bubble shape that extend over the entire surface of the bubble shows that, although re-entrant contact angles usually indicate instability, the profiles with re-entrant contact angles at the point of maximum volume are stable.

The determination of maximum bubble volume has been extended to account for the destabilizing effect of the solid support curving away from the bubble. The situation described applies exactly to a bubble growing on a hemispherical protrusion on the surface, and by extension, to a bubble growing on a wire or screen. The reduction in the maximum stable bubble volume for such a case can be described by the simple function

$$\frac{V_{max,\,r_w}}{V_{max,\,flat}} = \left(\frac{r_w}{r_w + L_c} \right)^{0.95\,\theta} \quad (\theta \text{ in radians}) \quad ,$$

where r_w is the radius of the protrusion.

This result is the first step in accounting for the role of the morphology of the substrate on bubble size, which profoundly affects the dynamics of gas-evolution on electrode surfaces. In practice, gas is often evolved on more complex electrode geometries and on orientations other than horizontal, and further extensions of the classical theory to describe these cases will prove valuable to understanding the factors affecting electrolytic gas evolution, and also nucleate boiling, and mineral flotation.

7. Chapter 2 Nomenclature

a	fitting parameter in Eq. (39)
b	fitting parameter in Eq. (39)
c	fitting parameter in Eq. (39)
E	energy to create bubble, ergs
E_0	dimensionless energy to create bubble
g	acceleration of gravity, 980 cm/s^2
h	bubble height, cm
L_c	characteristic length, defined by Eq. (14), cm
M	stability parameter, defined by Eq. (35)
N	stability parameter, defined by Eq. (32)
p	pressure, dyne/cm^2
r_c	radius of contact at bubble base, cm
r_w	radius of curvature of support, cm
R	stability parameter, defined by Eq. (33)
R_0	radius of curvature at origin, cm
R_1	radius of curvature of interface, given by Eq. (4)
R_2	radius of curvature of interface, given by Eq. (5)
s	arc length, cm
v	dimensionless volume
$V_{max,\,flat}$	maximum bubble volume, cm^3
$V_{max,\,r_w}$	maximum bubble volume, curved surface, cm^3
x	radial coordinate, cm
z	axial coordinate, cm
β	Bond number, given by Eq. (6)
γ	surface tension, dyne/cm
ϵ	arbitrary small number
ς	dimensionless vertical position

η	first perturbation variable
θ	angle of contact, degrees
θ_h	portion of θ above horizontal, degrees
κ	dimensionless bubble height
λ	dimensionless radius of contact
μ	capillary datum $= \frac{2L_c}{R_0}$
ν	second perturbation variable
ξ	dimensionless radial coordinate
ρ	density, g/cm^3

Subscripts and superscripts

$'$	derivative with respect to s
$*$	distance made dimensionless with R_0

8. Chapter 2 References

Bashforth, F., and Adams, J., 1883, *An Attempt to Test the Theory of Capillary Action*, Cambridge University Press and Deighton, Bell, and Co., Cambridge.

Blaisdell, B.E., 1940, *Journal of Mathematical Physics*, Vol. 19, pp. 186.

Cheh, H.Y., 1967, *On the Mechanism of Electrolytic Gas Evolution* Ph. D. Thesis, University of California, Berkeley, p.23. (Also University of California Radiation Laboratory Report No. UCRL-17324)

Fordham, S., 1948, "On the Calculation of Surface Tension from Measurements of Pendant Drops," *Proceedings of the Royal Society (London)*, Vol. 194A, pp. 1-16.

Fritz, V.W., 1935, "Berechnung des Maximalvolumens von Dampfblasen," *Physikalische Zeitschrift*, Vol. 36, pp. 379-384.

Gibbs, J.W., 1906, *Scientific Papers*, Dover Edition, 1961, original: Longmans and Green, 1906.

Gauss, 1830, *Principae Generalia Theoreticae Figurae Fluidorium in Statu Aequilibrii*, Gottingen.

Kabanow, B., and Frumkin, A., 1933, "On the Size of Electrolytically-Generated Gas Bubbles," *Zeitschrift für Physikalische Chemie*, Vol. 165A, pp. 433-452.

Laplace, P.S. de, 1805, *Mechanique Celeste, Suppl. au X Livre, Coureier*, Paris.

Lawal, A., and Brown, R.A., 1982, "The Stability of an Inclined Pendent Drop," *Journal of Colloid and Interface Science*, Vol. 89, pp. 332-345.

Mills, O.S., 1953, "Tables for use in the Measurement of Interfacial Tensions between Liquids with Small Density Differences," *British Journal of Applied Physics*, Vol. 4, pp. 247-252.

Padday, J.F., 1969, "Theory of Surface Tension," in *Surface and Colloid Science*, Vol. 1, E. Matifević, Ed., pp. 39-249.

Padday, J.F., 1972, "Tables of the Profiles of Axisymmetric Menisci," *Journal of Electoanalytical Chemistry and Interfacial Electrochemistry*, Vol. 37, pp. 313-316.

Pitts E., 1974, "The Stability of Pendent Liquid Drops. Part 2. Axial Symmetry," *Journal of Fluid Mechanics*, Vol. 63, pp. 487-508.

Poisson, 1831, *Nouvelle Theorie de l'Action Capillaire.*

Wark, I.W., 1933, "The Physical Chemistry of Flotation. I. The Significance of Contact Angle in Flotation," *Journal of Physical Chemistry*, Vol. 37, pp. 623-644.

Young, T., 1804, *Proceedings of the Royal Society*, Dec., 1804.

Chapter 3. Mass-Transfer Effects of Bubble Streams Rising Near Vertical Electrodes

1. Abstract

Mass-transfer enhancement by a stream of bubbles rising near a mass-transfer surface is resolved spatially and temporally using a micro-mosaic electrode. A stream of gas bubbles is generated electrolytically, either at a segment directly below and in the plane of the monitoring electrodes, or at a wire tip that can be positioned inside or outside of the mass-transfer boundary layer. The mass-transfer enhancement resulting from bubbles rising within the mass-transfer boundary layer is found to be strong and localized, in agreement with trends predicted by a surface-renewal model. Mass transfer resulting from bubbles rising outside the boundary layer is found to receive a steady, laminar enhancement, correlating well with predictions from an idealization of the bubble stream entraining a cylinder of liquid.

2. Introduction

Electrolytic gas evolution has been recognized in the literature since 1951 (Roald and Beck, 1951) as an efficient means of achieving high mass-transfer rates at solid surfaces. The magnitude of this effect can be illustrated by comparing the equivalent diffusion boundary-layer thicknesses for gas evolution and for forced convection. Ibl *et al.* (1971) measured mass-transfer rates during electrolysis by adding Fe^{+3} to the electrolyte as an indicator ion: the Fe^{+3} is reduced at limiting current simultaneously as the hydrogen ion is discharged. For hydrogen evolution at a planar vertical surface at a rate of 1 cm^3/cm^2-min , which corresponds to a current density of 130 mA $/cm^2$, they determined a diffusion-layer thickness δ of 15 μm , or a mass-transfer coefficient k of 3.6×10^{-4} cm/sec. For comparison, we calculate the average diffusion boundary-layer thickness for developed mass transfer in turbulent channel flow with the correlation of Landau and Tobias (1976)

$$Sh \equiv \frac{d}{\delta} = 0.0113\, Re^{0.87}\, Sc^{0.35} \qquad 2800 < Re < 12{,}000 \quad , \tag{1}$$

where d is the equivalent diameter, $Re \equiv ud/\nu$ and $Sc \equiv \nu/D_i$. For a Sc of 1800, the Re required to obtain the average diffusion boundary-layer thickness of 15 μm is 6700. In a 1-cm square channel, the equivalent diameter d is 0.5 cm and the required average velocity between parallel plate electrodes is 135 cm/sec. Thus gas evolution indeed provides a very effective stirring mechanism.

The reason gas evolution is so effective a stirring mechanism is that the bubble motion takes place in the near vicinity of the electrode surface, within and just outside the mass-transfer boundary layer. Gas evolution is itself a very complex process, involving bubble nucleation, growth, coalescence, and detachment

from the electrode. In addition to these local events, a macroscopic flow is generated by the rise of bubble swarms or curtains. In practice, forced convection is often superimposed to facilitate removal of the gas from the inter-electrode gap, thereby lowering the ohmic penalty for the presence of gas in the electrolyte.

The dominant mechanism for the high mass-transfer enhancement by gas evolution is not obvious. In fact, it may be different under different conditions of gas-evolution rate, and electrode coverage, orientation, or morphology. The traditional approach has been to assume a primary mode of mass transfer, quantify the mass-transfer rate for the chosen mode, and average over the electrode area to obtain a relation between the mass-transfer rate and the gas-evolution rate. An example of this approach would be to assume that the important mechanism of mass transfer is the diffusional mass transfer to the newly-exposed electrode site following each bubble disengagement. Several schools of thought have emerged over the past two decades, each one emphasizing a different mechanism as the main contributor. The example mentioned above is the penetration, or surface-renewal, model. These theories will be briefly reviewed in Section 3. This coverage is by no means exhaustive; the reader is referred to two recently-published reviews (Vogt (1983) and Sides (1986)) for more details on all aspects of electrolytic gas evolution.

Recent advances in integrated-circuit processing have allowed the limiting-current technique of measuring mass-transfer coefficients to be applied at electrodes that are sectioned on the microscopic scale. The first study of this type involving gas-evolving electrodes was conducted by Dees and Tobias (1987b). They resolved on a scale of 100 μm (an order of magnitude smaller than the bubble diameter) the mass-transfer resulting from a single bubble detaching from a horizontal electrode,

and also that resulting from two bubbles coalescing and rising from the electrode. They found that *the mass transfer following a coalescence event was significantly more intense than that following a disengagement.* A coalescence and simultaneous disengagement increased the mass-transfer rate by an order of magnitude over the free-convection limiting current, while a single-bubble disengagement increased the mass-transfer rate by only a few percent.

The present study is an effort to advance our understanding of local, transient mass-transfer during electrolytic gas evolution, in much the same way as have Dees and Tobias (1987b). The objective of this work is to resolve spatially and temporally the mass transfer resulting from a single stream of gas bubbles evolved at or near a *vertical* micro-mosaic electrode. Our aim is to characterize the nature of the enhancement in an effort to fill in the missing microscopic picture, so that the correlation of mass-transfer enhancement data, and ultimately, the engineering design of gas-evolving electrodes, may be based on the fundamental physico-chemical principles. The specific topic addressed in this study is the dependence of the magnitude and spatial distribution of the mass-transfer enhancement at vertical gas-evolving electrodes on bubble size, bubble stream position relative to the mass-transfer surface, and rate of gas evolution.

3. Models for Mass-Transfer Enhancement

Three theories of mass transfer at gas-evolving electrodes have been advanced, each one emphasizing a particular mechanism of mass-transfer enhancement. These theories are the penetration model, the hydrodynamic model,

and the micro-convection model.

3.1. *The Penetration Model*

The penetration model, or surface-renewal effect, was first proposed by Higbie (1935) in relation to the absorption of a gas into a liquid, and was adopted by Ibl and coworkers (Ibl and Venczel (1970)) for electrolytic gas evolution. In this description, a volume of fluid in the mass-transfer boundary layer, having been depleted of reactant, is renewed as each bubble detaches from the electrode and allows fresh electrolyte with bulk concentration of reactant to penetrate to the electrode. The transport of reactive species to the nucleation area at the electrode is by diffusion during a waiting period τ_w before a new bubble is nucleated. The reactant-ion limiting current during the waiting time falls with $t^{-1/2}$ following the Cottrell equation (1903),

$$i(t) = \frac{n_i F D_i {c_i}^{\infty}}{\sqrt{\pi D_i t}} \quad . \tag{2}$$

The average limiting current during the waiting time is

$$i = \frac{1}{\tau_w} \int_0^{\tau_w} i(t)dt = \frac{2 n_i F D_i {c_i}^{\infty}}{\sqrt{\pi D_i \tau_w}} \quad . \tag{3}$$

If one assumes that the bubble growth time is insignificant in comparison to the total life-cycle time, the waiting time τ_w is inversely proportional to the bubble frequency and hence to the volumetric flux of evolved gas. In this case, i and the mass-transfer coefficient k will depend on v, the volumetric rate of gas evolution per unit area, to the 1/2 power. The constant of proportionality is subject to various assumptions involving electrode coverage and the shape of attached bubbles.

Ibl and Venczel (1970) assumed that bubbles adhering to the electrode were hemispherical in shape, covering an area of $\pi {R_b}^2$. The waiting time was then the ratio of the gas volume per bubble to the product of the gas evolution rate per electrode area and the area per bubble, $\pi {R_b}^2$.

$$\tau_w = \frac{2\pi {R_b}^3}{3v\,\pi {R_b}^2} = \frac{2R_b}{3v} \quad . \tag{4}$$

To account for the fact that, on the average, a fraction θ of the electrode is blocked by attached bubbles, Ibl and Venczel multiplied τ_w and k by $1 - \theta$. Substituting Eq. (3) into Eq. (4), they obtained

$$i = n_i F c_i^{\infty} \left(\frac{6 D_i\, v\,(1-\theta)}{\pi R_b} \right)^{0.5} \tag{5}$$

Experimentally determined values of $\frac{\partial \ln k}{\partial \ln v}$ fall between 0.3 and 0.7. A summary is listed in Table 1.

3.2. *The Hydrodynamic Model*

The second theory of mass-transfer enhancement at gas-evolving electrodes is the hydrodynamic model, first proposed in relation to nucleate boiling by Zuber (1963). The model was discussed in relation to gas evolution by Janssen and Hoogland (1970, 1973) and described quantitatively by Janssen and Barendrecht (1979). This treatment emphasizes the electrolyte flow caused by the buoyant lift of the rising bubbles in the vicinity of the electrode. The mass-transfer correlation for turbulent natural convection at a plane wall,

Table 1. Experimentally determined values of $\frac{\partial \ln k}{\partial \ln v}$ (from Vogt (1983))

Gas	Electrolyte	$\frac{\partial \ln k}{\partial \ln v}$	Investigator
H_2	alkaline	0.43	Green and Robinson (1959)
		0.29	Vondrak and Balej (1970)
		0.36	Janssen and Hoogland (1973)
		0.25	Fouad and Sedahmed (1973)
		0.65	Rousar *et al.* (1975)
		0.17-0.30	Janssen (1978)
H_2	acidic	0.5(0.59)	Roald and Beck (1951)
		0.525	Venczel (1961)
		0.47	Janssen and Hoogland (1970)
		0.62(Pt)	Janssen and Hoogland (1973)
		0.36(Hg)	Janssen and Hoogland (1973)
		0.45	Kind (1975)
O_2	alkaline	0.87/0.33	Janssen and Hoogland (1973)
		0.4	Fouad and Sedahmed (1973)
O_2	acidic	0.5	Beck (1969)
		0.4	Janssen and Hoogland (1970)
		0.6	Ibl *et al.* (1971)
		0.57	Janssen and Hoogland (1973)
		0.66	Kind (1975)
Cl_2	acidic	0.71	Janssen and Hoogland (1970)

$$Sh_H \equiv \frac{kH}{D_i} = 0.16\,(GrSc)^{1/3} \quad , \tag{6}$$

is assumed to be applicable to the case of two-phase flow. The Grashof number Gr is defined

$$Gr \equiv \frac{gH^3}{\nu^2}\frac{\rho^\infty - \rho^0}{\rho^0} \quad , \tag{7}$$

where ρ^∞ is the density of the bulk solution, and ρ^0 is the mean density at the electrode surface. The bulk density ρ^∞ is equal to the density of the liquid ρ_L, and

ρ^0 is a function of the gas volume fraction ϵ: $\rho^0 = \epsilon\rho_G + (1-\epsilon)\rho_L$. For $\rho_L >> \rho_G$, the Grashof number becomes

$$Gr = \frac{gH^3}{\nu^2}\frac{\epsilon}{1-\epsilon} \quad . \tag{8}$$

Zuber (1963) related the volume fraction to the volumetric rate of gas evolution by

$$\frac{\epsilon}{1-\epsilon} = \frac{v}{v_t} \tag{9}$$

where v_t is the terminal velocity of a single bubble and, for a small spherical bubble with a rigid interface, is given by

$$v_t = \frac{1}{12}\frac{gd^2}{\nu}\frac{\rho_L - \rho_G}{\rho_L} \quad . \tag{10}$$

Equation (9) is valid in the "turbulent" regime, in which a net upward flow is induced by the rising bubbles. If the liquid were stationary, Equation (9) would be replaced by

$$v = \epsilon v_t \quad . \tag{11}$$

Similarly, if the net upward flow were zero, so that liquid flowed downward to replace the ascending gas, one would obtain the "laminar" result of Zuber (1963)

$$v = v_t\,\epsilon\,(1-\epsilon) \quad . \tag{12}$$

In any case, gas volume fractions are typically small compared to unity, so that $\epsilon/(1-\epsilon)$ in Equation (8) may be replaced by v/v_t. Substituting this result and Equations (8) and (10) into Equation (6), one obtains

$$Sh \equiv \frac{kd}{D_i} = 0.16\left(\frac{12\rho_L}{\rho_L - \rho_G}\right)^{1/3}\left(\frac{vd}{D_i}\right)^{1/3}$$

$$= 0.37 \left(ReSc\right)^{1/3} \quad . \tag{13}$$

The mass-transfer rate is proportional to the gas-evolution rate to the 1/3 power. This result may be applicable to gas evolution under certain conditions of current density and electrode coverage. Ibl and coworkers (1971) experimentally determined the slope of the $\ln k$-versus-$\ln v$ curve to be 0.36 for gas-sparged systems.

3.3. *The Micro-Convection Model*

The micro-convection model was developed by Vogt (1977) and Stephan and Vogt (1979). Their approach treats the mass transfer caused by the local convection generated by the growth of an attached bubble. The electrode area per bubble available for mass transfer is $1/(n/A) - \pi R_b^2$, where R_b is a function of time. The local, transient mass transfer for laminar flow is averaged over this area and over the time of bubble growth. In the resulting correlation,

$$Sh = 0.93\, Re^{0.5} Sc^{0.487} \quad , \tag{14}$$

Sh is a factor of approximately three below that calculated from the penetration model.

The important point to be gained from these mass-transfer theories is that single-bubble disturbances of the mass-transfer boundary layer, such as those emphasized in the penetration and the micro-convection models, result in a dependence of the mass-transfer coefficient on the gas-evolution rate to the 1/2 power. The mass-transfer enhancement resulting from macro-convection generated by the buoyant lift of bubble swarms depends on the gas-evolution rate to the 1/3 power.

4. Experimental

The micro-mosaic electrode used in this study was conceived by Dees and Tobias (1982) in this laboratory and was originally designed in a collaborative effort with the Hewlett-Packard Company. The design was modified for this investigation, and the electrodes were fabricated using integrated-circuit technology at Hewlett-Packard Laboratories, and later at AT&T Bell Laboratories. The electrode is fabricated on a 7.62-cm silicon wafer. The active area, shown in Figure 1, consists of a 5-mm platinum square. The center 1-mm square of the active area comprises a 10 $\times$ 10 array of 98-μm square, platinum segments on 100-μm centers; the remaining part of the active area acts as a "buffer" segment to eliminate edge effects in the center region. An enlargement of the center section is shown in Figure 2. The electrode simulates a continuous surface, but contains one hundred electrically-isolated electrode elements.

The micro-mosaic electrode is housed in a Plexiglas cell along with two platinum counter electrodes and a reference-electrode capillary. A printed-circuit board presses onto the electrode edges to bring out the electrical connections. An o-ring seal between the cell body and the wafer ensures leak-free containment of the electrolyte. A data acquisition system developed by Dees (1983) includes current-to-voltage converters for each of the 112 segments, and a Multiplexer channel scanner which can monitor the current to each of the electrode segments at rates from 1.25 to 10.0 KHz. The data are taken by a Hewlett-Packard 9825T desktop computer, stored on floppy disk, and later transferred to a mainframe. Dees and Tobias (1982, 1987a) give a detailed description of the fabrication of the first

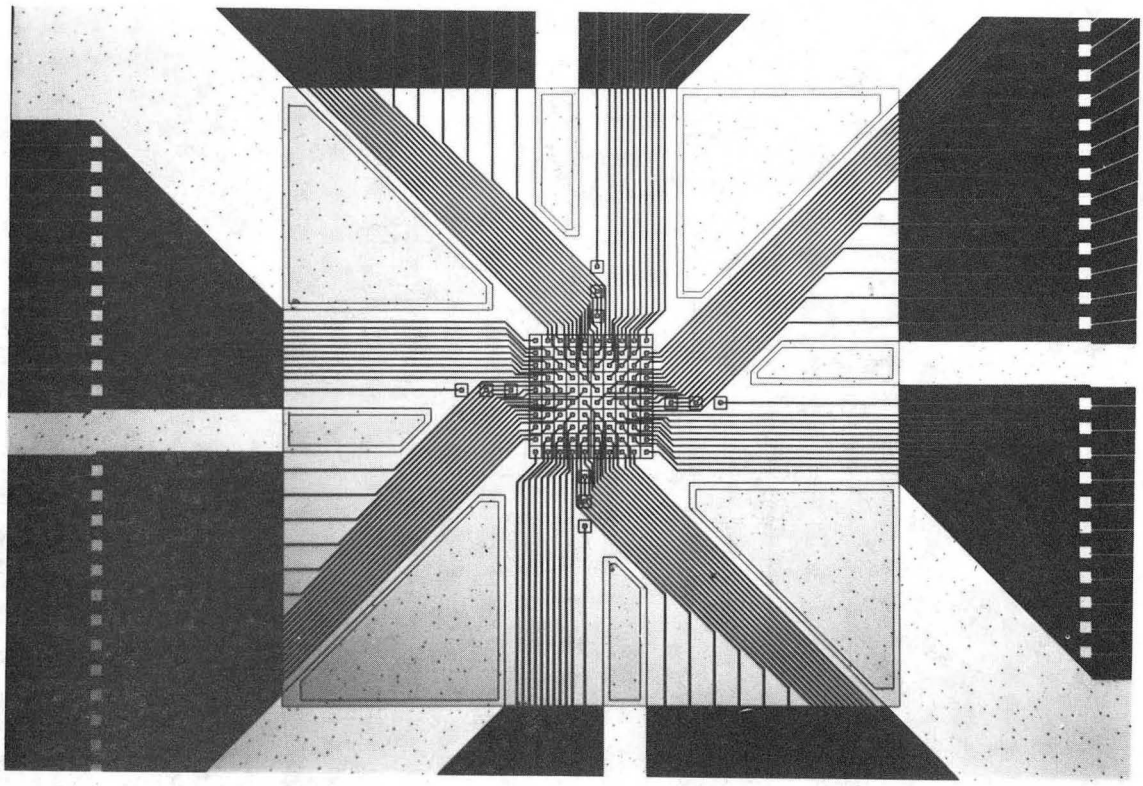

XBB 872-1333

Figure 1. Center 5-mm active area of the micro-mosaic electrode, including both segmented area and surrounding "buffer" section.

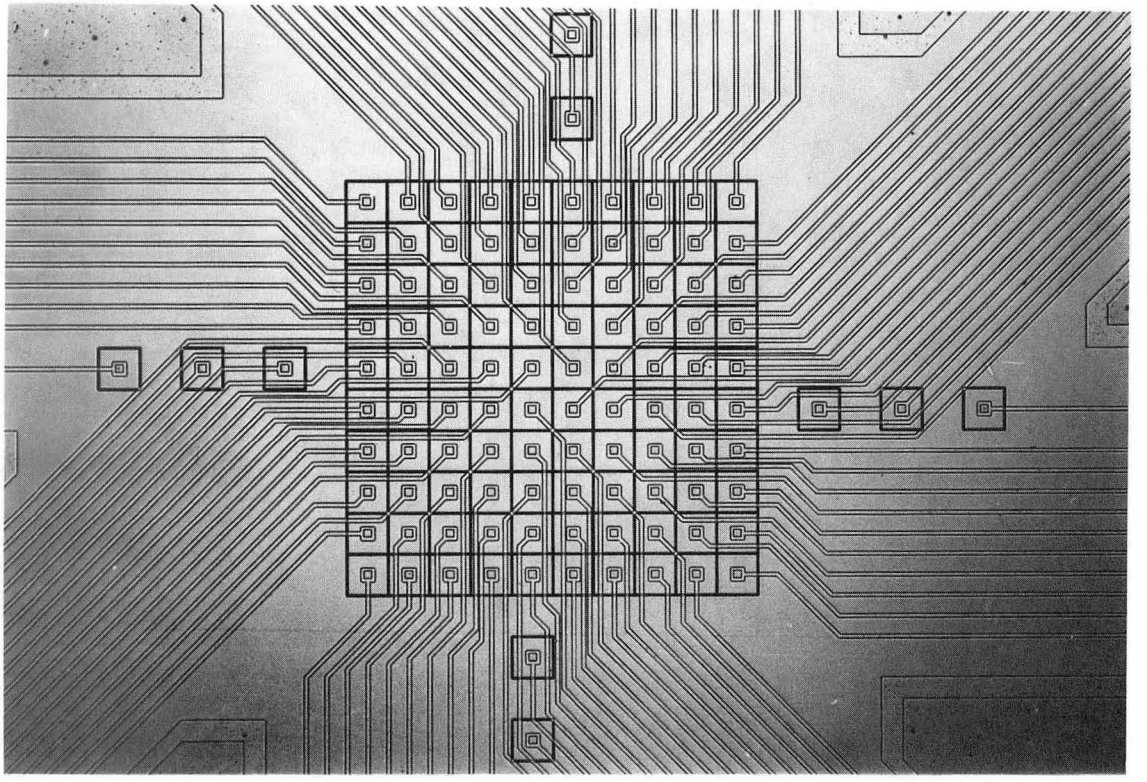

XBB 872-1401

Figure 2. Center segmented portion (1-mm square) of the micro-mosaic electrode.

generation of electrodes and of the data acquisition system. The electrode fabrication steps and materials used in the electrodes built for this study are given in Appendix A.

The working electrode potential is held at a value in the region of limiting current for the reduction of the indicator ion Fe^{+3} to Fe^{+2} from 0.0484-M $Fe_2(SO_4)_3$ in 0.5-M H_2SO_4. A bubble stream can be generated at one of the "satellite" segments in the plane of the micro-mosaic electrode by making the potential at that segment several hundred milivolts more cathodic than the rest of the electrode. The "satellite" segments were used for all of the experiments in which the bubble stream was rising within the mass-transfer boundary layer. An attempt was made in some early experiments to generate bubble streams at the segments in the bottom row of the 10 by 10 array of monitoring electrodes. The back reaction of dissolved hydrogen that was not captured by the bubble was found to overwhelm the indicator-ion reaction in the vicinity of the bubble evolution site. The magnitude of the back reaction of hydrogen was quantified by conducting experiments without addition of the indicator ion. These results are presented in Appendix B.

The experiments in which the bubble stream was generated away from the electrode surface were conducted using a modified cell top, shown in Figure 3. A post extending through the top of the cell (lower right in photo) holds a platinum wire electrode whose position with respect to the micro-mosaic electrode can be adjusted by turning the teflon nut. A Brown and Sharpe dial gauge (lower left) rests on top of the post and allows the measurement of position of the wire electrode with respect to the micro-mosaic to within about 12 μm . The completely-

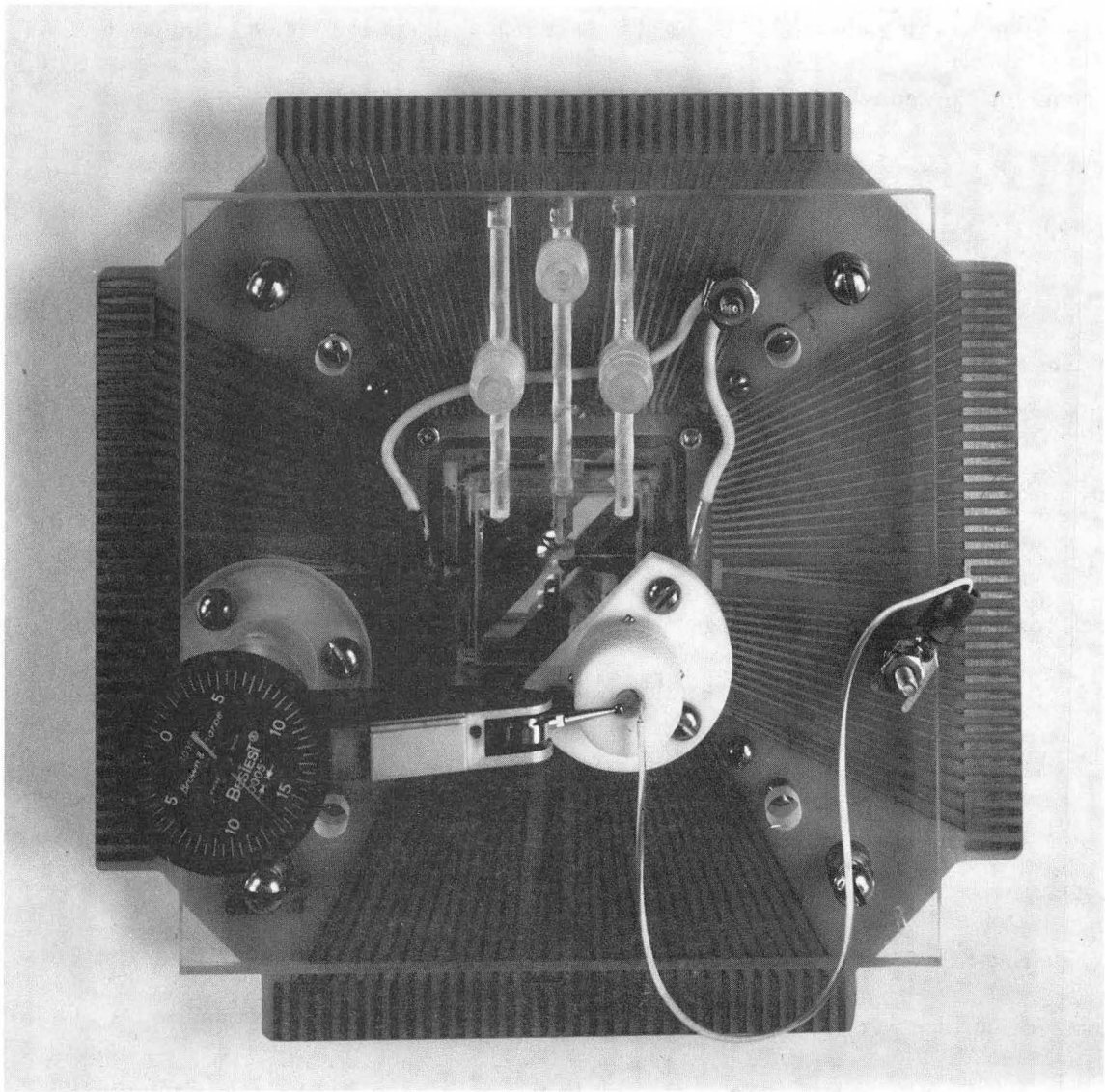

CBB 859-7903

Figure 3. Closeup of assembled cell holding micro-mosaic electrode. Brown and Sharpe dial gauge (lower left) measures position of bubble-generating electrode relative to micro-mosaic electrode.

assembled cell is shown in Figure 4, and the supporting electronics and researcher are shown in figure 5.

During the early experiments, in which the bubble stream was generated away from the electrode surface, the current was found to *decrease* as a result of the rising bubbles for bubble streams generated at 750 μm from the mass-transfer surface. It was determined that the reference-electrode capillary (shown in Figure 3) caused the upward natural convection along the electrode to deflect downward from that point. The reference-electrode capillary was modified so that it did not extend all of the way to the top of the mass-transfer surface. All results presented in this chapter were taken after the cell was modified. Some results from the earlier experiments are presented in Appendix C.

One problem with the type of experiment described here is that the micro-mosaic electrodes cannot withstand attack by the aggressive solutions in which they are immersed for long times. A photographic examination of several electrodes after use indicates that the less noble metal, which is used to enhance the adhesion of the noble electrode material to the insulator, is oxidized by the electrolyte solution. Eventually the noble electrode material can detach completely from the substrate. The results of the photographic examination are presented in Appendix D. A table showing the electrodes used and their operability before and after use is given in Appendix E.

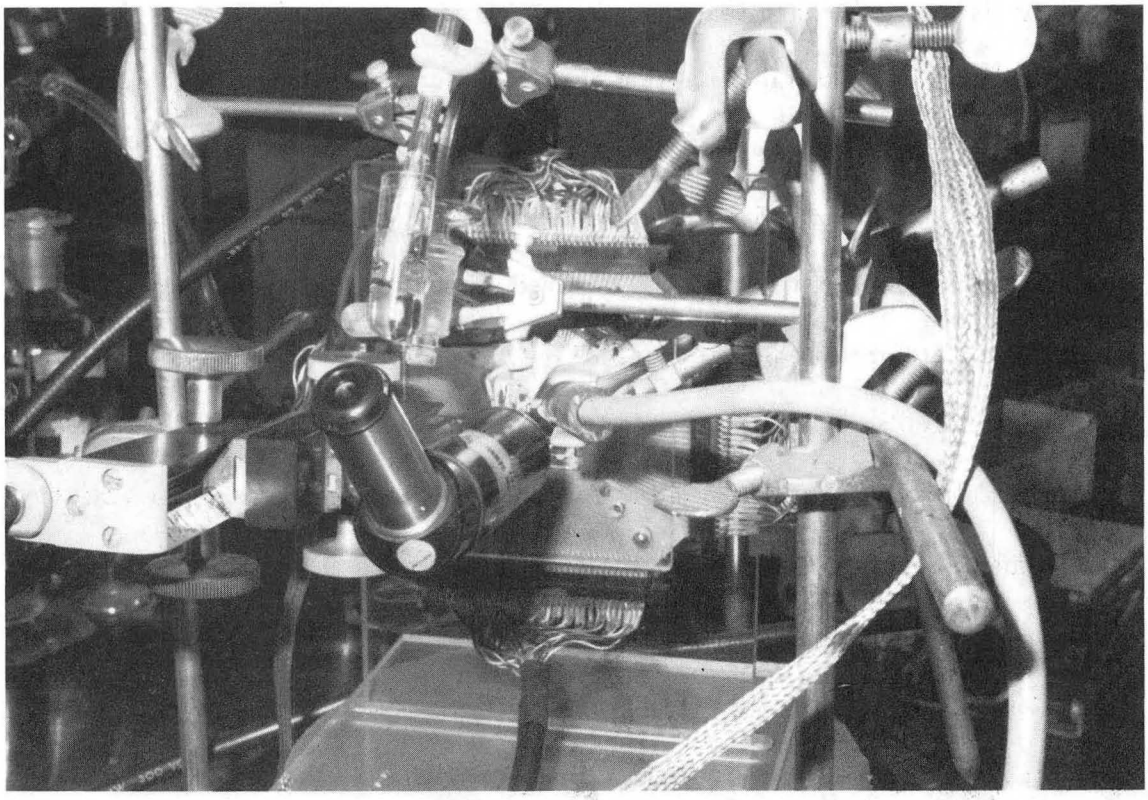

XBC 853-2164

Figure 4. Experimental apparatus for vertical gas-evolution experiments.

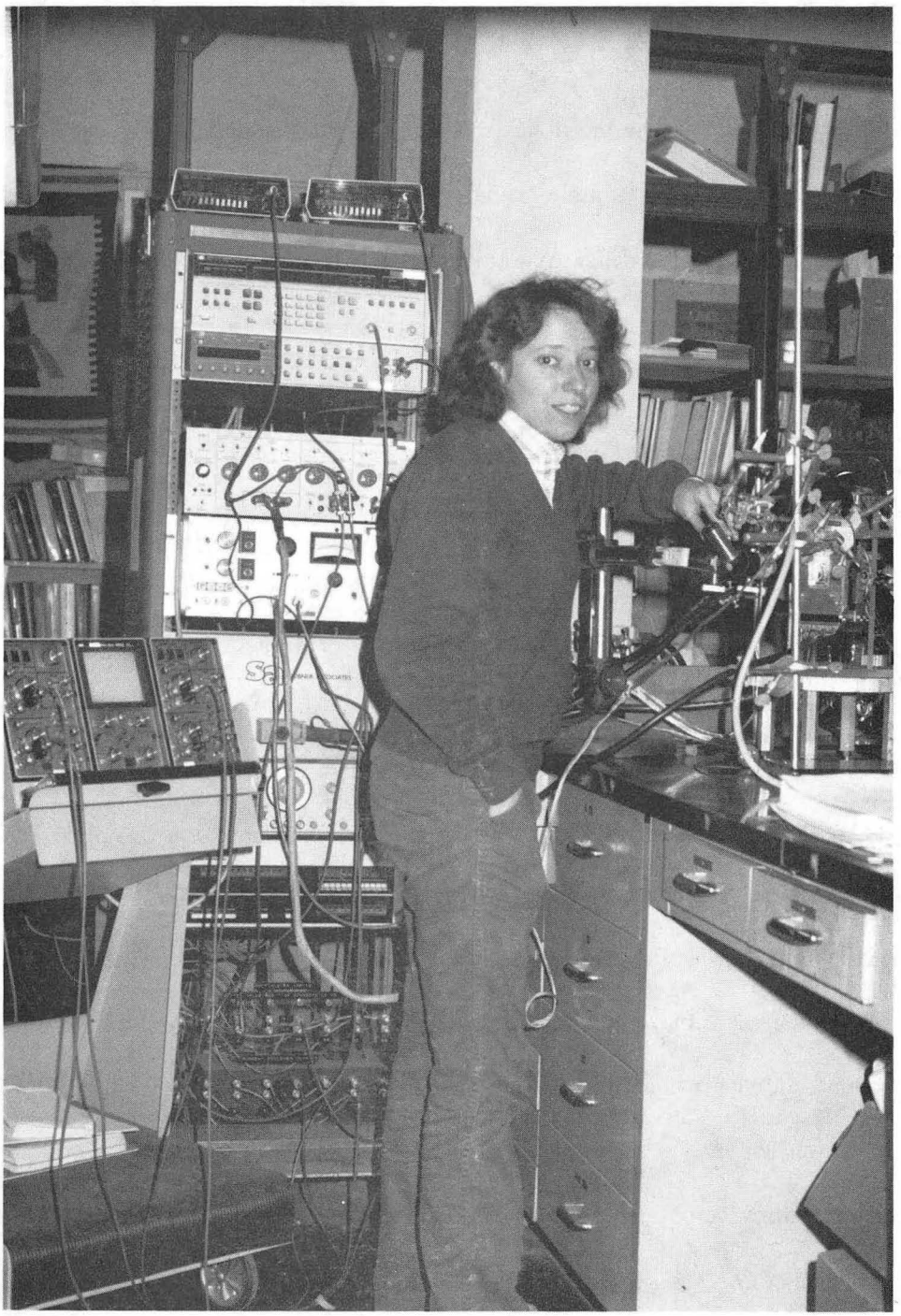

XBC 853-2162

Figure 5. Experimental apparatus with researcher *in situ* for vertical gas-evolution experiments.

5. Results

The modes of mass-transfer enhancement observed for the case of the bubbles rising *within* the mass-transfer boundary layer and for the case of the bubbles rising *outside* the mass-transfer boundary layer are qualitatively distinct and lend themselves to different analyses. In this section and in the Discussion section, the results and analyses for the two cases are presented separately.

5.1. *Bubbles Rising Within the Mass-Transfer Boundary Layer*

Bubbles generated at the plane of the micro-mosaic electrode surface at one of "satellite" segments below the 10 × 10 array of monitoring electrodes are typically 45 to 100 μm in diameter at the time of detachment. High-speed cinematography reveals that, upon leaving the growth site, a bubble slides along the electrode for a distance corresponding to several bubble diameters, and then separates from the electrode and rises at a constant separation of approximately one bubble radius. Thus the bubbles rise entirely within the free-convection mass-transfer boundary layer (approximately 200 μm in thickness), established by the indicator ion reaction. Figure 6 shows how these high-speed movies were taken. A micro-mosaic electrode was cut, and the center section mounted onto a Plexiglas strip which fits into a viewing cell. Contacts from the bonding pads at the edge of the electrode were connected with conductive silver epoxy to screws in the Plexiglas. One of the connected segments was used to generate a stream of hydrogen bubbles, and the other segments and the buffer section were polarized as they would be in a mass-transfer experiment. Figure 7 is taken from a high-speed movie of H_2

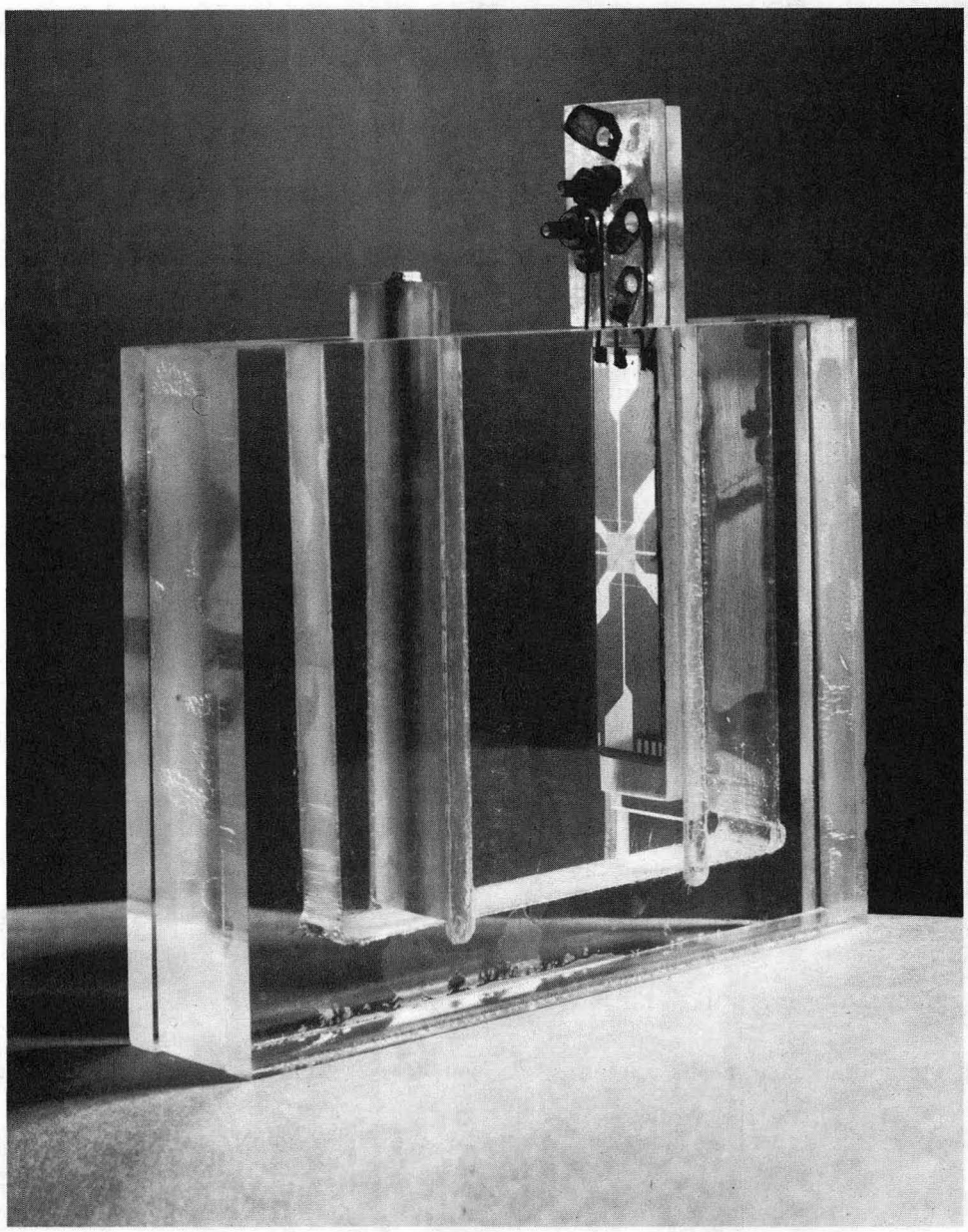

CBB 874-2835

Figure 6. Strip from micro-mosaic electrode and viewing cell, used for making high-speed motion pictures of bubbles rising along the micro-mosaic electrode.

evolution in this cell. The detached bubbles are 100 μm in diameter. The smallest bubble, approximately 30 μm in diameter, is still attached at the growth site. The bubble immediately above it is sliding along the electrode, and the uppermost bubble is rising at a separation of roughly 30 μm .

Figure 8 is a photograph taken during an experiment that uses the entire micro-mosaic electrode. A stream of 60-μm -diameter bubbles is generated by an 8.5-μA current at the lowest of the satellite segments below the array of monitoring electrodes. Figure 9 shows the current response of one of the monitoring segments directly in the path of the bubble stream. Time zero is the start of data acquisition; the transport processes are presumably in a steady, possibly periodic, state before this. The currents to two segments located at the same height, but 100 and 500 μm to the side, respectively, are also shown. One can see that the average mass-transfer rate to the segments close to the bubble path is enhanced by a factor of approximately 1.5. The frequency of the oscillations corresponds to the frequency of bubble evolution. The oscillatory behavior may be attributed at least in part to the increased mass-transfer rate immediately after the bubble has passed over the segment, trailing bulk fluid in its wake. The question arises as to whether the periodic decrease in the current is caused in part by the bubble directly over the segment blocking the field, or entirely by the decrease of mass transport. One way to determine this experimentally would be to conduct the same experiment at an applied overpotential well below that required for limiting current. Another would be to capture the transient behavior when the last bubble in a series passes by the electrode. These experiments were not performed. However, it is instructive to compare the current to a segment that is directly in the path of the bubble stream

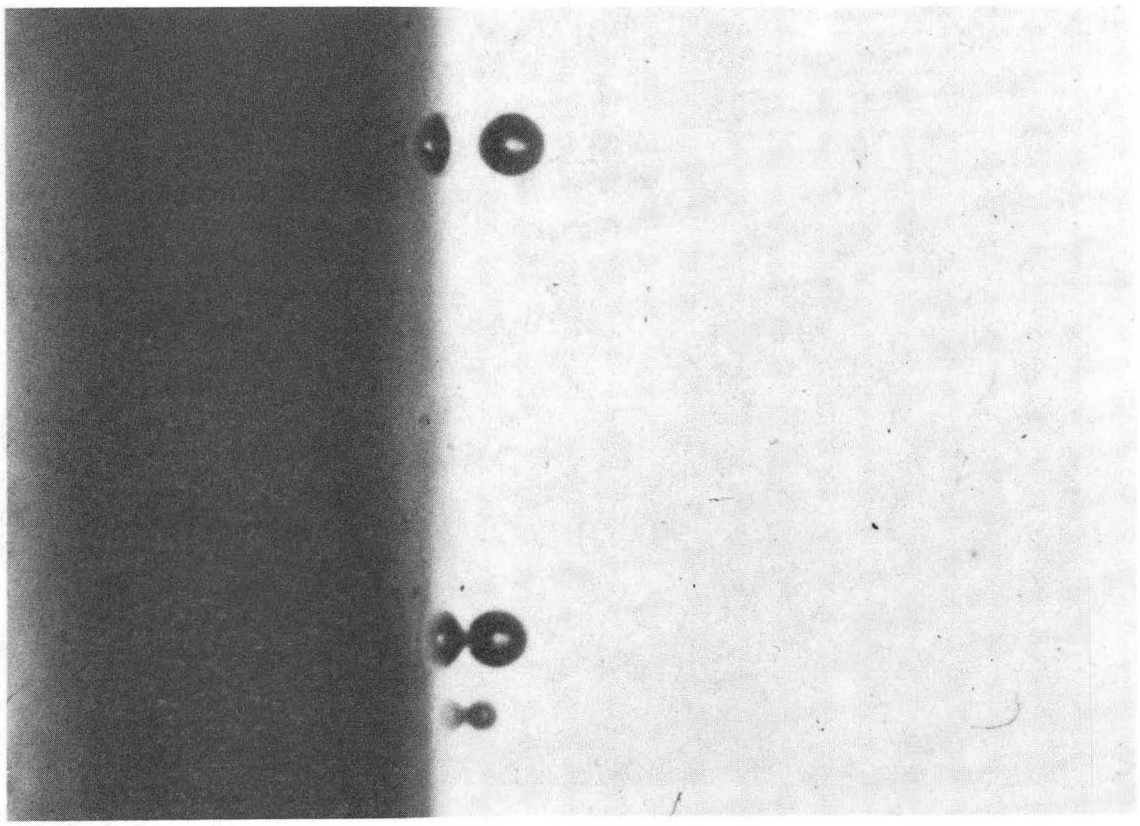

XBB 874-2789A

Figure 7. Frame from a high-speed movie of bubbles rising along micro-mosaic strip electrode. Frame is 1.4 mm wide and 1.1 mm high.

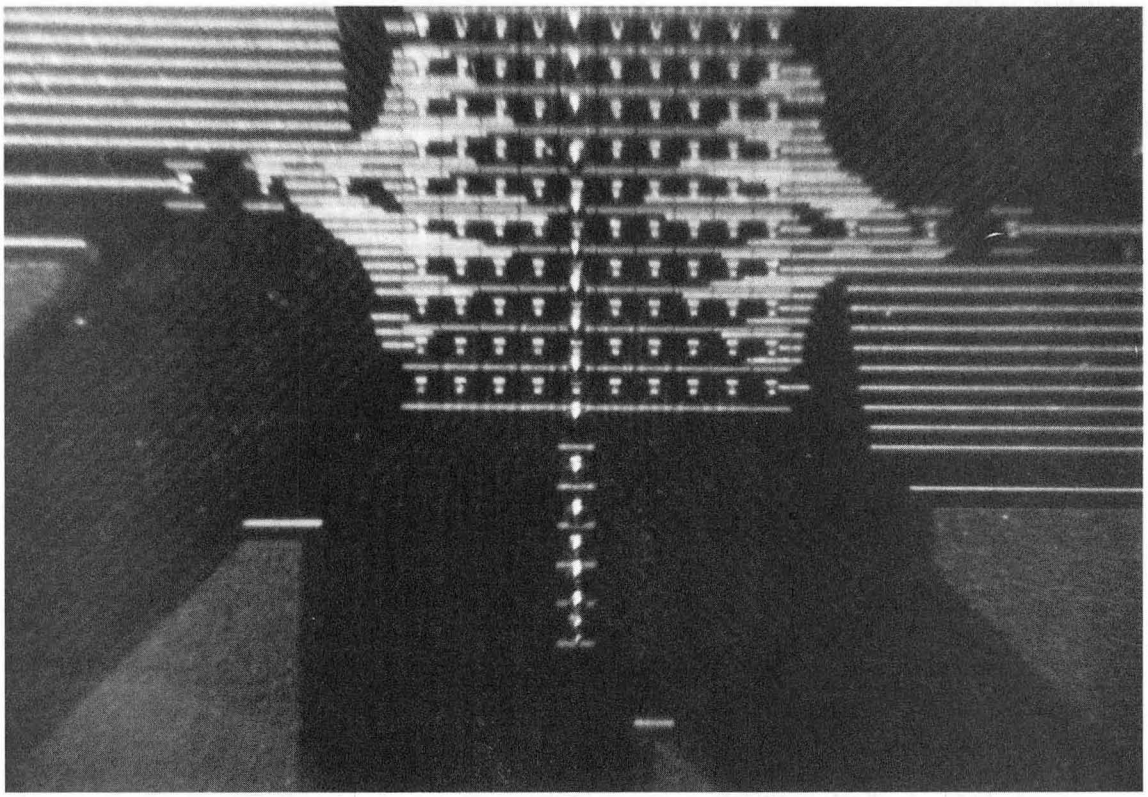

XBC 853-2187

Figure 8. Photograph taken during a mass-transfer experiment showing 60-μm diameter bubbles rising along micro-mosaic electrode.

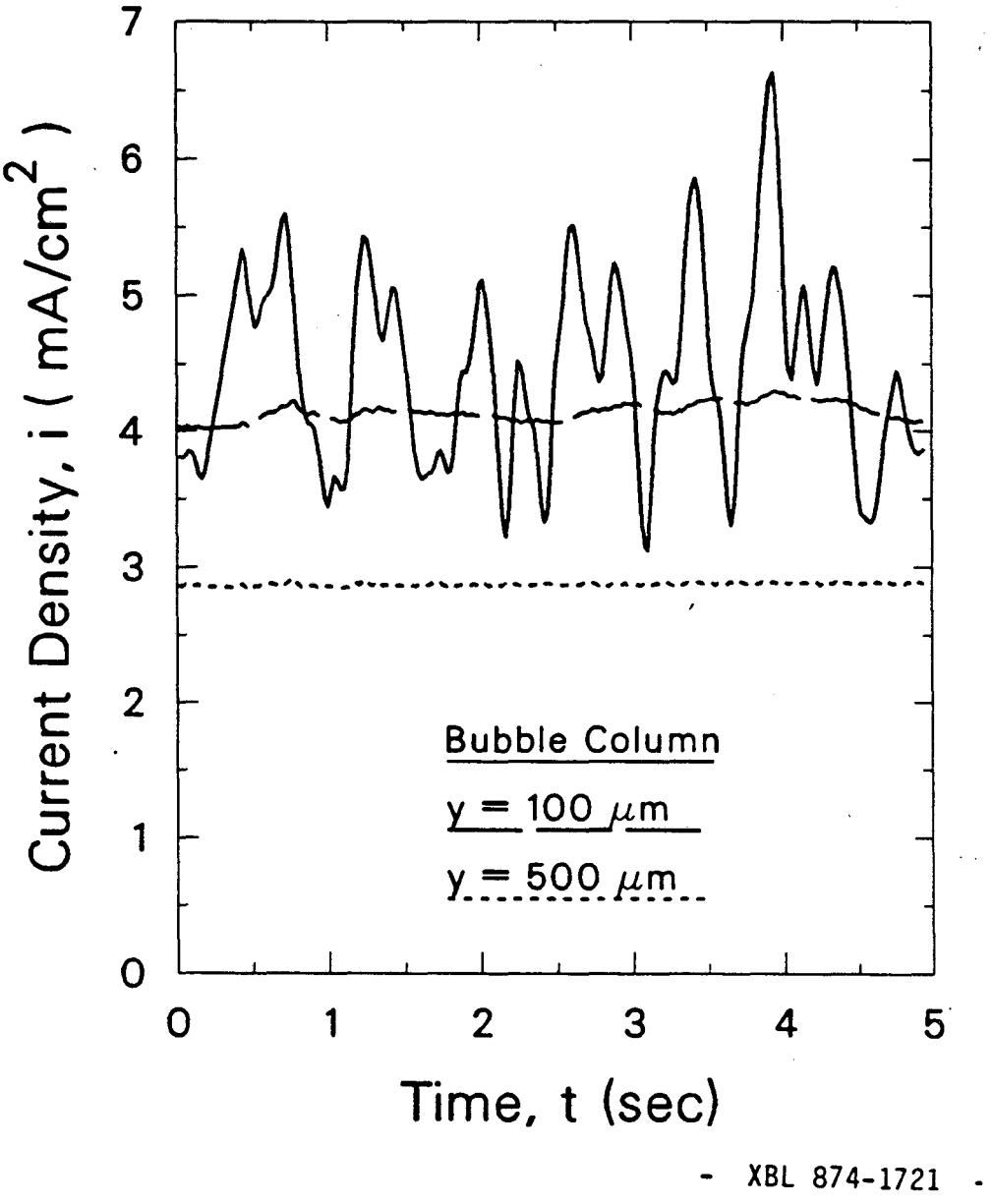

Figure 9. Current to three segments showing effect of 60-μm diameter H_2 bubbles rising within the mass-transfer boundary layer generated by an 8.5-μA current. The three segments are 1) directly in the bubble path and 2) 100 and 3) 500 μm to the side.

to that for a segment in the adjacent column. The segment 100 μm to the side would presumably experience an enhanced mass-transfer, but suffer no ohmic obstruction from the passing bubbles. The corresponding curve, shown in Figure 9, exhibits almost no oscillatory behavior, but the average value is nearly the same as that for the segment directly in the path. Evidently, the field-obstruction effect does contribute to the periodic behavior.

The spatial variation of the mass-transfer enhancement due to the rising bubble streams can be seen by comparing the curves in Figure 9; one can see that at least two columns receive enhanced mass transfer due to the rising bubbles. The edge column is unaffected by the bubble stream. Figure 10 shows the spatial distribution of mass-transfer rate for the matrix of monitoring electrodes averaged over the 5-second duration of the run. The site of bubble evolution is behind the monitoring electrodes in the figure and the bubbles rise toward the viewer, as indicated by the arrow. Figures 9 and 10 show that the mass-transfer enhancement is fairly localized, affecting an area approximately four columns, or seven bubble diameters, in width. The end columns are unaffected by the rising bubbles; the current to the end columns is approximately 0.25 μA per segment, which corresponds to 2.5 mA /cm ^{2} or a mass-transfer coefficient of 2.5 cm/s. This is the value of the background natural-convection current, generated by the redox reaction itself.

An example showing the magnitude of the mass-transfer effect is given in Figure 11, in which the current to one segment from the column closest to the bubble path is plotted as a function of time for several experiments with different bubble evolution rates. As expected, the mass-transfer rate increases with the

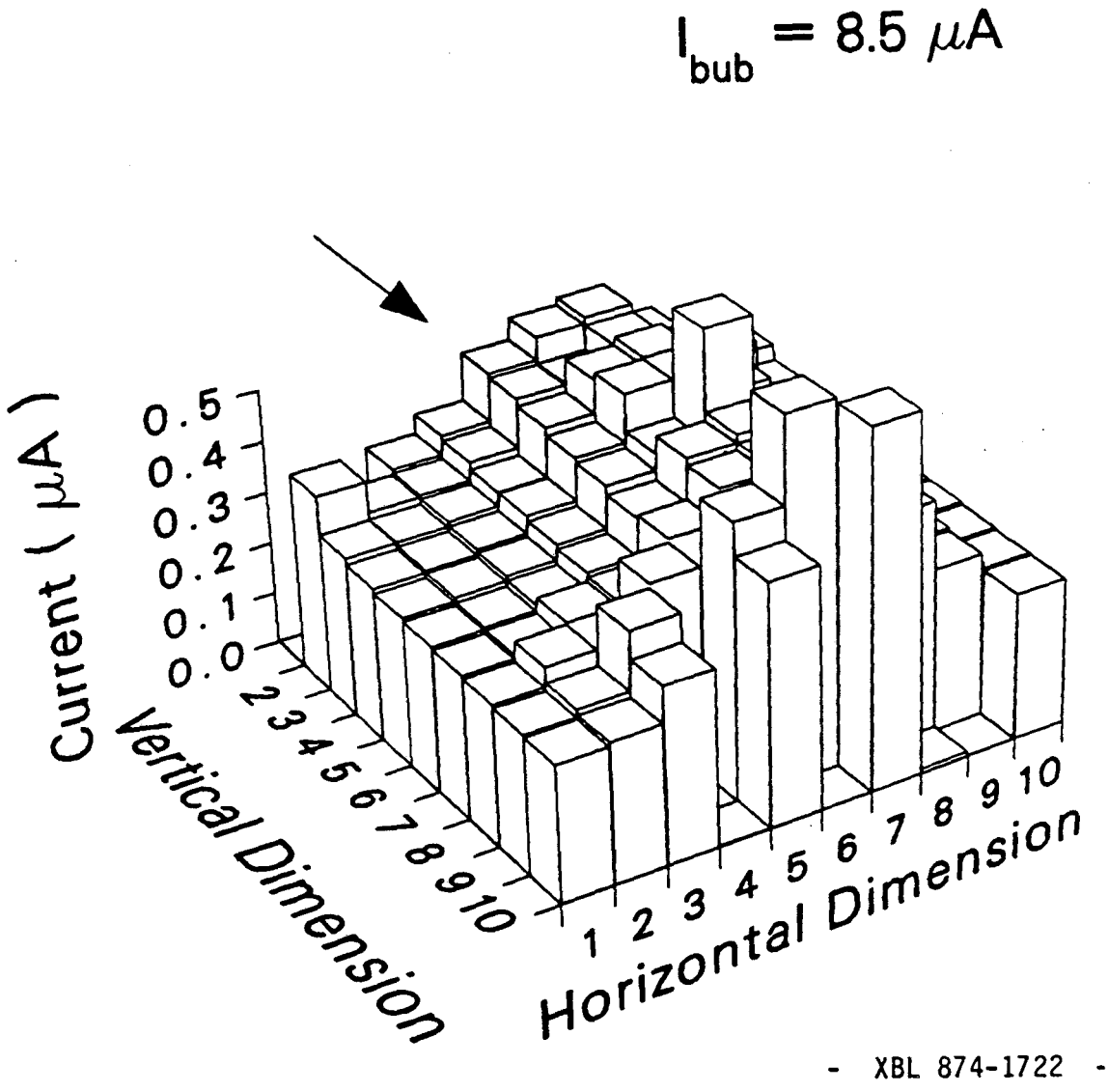

Figure 10. Spatial distribution of mass-transfer rate enhanced by 60-μm H_2 bubbles generated by an 8.5-μA current and rising within the mass-transfer boundary layer.

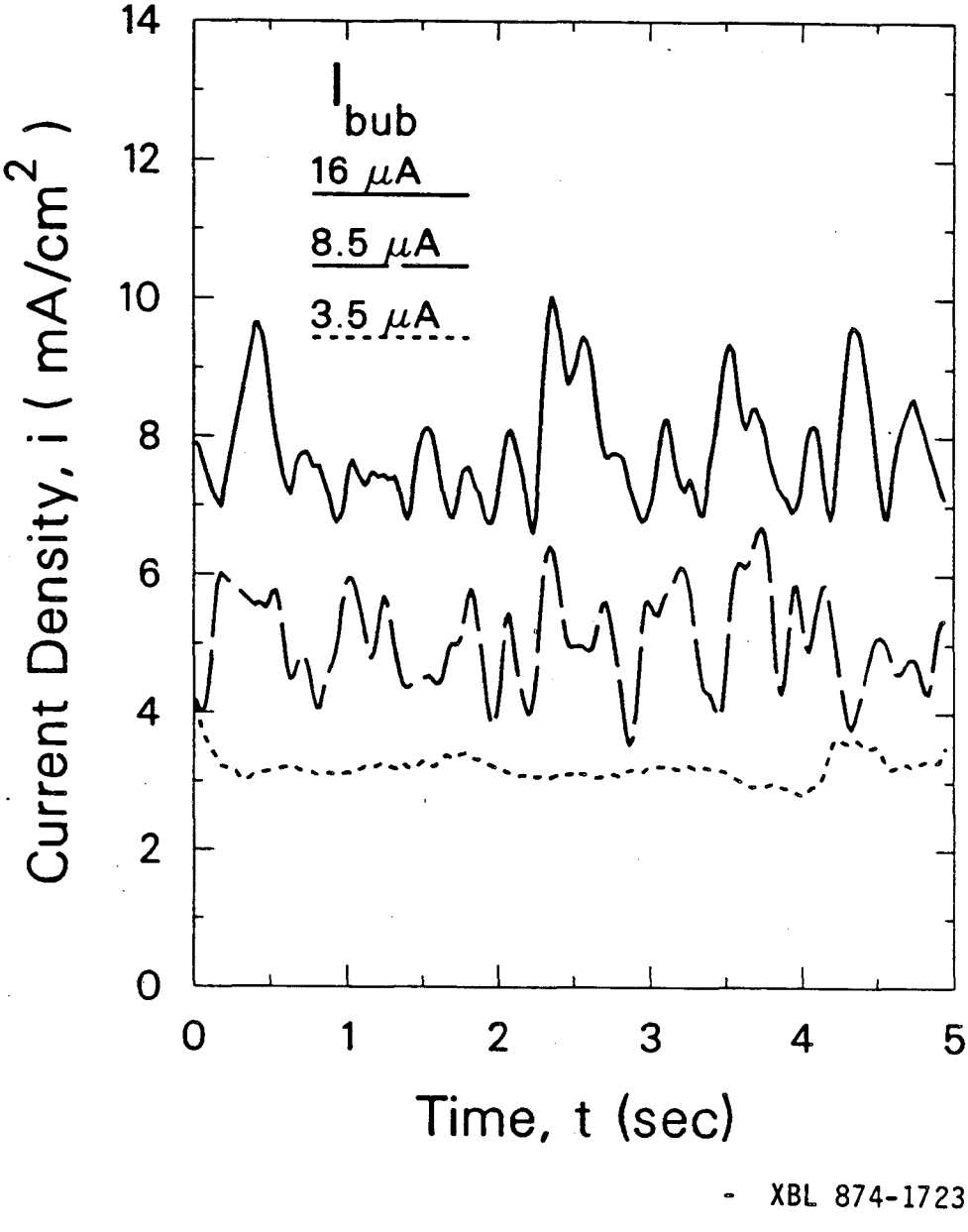

Figure 11. Transient mass-transfer to a segment in the column closest to the bubble stream for bubble evolution rates of 16, 8.5, and 3.5 μA.

bubble evolution frequency. The spatial distributions of the mass-transfer rate for 3.5- and 16-μA bubble streams can be seen in Figures 12 and 13. As the bubble evolution rate is increased, the mass-transfer rate to the segments within 200 μm of the bubble path is increased, but the current to the edge columns remains unaffected at the value of the background natural-convection current. As will be seen in the next section, these results are in good agreement with those provided by the surface-renewal theory of mass-transfer enhancement.

5.2. *Bubbles Rising Outside the Mass-Transfer Boundary Layer*

For the case of bubbles rising outside the mass-transfer boundary layer, the transient response of the monitoring electrodes is much more steady in time than for the case of bubbles rising very close to the electrode. Figure 14 shows the transient mass transfer to one segment, again closest to the path of the rising bubble stream, as a result of 30-μA bubble streams rising 200, 300 and 450 μm away from the electrode. One can see that the magnitude of the mass-transfer enhancement is strongly dependent on bubble-stream position. The oscillations in the mass-transfer rate due to the passing of individual bubbles are virtually absent when the bubble stream is 300 μm from the electrode or beyond.

Figures 15, 16, 17, and 18 show the time-averaged mass-transfer distributions for this same series of experiments, in which the distance between the bubble evolution site and the electrode is varied from 200 to 750 μm . The magnitude of the enhanced mass transfer decreases with increasing distance from the electrode. Note, however, that the currents to the edge columns are considerably higher than the background natural-convection current of 0.25 μA. Even at the greatest

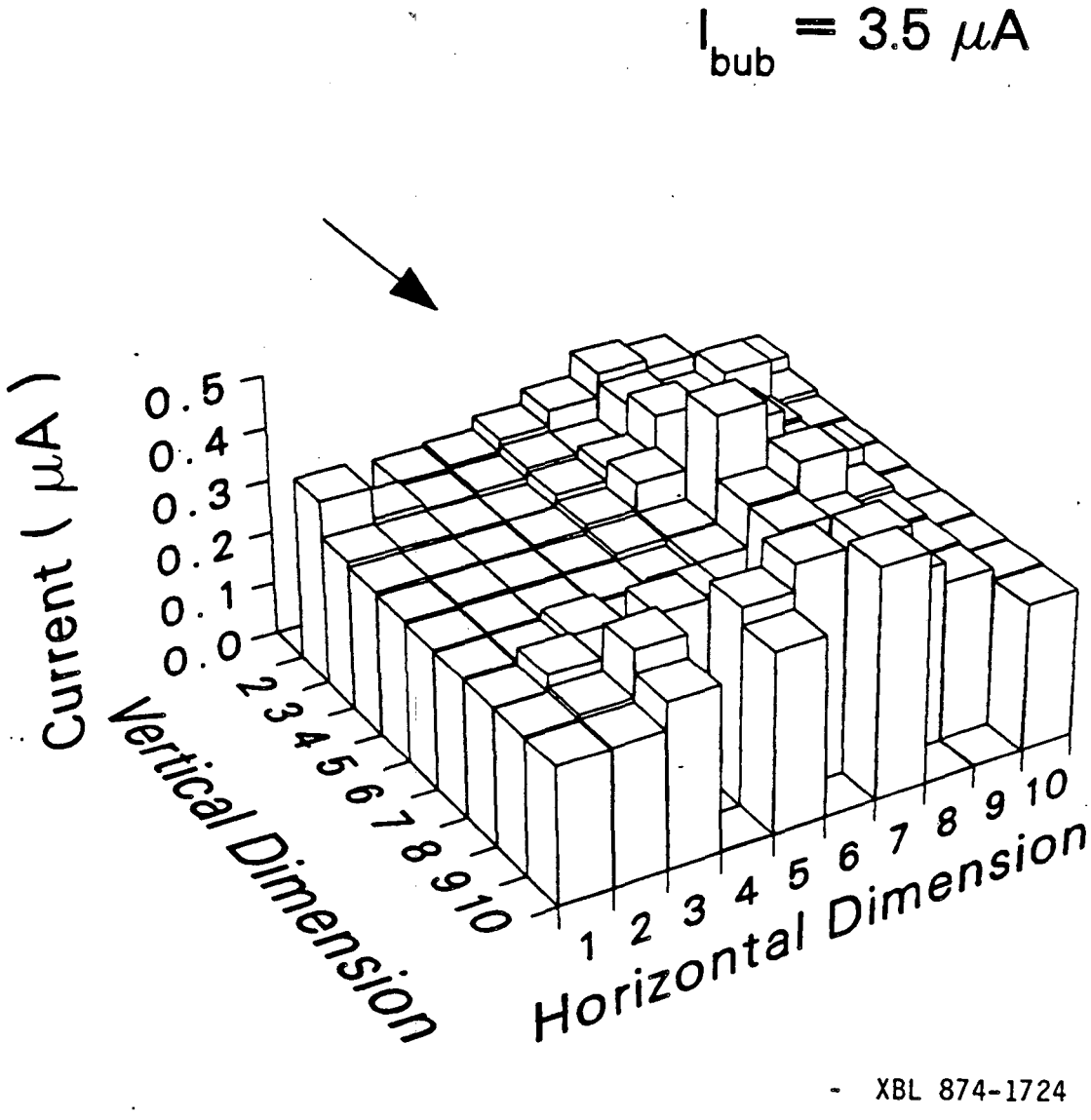

Figure 12. Spatial distribution of mass-transfer rate enhanced by 50-μm H_2 bubbles generated by a 3.5-μA current and rising within the mass-transfer boundary layer.

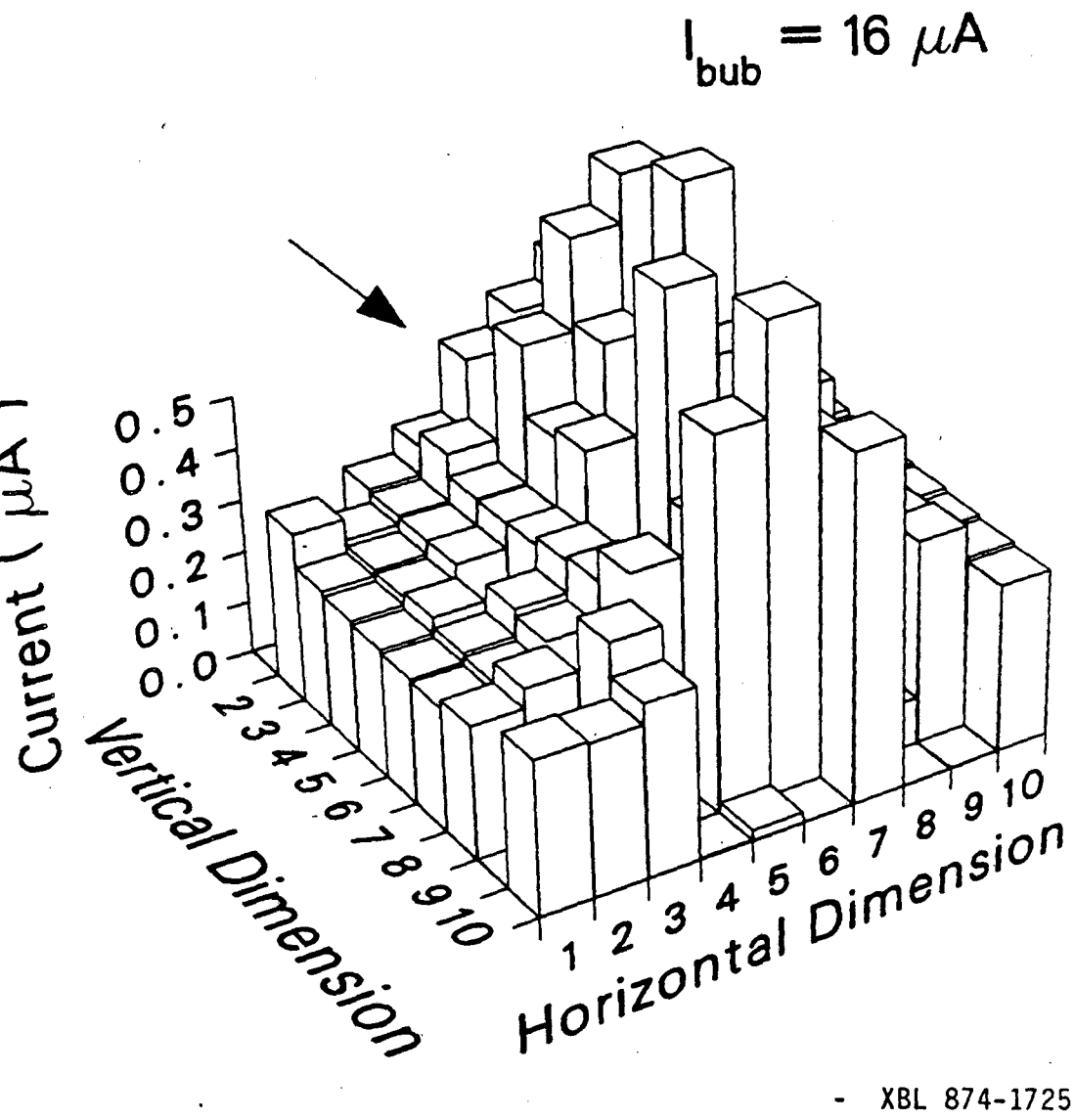

Figure 13. Spatial distribution of mass-transfer rate enhanced by 75-μm H_2 bubbles generated by a 16-μA current and rising within the mass-transfer boundary layer.

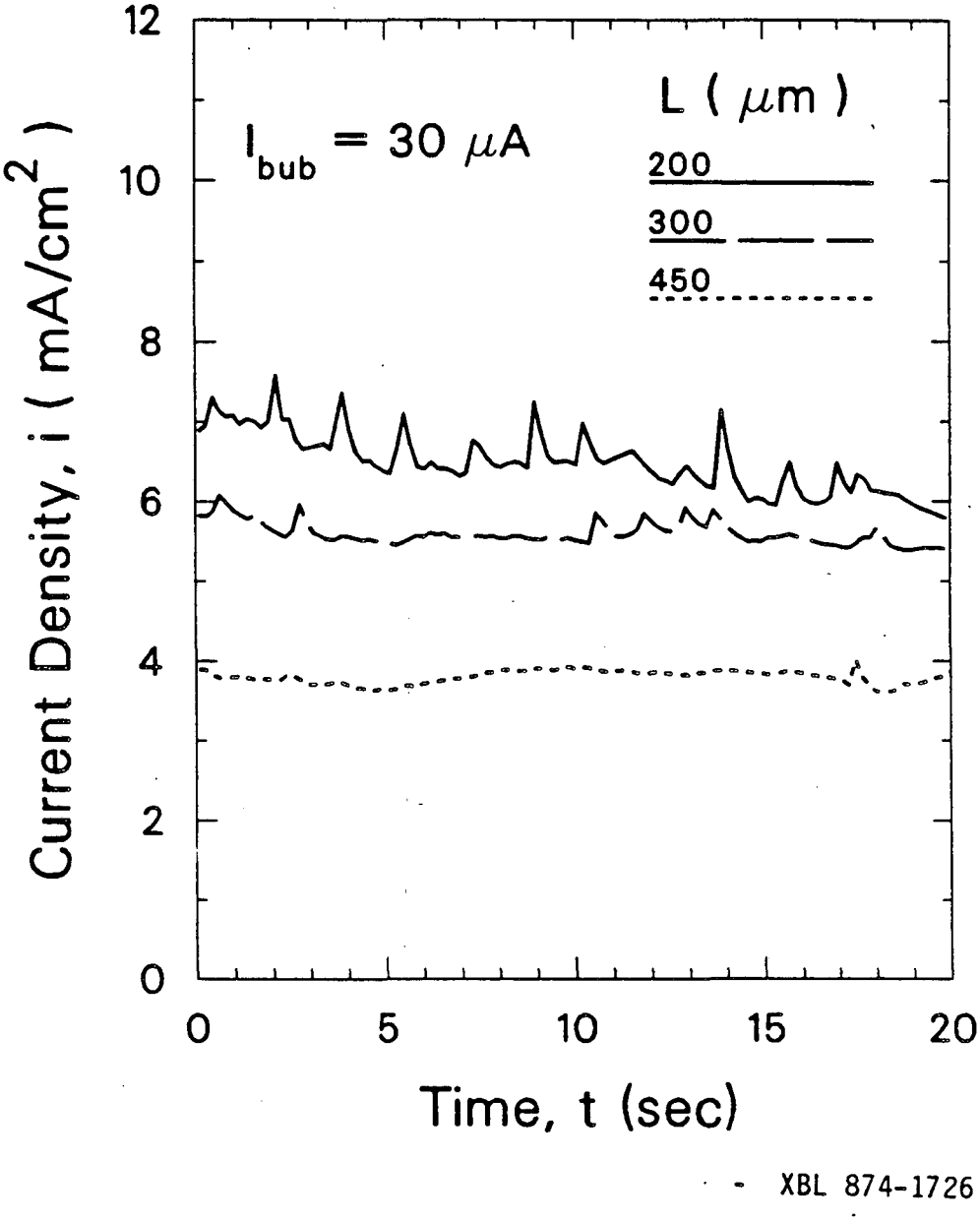

Figure 14. Transient mass-transfer to a segment in the column directly behind the bubble stream for a bubble evolution rate of 30 μA, and bubble stream positions of 200, 300 and 450 μm .

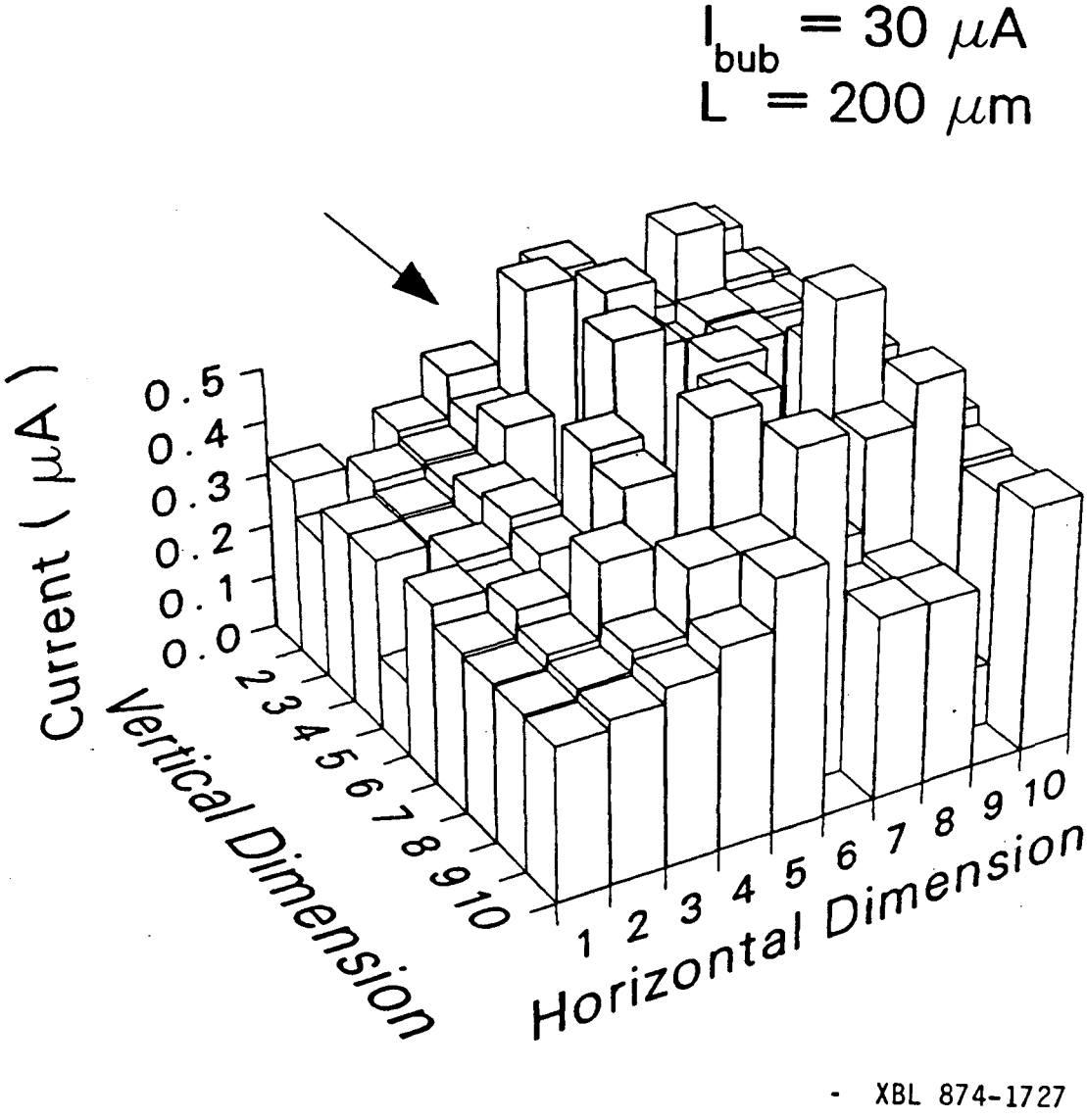

Figure 15. Spatial distribution of mass-transfer rate enhanced by 100-μm H_2 bubbles generated by a 30-μA current at 200 μm from the electrode surface.

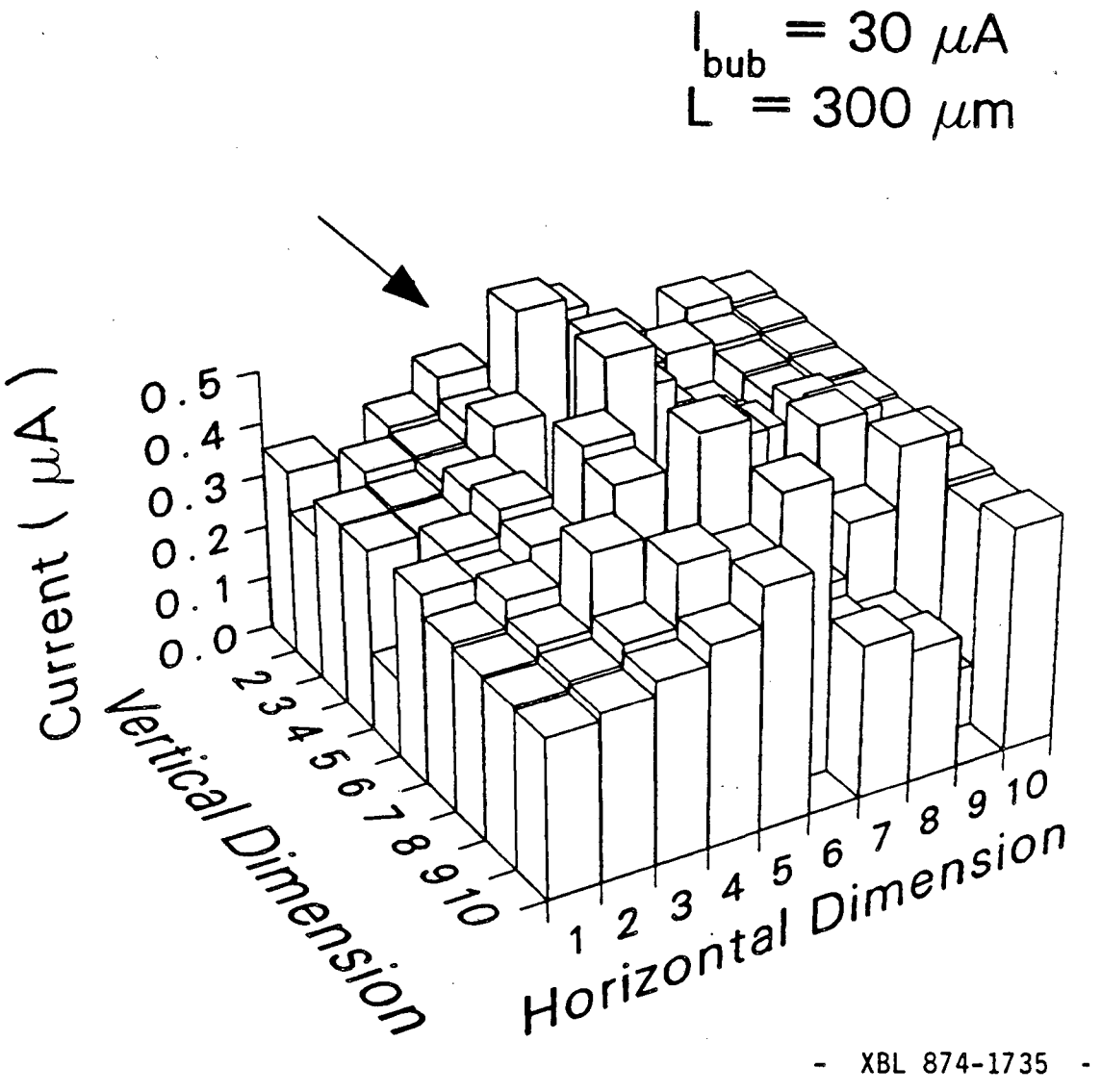

Figure 16. Spatial distribution of mass-transfer rate enhanced by 100-μm H_2 bubbles generated by a 30-μA current at 300 μm from the electrode surface.

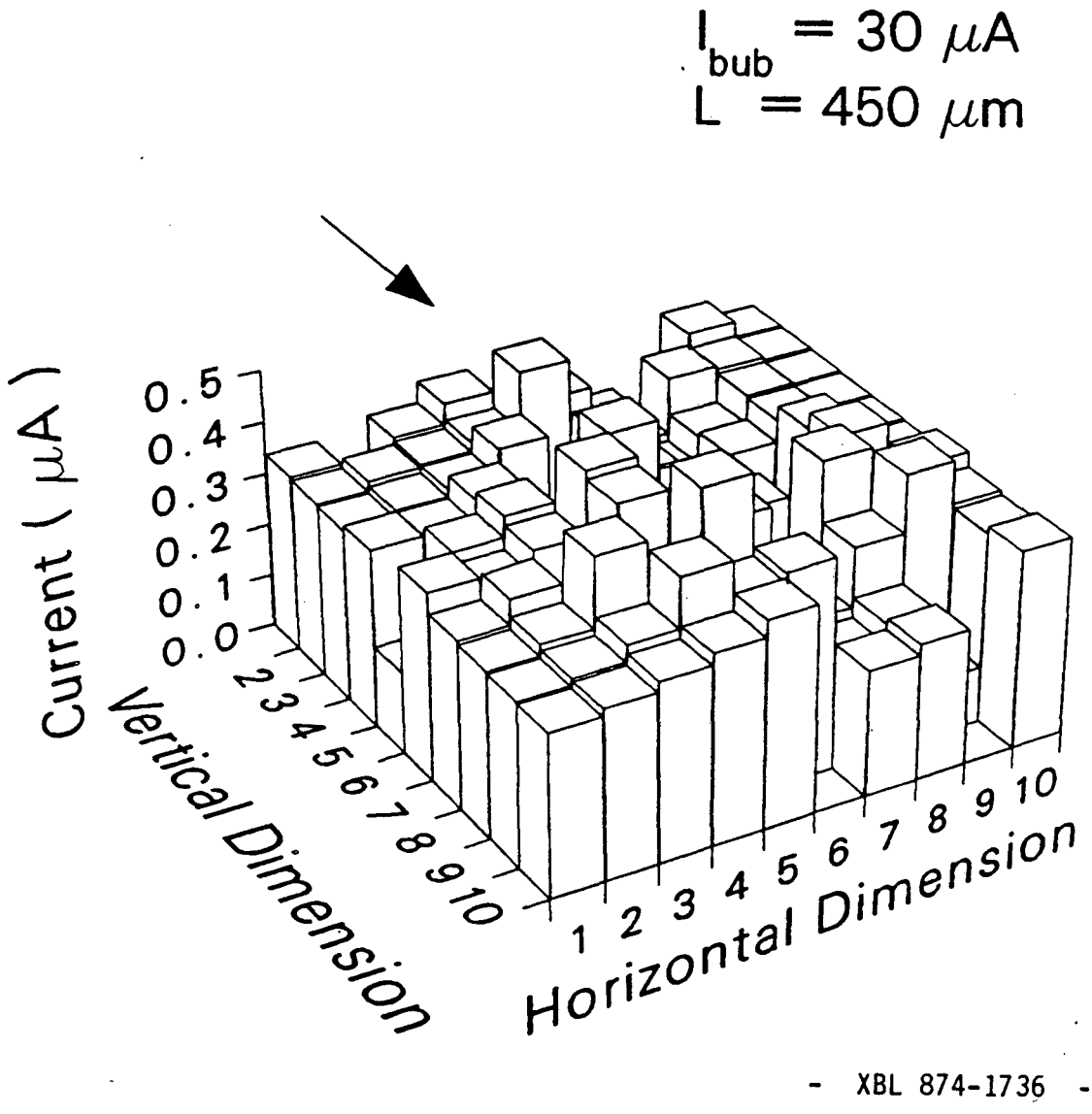

Figure 17. Spatial distribution of mass-transfer rate enhanced by 100-μm H_2 bubbles generated by a 30-μA current at 450 μm from the electrode surface.

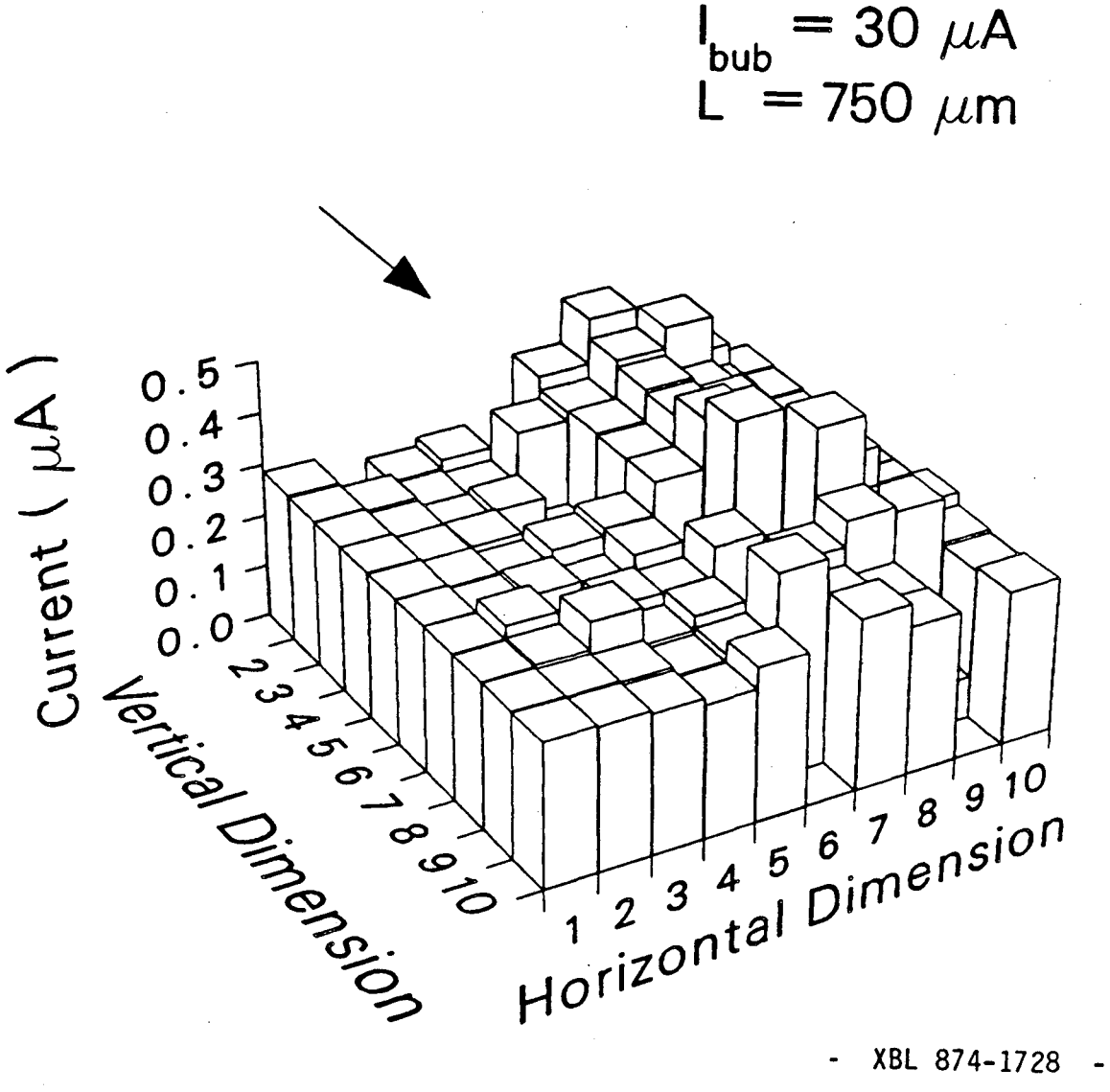

Figure 18. Spatial distribution of mass-transfer rate enhanced by 100-μm H_2 bubbles generated by a 30-μA current at 750 μm from the electrode surface.

distance of 750 μm (Figure 18), at which the current distribution is fairly flat, the average current is considerably higher than the background natural-convection current, even at the the edge of the segmented area. The enhancement from bubble streams rising outside the mass-transfer boundary layer is significant, steady, and less localized than that from bubble streams rising within the mass-transfer boundary layer.

The mass-transfer rate averaged over the 1 $\times$ 1 mm segmented area of the electrode and over the 20-second duration of data acquisition is plotted as a function of bubble evolution rate in Figure 19 and as a function of distance in Figure 20.

6. Analysis and Discussion

6.1. *Bubbles Rising Within the Mass-Transfer Boundary Layer*

Bubble streams rising within the mass-transfer boundary layer result in fluctuating, localized mass-transfer enhancement to the electrode surface. In light of this, we wish to examine our results in the context of a surface-renewal theory of mass-transfer enhancement. We first present a general derivation for surface renewal at vertical gas-evolving electrodes, and then consider the special case of a single bubble stream originating from one position on the electrode.

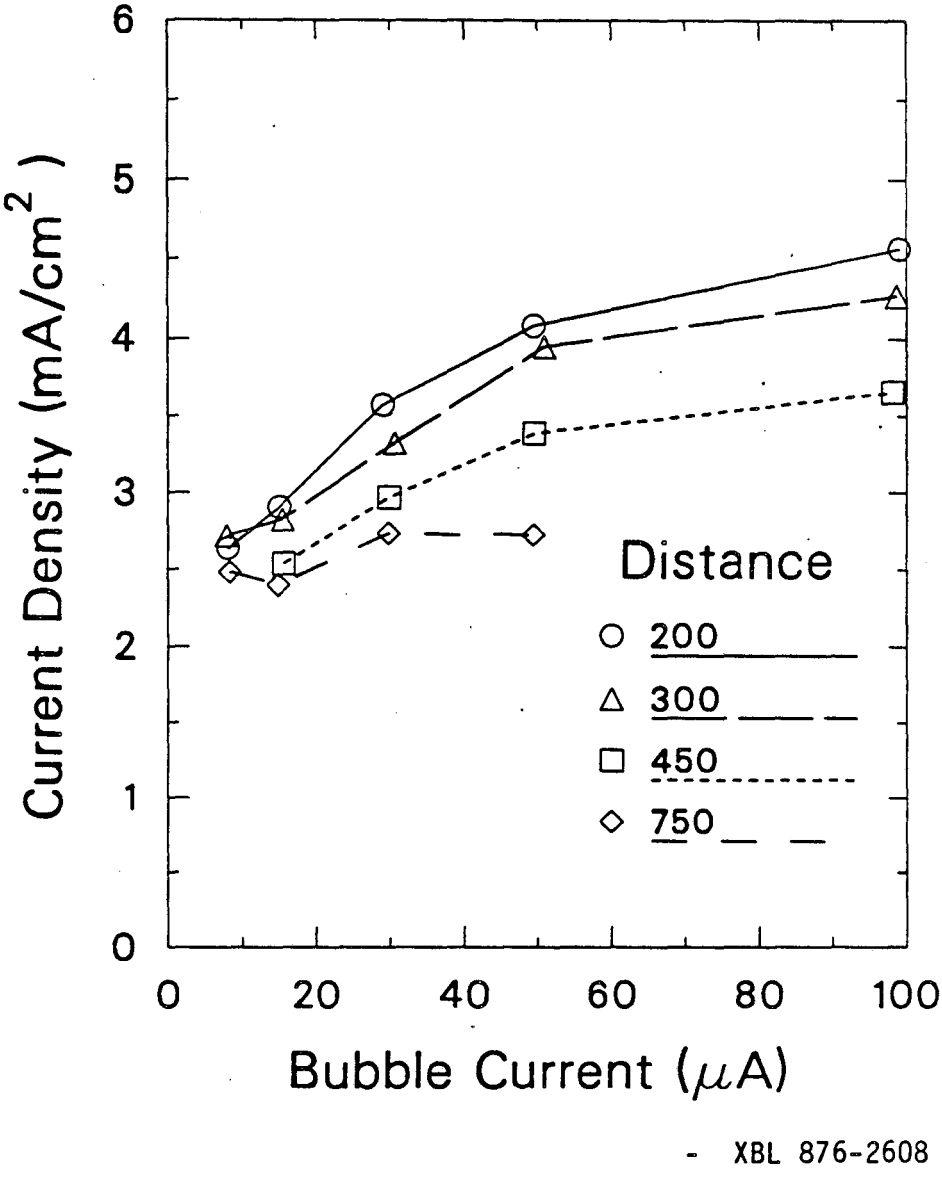

Figure 19. Mass-transfer rate, averaged over the area of the segmented portion of the electrode and over the time of data acquisition, as a function of bubble evolution rate.

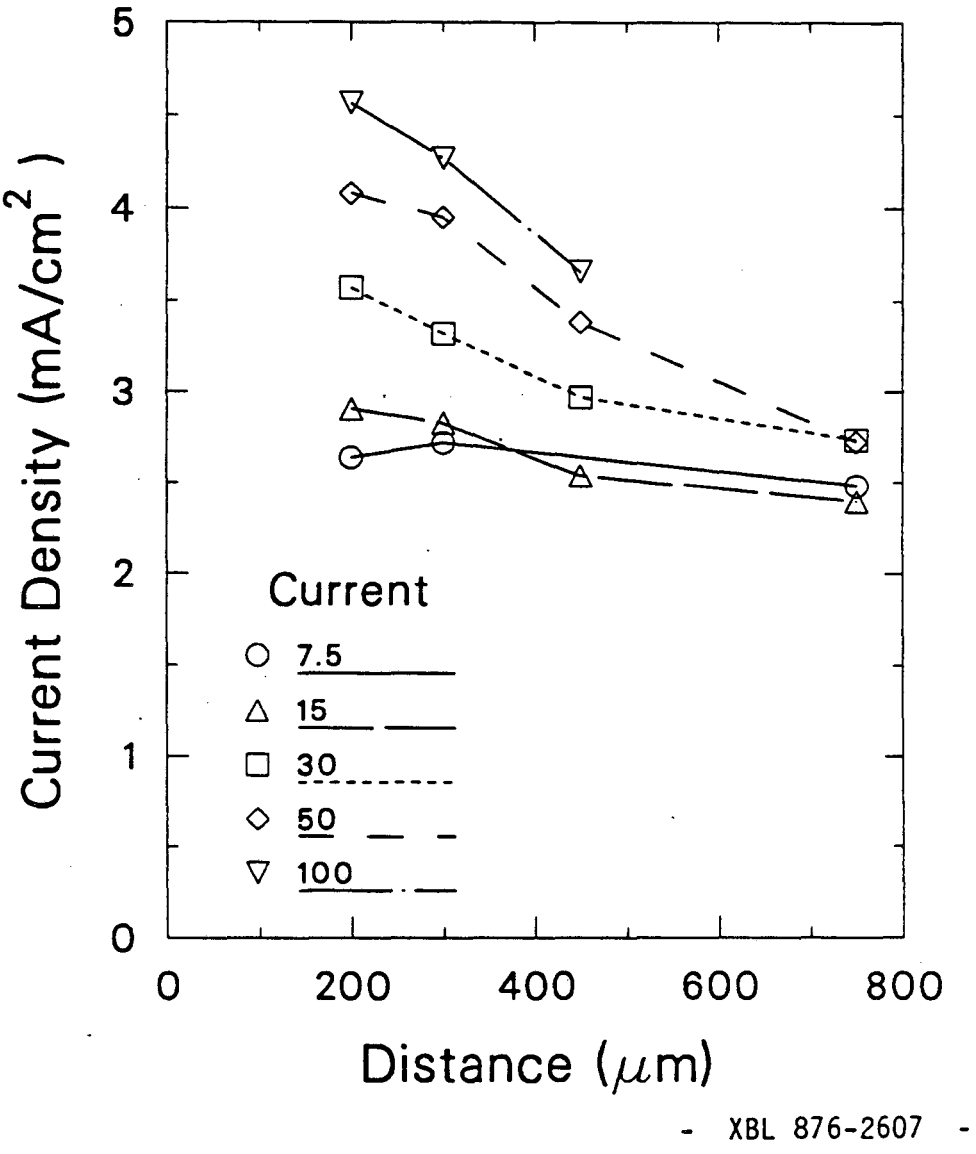

Figure 20. Average mass-transfer rate to the segmented portion of the electrode as a function of bubble-stream position.

6.1.1. *Surface Renewal at Vertical Gas-Evolving Electrodes*

Consider streams of bubbles of radius R_b rising upward along the electrode surface and sweeping a renewal path of width $2R_b$. From the time a bubble crosses a horizontal line at vertical position z, until the next bubble arrives, the current density at z falls according to the Cottrell (1903) equation for transient one-dimensional diffusion in a stagnant medium,

$$N = c_i^{\infty} \sqrt{\frac{D_i}{\pi t}} \quad . \tag{15}$$

The average flux over the surface of the electrode is N averaged over the electrode area and over the time between surface renewals. We will follow the description by Danckwerts (1951) in considering a distribution of surface ages. Let $\phi(t)dt$ be the fraction of surface area that is of a surface age, or time since last being renewed, between t and $t + dt$. Let s be the mean rate of fractional surface renewal, assumed constant in time, but possibly a function of position. The fraction of surface with surface age between t and $t + dt$ is equal to that with surface age between $t - dt$ and t minus the fraction renewed in time dt.

$$\phi(t)dt = \phi(t - dt)dt - \phi(t - dt)dt \cdot sdt \quad . \tag{16}$$

Dividing by dt and taking the limit as $dt \rightarrow 0$ gives

$$\frac{d\phi}{dt} = -s\phi \quad . \tag{17}$$

Integrating Eq. (17) with the condition that $\int_0^{\infty} \phi(t)dt = 1$ gives

$$\phi(t) = se^{-st} \quad . \tag{18}$$

The average flux over time is the integral of the transient flux times the fraction of

surface with surface age t.

$$\overline{N} = \int_0^\infty N(t)\,\phi(t)dt \tag{19}$$

$$\overline{N} = \int_0^\infty N(t)\,se^{-st}\,dt = c_i{}^\infty\sqrt{\frac{D_i}{\pi t}}\,se^{-st}\,dt \quad . \tag{20}$$

For the case of gas evolution at a vertical electrode, the mean rate of surface renewal by bubbles rising along the electrode is a function of vertical position z on the electrode. The fraction of surface area at height z that is renewed per unit time is equal to the rate at which bubbles cross a horizontal line of length w at height z, times the probability that any given point on the line is in the renewal path.

$$s(z) = \dot{n}_z\,\frac{2R_b}{w} \quad , \tag{21}$$

where R_b is the bubble radius and $2R_b$ is the renewal path width. $\dot{n}_z$ is the total bubble evolution rate below height z and, assuming the gas evolution rate v to be uniform, is given by

$$\dot{n}_z = \frac{v}{4/3\pi {R_b}^3}\,wz \quad . \tag{22}$$

Combining Eqs. (21) and (22), we obtain

$$s(z) = \frac{3vz}{2\pi {R_b}^2} \quad . \tag{23}$$

Integrating Eq. (20) over time gives

$$\overline{N} = \frac{1}{H}\int_0^H c_i{}^\infty\sqrt{D_i}\int_0^\infty \frac{1}{\sqrt{\pi t}}\,s(z)e^{-st}\,dtdz \tag{24}$$

$$= \frac{c_i^{\infty}\sqrt{D_i}}{H} \int_0^H s(z) \left[\int_0^{\infty} \frac{1}{\sqrt{\pi t}} e^{-st} \, dt \right] dz \tag{25}$$

$$= \frac{c_i^{\infty}\sqrt{D_i}}{H} \int_0^H \sqrt{s(z)} dz \quad . \tag{26}$$

The flux to the electrode must be averaged over electrode height z from 0 to H. If s were independent of z, we would obtain the result of Danckwerts (1951)

$$\bar{N} = c_i^{\infty}\sqrt{D_i s} \quad . \tag{27}$$

Inserting Eq. (23) into (26) and integrating, we finally obtain

$$\bar{N}_A = c_i^{\infty} \sqrt{\frac{2D_i vH}{3\pi R_b^2}} \quad . \tag{28}$$

We would expect the above description to have validity only at low current densities, where flow of the bulk fluid does not become appreciable. Fouad and Sedahmed (1972) found that the mass-transfer rate increases with increasing electrode height for low current densities (2 to 10 mA /cm ^{2}) of hydrogen evolution over the entire range of electrode heights investigated (2.5 to 50 cm), though not as strongly as a square-root dependence. For higher current densities of hydrogen evolution (15 to 40 mA /cm ^{2}), the mass-transfer rate *decreases* with increasing electrode height for the shorter electrodes (2.5 to 10 cm). For oxygen evolution, the mass-transfer rate increases with increasing electrode height, in this case for the entire range of electrode heights and current densities investigated (2.5 to 50 cm, and 2 to 60 mA /cm ^{2}). Janssen and Hoogland (1970) found the opposite trend to hold for oxygen evolution at vertical electrodes of height 0.3 to 2 cm and at current densities of 10 to 400 mA /cm ^{2}, the mass-transfer coefficient falling with electrode

height to the -0.13 power.

The observed decrease of mass-transfer rate with height at short electrodes may be simply due to the increasing diffusion boundary layer thickness with height as given by boundary layer theory. For the higher current densities, the increase in mass transfer with increasing height will undoubtedly be aided by bulk convection, which was not accounted for in the above treatment. We simply note at this point that the surface-renewal theory based on bubbles sweeping a path as they slide along the electrode gives the same value (1/2) of the exponent on the gas-evolution rate v as the other surface-renewal theories.

6.1.2. *Surface Renewal with a Single Bubble Stream*

The surface-renewal theory applied to the experiments described in Section 3 is simpler than presented above in that we do not have a random distribution of surface ages. The bubble stream rises along the electrode surface on a particular path and sweeps a region of width $2R_b$ with a frequency equal to the bubble evolution frequency, $3\dot{V}/4\pi{R_b}^3$. Substituting the bubble evolution frequency for $1/\tau$ in the integrated form of Eq. (15), we obtain the average flux $\overline{N}_\tau$ to the area being renewed:

$$\overline{N}_\tau = 2{c_i}^\infty \sqrt{\frac{3D_i\,\dot{V}}{4\pi^2{R_b}^3}} \quad . \tag{29}$$

The area that is periodically renewed is $2R_b\,H$. The average flux to an area wH is then

$$\overline{N}_{r,A} = \overline{N}_r \frac{2R_b H}{wH} = c_i^{\infty} \sqrt{\frac{12D_i \dot{V}}{\pi^2 R_b w^2}} \quad . \tag{30}$$

The above description does not include a contribution to the average flux from the electrode area lying outside the renewal path. In fact, the rest of the electrode is receiving a flux due to the background natural-convection current density i_{nc}. The overall flux to the electrode, expressed as a current density, includes contributions from the renewal area of width $2R_b$ and the non-renewed area of width $(w - 2R_b)$.

$$i_{avg} = (i_{nc} (w - 2R_b) + n_i F \overline{N}_r 2R_b)/w \tag{31}$$

$$i_{avg} = i_{nc} + \left(\frac{n_i F c_i^{\infty}}{\pi} \sqrt{\frac{12D_i RT\ I}{n_g Fp\ R_b}} - 2R_b i_{nc} \right) \frac{1}{w} \quad . \tag{32}$$

Equation (32) is valid for electrode width w greater than the renewal path $2R_b$. With the micro-mosaic electrode we can conveniently vary w by varying the number of columns of segments over which we average the mass-transfer rate. We can, in effect, vary the electrode width by simply grouping the data from the same experiment in different ways. If we plot the average current density as a function of $1/w$, where w is the electrode width over which we average, we should obtain a straight line with a slope of

$$b = \frac{n_i F c_i^{\infty}}{\pi} \sqrt{\frac{12D_i RT\ I}{n_g Fp\ R_b}} - 2R_b i_{nc} \quad . \tag{33}$$

and a y-intercept of i_{nc}. Knowing b, i_{nc}, and I, the current to generate the bubble stream, we can solve Eq. (33) for R_b, the effective bubble radius.

If $w < 2R_b$, Eq. (32) is no longer valid; the average current becomes equal to the renewal current, $n_i F \overline{N}_r$, where $\overline{N}_r$ is given by Eq. (29). Knowing R_b, we can calculate i_{max}, the renewal current. Thus using the slope and the y-intercept from

the part of the curve for small $1/w$, we can calculate the limiting value of the curve as $1/w$ becomes large with respect to $1/(2R_b)$.

Figure 21 is the plot of the average current density versus $1/w$ for two experiments, in which the bubble evolution rates were 3.5 μA and 8.5 μA. The current distribution plots for these two runs appear in Figures 12 and 10, respectively. For small $1/w$, the points lie on a straight line. The y-intercept of approximately 2.8 mA /cm ^{2} corresponds to the background natural-convection current measured independently. There is a region of transition from approximately 25 to 50 cm $^{-1}$, beyond which the current density reaches a plateau. The effective bubble radii from Eq. (33) for the two runs were found to be 160 and 170 μm, factors of 6.4 and 5.7 greater than visual estimates from photographs, such as the one shown in Figure 8 for the 8.5 μA run. Values of I and R_b were inserted into Eq. (29) to calculate the maximum current density for $1/w > 1/2R_b$. These values were found to agree within several percent with the experimentally measured values of the current to the 100-μm -wide column of electrodes in the bubble path. These are the values plotted in Figure 21 for 100 cm $^{-1}$.

Table 2 summarizes the application of the surface-renewal theory to a series of five experiments in which the bubble stream rises within the mass-transfer boundary layer. The effective bubble radius varies from 5.7 to 7.5 times the experimentally-determined bubble radius. This factor is not surprising when one considers the spatial distribution of the mass-transfer rate. Figure 22 shows this distribution averaged along the height of the electrode for one of the runs described above. The visually-observed bubble diameter for this experiment is 60 μm, while the effective bubble diameter was found to be 340 μm. From Figure 22, we can see

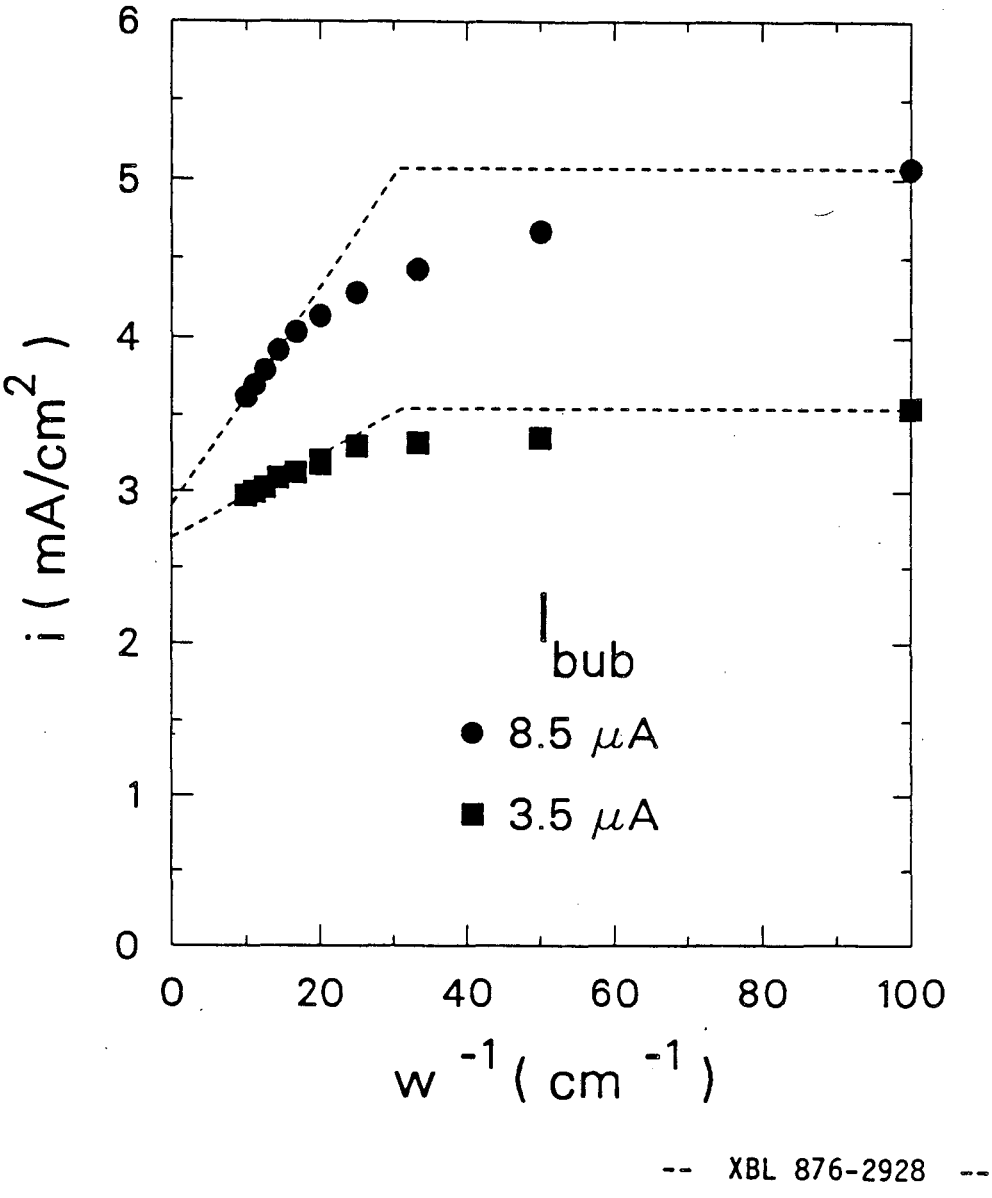

Figure 21. Enhanced mass-transfer rate versus the inverse of the averaging width w for two experiments. The top curve is for a 60-μm diameter H_2 bubble stream evolved at a rate of 8.5 μA within the mass-transfer boundary layer. The second is for a 50-μm diameter H_2 bubble stream evolved at a rate of 3.5 μA.

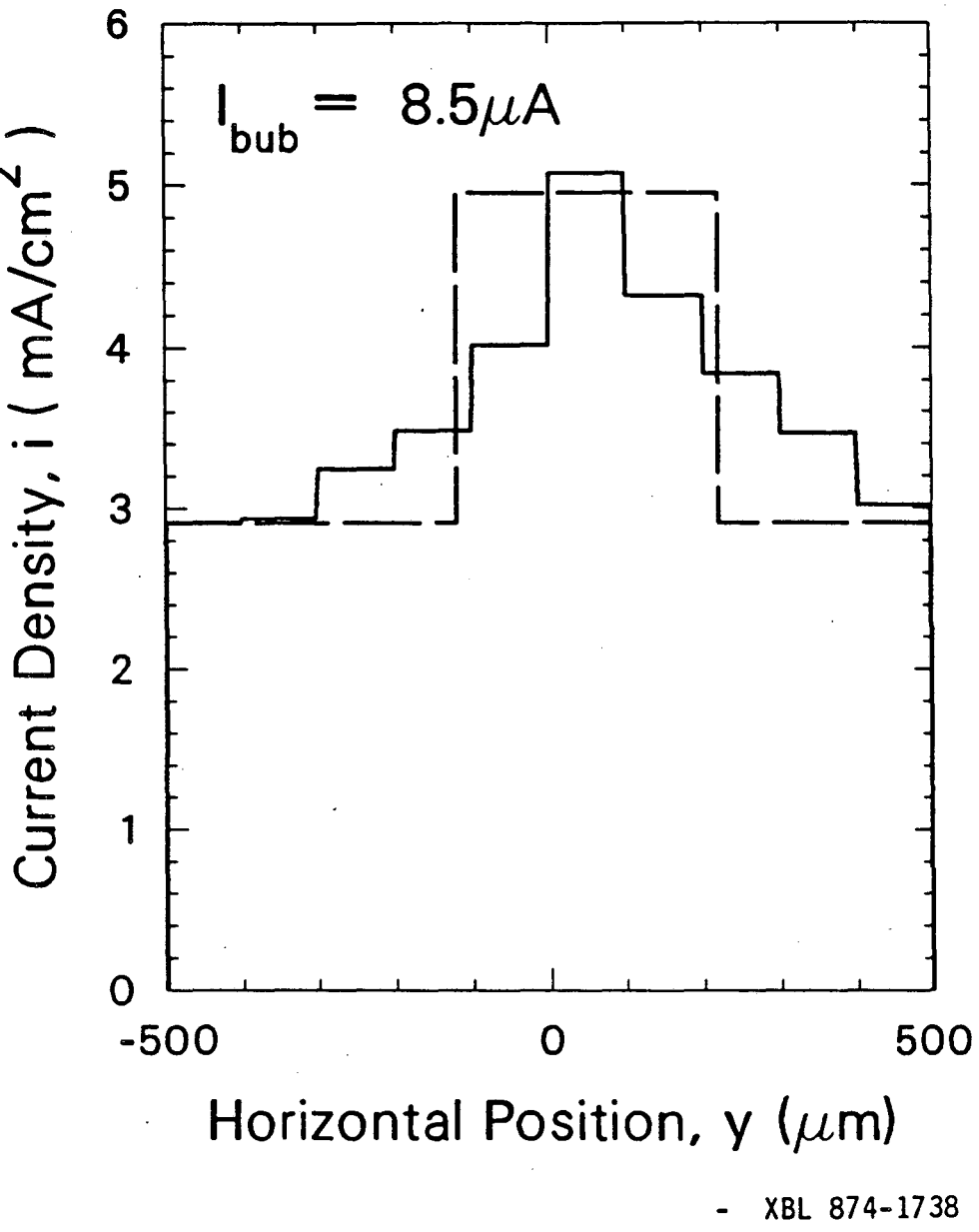

Figure 22. Measured (solid) and idealized (dashed) mass-transfer distribution across electrode produced by 60-μm diameter H_2 bubbles rising within the mass-transfer boundary layer at a rate of 8.5 μA. The width of the renewal path for this experiment was found to be 340 μm ; the effectiveness factor is 5.7.

Table 2. Effective bubble radii and renewal currents from Eqs. (33) and (29)

I (μA)	R_b (μm)	i_{nc} (mA /cm^2)	$10^2\, b$ (mA /cm)	$R_{b,eff}$ (μm)	Eff. factor	i_{max}^{exp} (mA /cm^2)	i_{max}^{calc} (mA /cm^2)	Δ %
3.5	25	2.69	2.73	160	6.4	3.54	3.54	0.0
4.5	22	2.51	4.88	159	7.2	4.06	4.04	0.4
8.5	30	2.91	7.01	172	5.7	5.07	4.95	2.4
9.0	22	2.82	8.67	164	7.5	5.66	5.46	3.5
16.0	38	2.71	8.93	218	5.7	5.46	4.76	12.8

that the path of enhanced mass transfer is appreciably wider than the actual bubble diameter. In the simplified theory described here, we consider the actual distribution shown in Figure 22 to be idealized as having only two possible values, as shown by the dashed curve: the value of the current to the renewal path is i_{max} and that to the rest of the electrode is i_{nc}. The width of the renewal path and the values of i_{max} and i_{nc} were taken from the low $1/w$ values; these are found to match i_{nc} measured in independent experiments, and also i_{max} for large $1/w$ values. Thus the effectiveness factor of 6 to 7.5 is a physically-meaningful quantity, representing the width of the renewal path for a bubble stream rising within the mass-transfer boundary layer.

6.2. *Bubbles Rising Outside the Mass-Transfer Boundary Layer*

When the bubble stream is rising outside the mass-transfer boundary layer, the mass-transfer enhancement is a relatively steady process; the effects of individual bubbles are averaged somewhat. This suggests a treatment in terms of an assisting laminar flow enhancement. We first attempt to account for the background natural-convection at the electrode.

6.2.1. *Background Natural Convection and Assisting Flows*

The redox reaction itself causes a density difference between the fluid at the electrode surface and the bulk fluid, the fluid near the electrode being less dense than that of the bulk. This phenomenon is rather complex, involving the multi-component diffusion and migration of ionic species in concentration and potential gradients. The subject is treated in considerable detail in Chapter 4. In the cell geometry used in this study, the less dense fluid generated at the electrode causes an upward laminar flow along the electrode surface, which dissipates beyond the upper edge of the active region on the electrode. Under mass-transfer control, in the absence of any bubble generation at the electrode, there is a non-uniform current distribution along the electrode: the local current density is proportional to the distance from the lower edge to the negative one-fourth power. The experimentally measured mass-transfer distribution for laminar, natural-convection flow at the micro-mosaic electrode is shown in Figure 23.

For the case of assisting laminar flows, Churchill (1977) has shown experimentally, and Ruckenstein and Rajagopalan (1980) have demonstrated using scaling arguments that the cube of the effective mass-transfer coefficient is equal to

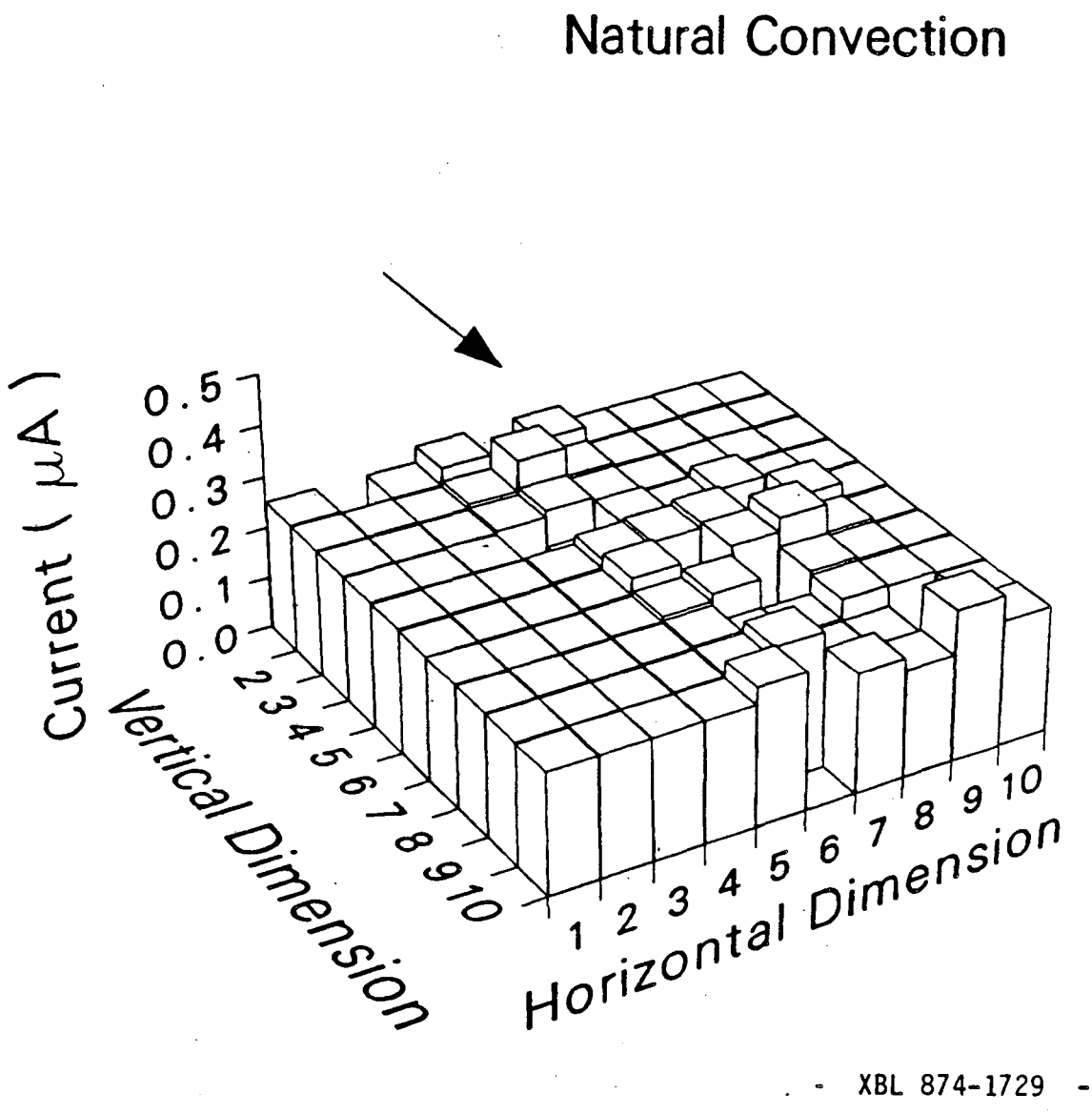

Figure 23. Spatial distribution of the background natural-convection mass-transfer rate generated by the redox reaction itself. The upward direction is indicated by the arrow in the figure.

the sum of the cubes of the component coefficients.

$$k_{tot}^3 = k_1^3 + k_2^3 \quad . \tag{34}$$

The mass-transfer coefficient is directly proportional to the current density as $i = n_i F k c_i^\infty$, so the measured current densities combine in the same way. The background natural-convection current density to the area of the 10 × 10 array of monitoring electrodes is measured between gas-evolution runs. This value is subtracted from the total mass-transfer rate measured during the gas-evolution experiments according to Eq. (34). The resulting mass-transfer rate due solely to the influence of the bubble stream is presented as a function of bubble evolution rate in Figure 24, and as a function of bubble stream position in Figure 25.

6.2.2. *Comparison to Rising Cylinder*

The steady nature of the mass-transfer enhancement when the bubble stream is outside the mass-transfer boundary layer suggests an idealization of the bubble stream as a steadily-rising column of bubbles and entrained fluid. The mass-transfer enhancement in such a case results from an increased velocity gradient in the vicinity of the electrode.

6.2.2.1. *Velocity Field around a Cylinder Rising Parallel to a Wall*

The velocity profile for an infinite cylinder rising parallel to a stationary wall can be derived analytically. In rectangular coordinates, x is the normal distance from the electrode, y is the horizontal distance parallel to the electrode, and z is the vertical distance parallel to the electrode and to the axis of the cylinder. The laminar flow problem involves only the z-component of velocity. For $v_z(x, y)$, the

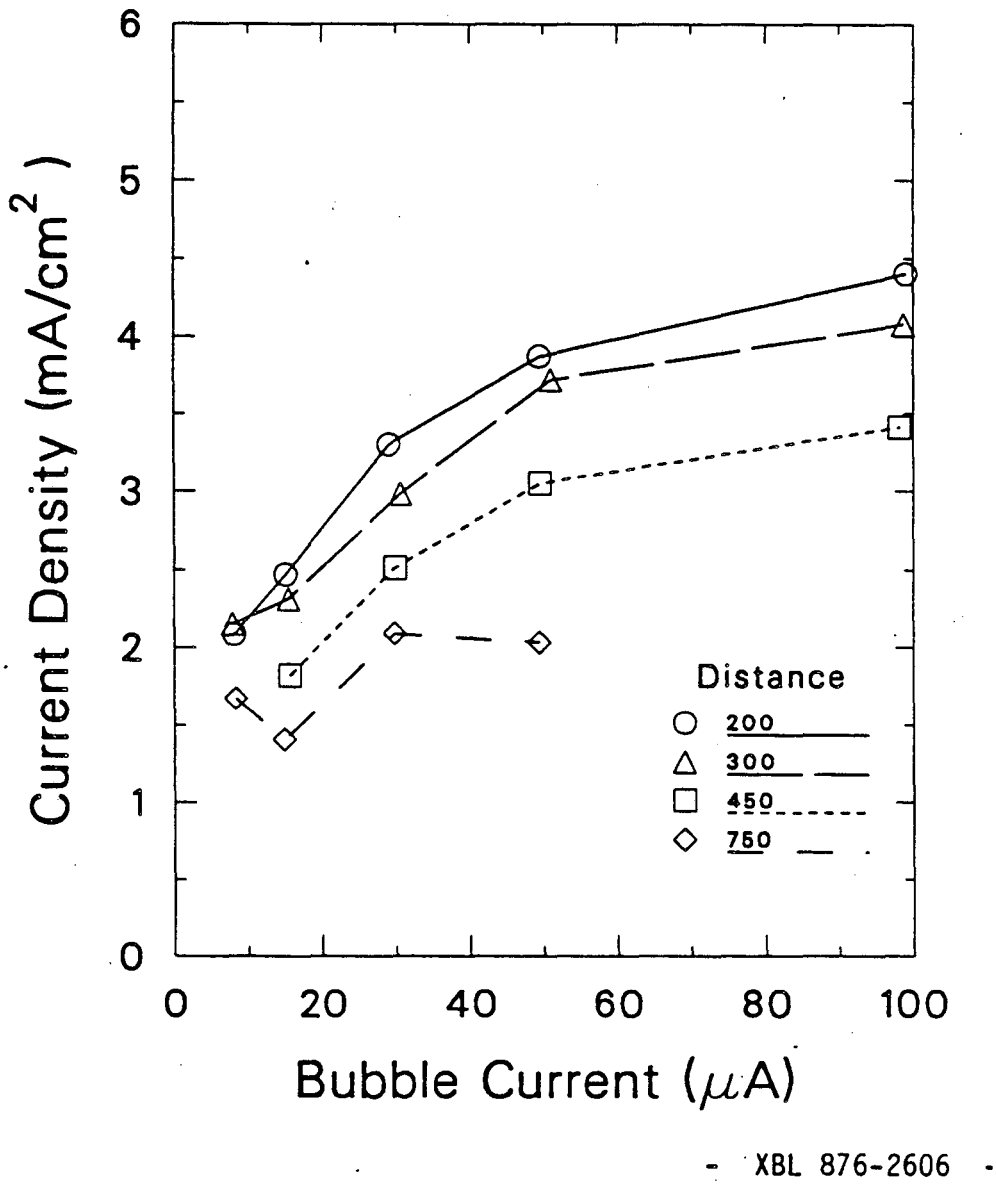

Figure 24. Mass-transfer enhancement, averaged over the segmented portion of the electrode and over the time of data acquisition, and corrected for the background natural-convection current, as a function of bubble evolution rate.

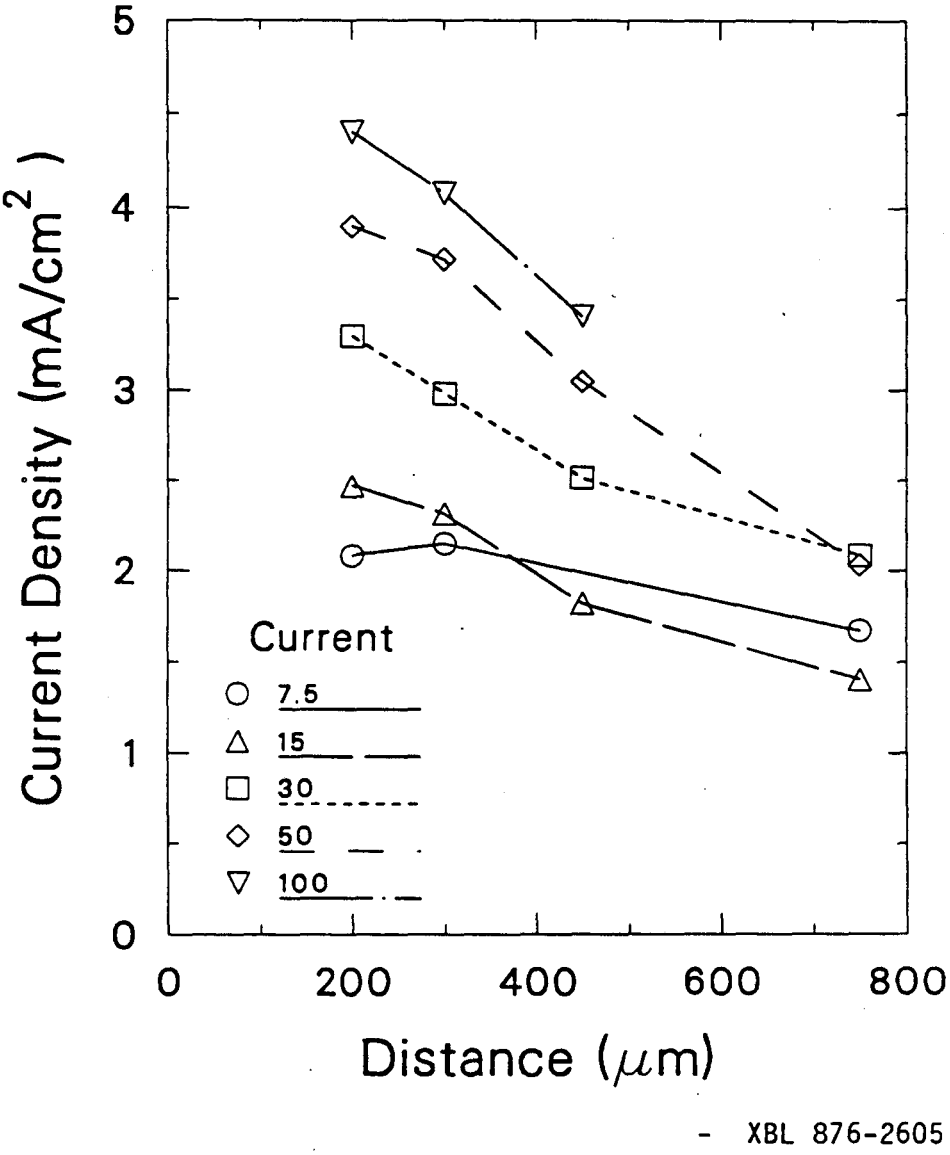

Figure 25. Average mass-transfer enhancement to the segmented portion of the electrode, corrected for the background natural convection current, as a function of bubble stream position.

Navier-Stokes equation reduces to

$$\frac{\partial^2 v_z}{\partial x^2} + \frac{\partial^2 v_z}{\partial y^2} = 0 \quad . \tag{35}$$

The problem can be solved by transforming to bi-cylindrical coordinates (Moon and Spencer, 1961), shown in Figure 26. In this geometry, Laplace's equation is

$$\nabla^2 v_z = \frac{(\cosh\eta - \cos\psi)^2}{a^2}\left(\frac{\partial^2 v_z}{\partial \psi^2} + \frac{\partial^2 v_z}{\partial \eta^2}\right) + \frac{\partial^2 v_z}{\partial z^2} \quad , \tag{36}$$

where

$$x = \frac{a \sinh\eta}{\cosh\eta - \cos\psi} \quad \text{and} \quad y = \frac{a \sin\psi}{\cosh\eta - \cos\psi} \tag{37-a,b}$$

and a is a constant of the geometry to be determined later. If $v_z \neq f(z)$, Eq. (36) reduces to

$$\nabla^2 v_z = \frac{\partial^2 v_z}{\partial \psi^2} + \frac{\partial^2 v_z}{\partial \eta^2} = 0 \quad . \tag{38}$$

The boundary conditions are that the velocity vanishes at the electrode and is equal to the velocity of the cylinder v_c at η_c:

$$v_z = 0 \quad \text{at} \quad \eta = 0 \tag{39-a}$$

$$v_z = v_c \quad \text{at} \quad \eta = \eta_c \quad . \tag{39-b}$$

The problem is symmetric at $\psi = 0$ and $\psi = \pi$ so we expect

$$\frac{\partial v_z}{\partial \psi} = 0 \quad \text{at} \quad \psi = 0 \tag{40-a}$$

$$\frac{\partial v_z}{\partial \psi} = 0 \quad \text{at} \quad \psi = \pi \quad . \tag{40-b}$$

There is in fact no reason to expect any dependence of the velocity field on ψ, and the solution to Eq. (38) is simply

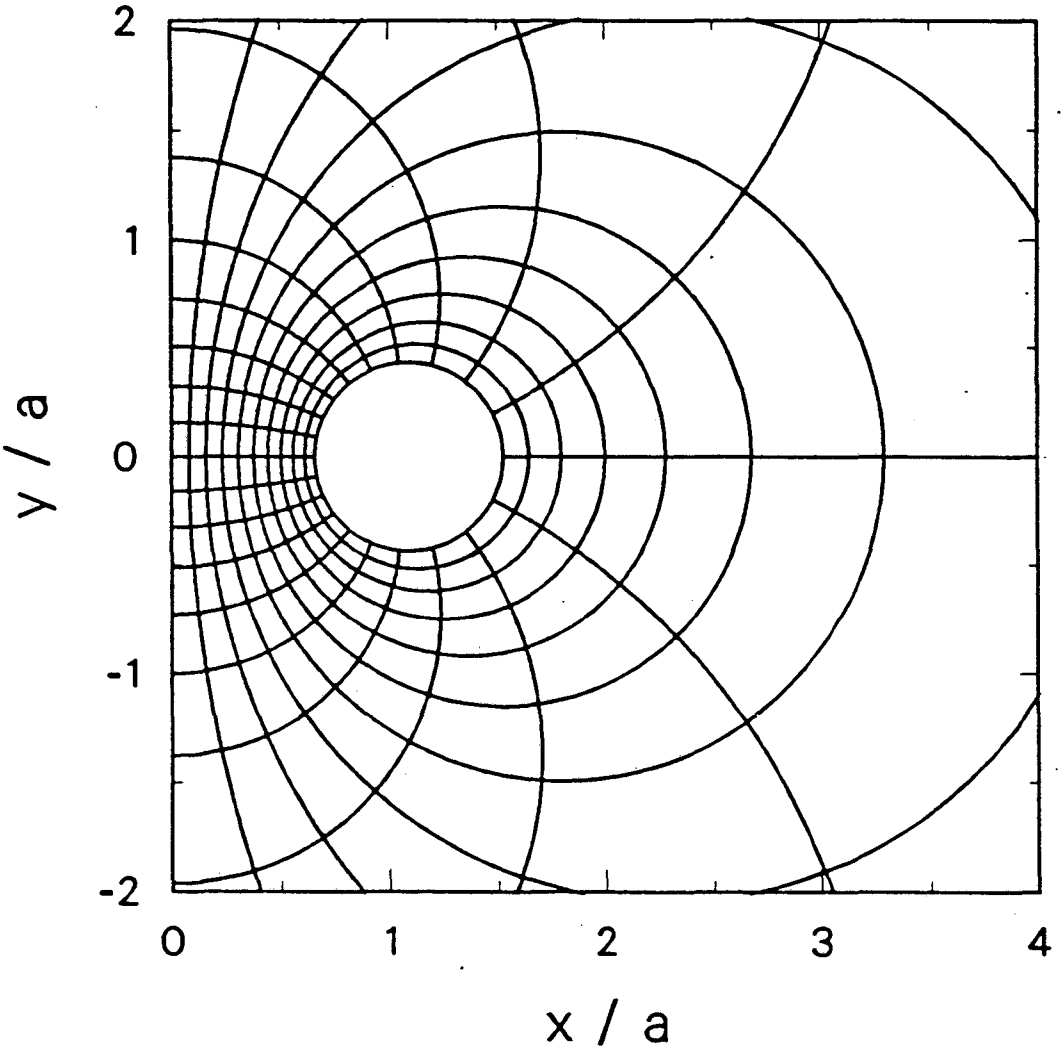

Figure 26. η–ψ plane (x-y plane) of bi-cylindrical coordinate system for an infinite cylinder rising parallel to a plane wall. Lines of constant η are eccentric circles with radius proportional to $1/\eta$; $\eta = 0$ is the wall.

$$v_z = A + B\eta \quad . \tag{41}$$

Inserting boundary conditions (40-a,b) we find

$$v_z = v_c \frac{\eta}{\eta_c} \quad . \tag{42}$$

The complexity of the problem arises from transforming the solution back to rectangular coordinates. Solving Eq. (37-a) for $\cos\psi$ and substituting into Eq. (37-b), we find the equation for a circle (constant η) to be

$$y^2 + (x - a\coth\eta)^2 = \frac{a^2}{\sinh^2\eta} \quad . \tag{43}$$

Solving Eq. (43) for η, we have

$$\eta = \frac{1}{2} \ln\left(\frac{x^2 + y^2 + a^2 + 2ax}{x^2 + y^2 + a^2 - 2ax} \right) \quad . \tag{44}$$

The cylinder is described by the circle at η_c. We need to solve for η_c and the constant a in terms of the radius R_c and the distance L from the center of the cylinder to the wall. By inspection of Eq. (43) we have

$$R_c = \frac{a}{\sinh\eta_c} \quad \text{and} \quad L = a\coth\eta_c \quad . \tag{45-a,b}$$

Combining Eqs. (45) we obtain

$$a = \sqrt{L^2 - R_c^2} \tag{46}$$

$$\eta_c = \cosh^{-1}\left(\frac{L}{R_c} \right) = \ln\left(\frac{1}{R_c}\left(L + \sqrt{L^2 - R_c^2} \right) \right) \quad . \tag{47}$$

The velocity contours from Eq. (42) are shown in Figure 27 for a 100-μm diameter cylinder rising at a center-to-wall distance of 200 μm , and in Figure 28 for 750 μm . Both the velocity gradient and the non-uniformity of the gradient along the electrode surface (y = –500 to 500μm) decrease as the cylinder is moved from

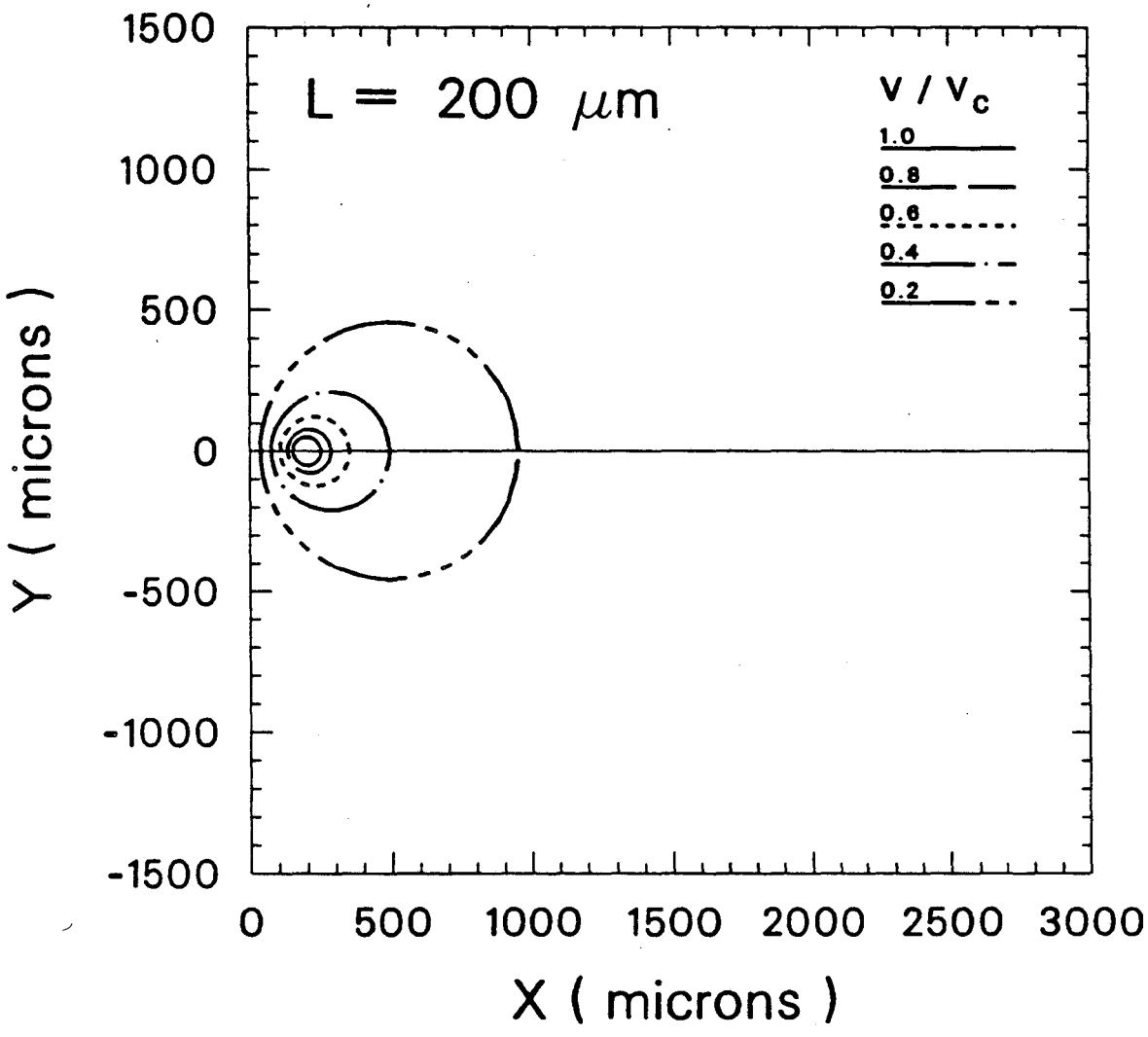

Figure 27. Lines of constant velocity for a 100-μm diameter cylinder rising at 200 μm from the electrode surface.

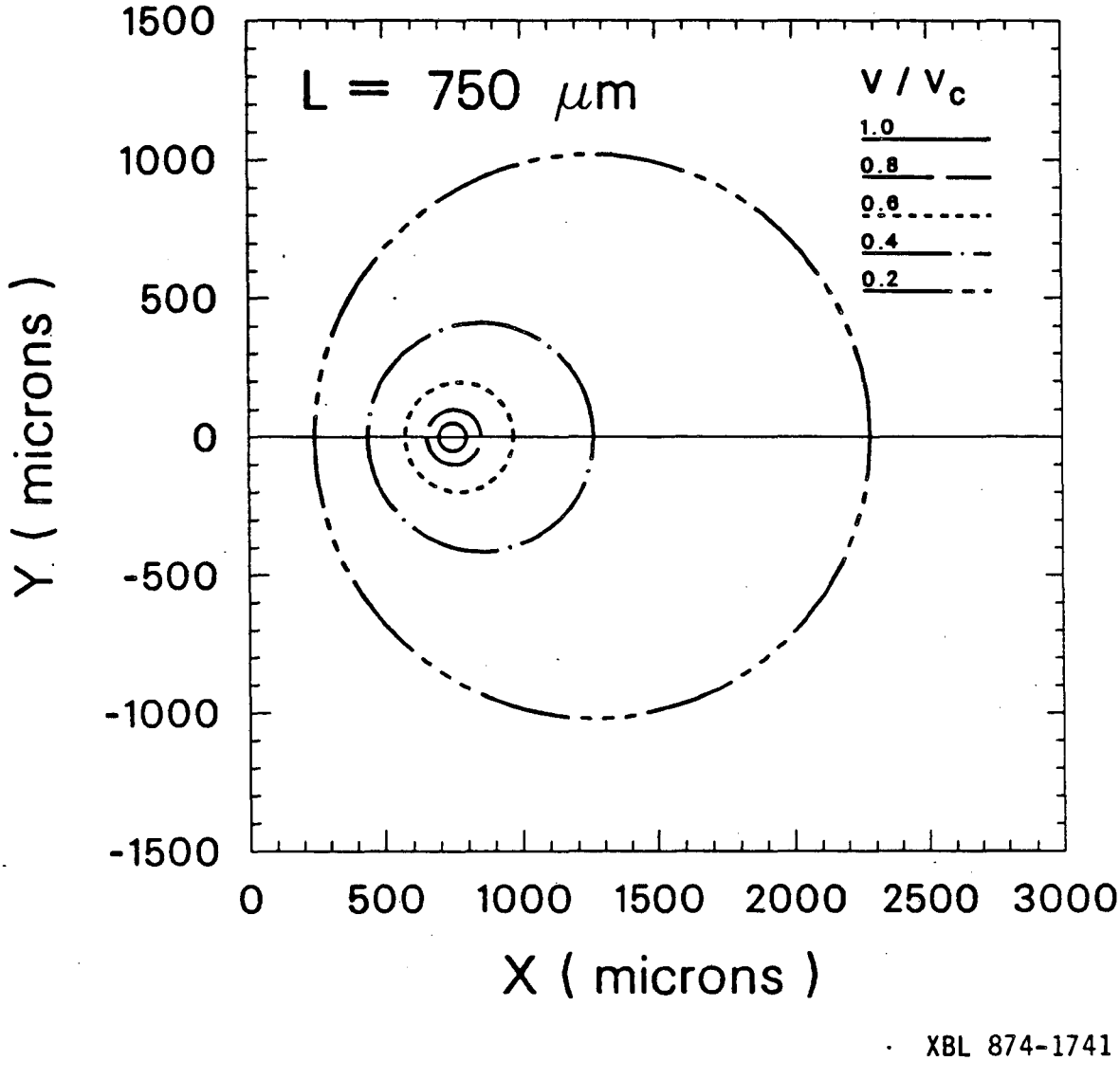

Figure 28. Velocity contours for a 100-μm diameter cylinder rising at 750 μm from the electrode surface.

200 to 750 μm . The essence of the idealization of the bubble stream as a rising cylinder can be seen in these two figures; the rising cylinder creates a high velocity gradient at the electrode surface. To obtain the same velocity gradient at the surface by forced convection of the bulk fluid, one would have to maintain fairly high flow rates *of all the fluid in the cell.* The cylinder or bubble stream drags the fluid that is very near the electrode surface upward, producing a high velocity gradient without carrying a large amount of fluid.

6.2.2.2. *Mass-Transfer Effect Caused by a Rising Cylinder*

We solve next for the mass-transfer rate to the electrode at $x = 0$ (*i.e.*, $\eta = 0$), and $z > 0$, by solving for the gradient of velocity at the wall and inserting this into the equation of convective diffusion. The equation of convective diffusion is

$$\frac{\partial c_i}{\partial t} + \mathbf{v}\cdot\nabla c_i = D_i \nabla^2 c_i \quad . \tag{48}$$

The first term is zero at steady state, and the only component of velocity is $v_z(x, y; L, R_c)$. In rectangular coordinates, Eq. (48) becomes

$$v_z \frac{\partial c_i}{\partial z} = D_i \left(\frac{\partial^2 c_i}{\partial x^2} + \frac{\partial^2 c_i}{\partial y^2} + \frac{\partial^2 c_i}{\partial z^2} \right) \quad . \tag{49}$$

The boundary conditions are

$$c_i(x = 0, \text{ all } y, z > 0) = c_i^{\,0} \tag{50-a}$$

$$c_i(x = 0, \text{ all } y, z \leq 0) = c_i^{\,\infty} \tag{50-b}$$

$$c_i(x \to \infty, \text{ all } y, \text{ all } z) = c_i^{\,\infty} \quad . \tag{50-c}$$

Diffusion in the y-direction may be neglected since the driving force for

concentration changes is primarily in the x-direction. We make Eq. (49) dimensionless with

$$v_z^* \equiv \frac{v_z}{v_c} \quad , \tag{51-a}$$

$$\theta_i \equiv \frac{c_i - c_i^0}{c_i^\infty - c_i^0} \quad , \tag{51-b}$$

and

$$\xi \equiv \frac{x}{a} \quad . \tag{51-c}$$

Substituting Eqs. (51) into Eq. (49), we obtain

$$\left(\frac{v_c\, a^2}{D_i} \right) v_z^* \frac{\partial \theta_i}{\partial z} = \frac{\partial^2 \theta_i}{\partial \xi^2} + a^2 \frac{\partial^2 \theta_i}{\partial z^2} \quad . \tag{52}$$

The appropriate scaling of z becomes obvious from Eq. (52):

$$\varsigma \equiv \frac{z}{\frac{v_c\, a^2}{D_i}} \quad . \tag{53}$$

Eq. (52) becomes

$$v_z^* \frac{\partial \theta_i}{\partial \varsigma} = \frac{\partial^2 \theta_i}{\partial \xi^2} + \left(\frac{D_i}{v_c\, a} \right)^2 \frac{\partial^2 \theta_i}{\partial \varsigma^2} \quad . \tag{54}$$

Defining the Peclet number Pe as $a v_c / D_i$ we have

$$v_z^* \frac{\partial \theta_i}{\partial \varsigma} = \frac{\partial^2 \theta_i}{\partial \xi^2} + \frac{1}{Pe^2} \frac{\partial^2 \theta_i}{\partial \varsigma^2} \quad . \tag{55}$$

Although the cases we will consider have Re on the order of unity, the Peclet number ($Pe \equiv ReSc$) is high because of the high Schmidt number (~ 2000). Thus we can neglect diffusion in the flow direction and solve

$$v_z^* \frac{\partial \theta_i}{\partial \varsigma} = \frac{\partial^2 \theta_i}{\partial \xi^2} \tag{56}$$

with boundary conditions

$$\theta_i(\xi = 0, \varsigma > 0) = 0 \tag{57-a}$$

$$\theta_i(\xi = 0, \varsigma \leq 0) = 1 \tag{57-b}$$

$$\theta_i(\xi \to \infty, \text{ all } \varsigma) = 1 \quad . \tag{57-c}$$

For small ξ we can approximate v_z as $\left.\frac{\partial v_z}{\partial \xi}\right|_{\xi = 0} \xi$.

$$v_z = \left.\frac{\partial v_z}{\partial \xi}\right|_{\xi = 0} \xi = \left.\frac{\partial v_z}{\partial x}\right|_{x = 0} x = \left.\frac{\partial v_z}{\partial \eta}\right|_{\eta = 0} \left.\frac{\partial \eta}{\partial x}\right|_{x = 0} x \quad . \tag{58}$$

From Eq. (42)

$$\frac{\partial v_z}{\partial \eta} = \frac{v_c}{\eta_c} \quad , \tag{59}$$

and from Eq. (44)

$$\left.\frac{\partial \eta}{\partial x}\right|_{x = 0} = \frac{2a}{y^2 + a^2} \quad . \tag{60}$$

Substituting Eqs. (58)-(60) into (56) and defining $f \equiv y/a$, we obtain

$$\frac{2\xi}{\eta_c (f^2 + 1)} \frac{\partial \theta_i}{\partial \varsigma} = \frac{\partial^2 \theta_i}{\partial \xi^2} \quad . \tag{61}$$

The similarity variable

$$\lambda \equiv \xi \left(\frac{2}{9\eta_c (f^2 + 1)\varsigma} \right)^{1/3} \tag{62}$$

transforms Eq. (61) to

$$\frac{d^2 \theta_i}{d\lambda^2} + 3\lambda^2 \frac{d\theta_i}{d\lambda} = 0 \quad . \tag{63}$$

Boundary conditions (57) become

$$\theta_i(\lambda = 0) = 1 \tag{64-a}$$

$$\theta_i(\lambda = \infty) = 0 \quad . \tag{64-b}$$

The solution to Eq. (63) with boundary conditions (64) is

$$\theta_i = \frac{1}{\Gamma(4/3)} \int_{\lambda}^{\infty} \exp(-\lambda^3)\, d\lambda \quad . \tag{65}$$

The flux to the electrode is found by

$$N_i = -D_i \left.\frac{\partial c_i}{\partial x}\right|_{x=0} = -D_i \left(c_i^{\infty} - c_i^{0} \right) \left.\frac{\partial \theta_i}{\partial \lambda}\right|_{\lambda=0} \frac{\partial \lambda}{\partial \xi} \frac{\partial \xi}{\partial x} \tag{66}$$

$$= \frac{-D_i \left(c_i^{\infty} - c_i^{0} \right)}{\Gamma(4/3)} \left(\frac{2av_c}{9D_i \eta_c} \right)^{1/3} \left(\frac{1}{y^2 + a^2} \right)^{1/3} \left(\frac{1}{z} \right)^{1/3} \quad . \tag{67}$$

6.2.2:3. *Equivalent Velocity of Rising Cylinder*

The only quantity in Eq. (67) still to be specified is v_c, the cylinder velocity. There are three possibilities: 1) equate the volumetric flow rate of the cylinder to that of the rising bubbles, 2) equate the drag on the rising cylinder to the drag on the rising bubbles, or 3) allow the cylinder to rise at the terminal velocity of the individual bubbles. The first option allows for no entrainment of the liquid by the rising bubbles, the second for intermediate entrainment, and the third for maximum entrainment. This last possibility can be eliminated by noting that v_c would not depend on bubble evolution rate, but only on bubble size, which is not the case (See Figure 24).

Equating the gas flows for the cylinder and the bubble stream, (Option 1), we find

$$v_c = \frac{\dot{V}}{\pi {R_b}^2} = \frac{IRT}{n_g\, Fp\, \pi {R_b}^2} \quad , \tag{68}$$

and the mass-transfer rate due to the rising cylinder is dependent on $I^{1/3}$.

In Option 2, the case of equal drag forces, the drag on the cylinder can be calculated by integrating the tangential force over the area of the cylinder. It is simpler, however, to calculate the drag on the wall (which must be equivalent since the wall is infinite). The drag on the wall is

$$F_D = 2 \int_0^{\infty} \int_0^{l} \mu \left. \frac{\partial v_z}{\partial x} \right|_{x\,=\,0} dz\ dy \tag{69}$$

$$\frac{F_D}{l} = 2 \int_0^{\infty} \mu \left. \frac{\partial v_z}{\partial x} \right|_{x\,=\,0} dy \quad . \tag{70}$$

Substituting Eqs. (59) and (60) for $\left. \frac{\partial v_z}{\partial x} \right|_{x\,=\,0}$ into (70) we obtain

$$\frac{F_D}{l} = \frac{4 a v_c\, \mu}{\eta_c} \int_0^{\infty} \frac{1}{y^2 + a^2}\, dy \tag{71}$$

$$= \frac{4 a v_c\, \mu}{\eta_c}\ \frac{1}{a}\ \tan^{-1}\frac{y}{a} \Bigg]_{y\,=\,0}^{y\,=\,\infty} \tag{72}$$

$$= \frac{4 \mu v_c}{\eta_c} \left(\frac{\pi}{2} - 0 \right) \tag{73}$$

$$\frac{F_D}{l} = \frac{2 \mu v_c\, \pi}{\eta_c} \quad . \tag{74}$$

The drag on a series of bubbles is computed by assuming that the bubbles act independently and rise in Stokes flow. Faxén (1923) solved for the total drag force on a single bubble rising at terminal velocity v_t and distance L from a wall:

$$\frac{F_D}{\text{bubble}} = \frac{6 \pi \mu R_b\, v_t}{f\,(R_b / L)} \quad , \tag{75}$$

where $f\,(R_b/L)$ is the correction for the presence of the wall and is given by (Happel and Brenner (1965), p.327)

$$f\left(\frac{R_b}{L}\right) = 1 - \frac{9}{16}\left(\frac{R_b}{L}\right) + \frac{1}{8}\left(\frac{R_b}{L}\right)^3 - \frac{45}{256}\left(\frac{R_b}{L}\right)^4 - \frac{1}{16}\left(\frac{R_b}{L}\right)^5 \quad . \tag{76}$$

The frictional drag force per unit length of a rising column of bubbles is the product of the frictional drag force per bubble (2/3 of the total drag force) and the bubble frequency, divided by the bubble velocity:

$$\frac{F_D}{l} = \frac{F_D}{\text{bubble}}\,\frac{\dot{V}}{\frac{4}{3}\pi R_b{}^3 v_t} = \frac{6\mu\dot{V}}{2R_b{}^2 f\,(R_b/L)} \quad . \tag{77}$$

Combining Eqs. (77) and (74), we finally obtain

$$v_c = \frac{\dot{V}}{\pi R_b{}^2}\,\frac{9\eta_c}{4f\,(R_b/L)} = \frac{IRT}{n_g\,Fp\,\pi R_b{}^2}\,\frac{9\eta_c}{4f\,(R_b/L)} \quad . \tag{78}$$

In the above treatment, we have chosen, somewhat arbitrarily, to exclude the form drag from the bubble force calculation. By this choice we attempt to account for the fact that the bubbles do not act independently: each bubble decreases the form drag on the bubble that follows.

We have also chosen to fix the radius of the cylinder (at the radius of the bubbles), and to vary the cylinder velocity. If we had done the reverse, we would obtain the same result in the maximum entrainment case (Option 3). In the case of equivalent volumetric flowrate (Option 1), we would obtain only a weak dependence on bubble evolution rate. In the case of equivalent drag (Option 2), we would obtain the identical result as that derived above (Eq. (78)).

The average mass-transfer enhancement due to the rising cylinder is evaluated in terms of the average current density by integrating Eq. (67) over the

electrode area:

$$i_{avg} = \frac{-nFD_i\,(\,c_i^{\infty} - c_i^{0}\,)}{s_i\,\Gamma(4/3)} \left(\frac{2av_c}{9D_i\,\eta_c} \right)^{1/3} \times$$

$$\frac{3}{2} \left(\frac{z_2^{(2/3)} - z_1^{(2/3)}}{z_2 - z_1} \right) \frac{1}{y_2 - y_1} \int_{y_1}^{y_2} \left(\frac{1}{y^2 + a^2} \right)^{1/3} dy \quad , \tag{79}$$

with v_c given by Eq. (68) or (78).

The predicted current distribution resulting from a rising cylinder that is equivalent, on the basis of equivalent drag, to a 30-μA bubble stream at 200 μm is shown in Figure 29. The current distribution resulting from a stream of the same diameter and rise velocity, but positioned at 750 μm is shown in Figure 30. Figures 29 and 30 include the background natural-convection mass transfer, added according to Eq. (34), so that they may be compared directly to the experimentally measured current distributions, Figures 15 and 18, respectively. The degree of non-uniformity in the calculated and experimental distributions agrees reasonably well. The agreement between the calculated and experimental average mass-transfer enhancement is excellent. Figure 31 compares, as a function of bubble evolution rate, the experimental and calculated mass-transfer rates for a bubble-stream-to-wall separation of 200 μm . The calculated results for both equivalent drag (Eq. (78)) and equivalent volummetric flow of gas (Eq. (68)) are shown. The former matches experiment very well; the latter would be expected to present a lower limit to the mass-transfer enhancement. The functionality of the dependence of mass-transfer enhancement on bubble evolution rate is seen to agree with the one-third power dependence predicted by the model. This result implies that the enhancement is due to a laminar flow of gas and liquid. Figure 32 shows the same comparison for a

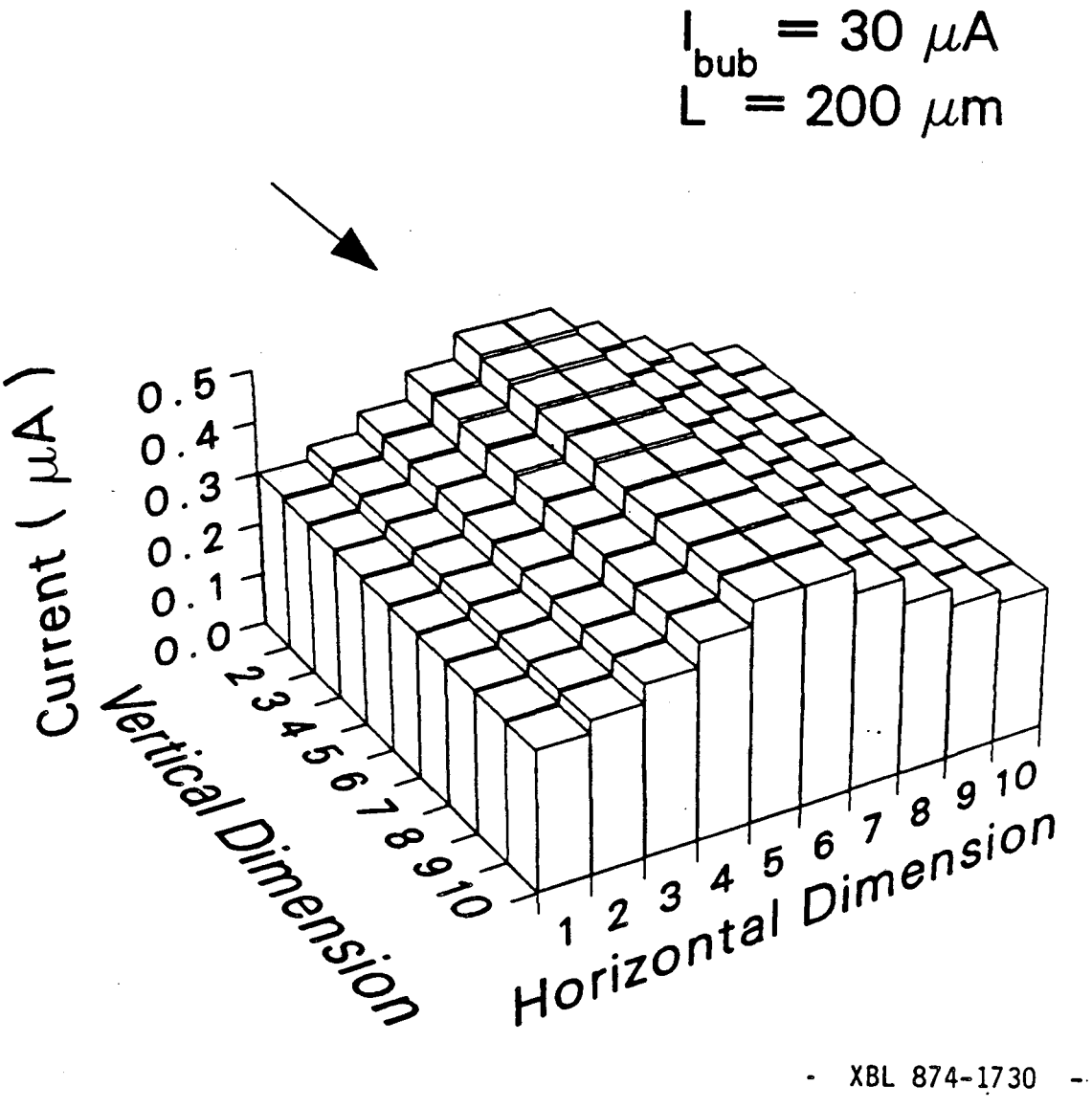

Figure 29. Mass-transfer distribution resulting from a 100-μm diameter cylinder rising at 200 μm from the electrode surface, at a rate equivalent to a 30-μA rate of gas evolution. The background natural-convection current is included.

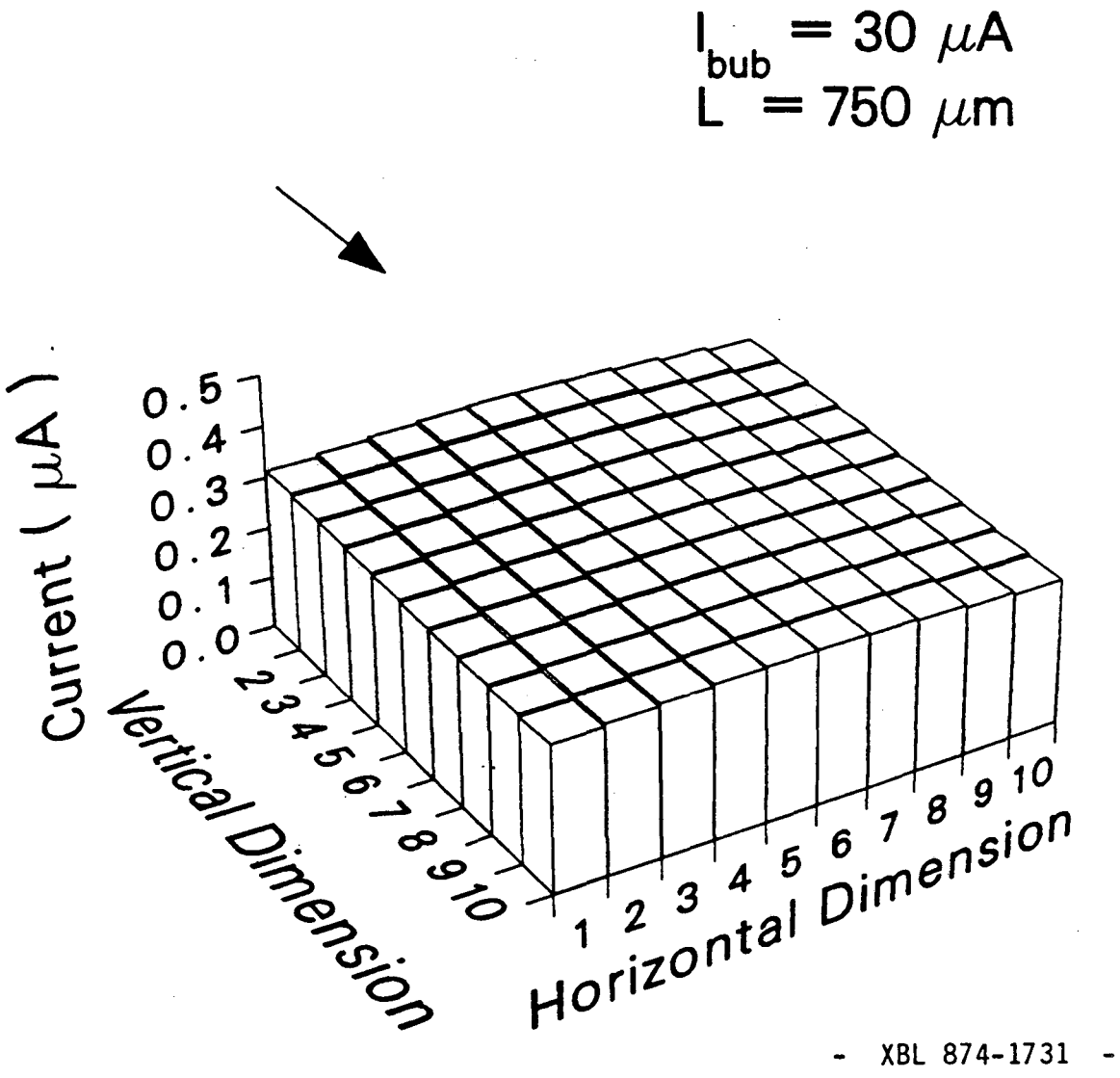

Figure 30. Mass-transfer distribution resulting from a 100-μm diameter cylinder rising at 750 μm from the electrode surface, at a rate equivalent to a 30-μA rate of gas evolution. The background natural-convection current is included.

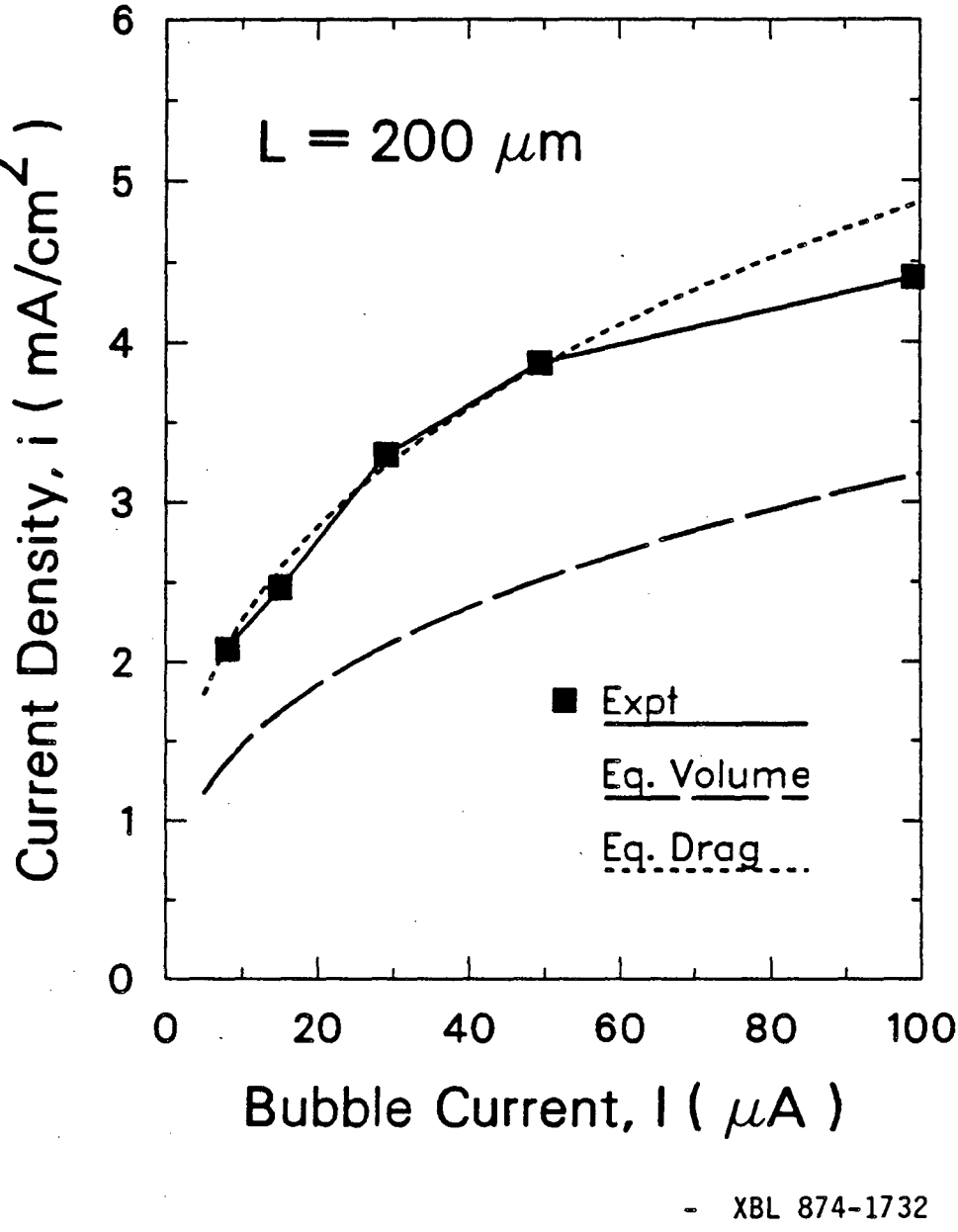

Figure 31. Comparison of mass-transfer enhancement as a function of bubble evolution rate 1) measured for a single stream of bubbles and 2) calculated for a steadily-rising cylinder, both centered at 200 μm from the electrode.

separation of 300 μm and Figure 33 for a separation of 450 μm . The agreement between experiment and theory decreases with increasing separation. In part this reflects a weakness of the theory, but also, as the total mass-transfer rate approaches the background natural-convection mass-transfer rate, the sensitivity of the determined value of the enhancement to experimental error increases.

In summary, the rising cylinder model describes the effect of an increased laminar flow along the electrode and neglects individual bubble effects. The resulting mass-transfer rate matches the experimentally measured values in both magnitude and distribution. The measured dependence of the mass-transfer enhancement on the bubble-stream-to-electrode separation is stronger than predicted by the cylinder model.

7. Conclusions

The mass-transfer enhancement due to a stream of bubbles rising along a vertical electrode has been characterized by transient and spatial resolution using an indicator ion reaction at a micro-mosaic electrode. Bubbles rising within the mass-transfer boundary layer create a strong, localized, periodic enhancement. Spatial resolution of these effects reveals a mechanism consistent with a surface-renewal theory of mass-transfer enhancement. The effective renewal path of the bubbles is typically 5 to 7 bubble diameters wide.

Bubble streams rising outside the mass-transfer boundary layer cause a steady increase in the mass-transfer rate over a large area. The mass-transfer enhancement in this case depends on the bubble evolution rate to the one-third

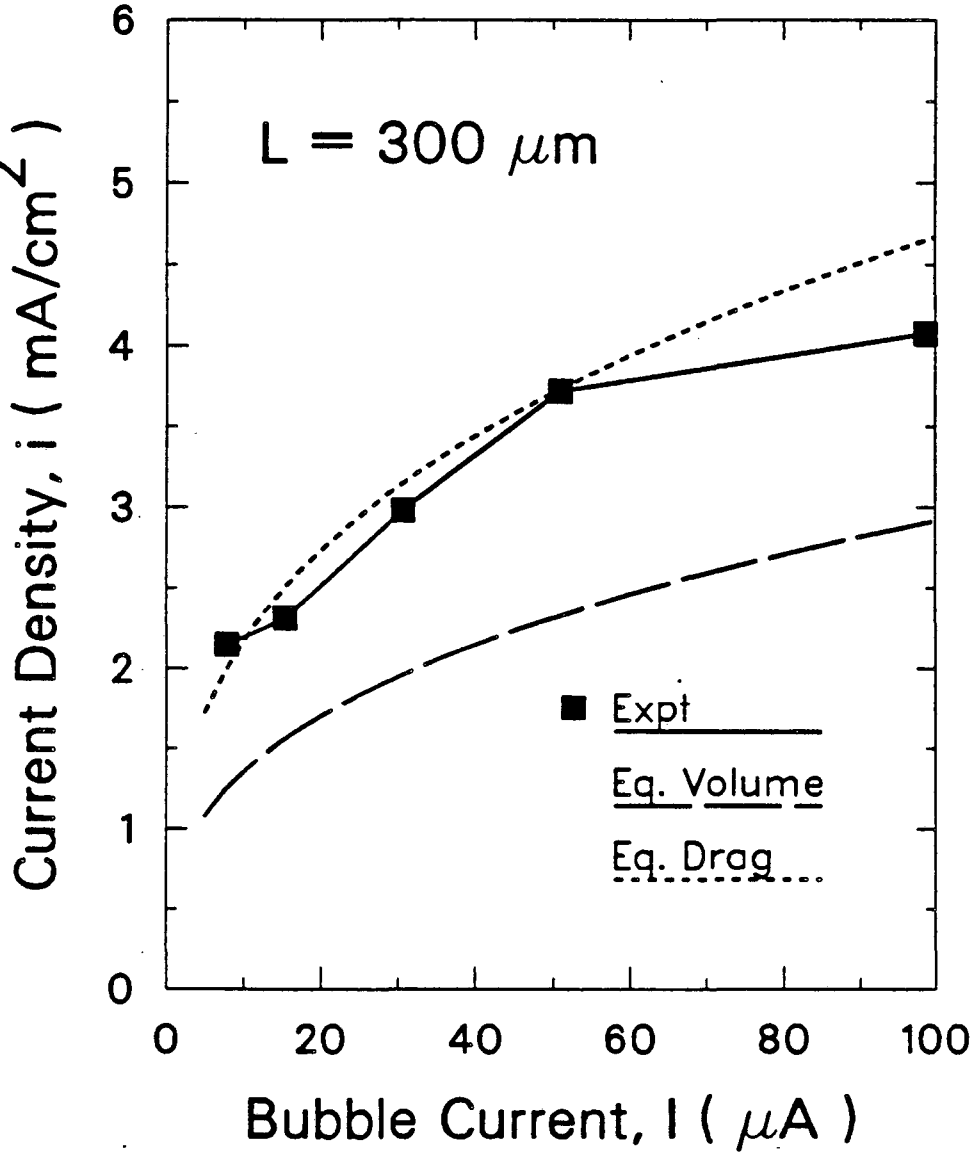

Figure 32. Comparison of mass-transfer enhancement as a function of bubble evolution rate 1) measured for a single stream of bubbles and 2) calculated for a steadily-rising cylinder, both centered at 300 μm from the electrode.

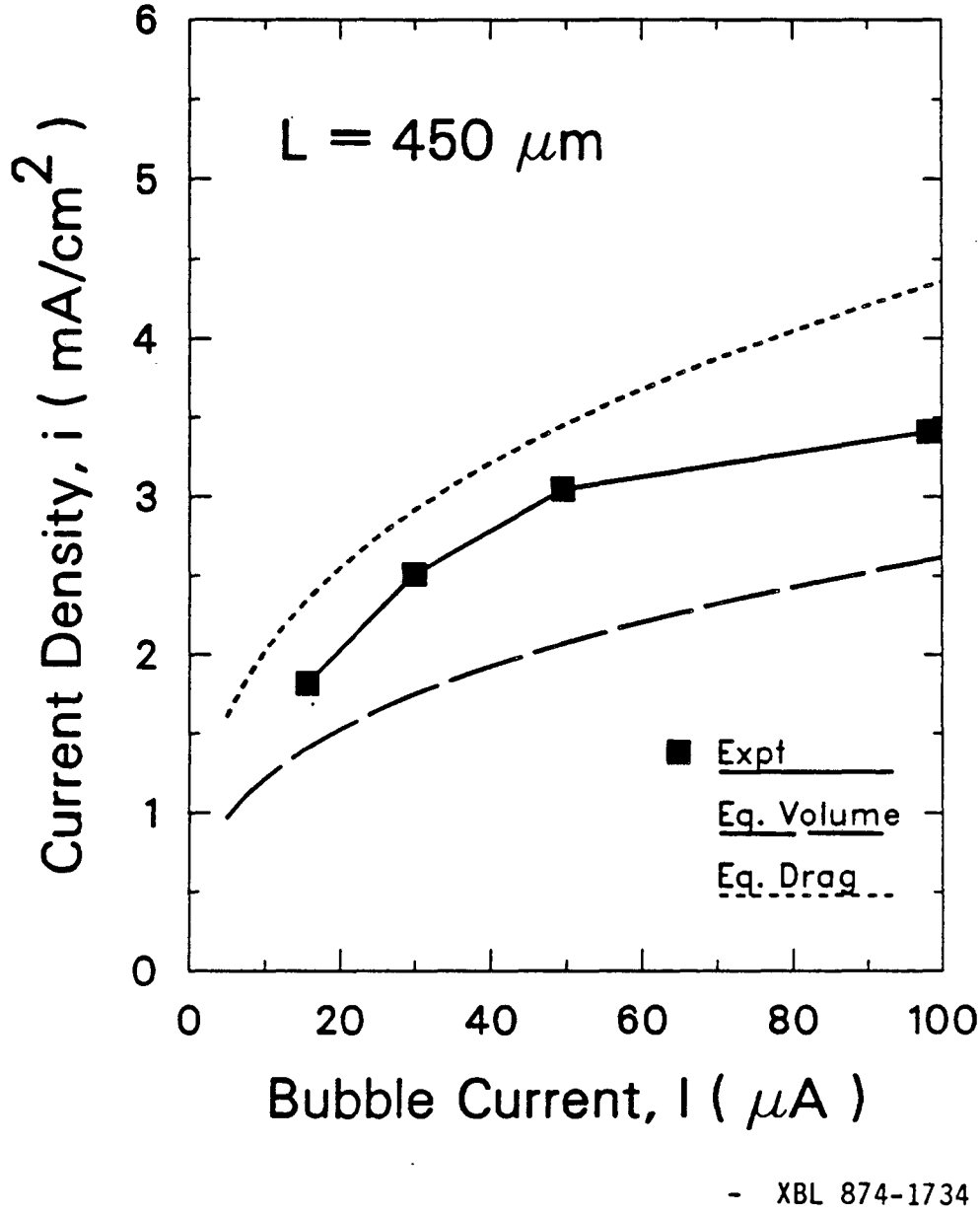

Figure 33. Comparison of mass-transfer enhancement as a function of bubble evolution rate 1) measured for a single stream of bubbles and 2) calculated for a steadily-rising cylinder, both centered at 450 μm from the electrode.

power, a result of an increased velocity gradient at the electrode surface. The experimental results are consistent with a laminar-flow model that treats the rising column of bubbles and entrained liquid as an equivalent cylinder rising with the same friction drag.

8. Chapter 3 Nomenclature

a	constant of bi-cylindrical geometry, given by Eq. (47), cm
b	slope of i vs $1/w$, given by Eq. (33)
c_i	concentration of indicator ion, mol /cm ^{3}
d	bubble diameter or equivalent channel diameter, cm
D_i	diffusivity of indicator ion, cm ^{2}/s
f	dimensionless y coordinate
F	Faraday constant, 96,487 C/eq
F_D	drag force, g-cm/s ^{2}
Gr	Grashof number
H	electrode length, cm
i	current density, A/cm ^{2}
i_{avg}	current density, averaged over electrode area, A/cm ^{2}
I_{bub}	bubble evolution rate, A
i_{nc}	natural-convection current density, A/cm ^{2}
$i_{\max}$	current density to renewal path, A/cm ^{2}
k	mass-transfer coefficient, cm/s
l	cylinder length, cm
L	distance between wall and bubble column distance or cylinder, cm
n_i	number of electrons transferred in the indicator reaction
n_g	number of electrons transferred in gas-evolution reaction

$\dot{n}_z$	cumulative bubble evolution rate below height z, s^{-1}
n/A	number of bubbles evolved per unit area, cm^{-2}
N	flux, mol/cm^2-s
$\overline{N}$	flux averaged over time, mol/cm^2-s
$\overline{N}_A$	flux averaged over time and area, mol/cm^2-s
$\overline{N}_\tau$	flux averaged over waiting time, mol/cm^2-s
$\overline{N}_{\tau,A}$	flux averaged over waiting time and area, mol/cm^2-s
p	pressure, atm
Pe	Peclet number, $v_c\, a/D_i$
R	universal gas constant, 82.055 cm^3-atm/mol-K
R_b	bubble radius, cm
R_c	cylinder radius, cm
Re	Reynolds number, $v_c\, a/\nu$
s	fraction of surface renewed per time, s^{-1}
s_i	stoichiometric coefficient of indicator ion in the electrode reaction
Sc	Schmidt number, ν/D_i
Sh	Sherwood number, dimensionless mass flux
t	time, s
T	temperature, K
u	liquid velocity, cm/s
v	gas evolution rate per unit area, cm^3/cm^2–s
v_c	cylinder velocity, cm/s
v_z	fluid velocity, cm/s
v_z^*	fluid velocity, made dimensionless with v_c
v_t	terminal velocity of rising bubble, cm/s
$\dot{V}$	volumetric gas evolution rate, cm^3/s
w	electrode width, cm
x	horizontal distance from electrode surface, cm
y	horizontal distance along electrode surface, cm
z	vertical distance along electrode surface, cm

δ	diffusion boundary-layer thickness, cm
ϵ	gas volume fraction
ς	dimensionless z coordinate
η	bi-cylindrical geometry coordinate
θ	fraction of electrode area shadowed by attached bubbles
θ_i	dimensionless concentration of indicator ion
λ	similarity variable defined by Eq. (62)
μ	viscosity, g/cm-s
ν	kinematic viscosity, cm^2/s
ξ	dimensionless x coordinate
ρ	density, g/cm^3
τ_w	waiting time between bubble departure and nucleation, s
ψ	bi-cylindrical geometry coordinate

Subscripts and superscripts

i	indicator ion
0	at the electrode surface
∞	in the bulk solution

9. Chapter 3 References

Beck, T.R., 1969, "A Contribution to the Theory of Electrolytic Chlorate Formation," *Journal of the Electrochemical Society*, Vol. 116, pp. 1038-1041.

Churchill, S.W., 1977, "A Comprehensive Correlating Equation for Laminar, Assisting, Forced and Free Convection," *The American Institute of Chemical Engineers Journal*, Vol. 23, pp. 10-16.

Cottrell, F.G., 1903, "Der Reststrom bei galvanischer Polarisation, betrachtet als ein Diffusionsproblem," *Zeitschrift für Physikalische Chemie*, Vol. 42, pp. 385-401.

Danckwerts, P.V., 1951, "Significance of Liquid-Film Coefficients in Gas Absorption," *Industrial and Engineering Chemistry*, Vol. 43, pp. 1460-1467.

Dees, D.W., 1983, *Mass Transfer at Gas-Evolving Surfaces in Electrolysis*, Ph. D. Thesis, University of California, Berkeley. (Also Lawrence Berkeley Laboratory Report No. LBL-16176)

Dees, D.W., and Tobias, C.W., 1982, "A Novel Micro-Mosaic Electrode for the Study of Transport Phenomena at Gas-Evolving Electrodes," *Extended Abstracts of the 33rd International Society of Electrochemistry Meeting*, Vol. I, pp. 456-458.

Dees, D.W., and Tobias, C.W., 1987a, "Experimental Studies of Free-Convection Mass Transfer to a Horizontal Surface with a Micro-Mosaic Electrode," *Journal of the Electrochemical Society*, Vol. 134, pp. 369-376.

Dees, D. W., and Tobias, C. W., 1987b, "Mass Transfer at Gas Evolving Surfaces: a Microscopic Study," *Journal of the Electrochemical Society*, Vol. 134, pp. 1702-1713.

Faxén, H., 1923, "Die Bewegung einer starren Kugel längs der Achse eines mit zäher Flüssigkeit gefüllten Rohres," *Arkiv för Matematik, Astronomi och Fysik*, Vol. 17, No. 27, pp. 1-28.

Fouad, M.G., and Sedahmed, G.H., 1972, "Effect of Gas Evolution on the Rate of Mass Transfer at Vertical Electrodes," *Electrochimica Acta*, Vol. 17, pp. 665-672.

Fouad, M.G., and Sedahmed, G.H., 1973, "Mass Transfer at Horizontal Gas-Evolving Electrodes," *Electrochimica Acta*, Vol. 18, pp. 55-58.

Green, M., and Robinson, P.H., 1959, "Kinetics of the Cathodic Reduction of Anions," *Journal of the Electrochemical Society*, Vol. 106, pp. 253-260.

Happel, J., and Brenner, H., 1965, *Low Reynolds Number Hydrodynamics*, Prentice-Hall, Inc., Englewood Cliffs, New Jersey, p. 327.

Higbie, R., 1935, "The Rate of Absorption of a Pure Gas into a Still Liquid During Short Times of Exposure," *Transactions of the American Institute of Chemical Engineers*, Vol. 31, pp. 365-389.

Ibl, N., and Venczel, J., 1970, "Untersuchung des Stofftransports an gasentwickelnden Elektroden," *Metalloberfläche*, Vol. 24, pp. 366-374.

Ibl, N., Adam, E., Venczel, J., and Schalch, E., 1971, "Stofftransport bei der Elektrolyse mit Gasrührung," *Chemie Ingenieur Technik*, Vol. 43, pp. 202-215.

Janssen, L.J.J., 1978, "Mass Transfer at Gas-Evolving Electrodes," *Electrochimica Acta*, Vol. 23, pp. 81-86.

Janssen, L.J.J., and Barendrecht, E., 1979, "The Effect of Electrolytic Gas Evolution on Mass Transfer at Electrodes," *Electrochimica Acta*, Vol. 24, pp. 693-699.

Janssen, L.J.J., and Hoogland, J.G., 1970, "The Effect of Electrolytically Evolved Gas Bubbles on the Thickness of the Diffusion Layer," *Electrochimica Acta*, Vol. 15, pp. 1013-1023.

Janssen, L.J.J., and Hoogland, J.G., 1973,"The Effect of Electrolytically Evolved Gas Bubbles on the Thickness of the Diffusion Layer - II," *Electrochimica Acta*, Vol. 18, pp. 543-550.

Kind, R., 1975, "Untersuchung des Stofftransports und der Rührwirkung bei gasentwickelnden Elektroden," Dissertation, ETH, Zurich.

Landau, U., and Tobias, C.W., 1976, "Mass Transport and Current Distribution in Channel Type Electrolyzers in the Laminar and Turbulent Flow Regimes," Extended Abstract No. 266, 159th Meeting of the Electrochemical Society, Washington D.C., May, 1976.

Moon P., and Spencer, D.E., 1961, *Field Theory Handbook*, Springer-Verlag, Berlin, pp. 64,89.

Roald, B., and Beck, W., 1951, "The Dissolution of Magnesium in Hydrochloric Acid," *Journal of the Electrochemical Society*, Vol. 98, pp. 277-290.

Ruckenstein, E., and Rajagopalan, R., 1980, "A Simple Algebraic Method for Obtaining the Heat or Mass Transfer Coefficients under Mixed Convection," *Chemical Engineering Communications*, Vol. 4, pp. 15-39.

Roušar, I., Kačin, J., Lippert, E., Šmirous, F., and Cezner, V., 1975, "Transport of Heat or Mass to a Electrode in the Region of Hydrogen Evolution. II," *Electrochimica Acta*, Vol. 20, pp. 295-299.

Sides, P.J., 1986, "Phenomena and Effects of Electrolytic Gas Evolution," in *Modern Aspects of Electrochemistry, No. 18*, R.E. White, J.O'M. Bockris, and B.E. Conway, Eds., Plenum Press, New York, pp. 303-354.

Stephan, K., and Vogt, H., 1979, "A Model for Correlating Mass-Transfer Data at Gas-Evolving Electrodes," *Electrochimica Acta*, Vol. 24, pp. 11-18.

Venczel, J., 1961, "Über den Stofftransport an gasentwickelnden Elektroden," Dissertation, ETH, Zurich.

Vogt, H., 1977, "Ein Beitrag zum Stoffübergang an gasentwickelnden Elektroden," Dissertation, University of Stuttgart.

Vogt, H., 1983, "Gas-Evolving Electrodes," in *Comprehensive Treatise of*

Electrochemistry, E. Yeager, J.O'M. Bockris, B.E. Conway, and S. Sarangapani, Eds., Plenum Press, New York, Vol. 6, pp. 445-489.

Vondrák, J., and Balej, J., 1970, "Influence of Mercury on Hydrogen Overvoltage on Solid Metal Electrodes. I.," *Electrochimica Acta,* Vol. 15, pp. 1653-1665.

Zuber, N., 1963, "Nucleate Boiling. The Region of Isolated Bubbles and the Similarity with Natural Convection," *International Journal of Heat and Mass Transfer,* Vol. 6, pp. 53-78.

Chapter 4. The Onset of Buoyancy-Induced Convection at a Micro-Mosaic Electrode

1. Abstract

The onset of convection is investigated for a case in which the density profile is evolving in time in a semi-infinite fluid, due to a step change in surface concentration at a rigid, conducting boundary. The limiting current technique at a micro-mosaic electrode, which is composed of 100-μm, square elements, is used to effect the concentration change and to monitor the resulting mass transfer. The equations of transient mass transport by diffusion and migration and the equation of electroneutrality are solved numerically to determine the concentration and density profiles before the onset of convection. The critical Rayleigh number based on the penetration depth of the concentration profile was found to be approximately 900, and the critical Rayleigh number based on the position and magnitude of the density profile was found to be approximately 1750. The micro-mosaic electrode is used to demonstrate the dependence of experimentally-determined onset times on the size of the sensing elements and the sensitivity of the monitoring instruments.

2. Introduction

An adverse density gradient in a horizontal fluid may induce convection if it is of sufficient magnitude and extends over a sufficient distance. The criterion for the onset of convection in such a fluid, confined between two rigid boundaries and containing a linear density profile, has become known as the Bénard-Rayleigh stability problem. Bénard-Rayleigh instability can result from temperature or concentration gradients. We consider here a variation of the Bénard-Rayleigh problem in which the density profile is nonlinear, time-dependent, and does not extend far enough into the fluid to be affected by the presence of the second boundary. This type of situation occurs in nature, as in heat transfer at the surface of a body of water. Several examples of engineering interest include thermal effects in buildings and electronic equipment, mass-transfer effects in chemical processes that involve gas-liquid contacting, and in electrochemical processes, which inherently involve concentration gradients extending into solution from a solid boundary.

Many electroanalytical techniques involve a variation of electrode potential in a stagnant medium. Even though the resulting concentration gradients may be small, significant density gradients may result due to the strong dependence of solution density on species concentrations. That this effect may be important for metal deposition reactions is more readily apparent than for redox reactions, in which there is no net removal of material at the electrode. However, the combined effects of diffusion and migration of ionic species in an electric field can result in significant density gradients in the vicinity of the electrode for redox systems as well. The key objective of this work is to quantify experimentally the criterion for

convection onset in electrochemical redox systems, and to relate this criterion to theoretical work on stability for this type of problem.

Several researchers have used electrochemical techniques to effect a density gradient at an electrode and monitor the resulting mass transfer. The earliest investigations (Wagner (1949), Wilke, Eisenberg, and Tobias (1953), and Ibl and Muller (1958)) involved determination of free-convection mass transfer at vertical electrodes. Fenech and Tobias (1960) deposited copper at limiting current from acid copper sulfate solutions onto a horizontal cathode facing upward. Depletion of the copper ion from the solution near the electrode resulted in an unstable density gradient. The buoyancy-affected mass-transfer distribution was measured using a sectioned electrode. The mass-transfer distribution could also be evaluated directly from the patterns in the electrodeposit. Boeffard (1966) extended this work using the ferri-ferrocyanide redox couple to measure the mass-transfer limited current to a nickel cathode in various orientations. Ward and Le Blanc (1984) used the ferric/ferrous couple in chloride solution to effect a density gradient between two closely-spaced electrodes. They repeated the classic Bénard-Rayleigh stability experiment by imposing a current (flux) step and monitoring the potential. At very low current densities, the potential gives a direct measure of the ratio of concentrations of Fe^{+3} to Fe^{+2} at the electrodes, from which they could estimate the difference in solution density between the two electrodes. They found the critical Rayleigh number to be 1350 ± 300. Dees and Tobias (1987) used the micro-mosaic electrode to study buoyancy-induced mass transfer at an upward-facing horizontal cathode. They observed both chaotic and regular fluctuations in the mass-transfer limited current to the electrode, sometimes occurring simultaneously on different

parts of the electrode. They also demonstrated that, while the current to a single electrode element (of area 0.01 mm^2) oscillated with a peak-to-peak amplitude as large as 83% of the average value, the current to the total electrode area (0.25 cm^2) varied by only about 3%. Apparently, the current oscillations are averaged over a large area. McLarnon, Muller, and Tobias (1982) used electrochemical and optical techniques in the study of combined free and forced convection. They deposited copper from unsupported $CuSO_4$ and used interferometry to measure the resulting concentration profile.

The above investigators have demonstrated the usefulness of electrochemical techniques for inducing density-driven flows as well as for monitoring the resulting mass transfer. The major advantage of the electrochemical technique over the more-traditional thermal method of generating a density gradient is that, by controlling the surface condition electrically, a step change in surface concentration can be effected uniformly and rapidly. The mass-transfer rate to the surface is monitored as the resulting current. This electrochemical detection of the onset of convection by monitoring the Sherwood number is more precise than flow visualization techniques; the latter cannot discern the initial stages of convection.

An important aspect of this work is the application of the electrochemical technique to the study of a classic Bénard-Rayleigh stability problem in an experiment that allows spatial resolution of 100 μm on the monitoring surface. This spatial resolution is achieved using a micro-mosaic electrode, which is designed to simulate a continuous surface. Fabricated on a 7.62-cm silicon wafer, it comprises a 10 x 10 array of 98-μm square, electrically-isolated, platinum segments on 100-μm centers. The problem we consider is the mass-transfer analog to the Bénard-

Rayleigh problem of a fluid contained in a deep cell whose lower surface is heated impulsively to a constant temperature. A potential step is imposed, resulting in a limiting current for the reduction of an indicator ion; the concentration of this species instantaneously becomes zero at the electrode. As a consequence of the ionic species transport by diffusion and migration, the fluid density near the electrode surface is less than that of the fluid above. The problem is analyzed in terms of a Rayleigh number based on the penetration depth of the reactant ion concentration profile, and one based on the position and magnitude of the density maximum. We investigate the effects of the size and sensitivity of the sensing element on the critical Rayleigh number.

3. Stability of Impulsively-Heated Fluids

Two different approaches were followed in the early theoretical work on the stability of fluids with a time-dependent density profile (reviewed by Homsy (1973) and Jhaveri and Homsy (1982)). The first workers in this area (Lick, 1965; Currie, 1967) assumed that the disturbance grows much faster than the evolving diffusive profile, so that one can examine the marginal stability of the evolving base state at a given time. Their approach has been criticized in the literature as not valid; this "quasi-steady state" assumption is common in engineering practice, however, and can be used subject to scaling arguments which demonstrate its applicability. For the case of a sudden change in surface concentration (or temperature), the parameter that should be examined is the Schmidt (or Prandtl) number, the ratio of momentum diffusivity to mass (or thermal) diffusivity. One would not expect the

quasi-steady state assumption to be valid for low values of the Schmidt number. In the case of a time-dependent surface condition, one would also not expect this type of analysis to be valid for high rates of surface heating. After extensive comparison of his own experimental data to the early theories, Davenport (1972) concluded that the problem with the quasi-steady state models is not with the quasi-steady state assumption itself, but that a destabilizing influence had been erroneously attributed to the bulk fluid. (For relatively deep pools, $\alpha t / h^2 < 0.1$, Currie's model predictions were a factor of 40 below Davenport's experimental results, even for high Prandtl number.)

The second early theoretical approach is that first used by Foster (1965a, 1968) and followed by several others (Elder (1968), Mahler *et al.* (1968), Mahler and Schechter (1970), and Gresho and Sani (1971)). In this approach the linear stability equations are integrated numerically and the growth rate of an initial velocity disturbance is followed in time. The onset time is determined as the time at which the magnitude of the disturbance has increased to a given multiple, or amplification, of the magnitude of the initial disturbance. The main objection to this approach is that the linearized equations may not be valid during the growth of the disturbance. In addition, the initial disturbance itself and the amplification factor at which one would presume that convection could be observed are somewhat arbitrary. Foster (1968) presented his results in terms of the times to achieve disturbance amplifications of 10 and 10^8. Gresho and Sani (1971) used an amplification factor of 1000.

In a recent study, Jhaveri and Homsy (1980, 1982) report an elegant stability analysis of the problem which retains quadratic interactions and uses

thermodynamic fluctuations as the disturbances. Their stability analysis was conducted for a step change of temperature, and also for a linear change, at a free surface with a Prandtl number of 7. Their results are presented in terms of a time-dependent, critical Rayleigh number Ra_t , which is the Rayleigh number based on total fluid depth multiplied by the dimensionless time; the total depth is removed from the problem with this scaling, and the Rayleigh number is based on a nominal penetration depth δ, where $\delta \equiv \sqrt{\alpha t}$. The time of onset of convection is defined as the time at which the thermal flux, or Nusselt number Nu, deviates from convection-free behavior by a given percentage. For a Prandtl number of 7, they found that the time-dependent Rayleigh number does not vary significantly if the Nusselt number deviation criterion is changed over a range of 1 to 10%. This result implies that the disturbance grows quickly relative to the evolution of the diffusive profile. Comparison of Jhaveri and Homsy's results at Pr = 7, for a step change at a free surface, to Foster's 1968 analysis shows that Jhaveri and Homsy's result of $Ra_t = 349$ (Nu variation of 5%) lies between Foster's limits of 61 (amplification = 10) and 630 (amplification = 10^8). (Jhaveri and Homsy's Ra_t corresponds to Foster's $t_c^{3/2}$.)

The early experimental investigations of this problem involved thermal studies (Spangenberg and Rowland (1961), Foster (1965b)), typically using evaporative cooling of water, for which the Prandtl number is approximately 7. In these experiments, neither surface temperature nor thermal flux is exactly constant; the surface temperature and evaporation rate are governed by the coupled mass and energy transfer at the surface. This type of experiment is also quite sensitive to trace impurities which affect the surface tension and hence the rigidity of the

surface. How dramatic this effect can be for water was shown theoretically by Berg and Acrivos (1965), who found that trace contamination, as low as 1% of that required to form a close-packed monolayer, should stabilize a water layer up to a depth of 1 cm. The most important result from these early experiments with water is that, for a deep cell, $\delta/h < 0.3$, the critical time for onset of convection is independent of total fluid depth.

The absorption of an inert gas at a free surface overcomes some of the difficulties associated with evaporative cooling. Plevan and Quinn (1966), Blair and Quinn (1969), and Mahler and Schechter (1970) used this technique to investigate the onset of buoyancy-induced convection. In a gas absorption experiment, the surface boundary condition can be altered by changing the pressure of the absorbing gas above the liquid. The concentration of dissolved gas at the surface is directly proportional to the gas pressure; the constant of proportionality is the Henry's constant. A sudden change in surface concentration can be effected, and an analytic solution is obtained for the concentration profile. The density of the fluid is linearly dependent on the dissolved gas concentration over a wide range, so that the density profile can be derived as well. With this technique, the surface properties will be sensitive to the presence of trace impurities of surface-active agents in the fluid; the effect can be minimized (or maximized), however, through the choice of the gas-liquid pairs.

Davenport and King (1974) conducted an extensive series of experiments with fluids covering a wide range of Prandtl numbers (0.7 to 8500). They contained the fluids between two plates and adjusted the heating rate to maintain either a constant lower plate temperature, or one which varied as a prescribed function of

time. Results are presented in terms of the Rayleigh number based on the nominal penetration depth described above. They also used a Rayleigh number Ra_l based on the equivalent linear-segment penetration depth originally proposed by Lick (1965):

$$l \equiv 2 \int_0^\infty \frac{(T - T^\infty)}{(T^0 - T^\infty)}\, dy \quad , \tag{1}$$

which, for the case of constant surface temperature, is equal to $\frac{2}{\sqrt{\pi}} \sqrt{4\alpha t}$. When Davenport and King compared their results to Foster's model, they found that the apparent amplification factor at convection onset decreases as the Prandtl number increases. Their value of Ra_l was independent of Prandtl number, and of total fluid depth, and was found to be approximately 1700, the critical Rayleigh number for the classic time-independent problem of a fluid contained between two rigid walls (Jeffreys, 1928).

The experimental procedure used in this study is closely related to the gas absorption experiments described above. In this study, an electrochemical technique is used to effect the change in surface concentration uniformly and rapidly. Our treatment of experimental results most closely parallels that of Davenport and King. We use a Rayleigh number based on penetration depth of the reacting species. The multi-component species problem that we encounter results in a density profile with a slight maximum so that we will also use a Rayleigh number based on the position and magnitude of the density maximum, as suggested by Bogar and Westwater (1967). The Schmidt number is high for the present case ($\sim$ 2300, typical of aqueous solutions), so that the quasi-steady state analysis should be applicable.

4. Experimental

The micro-mosaic electrode used in this study has been described in the preceding chapter. In the experiments presented here, the cell holding the micro-mosaic is oriented horizontally with the electrode facing upward. The cell is shown in Figure 1. We impose a potential step to the potential region of limiting current for the reduction of Fe^{+3} to Fe^{+2} from $Fe_2(SO_4)_3$ / H_2SO_4 solutions. Two different bulk solutions were used, 0.0484 M $Fe_2(SO_4)_3$ in 0.5 M H_2SO_4 (Solution 1) and 0.110 M $Fe_2(SO_4)_3$ in 1.0 M H_2SO_4 (Solution 2). The current responses of the electrode segments to the potential step are monitored and stored digitally.

Care was taken to ensure that the solution concentration was uniform and that the solution was quiescent prior to the start of an experiment. All cell parts were cleaned with distilled, deionized water and methanol. Reagent grade chemicals were used. Surface-tension driven flows were not a concern in our experiments, the electrode itself providing a rigid surface, so ultra-clean conditions were not a necessity. The cell temperature was monitored, but not controlled, in the experiments. Thermal effects due to heat generation are insignificant in our system. Even if all of the power dissipated in the system were released at the electrode surface, the density difference resulting from thermal effects would be less than 1% of that resulting from mass-transfer effects.

5. Analysis of the Base-State Profile

The description of a multi-component, electrochemical system is necessarily

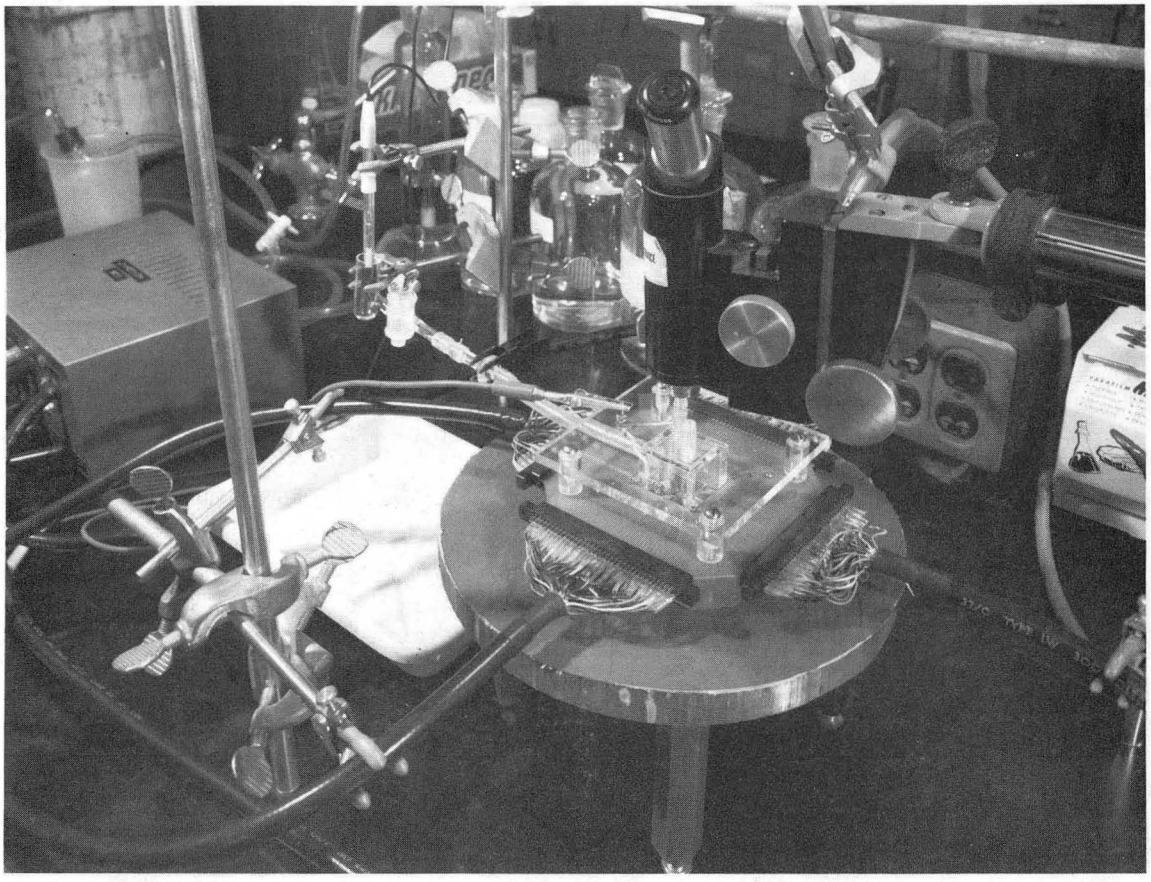

CBB 820-9965

Figure 1. Electrochemical cell that holds the micro-mosaic electrode in horizontal orientation (From Dees, 1983).

more complex than that of a thermal system. This analysis is conducted to obtain an estimate for the surface concentration of each of the ions in solution. From the surface concentrations, we can calculate the solution density at the electrode surface. We also obtain the concentration and density profiles through the solution and the flux at the surface (current) as a function of time.

A potential step to the limiting-current regime involves a sudden change in electrode potential to a value at which the rate of reaction is limited only by the mass transfer of the reactant ion to the surface. This step in potential results in an instantaneous drop in the concentration of the reactant ion Fe^{+3} at the electrode. At the same time, the reaction product Fe^{+2} starts to build up at the electrode. In the absence of convection, the region of depleted Fe^{+3} and enhanced Fe^{+2} extends farther and farther into the solution with time, increasing the resistance for mass transport to the electrode surface. The concentrations of the major supporting-electrolyte species, H^{+} and SO_4^{-2}, are governed by diffusion and by migration in the electric field in such a way that solution electroneutrality is maintained.

The equation governing the one-dimensional mass transport of species i due to diffusion and migration is (Newman, 1973)

$$\frac{\partial c_i}{\partial t} = D_i \frac{\partial^2 c_i}{\partial y^2} + z_i u_i F \frac{\partial \left(c_i \frac{\partial \phi}{\partial y} \right)}{\partial y} \quad . \tag{2}$$

u_i is the ionic mobility of species i and, for solutions dilute in species i, can be related to the diffusion coefficient by the Nernst-Einstein relation:

$$u_i = \frac{D_i}{RT} \quad . \tag{3}$$

The condition of electroneutrality is the other equation required to solve for the species concentrations and the potential, ϕ:

$$\sum_{i}^{4} z_i c_i = 0 \quad . \tag{4}$$

Initially, each species is at its bulk concentration,

$$c_i(0,y) = c_i^{\infty} \quad . \tag{5}$$

The boundary conditions at the electrode surface are

$$c_{Fe^{+3}}(t,0) = 0 \tag{6}$$

and

$$D_i \left(\frac{\partial c_i}{\partial y} + \frac{z_i F}{RT} c_i \frac{\partial \phi}{\partial y} \right) = \frac{s_i}{s_R} D_R \left(\frac{\partial c_R}{\partial y} + \frac{z_R F}{RT} c_R \frac{\partial \phi}{\partial y} \right) \quad , \tag{7}$$

where R refers to the reactant species Fe^{+3}, and s_i is the stoichiometric coefficient of species i when the electrode reaction is written as

$$\sum_{i} s_i M_i \rightarrow n e^{-} \quad . \tag{8}$$

For a nonreacting species, s_i is zero. The electrode reaction in our case is

$$- Fe^{+3} + Fe^{+2} \rightarrow e^{-} \quad . \tag{9}$$

The net flux of each of the non-reacting ions, H^{+} and SO_4^{-2}, is zero at the electrode surface. Far away from the electrode, the species concentrations are equal to their initial bulk values,

$$c_i(t,\infty) = c_i^{\infty} \quad . \tag{10}$$

For the H_2SO_4 concentration range of interest here (0.5 to 1.0 M) the dissociation of HSO_4^- is not complete. To account for the effect of bisulfate dissociation on solution density, the diffusion and migration equation (Eq. (2)) is written for the total hydrogen concentration ($c_{H^+} + c_{HSO_4^-}$) and for the total sulfate concentration ($c_{HSO_4^-} + c_{SO_4^{-2}}$), following Hsueh and Newman (1971). This formulation of the conservation equations is valid provided the dissociation equilibrium reaction of HSO_4^- is fast. The boundary conditions of no net flux at the electrode (Eq. (7)) apply for the total hydrogen and total sulfate. Eq. (2) as written for Fe^{+3} and Fe^{+2}, with boundary conditions (6) and (7), and the electroneutrality equation apply as before. The additional equation required to solve for bisulfate concentration is the dissociation equilibrium,

$$\frac{c_{H^+} c_{SO_4^{-2}}}{c_{HSO_4^-}} = K' \quad . \tag{11}$$

The dependence of the thermodynamic dissociation constant K' on ionic strength, determined by Young *et al* (1959) from Raman spectra, is given by

$$K' = K \exp\left(\frac{5.29\sqrt{I_r}}{1 + 0.56\sqrt{I_r}}\right) \tag{12}$$

over a range of 0 to 3-M H_2SO_4, where $K = 1.04 \times 10^{-5}$ mol /cm^3 and the true ionic strength of the bulk solution I_r in mol /l is

$$I_r = 1/2 \sum_i 1000\, c_i^{\infty} z_i^2 \quad . \tag{13}$$

The above set of equations describes the species transport in a quiescent solution. The equations may be transformed to ordinary differential equations using the similarity variable,

$$\eta \equiv \frac{y}{\sqrt{4D_R\, t}} \quad . \tag{14}$$

The transformed equations and boundary conditions are given in the Appendix. The set of transformed, coupled, ordinary differential equations was solved using the Galerkin finite-element method with linear basis functions and weighting functions.† The mesh was refined until the solution values remained unchanged to 5 significant figures. One thousand equally-spaced elements were used over a range of η from 0 to 4. Because the equations are nonlinear, a Newton-Raphson iterative technique was used. An IMSL Library subroutine (1982) was used to solve the linearized equations at each iteration. The solution was considered to be converged when the root mean square of the corrections to the previous iteration's values was less than 10^{-10}. The number of iterations required to achieve convergence depends on the initial guess, but usually no more than four were necessary, consuming 16 seconds of CPU time per iteration on a Vax 8600 computer.

The current is proportional to the derivative of the concentration of reactant ion at $\eta = 0$, which is a function of the diffusion coefficients and bulk concentrations of all of the ions:

† A Fortran program that solves the same set of coupled equations using a finite-difference method is given in Newman (1973, pp. 423-24)

$$i = \frac{nFD_R}{s_R\sqrt{4D_R\,t}}\left(\frac{dc_R}{d\eta}\right)_{(\eta=0)} \quad . \tag{15}$$

The solution to the above equations reduces to the Cottrell equation (Bard and Faulkner, 1980) for the current resulting from a potential step when the reactant is in an infinitely-supported solution. In such a case, transport of the reactant ion by migration is negligible, and $\left(\frac{dc_R}{d\eta}\right)_{(\eta=0)} = \frac{2c_R^{\infty}}{\sqrt{\pi}}$.

The reason for a density difference across the diffusion layer can best be seen by writing the electrode reaction as

$$Fe_2(SO_4)_3 + 2e^- \rightarrow 2FeSO_4 + SO_4^{-2} \quad . \tag{16}$$

SO_4^{-2} is transported away from the electrode and H^+ is transported to the electrode, maintaining electroneutrality. The net result is that the solution near the electrode is less dense than that in the bulk. The extent to which each of these two ions is accumulated or depleted at the electrode surface is a complex function of the diffusion coefficients and charges of *all* ionic species present in the electrolyte.

The density profile is obtained from the concentration profiles using

$$\rho = c_1 + \sum_i \alpha_i\ c_i \tag{17}$$

where α_i is the densification coefficient for species i. Since ionic species may occur only in the form of neutral pairs, the densification coefficient of any one of the ionic species may be set to zero without loss of generality. For convenience, SO_4^{-2} is chosen because it is common to all of the neutral pairs; the densification effect of SO_4^{-2} is then included with that of the associated cation. Since the major

electrolyte species is H_2SO_4, the densification coefficients of H^+ and HSO_4^- were obtained by a least-squares fit of H_2SO_4 solution density data (Weast, 1976) from 0.4 to 1.09 M. The densification coefficient for Fe^{+3} was estimated in two ways: (1) by least-squares fit of literature density information for pure $Fe_2(SO_4)_3$ solutions (Perry and Chilton, 1973), and (2) by fitting our own density measurements for the $Fe_2(SO_4)_3/H_2SO_4$ system. These two values differed by 4.2% An estimate for $\alpha_{Fe^{+2}}$ was obtained using literature data (Perry and Chilton, 1973) for pure $FeSO_4$ solution densities.

The diffusion coefficients for H^+, HSO_4^- and SO_4^{-2} were taken from literature data (Newman, 1973, p.230). The diffusion coefficient for Fe^{+3} was obtained from the initial part of the potential step experiment before convection onset (Eq. (10)). The product Fe^{+2} diffusion coefficient was calculated from that of Fe^{+3} on the basis of published values (Dean, 1979) of the equivalent ionic conductances of the two ions.

6. Results and Discussion

Our main objective in solving the model presented in the previous section is to calculate the concentration profiles and density profile for the base state. Had we been depositing a metal from an unsupported electrolyte, rather than using a redox reaction, the equations would reduce to the thermal equations for which an analytic solution is available. The advantage of the redox system is that there are no surface-roughening effects, which commonly occur in metal deposition.

The concentration profile of the reactant ion is shown in Figure 2 for a

potential step using Solution 1. The equivalent, linear-segment penetration depth l_c was calculated from the mass-transfer analog to Eq. (1),

$$l_c \equiv 2 \int_0^\infty \frac{(c_R - c_R^\infty)}{(c_R^0 - c_R^\infty)}\, dy \quad . \tag{18}$$

l_c was found to correspond to a dimensionless distance η_c of 1.1492 for Solution 1 and 1.1498 for Solution 2. The density profile is calculated from the ion concentration profiles according to Eq. (17) and is shown in Figure 3 for Solution 1. There is a slight density maximum in the density profile (also noted by Selman and Newman, 1971), which occurs at η_m of 1.344 for Solution 1 and 1.340 for Solution 2. Surface and bulk concentrations and the parameters used in the model are given in Table 1.

An example of the current response of a single segment to a potential step to limiting current is given in Figure 4. The time to onset of convection is more clearly seen when the same data are plotted versus the inverse square root of time, as suggested by the similarity variable. This curve, shown in Figure 5, is typical of those obtained for most of the working segments. There are, however, some segments, each of which was adjacent to a non-working segment, for which the inverse-square-root-of-time plot exhibits significant curvature throughout the period before convection starts. Because of a non-functioning adjacent segment, the assumption of one-dimensional diffusion is invalid. An example is given in Figure 6. Although the onset of convection is still observable, these segments were not used in the determination of the critical Rayleigh number. Only those segments that showed no appreciable curvature and had straight-line correlation coefficients

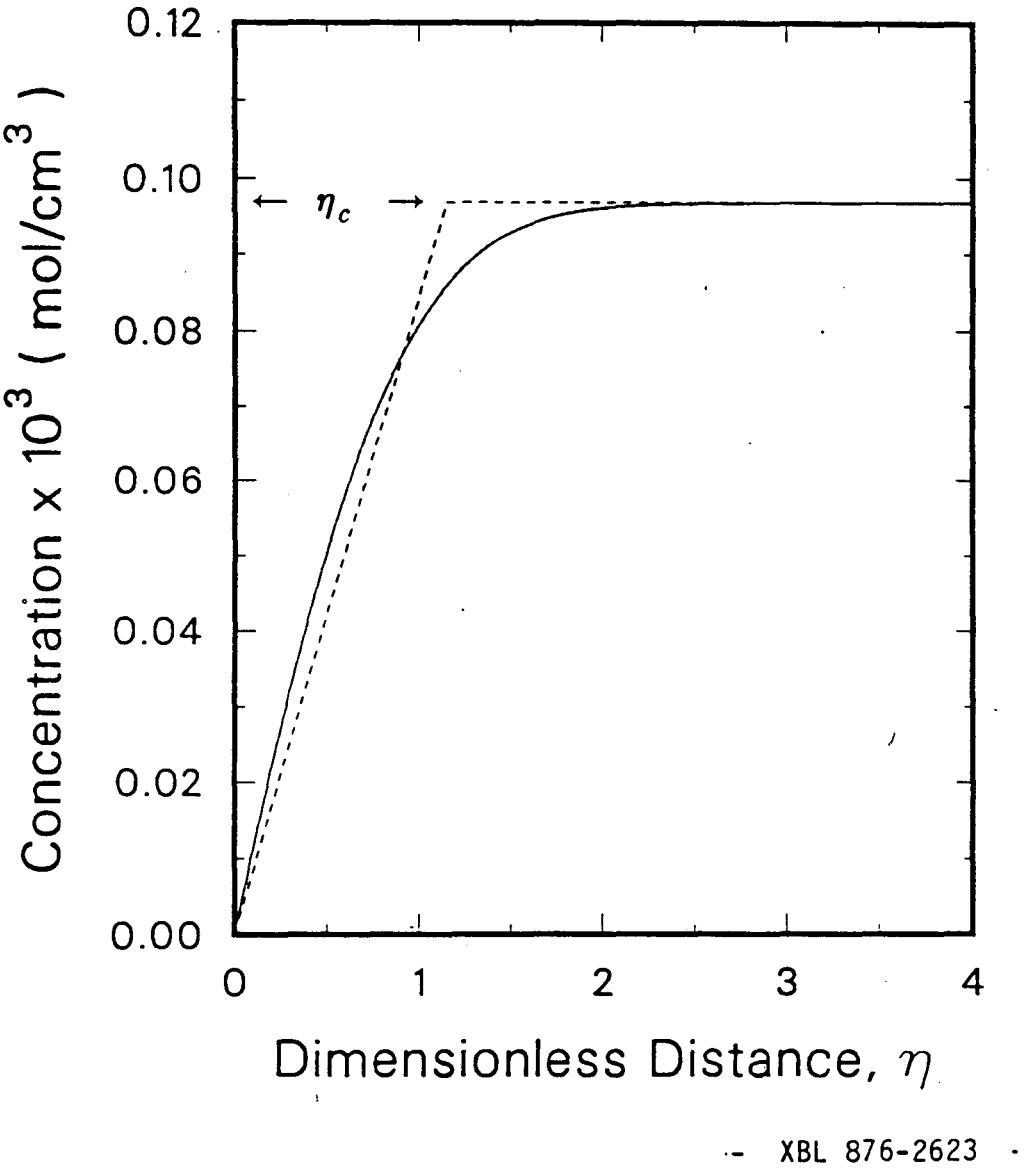

Figure 2. Calculated concentration profile of reactant Fe^{+3} following a potential step to limiting current. Dimensionless penetration length η_c is shown.

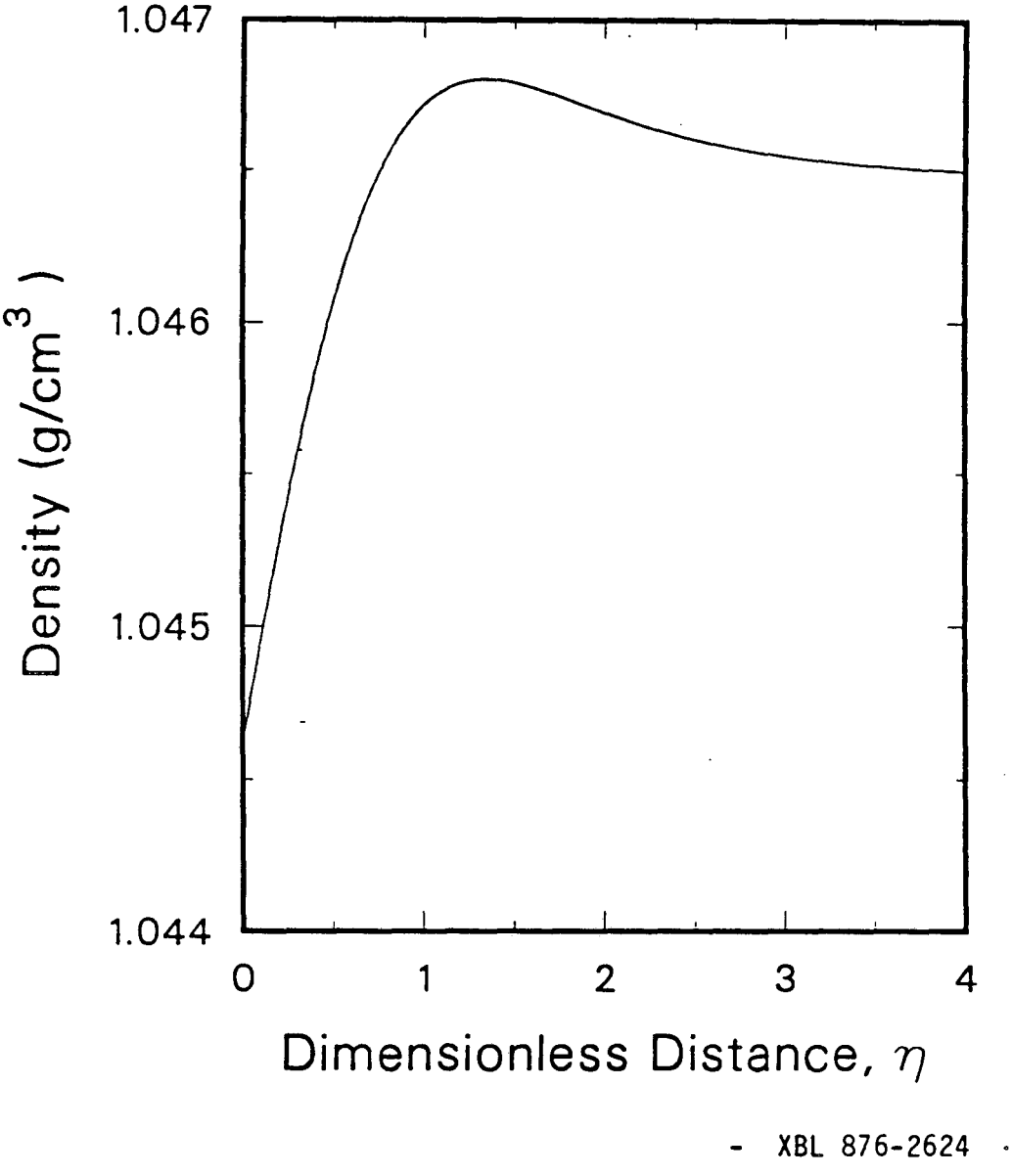

Figure 3. Calculated density profile following a potential step to limiting current for bulk Solution 1.

Table 1. Model Input Parameters and Surface Concentrations

			Solution 1		Solution 2	
Species	$D_i \times 10^6$ $\left(\frac{cm^2}{sec}\right)$	α_i $\left(\frac{g}{mol}\right)$	$c_i^{\infty} \times 10^3$ $\left(\frac{mol}{cm^3}\right)$	$c_i^{0} \times 10^3$ $\left(\frac{mol}{cm^3}\right)$	$c_i^{\infty} \times 10^3$ $\left(\frac{mol}{cm^3}\right)$	$c_i^{0} \times 10^3$ $\left(\frac{mol}{cm^3}\right)$
H^+	93.12	16.99	0.63385	0.67393	1.30743	1.39528
HSO_4^-	13.3	56.12	0.36615	0.35552	0.69257	0.67224
SO_4^{-2}	10.65	0.0	0.27920	0.25496	0.63743	0.57977
Fe^{+2}	5.135	141.65	0.0	0.09576	0.0	0.21825
Fe^{+3}	4.351	160.34	0.0969	0.0	0.220	0.0
			$\rho^{\infty} = 1.0465$		$\rho^{\infty} = 1.0960$	
			$\rho^{0} = 1.0446$		$\rho^{0} = 1.0920$	
			$\rho^{m} = 1.0468$		$\rho^{m} = 1.0966$	

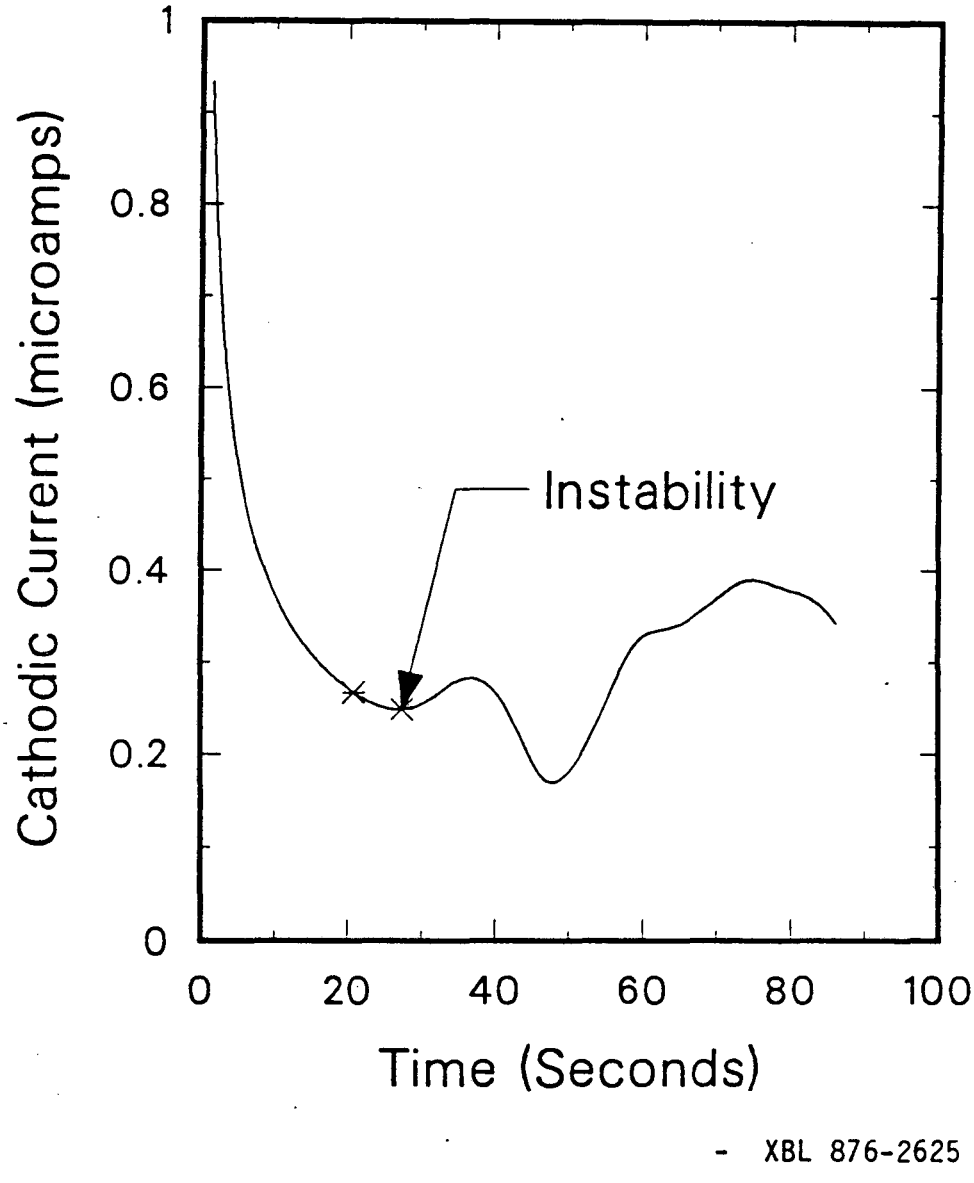

Figure 4. Current response of a single segment following a potential step to limiting current.

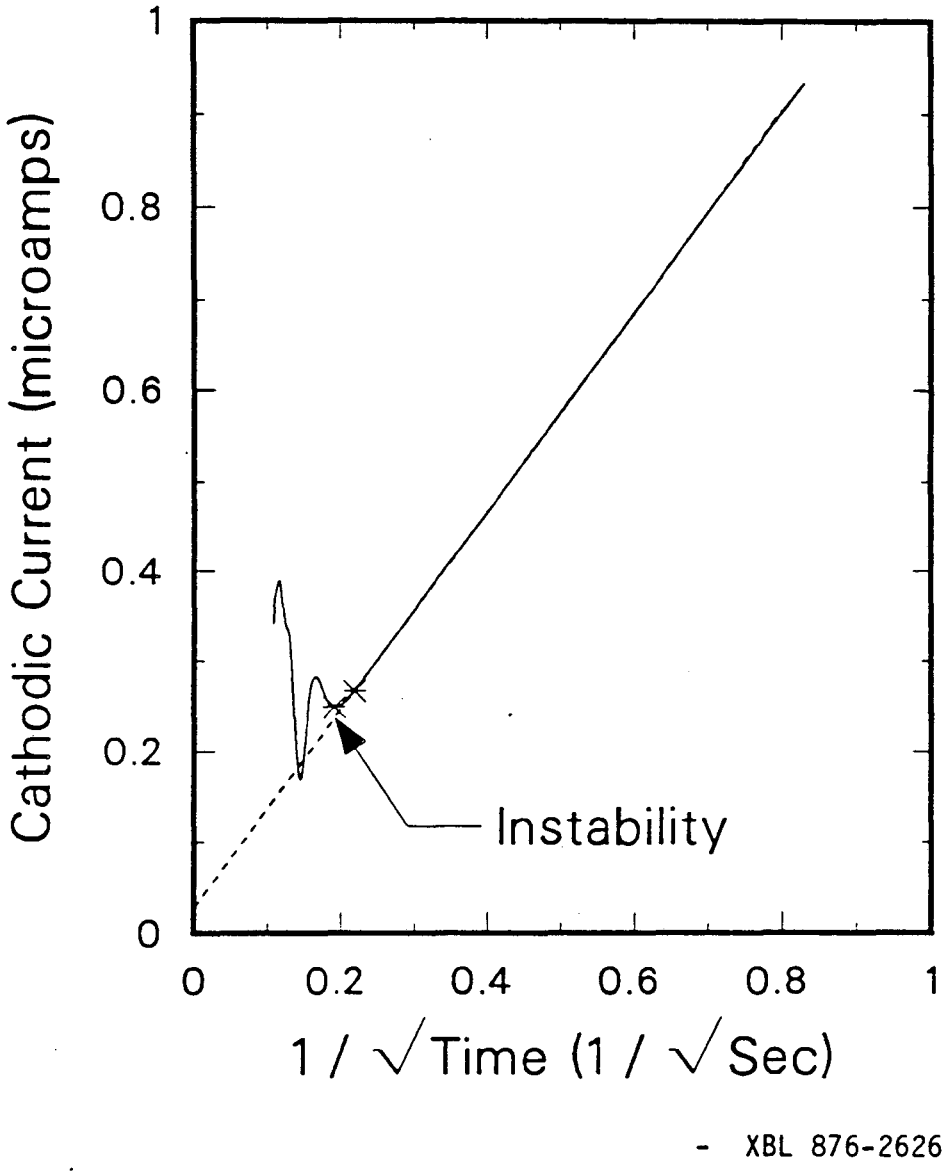

Figure 5. Current response from Figure 4 plotted versus the inverse square root of time. The first (right) marker shows the last point used for calculating the diffusion coefficient. The second marker (left) shows the point of 5% deviation from linearity.

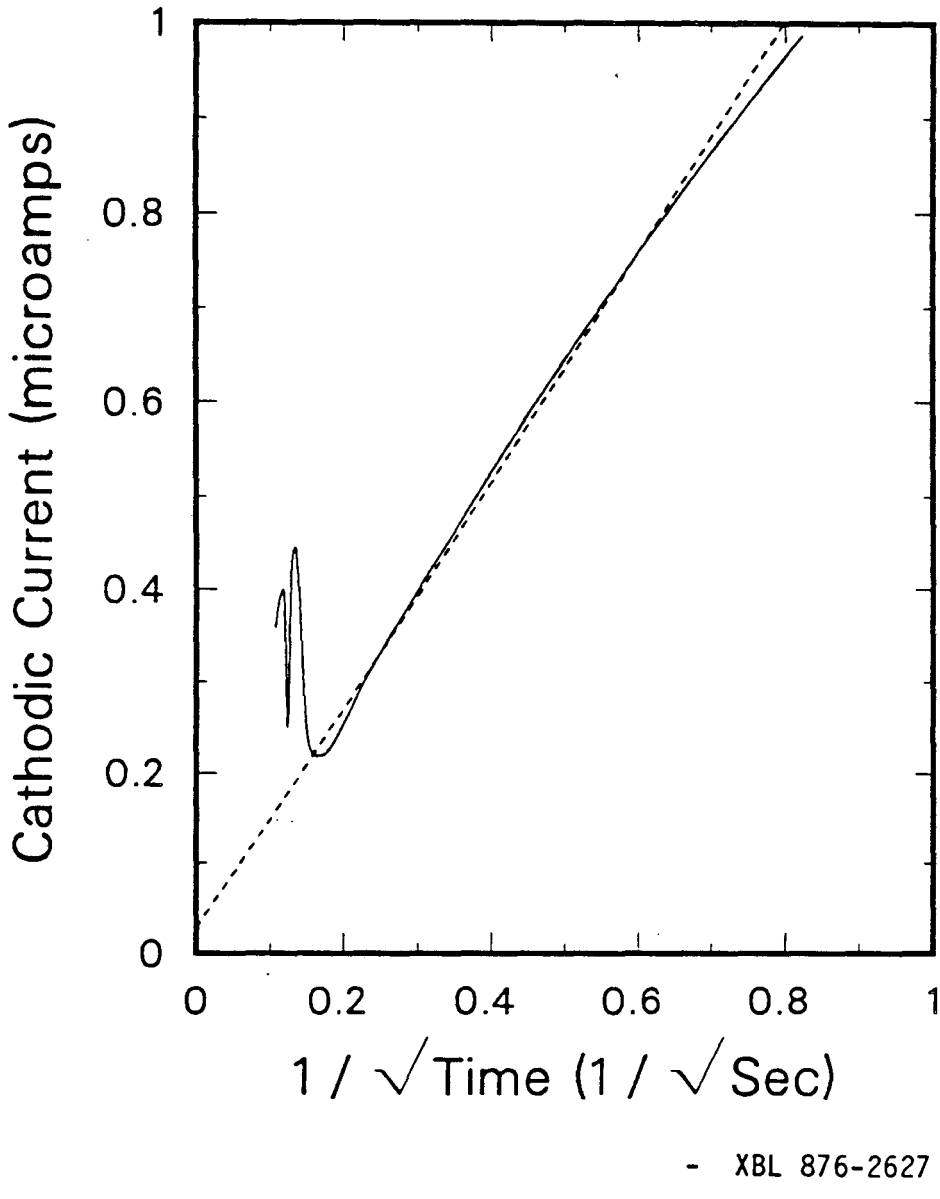

Figure 6. Current response of a single segment following a potential step to limiting current, showing curvature due to an adjacent non-working segment.

greater than 0.999 were used. Typically data from 50 to 60 segments were deemed acceptable.

The diffusion coefficient of Fe^{+3} was calculated from data obtained from each of 55 segments for an experiment using Solution 1. The average value is 4.335 $\times 10^{-6}$ cm ^{2}/sec, with a standard deviation of 0.32 $\times 10^{-6}$ cm ^{2}/sec. The total current response for all 55 segments from the same experiment is plotted versus time in Figure 7, and versus the inverse square root of time in Figure 8. The diffusion coefficient for Fe^{+3} from Figure 8 is 4.351 $\times 10^{-6}$ cm ^{2}/sec. The correlation coefficient for straight-line behavior up to the first marker is greater than 0.9999.

The critical Rayleigh number based on the concentration profile is

$$Ra_l \equiv \frac{\Delta\rho \; g l_c^{\,3}}{\rho^{\infty} \nu D_R} \quad , \tag{19}$$

where l_c , calculated from the model results (Eq. (18)), is

$$l_c = \eta_c \sqrt{4 D_R \, t_c} \quad . \tag{20}$$

$\Delta\rho$ is calculated from

$$\Delta\rho = \sum_i \alpha_i \left(c_i^{\infty} - c_i^{0} \right) \quad . \tag{21}$$

t_c was identified as the time when a deviation greater than 5% occurred in the current (Sherwood number) versus inverse-square-root-of-time plot. The choice of a 5% deviation criterion is somewhat arbitrary; however, Jhaveri and Homsy (1982) predicted that the critical Rayleigh number should be fairly insensitive to this

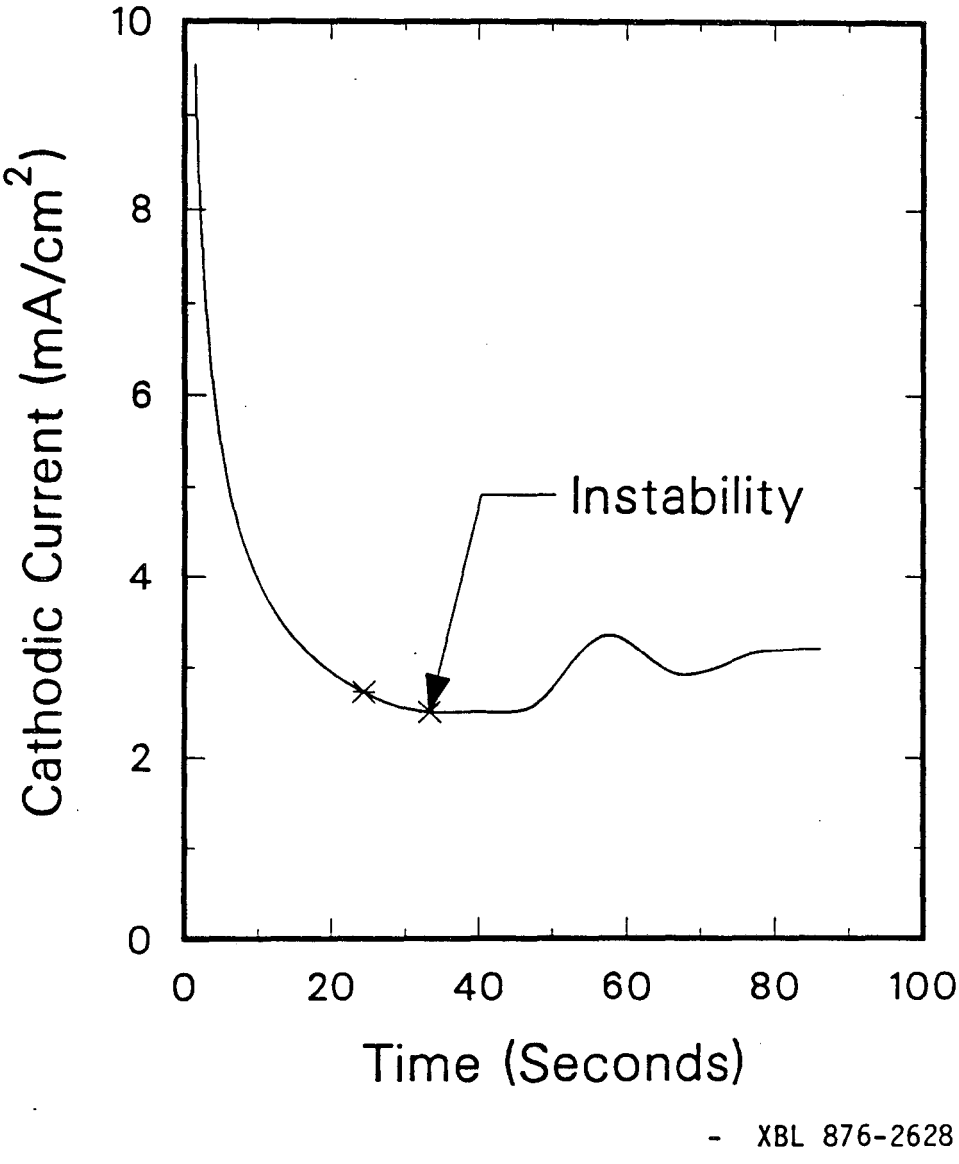

Figure 7. Total of the current responses obtained from all 55 segments following a potential step to limiting current.

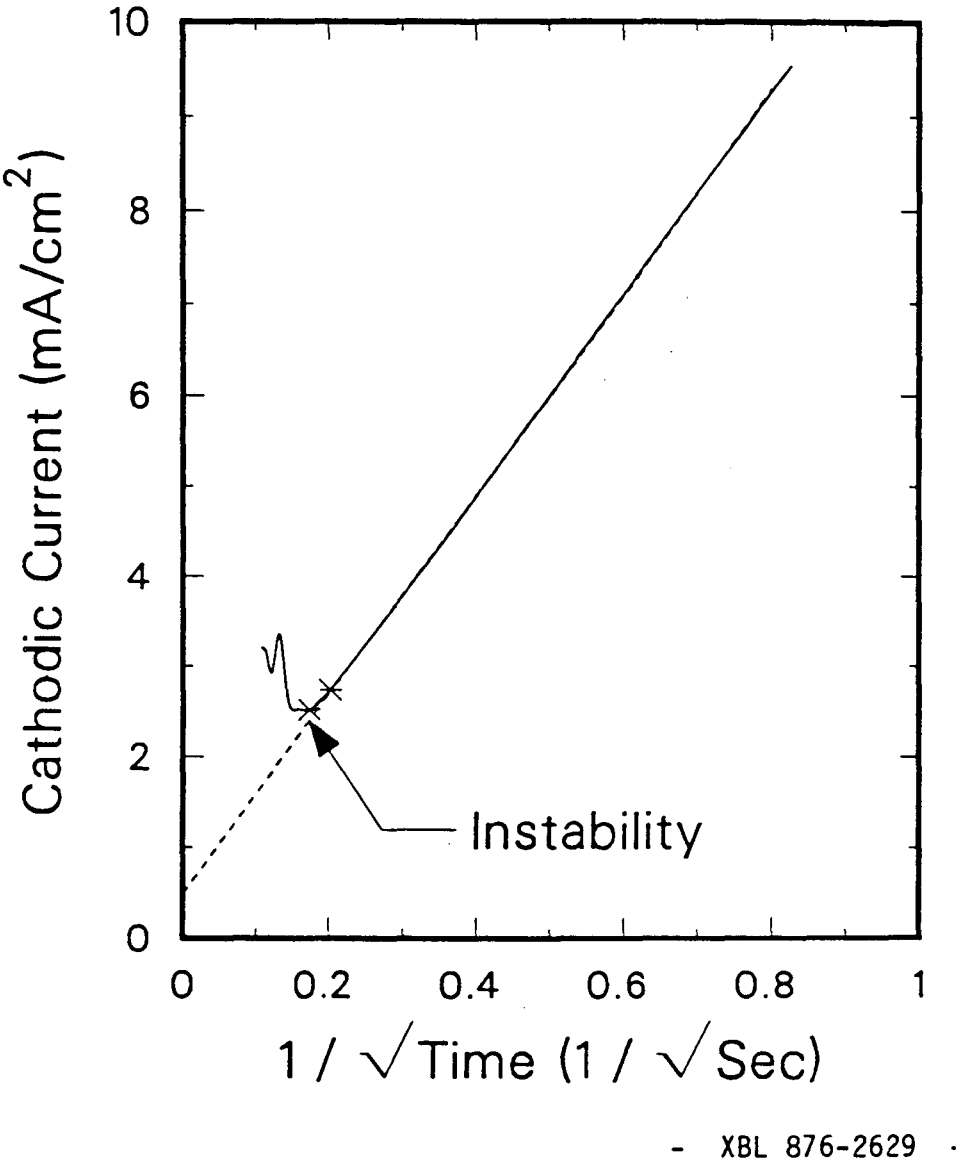

Figure 8. Inverse-square-root-of-time plot of the total current response obtained from all 55 segments following a potential step to limiting current.

criterion in the range between 1 and 10%.

The critical time for onset of convection was determined for each of the acceptable segments. The average value for Solution 1 is 30.8 seconds, with a standard deviation of 6.6 seconds. The corresponding Rayleigh number is 766, and l_c is 266 μm. The critical time determined from the curve of the sum of all of the segments (Figures 7,8) is 33.3 seconds, which gives a Ra_l of 861 and l_c of 277 μm.

Upon repeating the experiments using different electrodes, the measured onset times were 32.5, 32.9, and 34.1 seconds; the average value for the four runs is thus 33.2 seconds with a maximum deviation of 1.9 seconds. Blair and Quinn (1969) obtained an average onset time of 27 seconds with a range of 24 to 30 seconds in a typical set of gas-absorption experiments. The good reproducibility we observe is an indication of the precision of the electrochemical technique.

Three experiments were carried out using the more dense Solution 2. The average of the individual segments in one experiment was 20.5 with a standard deviation of 2.9 seconds. The onset time measured with the entire electrode was 21.9 in the same experiment. In repeated experiments, onset times for the entire electrode of 22.7, and 21.8 were measured. The average value, 22.1 seconds, corresponds to a penetration length l_c of 225 μm and Ra_l of 945.

The appropriate comparison of our data to theory would involve consideration of the model of Jhaveri and Homsy (1982); however, they did not analyze the problem with a rigid surface or for Prandtl number other than 7. The most direct comparison to theory that we can attempt is to consider Foster's (1968) limiting values obtained using amplification theory. Our Ra_l values are very near those of Foster for $Pr \rightarrow \infty$. He reports Ra_l of approximately 900 for an

amplification factor of 10 and approximately 5000 for an amplification factor of 10^8. Davenport and King (1974) found that, with increasing Pr, their experimentally-determined values of Ra_l decreased to an amplification factor of 10 according to Foster's theory.

6.1. *The Effect of a Density Maximum*

The effect of a density maximum, which occurs in the multi-component diffusion problem encountered here, was first treated by Veronis (1963) in connection with the problem of thermal gradients in water near 3.98 ° C confined between two boundaries. The topic remains a subject of current investigation (see Blake *et al.*, 1984, and references therein). The problem of determining the relevant length for such a system has not been resolved (see, for example, Merker *et al.*, 1979), and is even more complex for the semi-infinite system which we encounter. The linear-segment penetration depth was originally proposed (Lick, 1965) to represent an equivalent integrated buoyant force,

$$l \equiv 2 \int_0^\infty \frac{(\rho - \rho^\infty)}{(\rho^0 - \rho^\infty)}\, dy \quad , \tag{22}$$

and reduces to Eq. (1) when density can be treated as a linear function of temperature. Similarly, it would reduce to Eq. (18) if density were a linear function of c_R. The use of Eq. (22) when there is a density maximum results in the maximum contributing an artificial stabilization by *decreasing* l. Bogar and Westwater (1967) studied experimentally the conditions for convection onset in the melting of ice and found that the significant length for their analog to the problem

we encounter is the position of the density maximum. They also concluded that the correct density difference is the maximum density less the density at the lower boundary. The Rayleigh number defined in this way is

$$Ra_m \equiv \frac{(\rho^m - \rho^0)\, g l_m^3}{\rho^{avg}\, \nu D_R} \quad , \tag{23}$$

where $l_m \equiv \eta_m \sqrt{4 D_R t_c}$ is the calculated position of the density maximum. There is no *a priori* way to relate the two lengths l_c and l_m; l_c is a function of the diffusion coefficients, charges, and bulk concentrations of all of the species, while l_m is a function of all of the above *and* the densification coefficients. The critical Rayleigh number Ra_m according to Eq. (23) is 1829 for the Solution 1 experiments and 1718 Solution 2 experiments. Bogar and Westwater found that Ra_m for the analogous situation of melting ice was about 1700.

There has long been some uncertainty regarding the effect of the sensitivity of the monitoring technique on the critical Rayleigh number determined. With the micro-mosaic electrode we can conveniently investigate two effects: (1) the size of the sensing element relative to the that of the convective disturbance and (2) the effect of the chosen deviation criterion.

6.2. *The Effect of the Size of the Sensing Element*

Single electrode segments are 100 μm square. According to traditional stability theory, the wavelength of the disturbance is of the order of twice the characteristic length, which for our case is l_c. Thus our sensing elements are significantly smaller than the wavelength of the disturbance. Together they form a

cluster (1 mm square) of the same order as the disturbance, which is in turn surrounded by a larger "buffer" section. The effects of averaging on a large scale can be seen by simply comparing the time of the onset of convection for the individual segments to that for the larger cluster of segments, 30.8 versus 33.3 seconds. The longer time required until the onset of convection can be discernible for the larger cluster is the result of mass-transfer fluctuations being averaged on the larger scale.

Close inspection of Figure 4, the response of a single segment, and Figure 7, the response of the entire electrode, reveals another interesting point in regard to the effect of the size of the sensing element. Let us for the moment relax the 5% deviation criterion and consider instead the time until a *major* enhancement of the mass-transfer rate due to convection is established. This significant enhancement is the onset criterion one would probably detect in gas absorption experiments at a free surface without a very sensitive monitoring instrument. That the deviation from base-state behavior, according to our 5% criterion, significantly precedes any *major* enhancement in the current for the entire electrode can be seen in Figure 7. By contrast, the response for a single electrode element, shown in Figure 4, exhibits a significant increase in current immediately following the first deviation and much sooner than the entire electrode. If the Rayleigh number were based on the beginning of the sharp increase in current to the entire electrode ($\sim$ 50 seconds), it would be a factor of approximately 1.9 higher than the one determined from the 5% criterion we used. For the single-electrode data, the Rayleigh number would increase considerably less, by a factor of 1.3.

6.3. *The Effect of the Chosen Deviation Criterion*

The effect of varying the Sherwood number deviation criterion from 5 to 10% was investigated using the total current for all of the segments, shown in Figure 8. Over this range of onset criteria, the critical time varied from 33.3 seconds (at 5%) to 37.6 seconds (at 10%), an increase of 13%. The consequent increase in the calculated Ra_l is 20%. Jhaveri and Homsy (1982) predict that for $Pr = 7$ at a free surface, the measured Ra_l would increase by only 4% if the flux criterion is changed from 5 to 10%. Since we have a very high Schmidt number (2300), we might expect less of an effect of the onset criterion than predicted by Jhaveri and Homsy. Inspection of Figure 7 shows a definite departure from the base-state behavior at the marker for 5% deviation; however, the current response is still somewhat flat before the convection dominates and a very strong increase is seen. If we consider the current response of a single segment, we might see a sharper increase (or decrease) at convection onset than in the case of the sum of all the segments, where some averaging will undoubtedly take place. Figure 9 illustrates the current response for a segment showing a sharp negative deviation from the base-state behavior. The first marker (to the right in the figure) shows the last point for the calculation of the slope and correlation coefficient. The second marker (to the left) shows the point of 5% deviation. The time of convection onset for this curve is 39.8 seconds for a 5% deviation and 43.1 seconds for a 10% deviation, an 8.3% increase. The corresponding effect on the Rayleigh number is an increase of 12.7%, closer to the predicted value, but still significantly higher. One reason why we might not expect a close comparison between our result and Jhaveri and Homsy's model is that the model was established for a free surface condition, which means that there is no

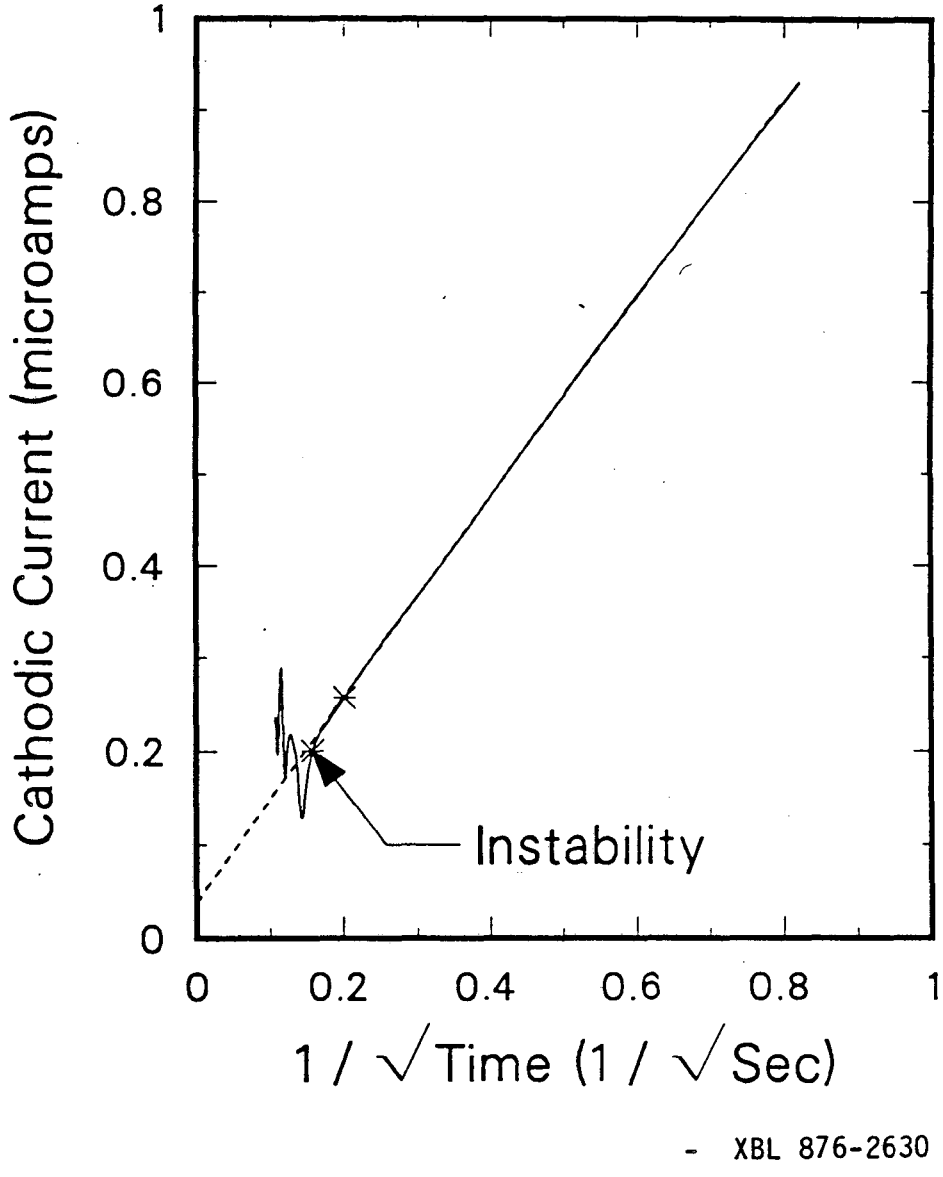

Figure 9. Current response of a single segment following a potential step to limiting current, showing a sharp decrease in Sh at the time of onset of convection.

shear stress at that surface to retard flow development.

It is of particular interest to consider the temporal and spatial variation of the direction of the change in mass transfer at the onset of convection. In the development of a cellular motion, we might expect to see areas where the initial deviation from the base-state current-time behavior is an enhanced transport rate and others where the rate is lowered. Indeed this was the case. In nearly every experiment, about two-thirds of the electrode surface showed a positive deviation, while a negative deviation occurred on the rest. The current to a segment showing a positive deviation is given in Figure 10, and that for a segment 100 microns away showing a negative deviation is given in Figure 11. The segment between these two, shown in Figure 12, underwent two slight negative deviations followed finally by a large increase in the current. The segmented area of the micro-mosaic electrode is too small to completely surround the entire area of segments showing the same type deviation. This distribution of deviations was not investigated in repeated experiments; however, all runs showed an overall *increase* in mass-transfer rate at the time of convection onset.

7. Conclusions

The use of a micro-mosaic electrode with an electrochemical redox system has been demonstrated in a study of the Bénard-Rayleigh problem of onset of convection in a fluid with a time-dependent density profile contained in a deep cell. The electrochemical technique offers several advantages over thermal techniques, the most important one being the precise control of the surface condition. The well-

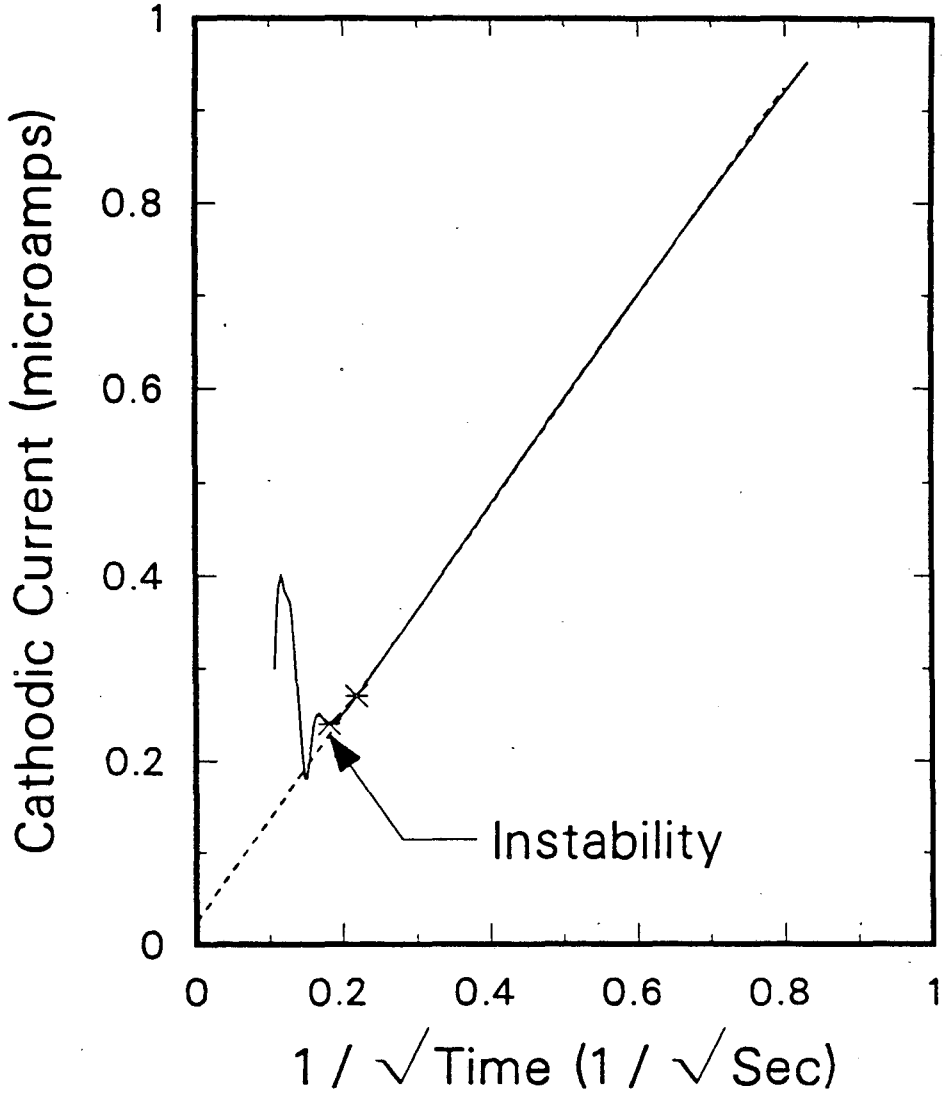

Figure 10. Current response of a segment following a potential step to limiting current, showing an *increase* in Sh at the time of onset of convection.

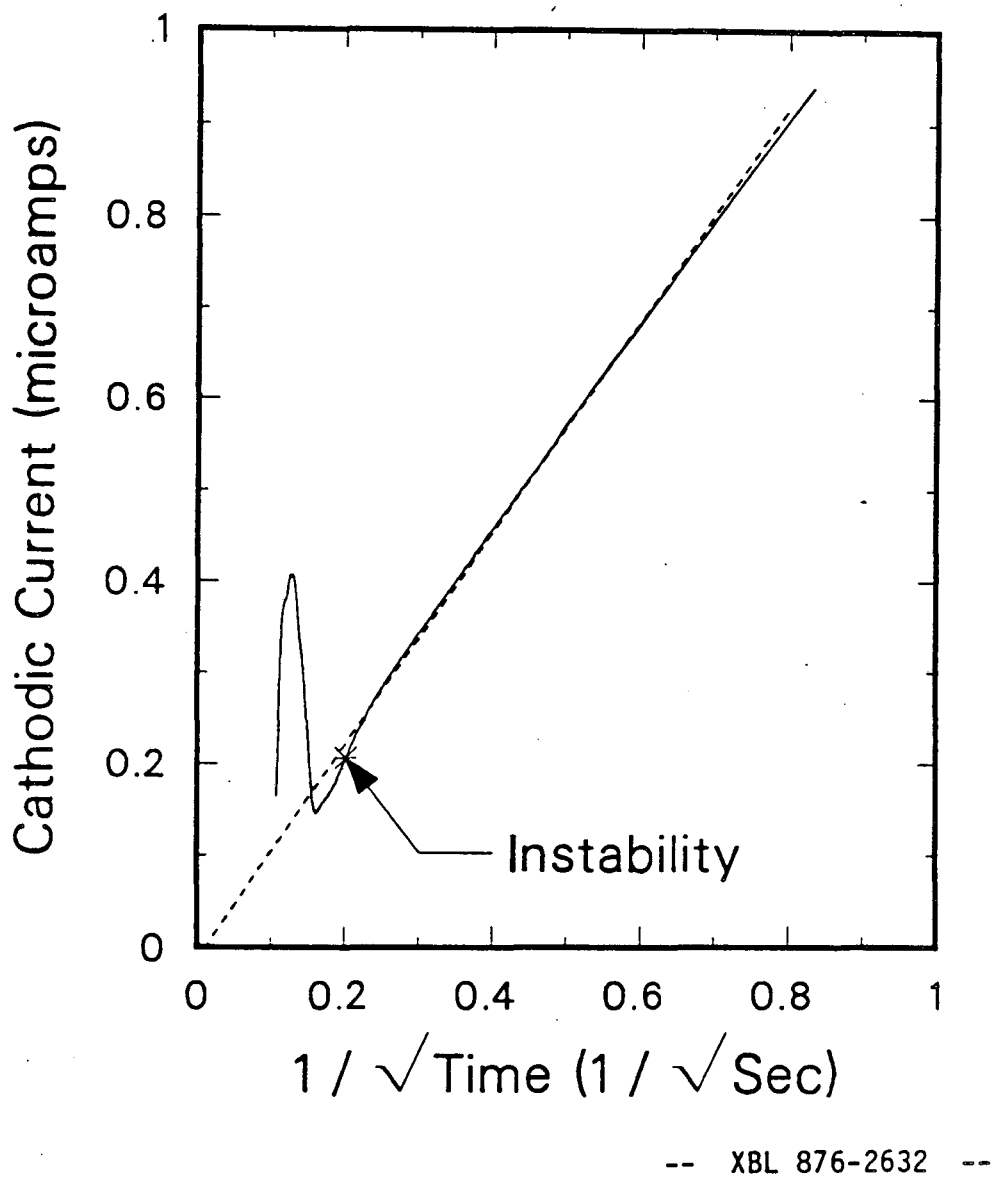

Figure 11. Current response of a segment that is 200 μm from that shown in Figure 10, exhibiting a *decrease* in Sh at the time of onset of convection.

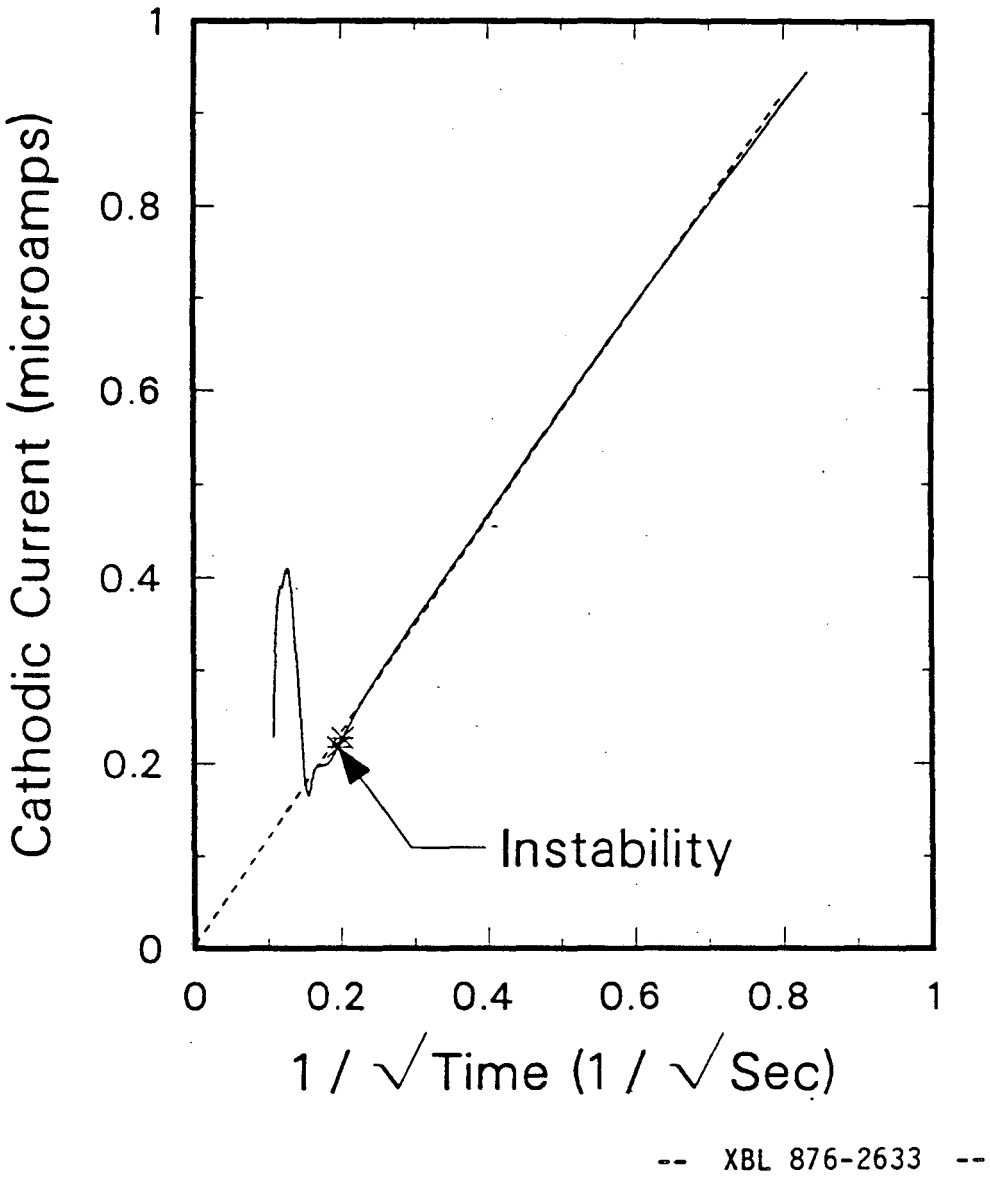

Figure 12. Current response of the segment between the two shown in Figures 10 and 11, showing two slight decreases, followed by a large increase in Sh at the time of convection onset.

controlled experiment lends itself to a thorough analysis of the time-dependent base state, the case of diffusion and migration into a semi-infinite column of electrolyte. In addition, the electrode serves as the monitoring device, allowing a precise detection of the onset of convection, the criterion for which is a percentage deviation of the Sherwood number (current) from base-state behavior.

The critical Rayleigh number Ra_l for the problem of onset of convection at a rigid, conducting boundary, due to a step change in the surface condition, was found to be approximately 900, based on the equivalent, linear-segment concentration profile and using a deviation criterion of 5% in the Sherwood number. For the redox system employed here, we calculate a maximum in the density profile. The critical Rayleigh number Ra_m based on the position and magnitude of the density maximum is approximately 1750.

At sensing elements much smaller than the wavelength of the disturbance, a sharp increase (or decrease) in mass-transfer rate occurs immediately after the first deviation from convection-free behavior. Over a larger area, some averaging takes place and a significant enhancement of the mass-transfer rate does not occur until tens of seconds after the first deviation in the mass-transfer rate is detected. For these reasons the single-segment data are less sensitive to the choice of the criterion that defines the time of deviation from convection-free behavior than are the data obtained from the entire electrode. Ra_l for single segments increased approximately 13% when the onset criterion was raised from a 5 to 10% deviation, while Ra_l derived from the entire electrode increased by 20%.

8. Chapter 4 Nomenclature

c_i	concentration of species i, mol /cm ^{3}
c_1	constant in density equation, 0.9996457 g /cm ^{3}
D_i	diffusivity of species i, cm ^{2}/sec
F	Faraday constant, 96,487 C/eq
h	total liquid depth, cm
i	current density, A/cm ^{2}
I_r	true ionic strength of bulk solution, mol/l
K	dissociation constant at infinite dilution, mol /cm ^{3}
K'	thermodynamic dissociation constant, mol /cm ^{3}
l	linear-segment penetration depth, defined in Eq. (1), cm
l_c	linear-segment penetration depth, based on concentration, cm
l_m	linear-segment penetration depth, based on density profile, cm
n	number of electrons transferred in the electrode reaction
Nu	Nusselt number, dimensionless thermal energy flux
Pr	Prandtl number, ν/α
R	universal gas constant, 8.3144 J/mol-K
Ra	Rayleigh number
s_i	stoichiometric coefficient of species i in the electrode reaction
Sc	Schmidt number, ν/D_R
Sh	Sherwood number, dimensionless mass flux
t	time, sec
T	temperature, K
u_i	mobility of species i, cm ^{2}-mol/J-sec
y	vertical distance from electrode surface, cm
z_i	charge number of species i
α	thermal diffusivity, cm ^{2}/sec
α_i	densification coefficient of species i, g/mol

δ	nominal penetration depth $= \sqrt{\alpha t}$, cm
η	similarity variable for semi-infinite diffusion
ϕ	potential, volt
ν	kinematic viscosity, cm^2/sec
ρ	density, g/cm^3

Subscripts and superscripts

c	referring to time of convection onset
l	Ra based on linear-segment penetration depth
m	l , η, ρ at the density maximum Ra based on density maximum
R	limiting reactant
t	Ra based on nominal penetration depth δ
0	at the electrode surface
∞	in the bulk solution

9. Chapter 4 References

Bard, A. J., and Faulkner, L. R., 1980, *Electrochemical Methods*, John Wiley & Sons, New York, pp. 142-144.

Berg, J. C., and Acrivos, A., 1965, "The Effect of Surface Active Agents on Convection Cells Induced by Surface Tension," *Chemical Engineering Science*," Vol. 20, pp. 737-745.

Blair, L. M., and Quinn, J. A., 1969, "The Onset of Cellular Convection in a Fluid Layer with Time-Dependent Density Gradients," *Journal of Fluid Mechanics*, Vol. 36, part 2, pp. 385-400.

Blake, K. R., Poulikakos, D., and Bejan, A., 1984, "Natural Convection near 4 ° C in a Horizontal Water Layer Heated from Below," *The Physics of Fluids*, Vol. 27, pp. 2608-2616.

Boeffard, A. J.-L., 1966, *Ionic Mass Transport by Free Convection in a Redox System*, M. S. Thesis, University of California, Berkeley. (Also Lawrence Radiation Laboratory Report No. UCRL-16624)

Bogar, D. V., and Westwater, J. W., 1967, "Effect of Buoyancy on the Melting and Freezing Process," *Journal of Heat Transfer, Transactions of the ASME*, Vol. 89, pp. 81-89.

Currie, I. G., 1967, "The Effect of Heating Rate on the Stability of Stationary Fluids," *Journal of Fluid Mechanics*, Vol. 29, part 2, pp. 337-347.

Davenport, I. F., 1972, *The Initiation of Natural Convection Caused by Time-Dependent Profiles*, Ph. D. Thesis, University of California, Berkeley. (Also Lawrence Berkeley Laboratory Report No. LBL-660)

Davenport, I. F. and King, C. J., 1974, "The Onset of Convection from Time-Dependent Profiles," *International Journal of Heat and Mass Transfer*, Vol. 17, pp. 69-76.

Dean, J. A., Ed., 1979, *Lange's Handbook of Chemistry, Twelfth Edition*, McGraw-Hill Book Company, New York, New York, p. **6**-34.

Dees, D. W., 1983, *Mass Transfer at Gas-Evolving Surfaces in Electrolysis*, Ph. D. Thesis, University of California, Berkeley. (Also Lawrence Berkeley Laboratory Report No. LBL-16176)

Dees, D. W., and Tobias, C. W., 1982, "A Novel Micro-Mosaic Electrode for the Study of Transport Phenomena at Gas-Evolving Electrodes," *Extended Abstracts of the 33rd International Society of Electrochemistry Meeting*, Vol. I, pp. 456-458.

Dees, D. W., and Tobias, C. W., 1987, "Experimental Studies of Free-Convection Mass Transfer to a Horizontal Surface with a Micro-Mosaic Electrode," *Journal of the Electrochemical Society*, Vol. 134, pp. 369-376.

Elder, J. W., 1968, "The Unstable Thermal Interface," *Journal of Fluid Mechanics*, Vol. 32, part 1, pp. 69-96.

Fenech, E. J. and Tobias, C. W., 1960, "Mass Transfer by Free Convection at Horizontal Electrodes," *Electrochimica Acta*, Vol. 2, pp. 311-325.

Foster, T. D., 1965a, "Stability of a Homogeneous Fluid Cooled Uniformly from Above," *The Physics of Fluids*, Vol. 8, pp. 1249-1257.

Foster, T. D., 1965b, "Onset of Convection in a Layer of Fluid Cooled from Above," *The Physics of Fluids*, Vol. 8, pp. 1770-1774.

Foster, T. D., 1968, "Effect of Boundary Conditions on the Onset of Convection,"

The Physics of Fluids, Vol. 11, pp. 1257-1262.

Gresho, P. M. and Sani, R. L., 1971, "The Stability of a Fluid Layer Subjected to a Step Change in Temperature: Transient versus Frozen Time Analyses," *International Journal of Heat and Mass Transfer*, Vol. 14, pp. 207-221.

Homsy, G. M., 1973, "Global Stability of Time-Dependent Flows: Impulsively Heated or Cooled Fluid Layers," *Journal of Fluid Mechanics*, Vol. 60, part 1, pp. 129-139.

Hsueh, L. and Newman, J., 1971, "The Role of Bisulfate Ions in Ionic Migration," *Industrial and Engineering Chemistry, Fundamentals*," Vol. 10, pp. 615-620.

Ibl, N. and Muller, R. H., 1958, "Studies of Natural Convection at Vertical electrodes," *Journal of the Electrochemical Society*, Vol. 105, pp. 346-353.

IMSL Inc., 1982, IMSL Library, Edition 9, IMSL, Inc., Houston, Texas.

Jeffreys, H., 1928, "Some Cases of Instability in Fluid Motion," *Proceedings of the Royal Society of London, Series A*, Vol. 118, pp. 195-208.

Jhaveri, B. S. and Homsy, G. M., 1980, "Randomly-Forced Rayleigh- Bénard Convection," *Journal of Fluid Mechanics*, Vol. 98, part 2, pp. 329-348.

Jhaveri, B. S. and Homsy, G. M., 1982, "The Onset of Convection in Fluid Layers Heated Rapidly in a Time-Dependent Manner," *Journal of Fluid Mechanics*, Vol. 114, pp. 251-260.

Lick, W., 1965, "The Instability of a Fluid Layer with Time-Dependent Heating," *Journal of Fluid Mechanics*, Vol. 21, part 3, pp. 565-576.

Mahler, E. G. and Schechter, R. S., 1970, "The Stability of a Fluid Layer with Gas Absorption," Vol. 25, *Chemical Engineering Science*, pp. 955-968.

Mahler, E. G., Schechter, R. S., and Wissler, E. H., 1968, "Stability of a Fluid Layer with Time-Dependent Density Gradients," *The Physics of Fluids*, Vol. 11, pp. 1901-1912.

McLarnon, F. R., Muller, R. H., and Tobias, C. W., 1982, "Interferometric Study of Combined Forced and Natural Convection," *Journal of the Electrochemical Society*, Vol. 129, pp. 2201-2206.

Merker, G. P., Waas, P., and Grigull, U., 1979, "Onset of Convection in a Horizontal Water Layer with Maximum Density Effects," *International Journal of Heat and Mass Transfer*, Vol. 22, pp. 505-515.

Newman, J. S., 1973, *Electrochemical Systems*, Prentice-Hall, Inc., Englewood Cliffs,

New Jersey, pp. 355-357.

Perry, R. H. and Chilton, C. H., Eds., 1973, *Chemical Engineers' Handbook, 5th Edition*, McGraw-Hill Book Company, New York, New York, p. 3-75.

Plevan, R. E., and Quinn, J. A., 1966, "The Effect of Monomolecular Films on the Rate of Gas Absorption into a Quiescent Liquid," *The American Institute of Chemical Engineers Journal*, Vol. 12, pp. 894-902.

Selman, J. R., and Newman, J., 1971, "Free Convection Mass Transfer with a Supporting Electrolyte," *Journal of the Electrochemical Society*, Vol. 118, pp. 1070-1078.

Spangenberg, W. G, and Rowland, W. R., 1961, "Convective Circulation in Water of Induced by Evaporative Cooling," *The Physics of Fluids*, Vol. 4, pp. 743-750.

Veronis, G., 1963, "Penetrative Convection," *Astrophysical Journal*, Vol. 137, pp. 641-663.

Wagner, C., 1949, "The Role of Natural Convection in Electrolytic Processes," *Transactions of the Electrochemical Society*, Vol. 95, pp. 161-173.

Ward, W. J., III, and LeBlanc, O. H., Jr., 1984, "Rayleigh-Bénard Convection in an Electrochemical Redox Cell," *Science*, Vol. 225, pp. 1472-1473.

Weast, R. C., Ed., 1976, *CRC Handbook of Chemistry and Physics, 57th Edition*, CRC Press, Inc., West Palm Beach, Florida, p. D-262.

Wilke, C. R., Eisenberg, M., and Tobias, C. W., 1953, "Correlation of Limiting Current under Free Convection Conditions," *Journal of the Electrochemical Society*, Vol. 100, pp. 513-523.

Young, T. F., Maranville, L. F., Smith, H. M., 1959, "The Structure of Electrolytic Solutions," W. J. Hammer, Ed., Wiley, New York, N. Y., pp. 35-63.

10. Chapter 4 Appendix

The dependent variables in the equation for mass transport by diffusion and migration in a semi-infinite column of electrolyte (Eq. (2)) are made dimensionless as

$$\theta_i \equiv \frac{c_i}{c_R^{\infty}} \qquad \text{(A-1)}$$

$$\Phi \equiv \frac{\phi F}{RT} \quad . \tag{A-2}$$

Substituting these into Eq. (2) gives

$$\frac{\partial \theta_i}{\partial t} = D_i \frac{\partial^2 \theta_i}{\partial y^2} + z_i D_i \left(\frac{\partial \theta_i}{\partial y} \frac{\partial \Phi}{\partial y} + \theta_i \frac{\partial^2 \Phi}{\partial y^2} \right) \quad . \tag{A-3}$$

Eq (A-3) is transformed to an ordinary differential equation using the similarity variable

$$\eta \equiv \frac{y}{\sqrt{4 D_R t}} \quad , \tag{A-4}$$

and becomes

$$2\eta \frac{d\theta_i}{d\eta} + \frac{D_i}{D_R} \frac{d^2 \theta_i}{d\eta^2} + \frac{D_i}{D_R} z_i \left(\frac{d\theta_i}{d\eta} \frac{d\Phi}{d\eta} + \theta_i \frac{d^2 \Phi}{d\eta^2} \right) = 0 \quad . \tag{A-5}$$

The boundary conditions at $y = \infty$ and the initial conditions combine to give

$$\theta_i = \frac{c_i^{\infty}}{c_R^{\infty}} \tag{A-6}$$

$$\Phi = 0 \tag{A-7}$$

at $\eta = \infty$. The surface boundary conditions at $\eta = 0$ become

$$\theta_R = 0 \tag{A-8}$$

$$D_i \left(\frac{d\theta_i}{d\eta} + z_i \theta_i \frac{d\Phi}{d\eta} \right) = \frac{s_i}{s_R} D_R \left(\frac{d\theta_R}{d\eta} + z_R \theta_R \frac{d\Phi}{d\eta} \right) \tag{A-9}$$

The equation of electroneutrality (Eq. (4)) becomes

$$\sum_i^4 z_i \theta_i = 0 \quad . \tag{A-10}$$

The equation for the dissociation of bisulfate is

$$\frac{\theta_{H^+} \theta_{SO_4^{-2}}}{\theta_{HSO_4^-}} = \frac{K'}{c_R^{\infty}} \quad . \tag{A-11}$$

Chapter 5. Observations of Bubble Growth and Disengagement

1. Abstract

Observations of galvanostatic growth and disengagement of hydrogen bubbles at a 127-μm-diameter micro-electrode embedded in a large, coplanar, horizontal electrode in 1.0-M H_2SO_4 are reported. Time scales for the collapse of the contact area, bubble disengagement and rise are obtained using high-speed cinematography. The collapse of the contact area takes place in less than two miliseconds and precedes the actual disengagement by up to 180 miliseconds. Observations of hydrogen evolution in free convection along vertical platinum electrodes in 0.5-M H_2SO_4 are also reported. The average diameter and position relative to the electrode surface of rising bubbles both increase with current density.

2. Introduction

An understanding of the mechanism by which electrolytically evolved gas bubbles influence mass transfer to and from the electrode surface requires intimate familiarity with the dynamics of bubble nucleation, growth, coalescence, and detachment. Optical observations are not easy to make because electrolytically evolved bubbles are small (at most a few hundred microns following detachment), and the events of coalescence and separation from the surface are completed within 10^{-4} and 10^{-3} seconds. Further, the movements of swarms of bubbles surrounding a given bubble render any precise observation of a single bubble difficult. It should not therefore be surprising that there is a paucity of information in the literature regarding the dynamics of bubble phenomena.

Coehn and Neumann (1923) and Kabanow and Frumkin (1933) grew bubbles at very low rates and obtained bubble diameters at breakoff. They were concerned with the forces that determine the size of the largest bubble that can adhere to a solid support, and not with bubble growth rates or dynamics.

The first report of electrolytic bubble growth was that of Westerheide and Westwater (1961), who photographed hydrogen bubbles growing in sulfuric acid at a 127-μm-diameter platinum micro-electrode encased in glass, using high-speed motion pictures. They found that the bubble diameter increased with the square root of time, indicating a mechanism of growth by diffusion from a supersaturated solution, according to the model of Scriven (1959). They also found that when two bubbles coalesced, the new bubble would sometimes jump off the electrode surface and return to it. They also recorded slip of bubbles along the electrode.

Glas and Westwater (1964) recorded the electrolytic growth of H_2, O_2, Cl_2 and CO_2 on platinum, nickel, copper, and iron electrodes with diameters from 127 to 508 μm. Bubble diameters were found to increase with the square root of time, following Scriven's model. The largest diameters recorded were approximately 160 μm. Bubble heights during growth were also measured, and contact angles were computed from the measured heights and maximum diameters, *assuming the bubbles to be spherical segments.* On this basis, it was concluded that the contact angle decreases with increasing bubble diameter. However, even for small, nearly spherical bubbles, a spherical segment is not a good approximation to its shape *if one is trying to determine the contact angle.* Any deviation from sphericity will be manifest in the shape of the bubble interface near the base (See Figure 2, Chapter 2).

Putt (1975) tried a different approach to observing bubble growth at vertical electrodes. He photographed H_2 and O_2 bubbles in 5-M KOH and 5-M H_2SO_4, at very short times (13-300 msec) after the start of electrolysis, through a glass window in the center of an opposing counter electrode. He also measured the sizes of free stream bubbles rising above the active electrode. Strong evidence has been presented by Putt showing the dense nucleation of bubbles following imposition of the current, subsequent rapid coalescence *while still attached to the electrode surface,* and eventual detachment of bubbles of uniform size. Hydrogen bubbles in H_2SO_4 also grew by sliding along the electrode surface, scavenging smaller bubbles in their paths. Steady-state flow of bubbles along the electrode was typically established within one second of the start of electrolysis. Putt concluded that the size of detaching bubbles at practical rates of gas evolution is governed by the dynamics of

bubble interactions.

Cettou and Tobias (1981) combined Putt's technique with high-speed motion pictures and extended the range of electrode materials to include nickel 200, stainless steel 304, and electrodeposited gold. They used sulfuric acid, sodium sulfate and sodium hydroxide electrolytes. The density of bubbles nucleated per electrode area was found to vary with electrode material, electrolyte, and the gas evolved, being much higher, for example, with H_2 on nickel or stainless steel in H_2SO_4 (1000/mm^2) than in NaOH (150/mm^2), and intermediate (600/mm^2) for H_2 on gold in both electrolytes. Comparisons of bubble sizes at detachment to bubble sizes in the bulk at steady state, show that coalescence is the most important mode of bubble growth in H_2SO_4 for both H_2 and O_2 on all electrode materials studied.

The other approach to viewing gas evolution has been to take photographs though the back side of a transparent metal or conductive metal-oxide electrode. Venczel (1970) vapor-deposited thin layers of platinum, chromium, nickel and gold on glass plates and observed H_2 bubbles in H_2SO_4. He found that bubble size is dependent on electrode material used: the coalescence of uniformly-sized bubbles on platinum and graphite electrodes forms large bubbles, and uneven growth on iron and copper (solid) electrodes results in bubbles separating before coalescence. Janssen and van Stralen (1981) evolved O_2 from KOH on transparent nickel electrodes and noted the important role of bubble coalescence in this system. Bubbles often slip across the electrode and coalesce into a larger bubble. Sides and Tobias (1985) observed this phenomenon during O_2 evolution in NaOH through transparent SnO_2 electrodes, and also noted the scavenging effect of large bubbles

sliding along the electrode and coalescing with smaller bubbles in their paths, reported earlier by Putt (1975).

The objective of the present investigation is to characterize H_2 evolution in H_2SO_4 by obtaining a *profile* view of bubble formation on flat electrodes. We are interested in the shape and size of individual bubbles during growth and detachment, and the movements of bubbles following coalescence. We hope to learn whether scavenging bubbles that slide along the electrode and coalesce with smaller bubbles are actually attached to the surface. We are also interested in the distances from the electrode at which free stream bubbles rise, and the dependence of the size of such bubbles on current density.

The method used in the present study to observe individual bubble growth and detachment is to grow bubbles at constant current at an electrically-isolated micro-electrode embedded in a relatively large planar electrode. The recording of bubble growth and coalescence at vertical electrodes is accomplished using narrow platinum strip electrodes. By restricting the electrode dimension in the horizontal direction to a few milimeters, only a few columns of bubbles are able to form, allowing an unobstructed view of multiple-bubble phenomena to be recorded.

3. Disengagement and Growth of Single Bubbles Formed at Micro-Electrodes

3.1. *Experimental*

Hydrogen bubbles were produced at constant current at a horizontal, platinum, two-section electrode. The electrode was constructed by inserting a 127-μm-diameter platinum wire through a hole drilled in the center of a 1 x 1 cm platinum sheet, filling the gap with epoxy, and facing the top surface. The epoxy ring separating the two electrodes is 50 to 75 μm in width. The surrounding platinum electrode can be used as a second working electrode or as a reference electrode. The sectioned electrode fits into a plexiglass cell that has a platinum counter electrode, and a reference-electrode capillary built into the wall at the edge of the second working electrode. A schematic of the cell is shown in Figure 1.

The electrode was polished to 1 μm with diamond paste, and rinsed with cyclohexane, methanol, de-ionized distilled water and the electrolyte, before being inserted in the cell. The central platinum electrode was polarized cathodically to generate hydrogen bubbles from 1-M H_2SO_4. Experiments were conducted in galvanostatic mode, using an EG&G PAR 173/176 potentiostat/galvanostat, and the potential waveforms were stored on a Nicolet 4094 digital oscilloscope. The data were transferred to an Hewlett-Packard HP9825T desktop computer, stored on floppy disk, and later transferred to a mainframe. A Redlake Hycam camera, capable of filming at rates up to 11,000 full frames per second, was used to record visual observations. Primary lighting was supplied by an optical fiber aimed directly into the microscope from behind the growing bubble; a second optical fiber lit the bubble from in front and above.

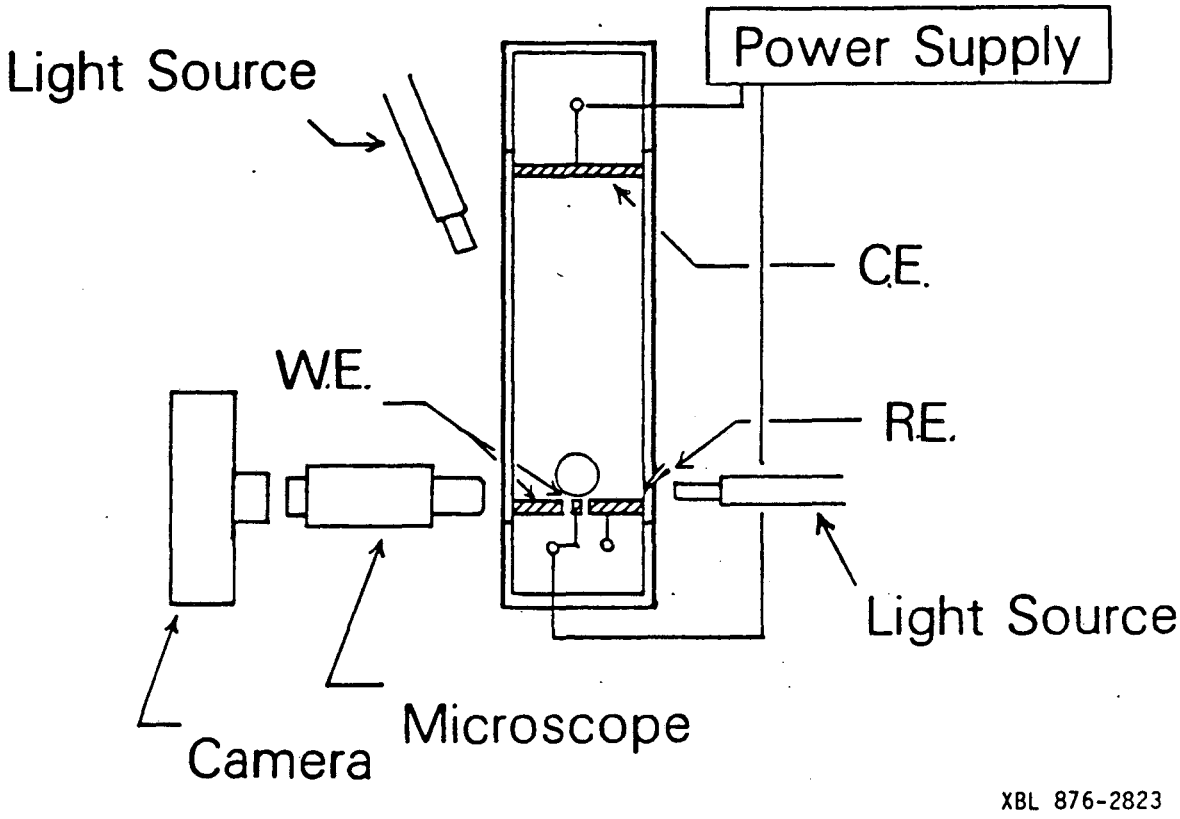

Figure 1. Electrochemical cell and equipment for observations of bubble growth at micro-electrodes.

3.2. *Overpotential Measurements*

The total potential, measured with respect to a mercury/mercurous sulfate reference, is shown in Figure 2 for bubble evolution rates of 100, 200, 500, and 1000 μA. The corresponding current densities are quite high (0.79, 1.58, 3.95, and 7.89 A/cm ^{2}), owing to the small area of the active electrode. The thermodynamic component of the total potential is 0.64 V. Two features are readily apparent from the overpotential curves. First, there is a sharp increase in the overpotential just before bubble disengagement, which may be attributed to the bubble base, having grown to the electrode edge, obstructing the flow of current. This is supported by the increasing magnitude of the potential jump with current. Second, the frequency of bubble evolution is roughly proportional to the current, from which it can be inferred that the bubbles are nearly the same size at detachment.

3.3. *Time Scale of Bubble Disengagement*

The time scale of the events preceding the actual tearing loose of the bubble from its base was determined using high-speed cinematography. A series of frames from a 1500 frame-per-second movie of a hydrogen bubble growing at 200 μA is shown in Figure 3. Times shown are relative to the first frame in the series; the bubble had been growing for approximately 25 seconds before this frame. The collapse of the contact area occurs in less than two miliseconds (frames 1-3). In the next 15 miliseconds (frames 4,5) the bubble rises slightly from its base and shifts horizontally. For a period of about 160 miliseconds, there is little bubble movement. It grows by coalescence with a series of small bubbles nucleated at its

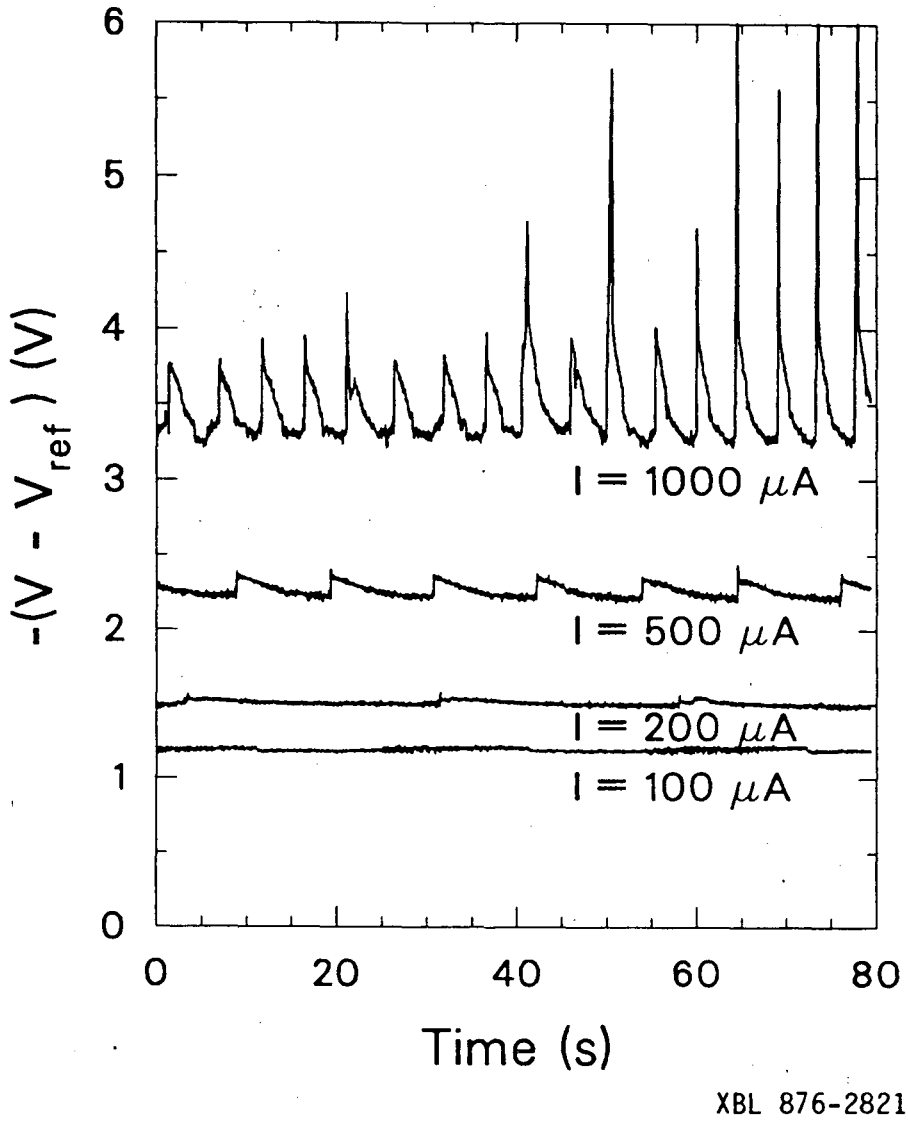

Figure 2. Micro-electrode potential with respect to a mercury/mercurous reference electrode for currents of 100, 200, 500, and 1000 μA.

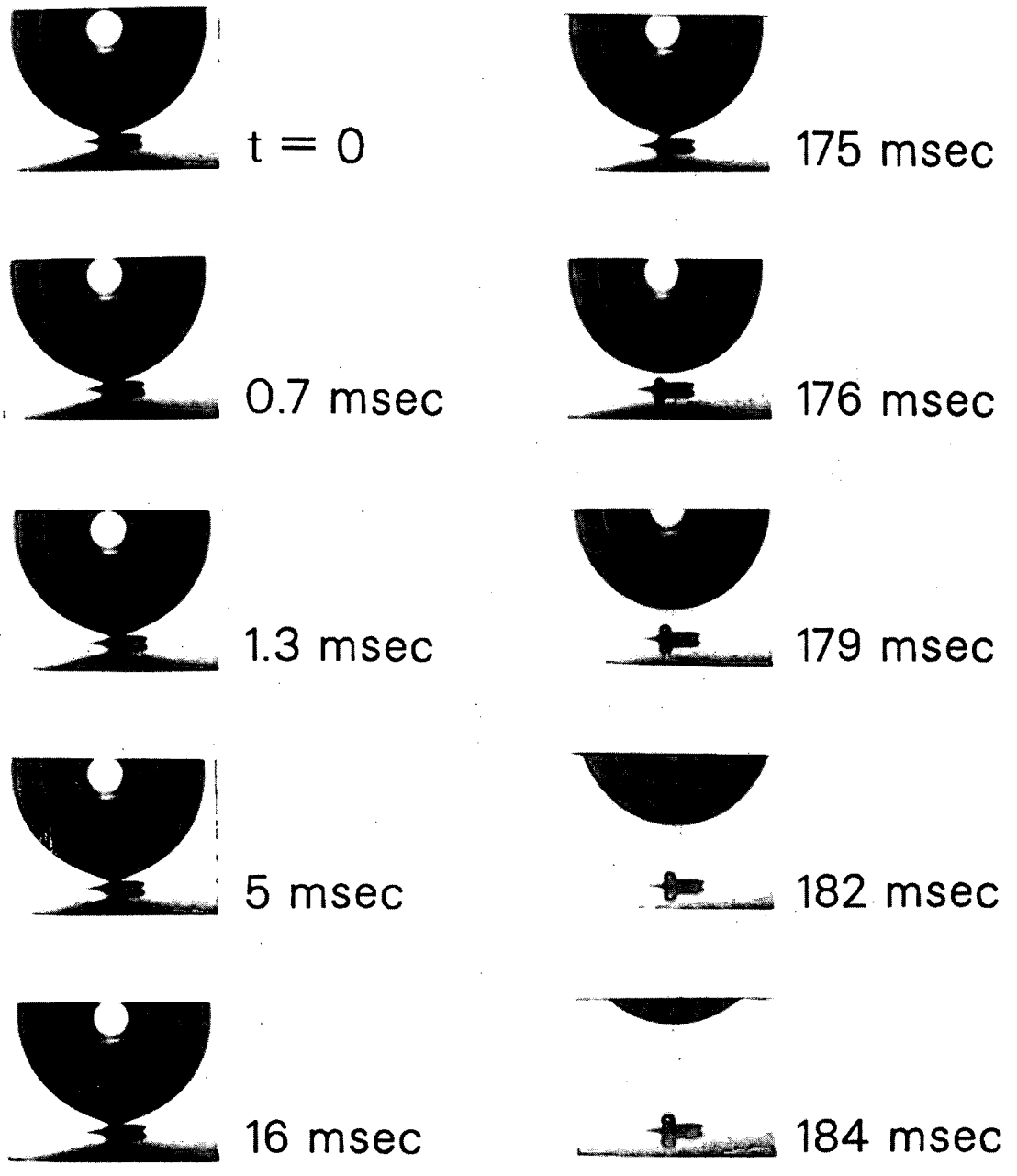

Figure 3. Bubble detachment from platinum micro-electrode in 1-M H_2SO_4. Bubble had been growing at 200 μA for 25 seconds before first frame shown here.

base. The tearing loose of the bubble from its base takes place between the sixth and seventh frames, almost 180 miliseconds after the collapse of the contact area. In another 8 miliseconds, the bubble has risen out of the frame (1mm height) and a new bubble is growing. The series of events is presented in a set of sketches, traced from the same film, in Figure 4. The asymmetric collapse of the contact area and subsequent horizontal movement can be more clearly seen in this presentation.

Tracings from movies of bubbles generated at 500 μA are similar to those for 200 μA; the time intervals, however, are considerably shorter. Figure 5 shows the disengagement of a hydrogen bubble grown at 500 μA for roughly 11 seconds prior to the first contour. The time from the beginning of the decrease of the contact area to the detachment of the bubble is 15 miliseconds at this current density.

3.4. *Rate of Bubble Growth*

The radius of a bubble growing by diffusion in a uniformly supersaturated solution will increase with the square root of time, as shown by Scriven (1959). Bubble growth at micro-electrodes is different from that at macro-electrodes in that the only source of hydrogen is directly at the base of the bubble. It is possible for the bubble to capture all or most of the dissolved gas directly from the area at its base, rather than from the bulk liquid. If this is the case, the bubble radius should increase with the cube root of time. Figure 6 is a plot of the radius of a bubble grown at 500 μA versus the cube root of time. The curve for 100% capture of dissolved hydrogen is also shown; it appears that the capture efficiency is almost 100%.

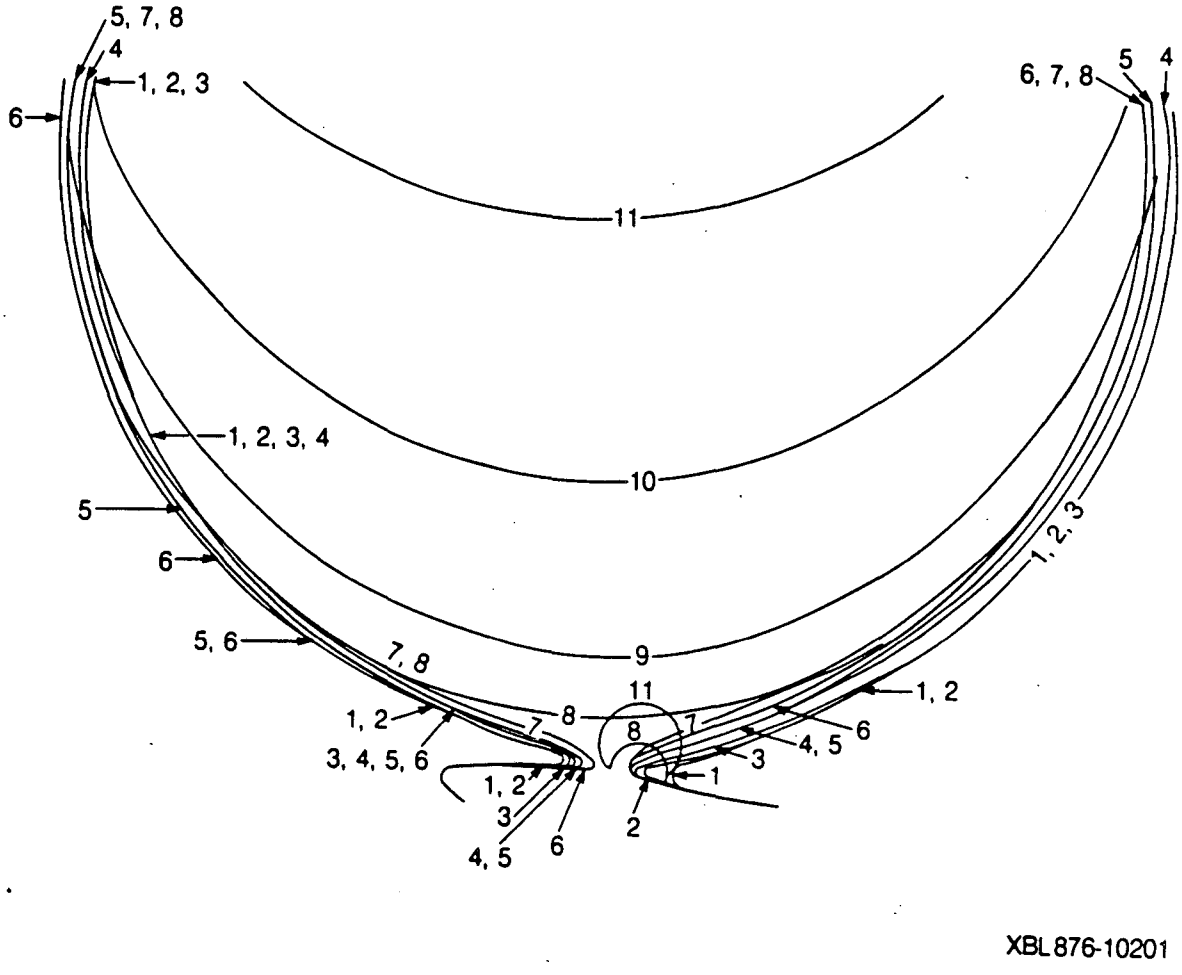

Figure 4. Change in shape of bubble at time of detachment from platinum microelectrode in 1-M H_2SO_4. Bubble had been growing at 200 μA for 25 sec before first sketch. Times in miliseconds relative to curve 1: (2) 0.7, (3) 1.3, (4) 5.3, (5) 11, (6) 159, (7) 175, (8) 176, (9) 179, (10) 182, (11) 184.

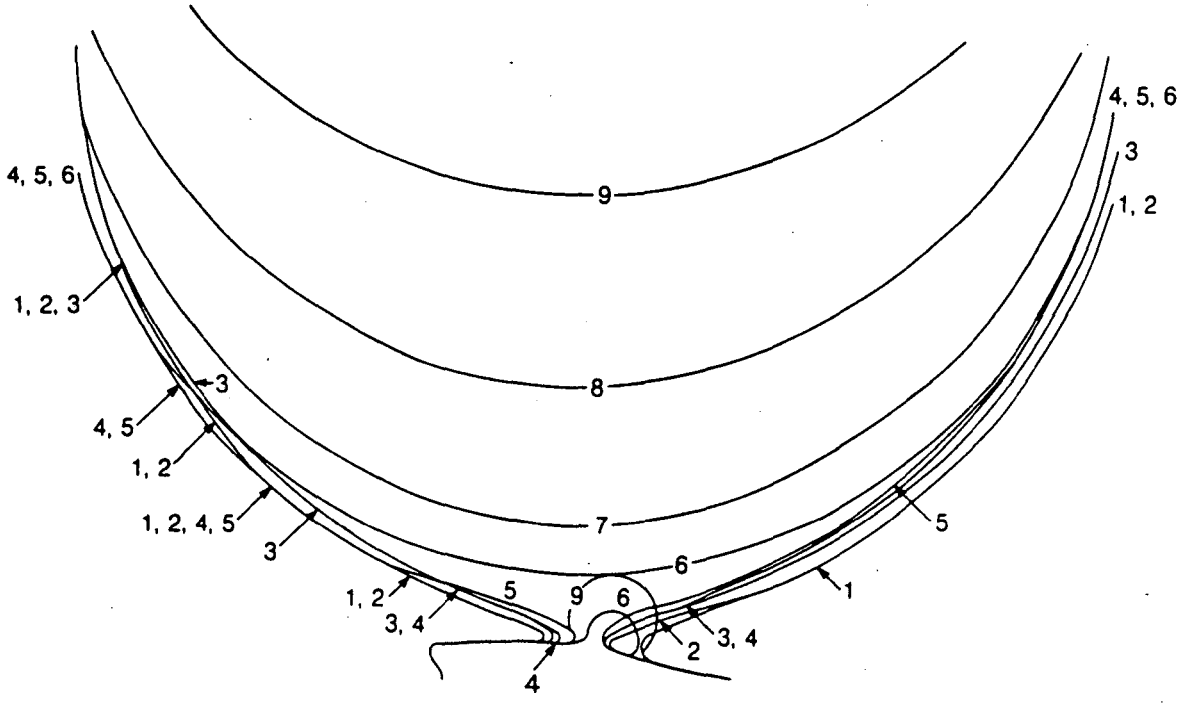

Figure 5. Bubble detachment from platinum micro-electrode in 1-M H_2SO_4. Bubble had been growing at 500 μA for 11 seconds prior to first contour shown. Times in miliseconds relative to curve 1: (2) 2, (3) 6, (4) 12, (5) 15, (6) 16, (7) 18, (8) 20, (9) 22.

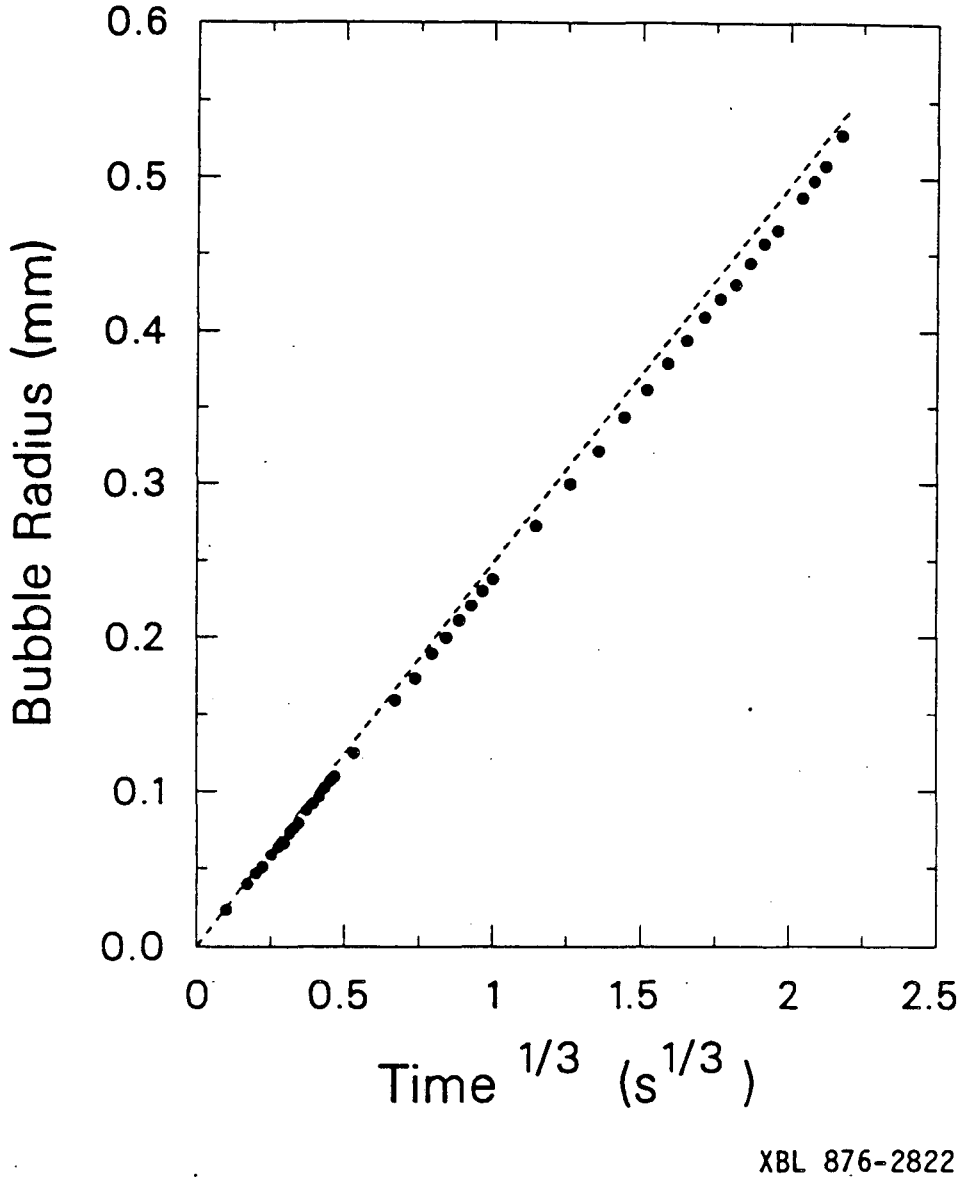

Figure 6. Bubble radius plotted against the cube root of time. The dashed line is the calculated bubble radius assuming a spherical bubble and 100% hydrogen capture efficiency.

4. Hydrogen Evolution at Vertical Platinum Electrodes

4.1. *Experimental*

Hydrogen was evolved from 0.5-M H_2SO_4 at vertical platinum strip electrodes 75 mm high and 1.3 mm wide. This electrode width proved small enough to allow an unobstructed side view of bubbles to be obtained. The platinum strips were encased in Plexiglas with epoxy. The entire piece fits into a small Plexiglas cell of dimensions 75 x 70 x 12 mm, shown in Figure 7. The electrodes were polished, and rinsed with methanol, de-ionized distilled water, and the electrolyte, prior to immersion in the cell.

4.2. *Results*

Three frames taken from a movie of hydrogen evolved at a rate of 14 mA /cm ^{2} at a vertical platinum electrode are shown in Figure 8. The scale of the frame is 1.1 x 1.4 mm. Coverage of the electrode area by attached bubbles is not high, and, periodically, a large bubble would slide along the electrode, coalescing with or causing the detachment of smaller bubbles. Bubbles on the surface are typically about 100 μm in diameter; the largest bubbles observed at this current density were about 250 μm in diameter. Bubbles rise at distances up to 600 μm from the electrode.

Figure 9 includes three frames from a film of hydrogen evolution at vertical platinum electrodes at a current density of 28 mA /cm ^{2}. The bubbles on the surface are somewhat larger than those at 14 mA /cm ^{2}; a typical diameter is 140

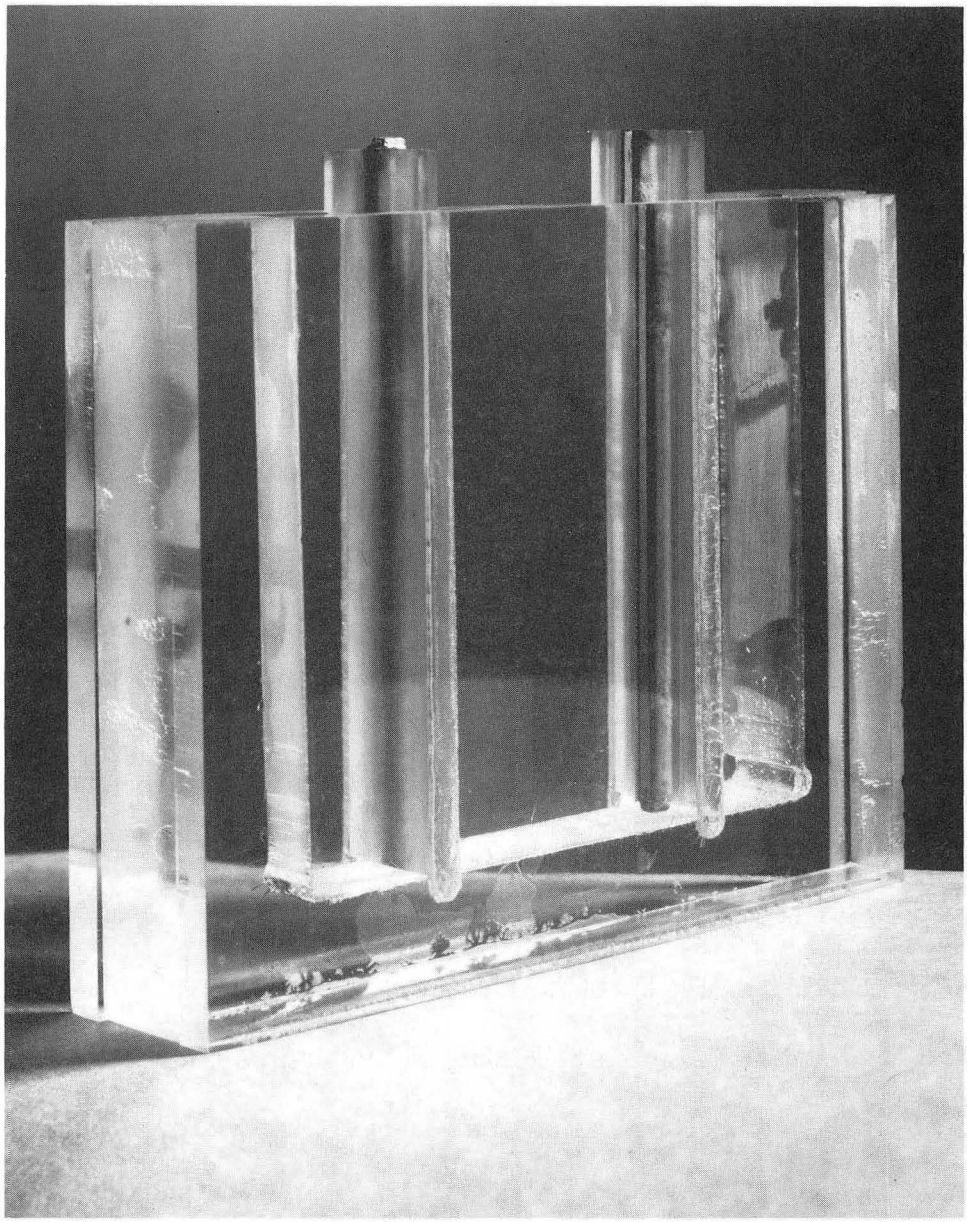

CBB 874-2837

Figure 7. Electrochemical cell and platinum electrodes for observing gas evolution at vertical macro-electrodes.

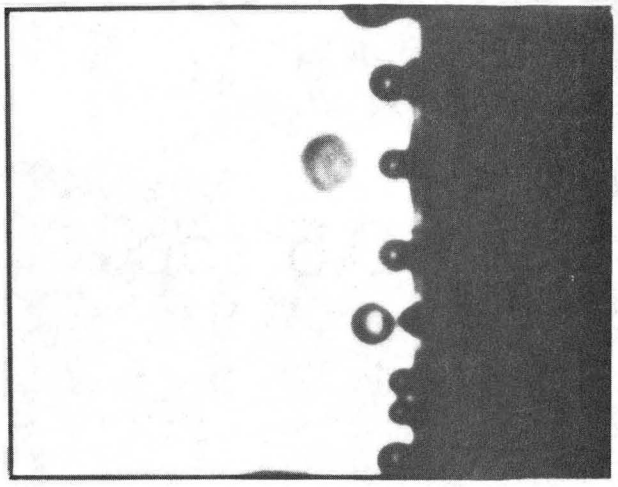

1.0 sec

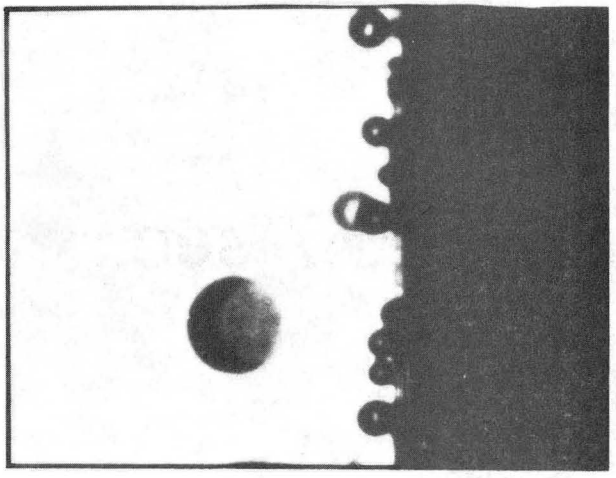

1.5 sec

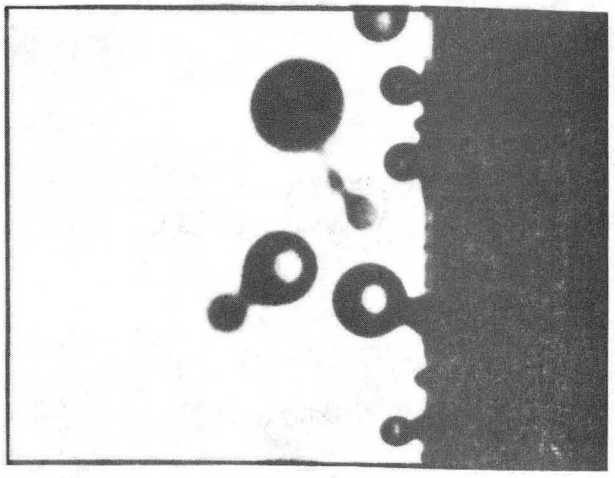

2.0 sec

XBB 860-8668A

Figure 8. Three frames, 0.5 seconds apart, from a movie of hydrogen evolution at a vertical platinum electrode at a current density of 14 mA /cm ^{2}. Each frame is 1.1 x 1.4 mm.

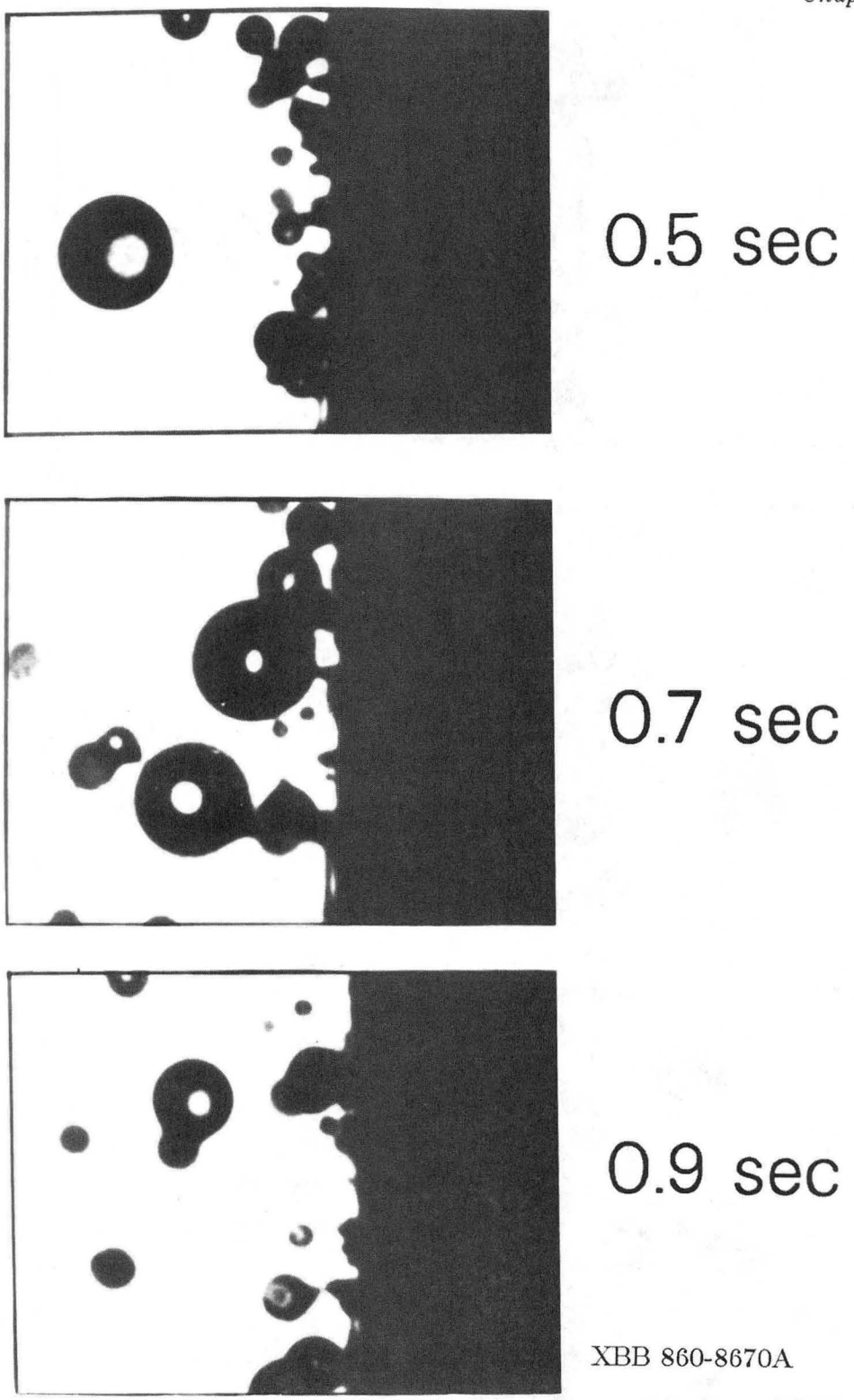

Figure 9. Three frames, 0.2 seconds apart, from a movie of hydrogen evolution at a vertical platinum electrode at a current density of 28 mA /cm ^{2}. Each frame is 1.1 x 1.4 mm.

μm. A higher fraction of bubbles rise unattached and at greater distances from the electrode then at the lower current density. The largest bubble in this set of photographs is about 350 μm in diameter.

5. Other Observations

The following qualitative observations of hydrogen evolution in sulfuric acid were also made:

1. Bubble size at detachment from a micro-electrode is independent of current density, and is larger than on a continuous electrode. This is presumably a result of the lack of convection or other disturbances that would be present were other bubbles growing or detaching nearby. The eventual bubble detachment is typically caused by a small secondary bubble coalescing into the base of the primary bubble.

2. The size of bubbles adhering to vertical electrodes increases with current density, while the number density of attached bubbles remains constant. The size of free stream bubbles generally increases with current density.

3. Periodically, in gas evolution along vertical electrodes, large bubbles (whose size appears to increase with current density) slide along the electrode, coalescing with adhering bubbles and exposing fresh electrode area. New bubbles are nucleated at previously occupied sites.

4. Coalescence in the free stream is very rare. A large bubble overtaking a smaller one usually slips around it. Only if the two bubbles' axes of motion are colinear, do

two bubbles coalesce without being attached to the electrode.

6. Conclusions

Observations of galvanostatic growth and disengagement of hydrogen bubbles have been recorded using high-speed cinematography with a 127-μm-diameter horizontal micro-electrode embedded in a large, coplanar electrode. In 1.0-M H_2SO_4 the collapse of the contact area takes place in less than two miliseconds and precedes the actual disengagement by up to 180 miliseconds. The total time for contact area collapse, bubble disengagement, and bubble rise to one diameter above the electrode decreases with increasing current density. Because of the bubble shielding the electrode area, a sharp increase in overpotential occurs just before the actual disengagement, at which time the overpotential drops. Hydrogen evolution has also been observed by high-speed cinematography in free convection along vertical platinum electrodes, 7.5 cm in height. At moderate current densities (15-30 mA /cm ^{2}) in 0.5-M H_2SO_4, bubble sizes after separation are in the range of 50 to 400 μm in diameter, and, as they rise, they drift to distances up to 800 μm away from the electrode surface. The average diameter and the path of rising bubbles both increase with current density.

7. Chapter 5 References

Cettou, P, and Tobias, C.W., 1981, "The First Generation of Bubbles at Gas Evolving Electrodes," Lawrence Berkeley Laboratory Report No. LBL-13632.

Coehn, A., and Neumann, H., 1923, "Elektrostatische Erscheinungen an Elektrolytisch Entwickelten Gasblasen. I," *Zeitschrift für Physik*, Vol. 20, pp. 54-68.

Glas, J.P., and Westwater, J.W., 1964, "Measurements of the Growth of Electrolytic Bubbles," *International Journal of Heat and Mass Transfer*, Vol. 7, pp. 1427-1443.

Janssen, L.J.J., and van Stralen, S.J.D., 1981, "Bubble Behavior on and Mass Transfer to an Oxygen-Evolving Transparent Nickel Electrode in Alkaline Solution," *Electrochimica Acta*, Vol. 26, pp. 1011-1022.

Kabanow, B., and Frumkin, A., 1933, "On the Size of Electrolytically-Generated Gas Bubbles," *Zeitschrift für Physikalische Chemie*, Vol. 165A, pp. 433-452.

Putt, R.A., 1975, *Studies of the Events Occurring at Gas-Evolving Electrodes*, M.S. Thesis, University of California, Berkeley (Also Lawrence Berkeley Laboratory Report No. LBL-3989).

Scriven, L.E., 1959, "On the Dynamics of Phase Growth," *Chemical Engineering Science*, Vol. 10, pp. 1-13.

Sides, P.J., and Tobias, C.W., 1985, "A Close View of Gas Evolution from the Back Side of a Transparent Electrode," *Journal of the Electrochemical Society*, pp. 583-587.

Venczel, J., 1970, "Über Gasblasen bei Elektrochemischen Prozessen," *Electrochimica Acta*, Vol. 15, pp. 1909-1920.

Westerheide, D.E., and Westwater, J.W., 1961, "Isothermal Growth of Hydrogen Bubbles During Electrolysis," *The American Institute of Chemical Engineers Journal*, Vol. 7, pp. 357-362.

Appendix A. Electrode Fabrication

Fifteen electrodes were received from Hewlett-Packard Laboratories in July, 1984. These electrodes were labeled HP-01 and numbered one through fifteen. In August of 1984, twenty electrodes were received from AT&T Bell Laboratories, labeled BL-01. Later in 1984, two more electrodes of the same materials and eleven electrodes of different materials, batch BL-02, were received. The following table shows the materials of construction of the three sets of electrodes. Appendix E shows the electrodes used in experiments and the operability before and after use.

	HP-01	BL-01	BL-02
base	(100)-Si	(100)-Si	(100)-Si
isolation	1.5μm SiO_2/1500Å Si_3N_4	SiO_2	SiO_2
conductors	1200Å Al	5000Å $TaSi_x$	1μm Al
insulator	4500Å SiO_2	1250Å SiN:H	polyimide
electrode	300/600Å Cr/Pt	500/5000/500Å Ti/Pd/Au	500/5000/500Å Ti/Pd/Au
number	15	22	11
line widths	4-5.5 μm	6-13 μm	7-9 μm

Appendix B. Dissolved Hydrogen Oxidation

In preliminary experiments on the nature of mass-transfer enhancement by bubble streams rising within the mass-transfer boundary layer, the bubble stream was generated at the lowest row in the 10 × 10 array of segments on the micro-mosaic electrode. Part of the motivation for this approach was the quantification of mass transfer due to multiple bubble streams, which could be generated at several segments in the bottom row. Anodic currents were measured over much of the segmented area in these experiments, obscuring any conclusions regarding mass-transfer enhancement by the bubbles. It is believed that the anodic currents were the result of dissolved H_2 being oxidized at the mass-transfer monitoring segments. During a typical experiment, the entire electrode is polarized roughly 650 mV cathodic to the Fe^{+3}/Fe^{+2} redox potential, and the gas-evolving segment is polarized about 500 mV further cathodic. The Fe^{+3}/Fe^{+2} redox potential is 770 mV anodic to the normal hydrogen electrode, so the mass-transfer monitoring segments are "cathodic" for the Fe^{+3}/Fe^{+2} reaction, but "anodic" for the H^+/H_2 reaction. This presents no problem as long as there is no significant amount of dissolved hydrogen that can be oxidized by these segments.

Experiments were performed to determine whether the hydrogen reaction was the cause of the anodic currents and to determine the area over which this reaction is likely to interfere with the indicator-ion reaction. This was accomplished by repeating the mass-transfer experiments in pure 0.5-M H_2SO_4 with no Fe^{+3} added.

Once the magnitude of the anodic reaction of dissolved hydrogen was known, experiments could be performed under conditions that minimize this reaction. The results of the experiments conducted to determine the magnitude of the oxidation reaction of dissolved hydrogen are presented in the following.

Figure 1 shows the transient mass transfer to several segments directly above a single bubble-evolution site. The electrolyte is 0.0484-M $Fe_2(SO_4)_3$ in 0.5-M H_2SO_4, and the bubble evolution rate is 31 μA. Segments within 300 μm of the gas-evolving segment receive a net anodic current, the result of the combined oxidation of H_2 and reduction of Fe^{+3}. It is not until a height of 800 μm above the gas-evolving segment that the mass-transfer rate reaches the background natural-convection current of approximately 0.2 μA (= 2 mA /cm ^{2}). Figure 2 shows the analogous experiment with no Fe^{+3} added to the electrolyte, with *anodic* currents plotted as *positive*. The bubble evolution rate here is 28 μA. The high anodic currents recorded show that the oxidation of dissolved hydrogen is indeed significant within 900 μm of the gas-evolving segment. Figure 3 is the current distribution plot for the same run, also with anodic currents positive. The gas-evolving segment is the fifth from the left in the bottom (rear) row.

Figure 4 depicts the distribution of anodic current in an experiment similar to that shown in Figure 3, except that here the bubble stream was generated at the lowest of the satellite segments, 600 μm below the lowest row of micro-electrodes, and in line with the sixth column of segments. It can be seen that this configuration minimizes the effect of the reaction of dissolved hydrogen on the mass-transfer rate to the segmented area of the micro-mosaic electrode. Most of the hydrogen not captured by the bubbles is oxidized at the buffer electrode, or is transported away

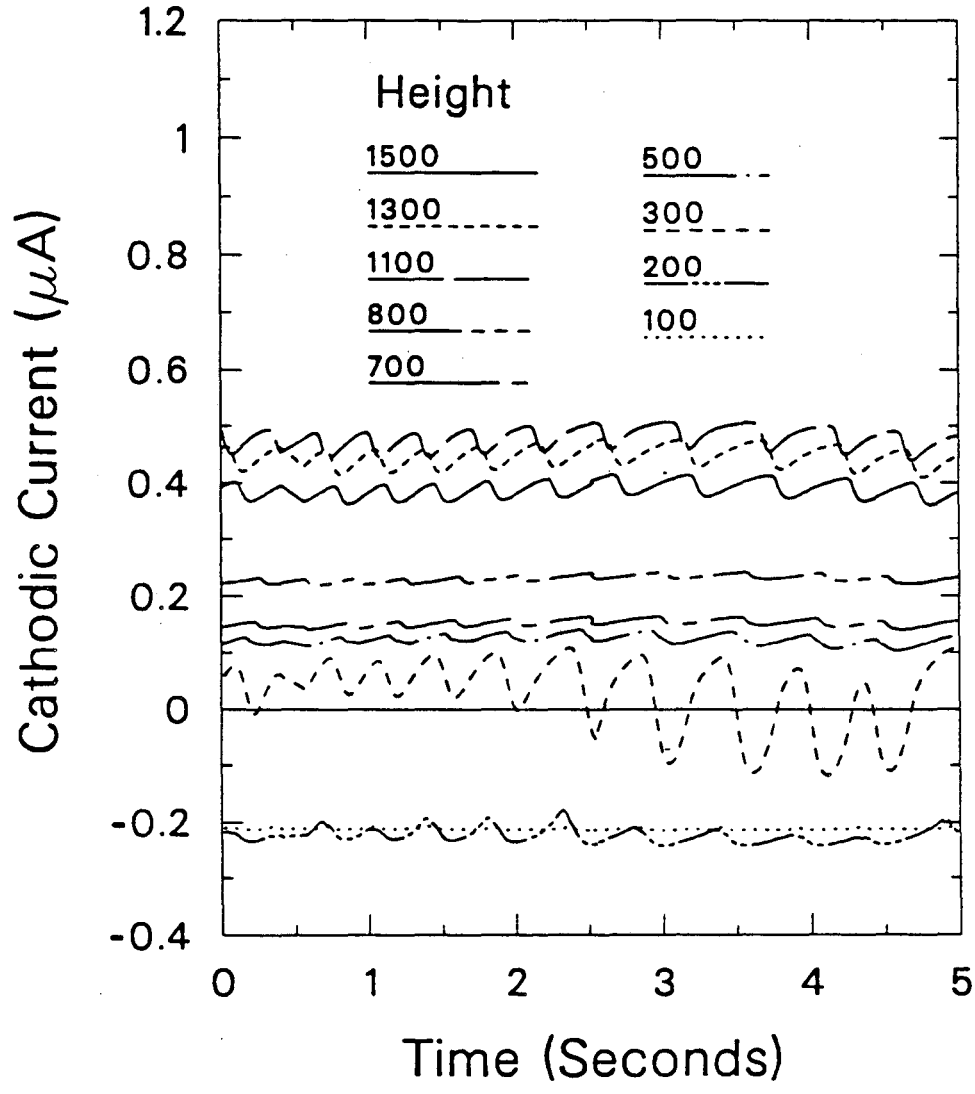

Figure 1. Current to several segments directly above the point of generation of a 31-μA bubble stream rising within the mass-transfer boundary layer. Parameter is distance above bubble-evolving segment. The electrolyte is 0.0484-M $Fe_2(SO_4)_3$ in 0.5-M H_2SO_4.

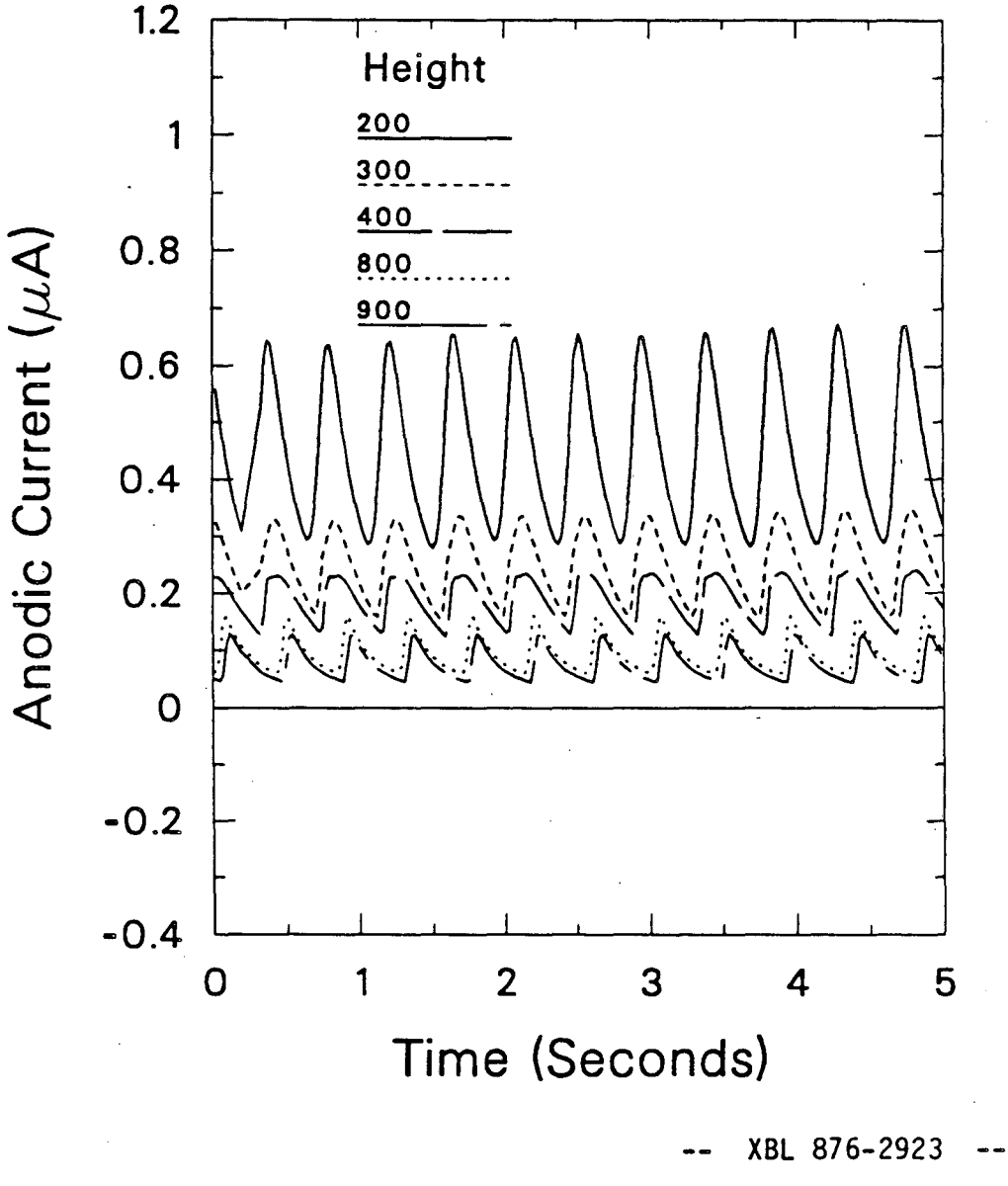

Figure 2. Anodic current to several segments directly above the point of generation of a 28-μA bubble stream rising within the mass-transfer boundary layer, in 0.5-M H_2SO_4. Parameter is distance above bubble-evolving segment.

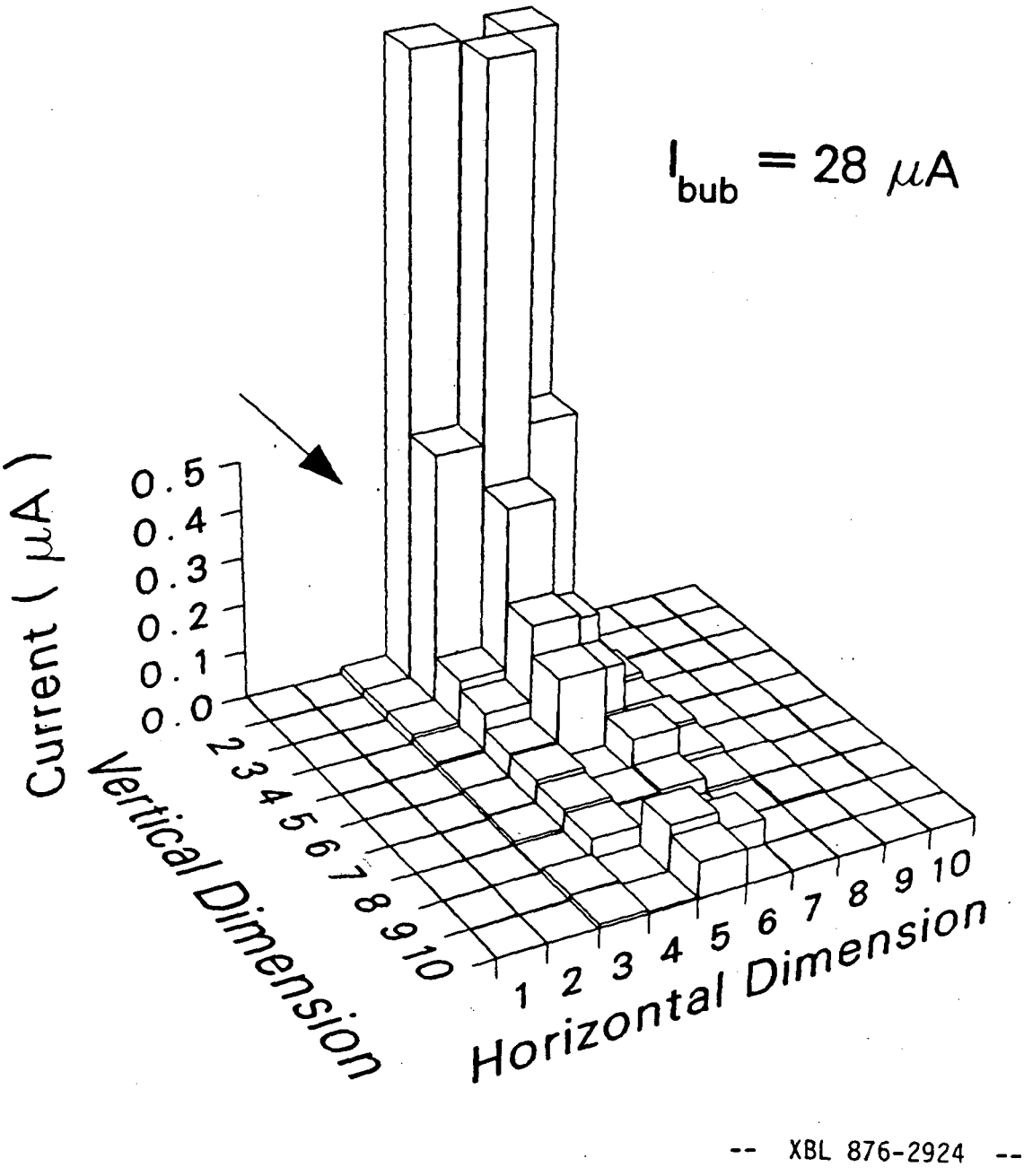

Figure 3. Distribution of anodic current over the segmented portion of the micromosaic electrode when the bubble-evolution site is the fifth from the left in the lowest (rear) row. The bubble evolution rate is 28-μA, and the electrolyte is 0.5-M H_2SO_4.

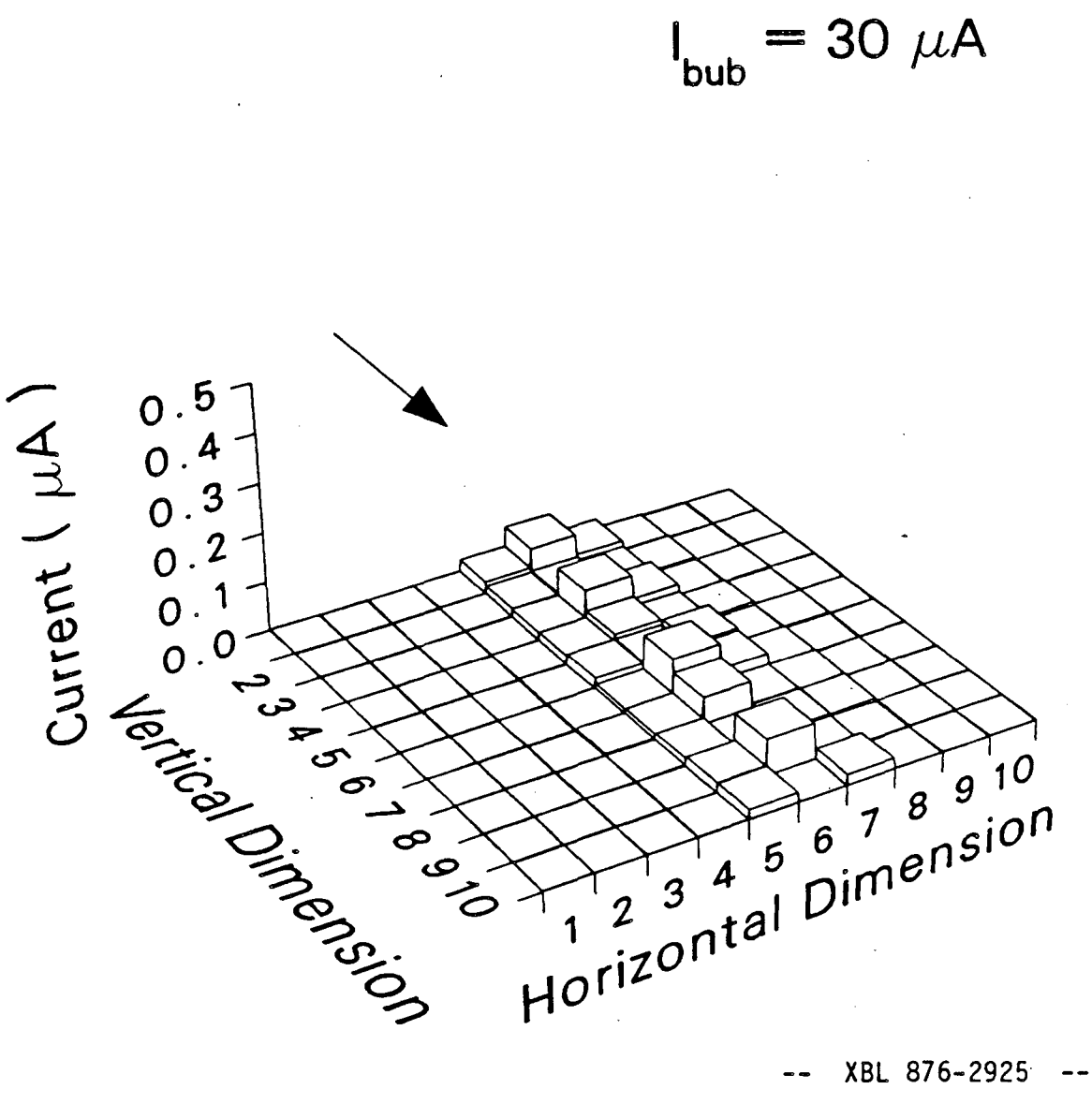

Figure 4. Distribution of anodic current over the segmented portion of the micromosaic electrode when the bubble-evolution site is 600 μm below the bottom (rear) row and in line with the sixth column from the left. The bubble evolution rate is 30-μA, and the electrolyte is 0.5-M H_2SO_4.

from the mass-transfer surface before it reaches the 10 × 10 array of monitoring electrodes. The average anodic current to the segmented area of the micro-mosaic is 0.16 mA /cm ^{2} for the run shown in Figure 4, compared to 0.75 mA /cm ^{2} for the run shown in Figures 2 and 3.

In all of the experiments presented in Chapter 3, in which the bubble stream was generated within the mass-transfer boundary layer, the bubbles were generated at the lowest of the satellite segments to minimize the effect of the oxidation of dissolved hydrogen.

Appendix C. Mass Transfer with Opposing Flows

Some of the preliminary experiments on the effect of bubble streams rising outside the mass-transfer boundary layer showed a destructive interference when the bubbles were rising at distances greater than 450 μm from the micro-mosaic electrode. In the experiments described here, the bubble stream originated from a microelectrode positioned between 200 and 750 μm from the micro-mosaic surface. These experiments were identical to those described in Chapter 3, except that a reference-electrode capillary extended from the top of the cell to the top of the active area of the micro-mosaic electrode. The reference-electrode capillary, as it was in these experiments, can be seen in Figure 3 of Chapter 3.

When the bubble stream originated at 200 or 300 μm from the mass-transfer surface, the mass-transfer rate to the electrode was enhanced by the flow from the ascending bubbles. When the bubble stream was positioned at 450 μm distance, however, the bubble stream had little effect on the mass-transfer rate, and at 750 μm, the rising bubble stream actually caused a *decrease* in the mass-transfer rate. It was concluded that the reference-electrode capillary caused the upward laminar natural-convection along the electrode to deflect downward. In the absence of the capillary, the natural-convection flow would simply dissipate above the active electrode area.

Figure 1 shows the mass-transfer effect of the bubble stream, isolated from the total mass-transfer rate according to Equation 34 of Chapter 3, as a function of

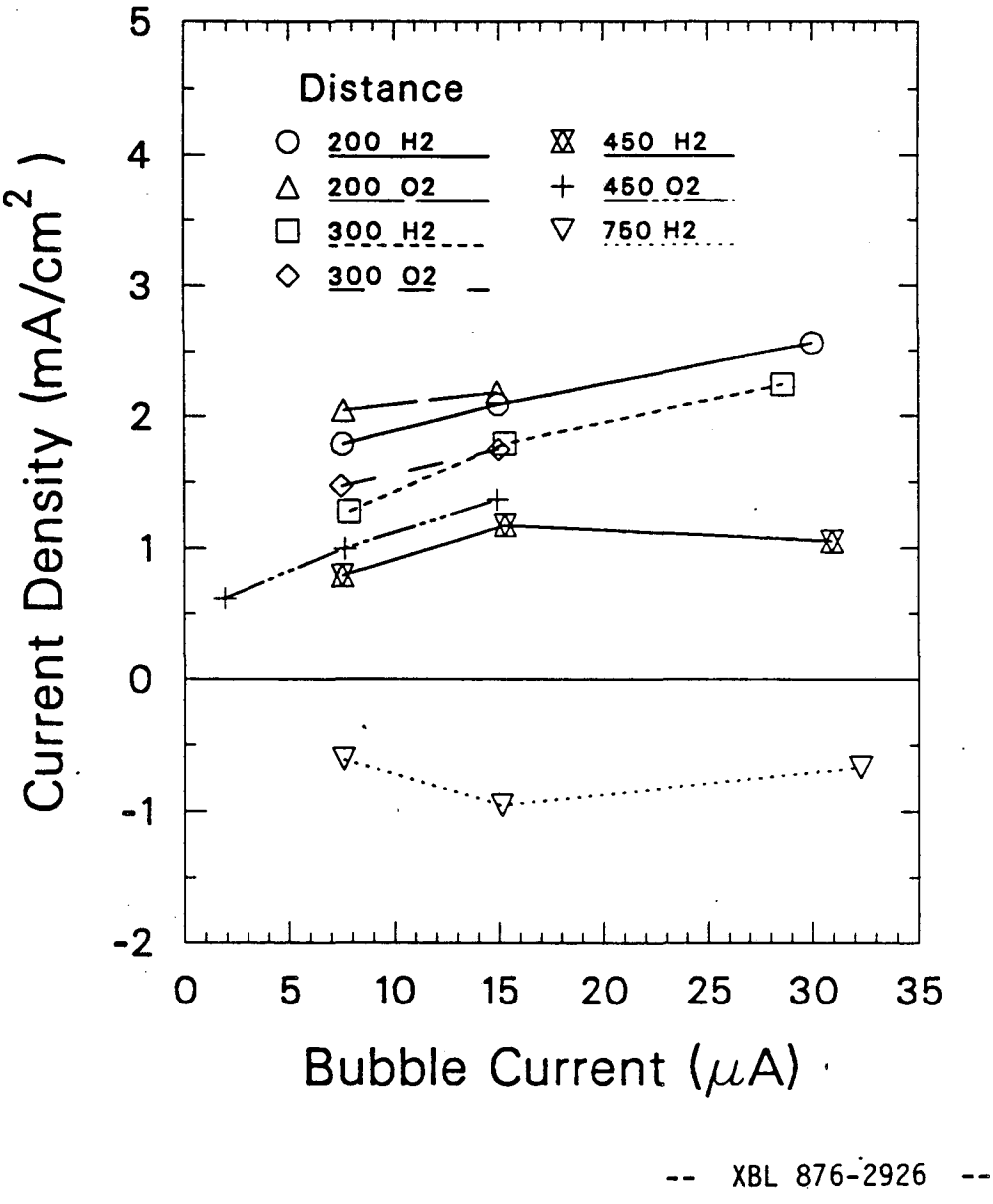

Figure 1. Mass-transfer effect of rising bubbles, averaged over the segmented portion of the electrode and over the time of data acquisition, corrected for the background natural-convection current, as a function of bubble evolution rate. Distance in μm. H2: hydrogen evolution; O2: oxygen evolution.

bubble-evolution rate. Stream distances shown are 200, 300, 450, and 750 μm relative to the micro-mosaic electrode, for both hydrogen (H2) and oxygen (O2). Figure 2 shows the mass-transfer rate plotted against stream position for various bubble currents. In both figures, the oxygen currents have been divided by two to give a volummetric rate equivalent to that of hydrogen. The use of Equation 34 when the bubble-induced convection opposes the free convection may not be strictly valid; however, the effect of bubble-stream position can be seen clearly in this presentation. The interference caused by the downflow can be seen by comparing Figures 1 and 2 to Figures 24 and 25 in Chapter 3, obtained after the cell was modified to eliminate the effect of the reference-electrode capillary.

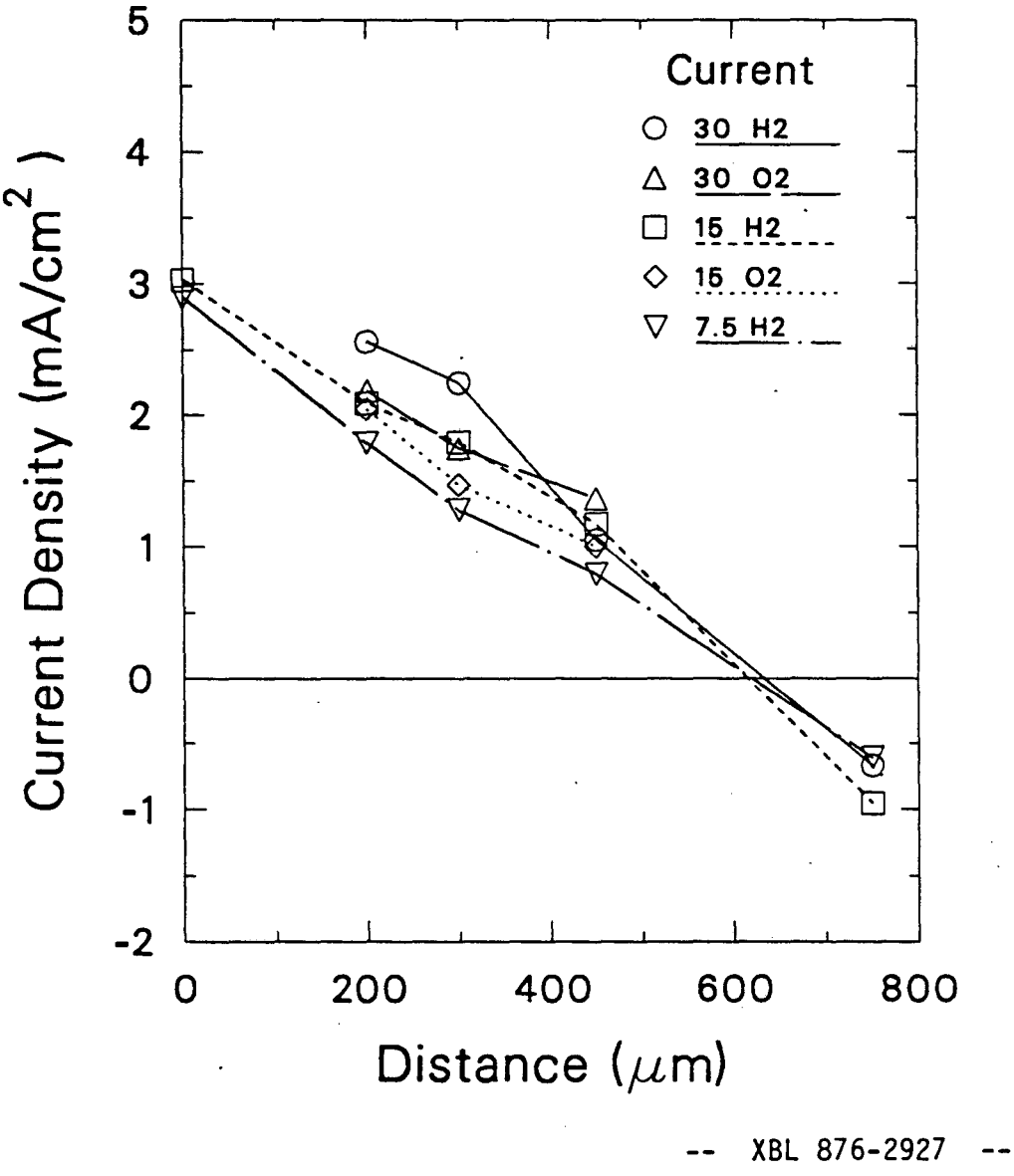

Figure 2. Mass-transfer effect of rising bubbles, averaged over the segmented portion of the electrode, and corrected for the background natural convection current, as a function of bubble stream position. Currents in μA. H2: hydrogen evolution; O2: oxygen evolution.

Appendix D. Stability of the Micro-Mosaic Electrode

Two modes of deterioration of the micro-mosaic electrodes have been identified by photographic examination of used electrodes. One is the formation of a surface film on the electrode and the other is the dissolution of the metal used to enhance the adhesion of the electrode to the insulator. Figure 1 is a photograph at approximately 16× magnification of a used electrode that has what appears to be a surface film. Figures 2 and 3 show the same electrode at 55× and at roughly 110× magnification, respectively. This electrode, #HP01-08, was used for convection-onset experiments, but an unusually high number (33) of segments would not pass current. The segments in Figure 3 that appear the darkest were all working segments. What appears to be a patchy film on this electrode may be the product of an organic impurity in the electrolyte having been reduced at the electrode, or more likely, photoresist that was incompletely removed in processing.

Figure 4 shows electrode #HP01-07, which was immersed in the electrolyte for approximately five hours, but would not pass any current. This was a problem with several electrodes: either the oxide holes were incompletely etched, leaving the surface platinum segments electrically isolated from the aluminum conductors, or again, the photoresist was not removed properly. Since cleaning in organic solvents did not solve this problem, it is more likely that the oxide holes were not completely etched. This would help to explain the rapid deterioration of this particular electrode. Figure 5 is a closeup of the upper left corner of the electrode. There is a

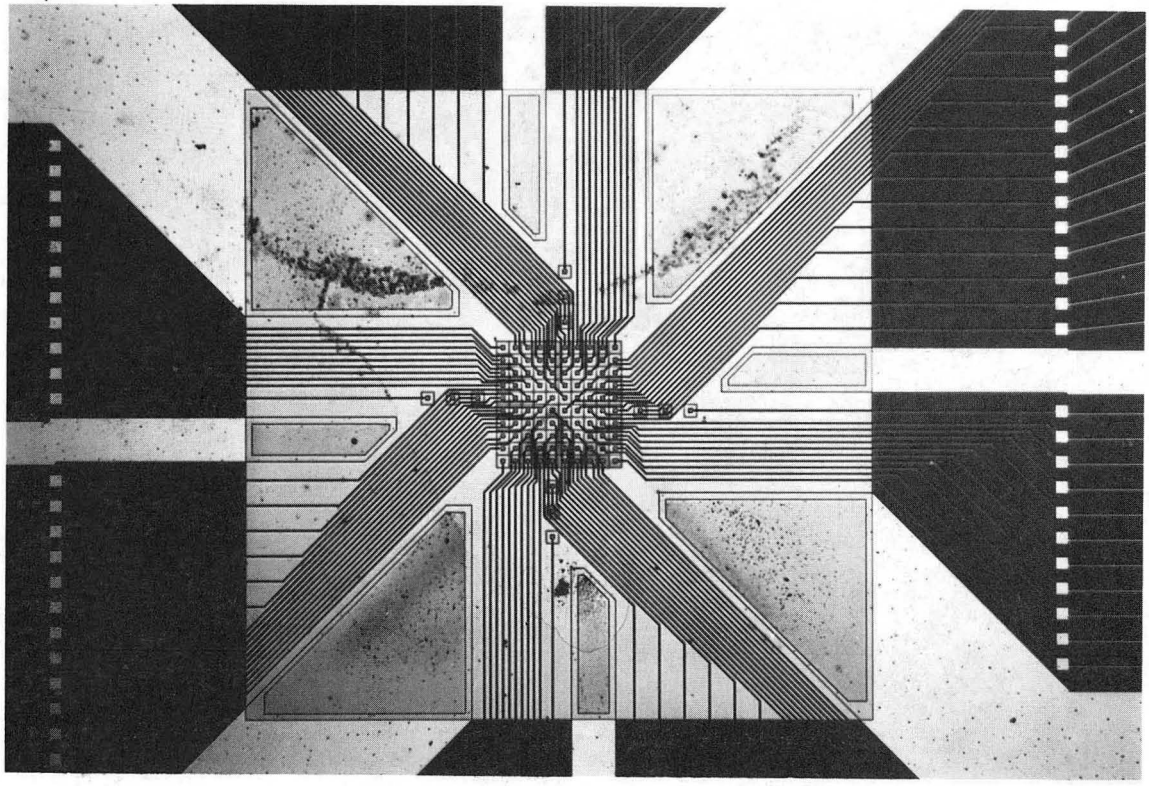

XBB 872-1323

Figure 1. Used micro-mosaic electrode #HP01-08, showing what appears to be a surface film, at approximately 16× magnification.

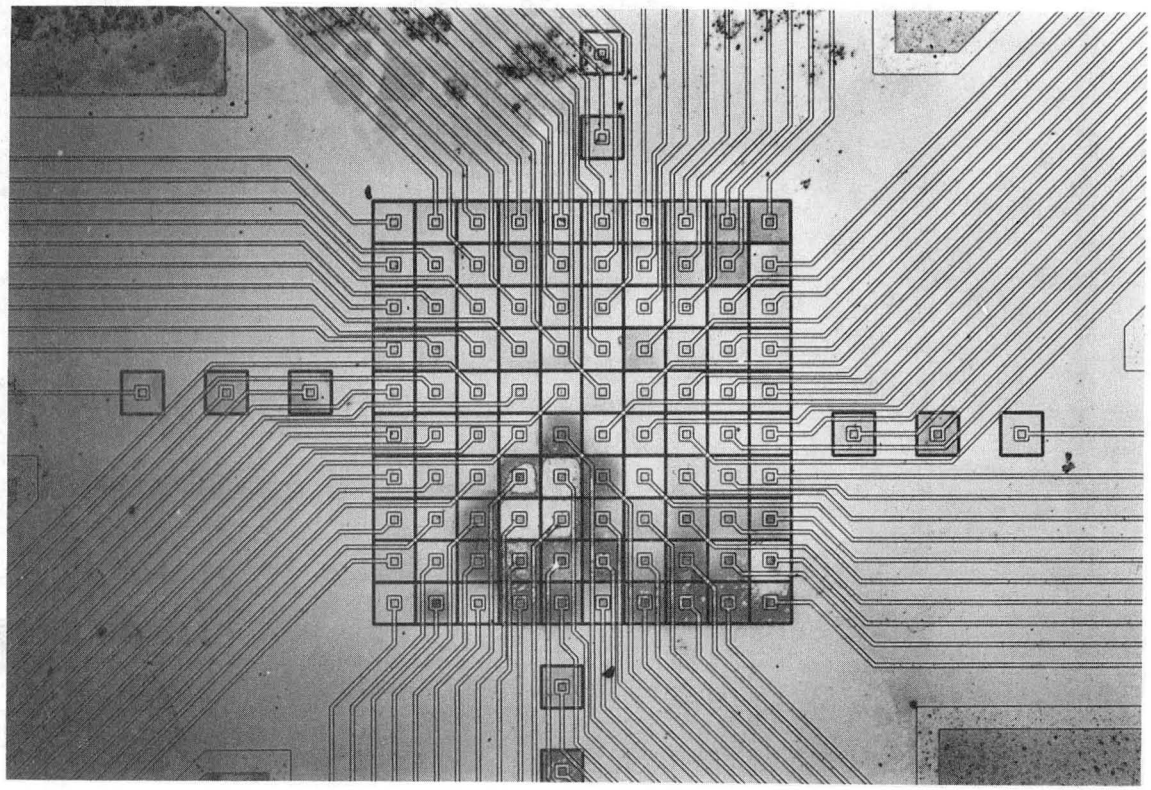

XBB 872-1322

Figure 2. Used micro-mosaic electrode #HP01-08, with what appears to be a surface film, at approximately 55× magnification.

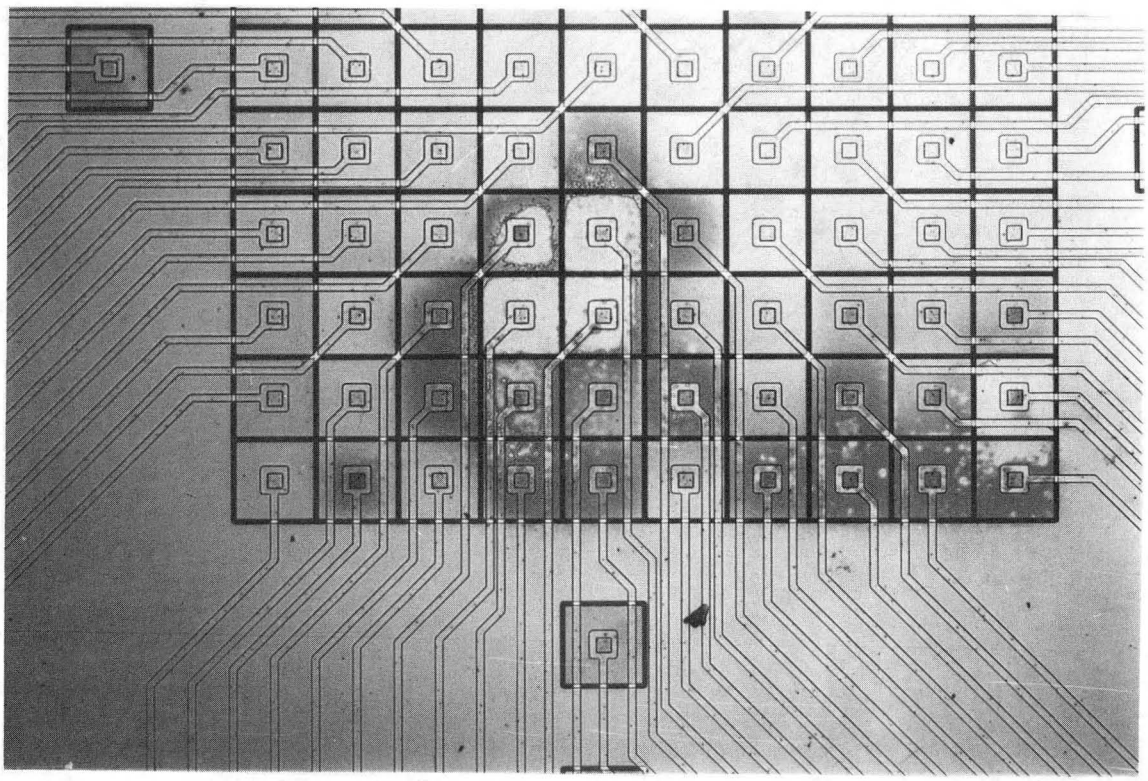

XBB 872-1324

Figure 3. Used micro-mosaic electrode #HP01-08, which apparently has a surface film, at approximately 110× magnification.

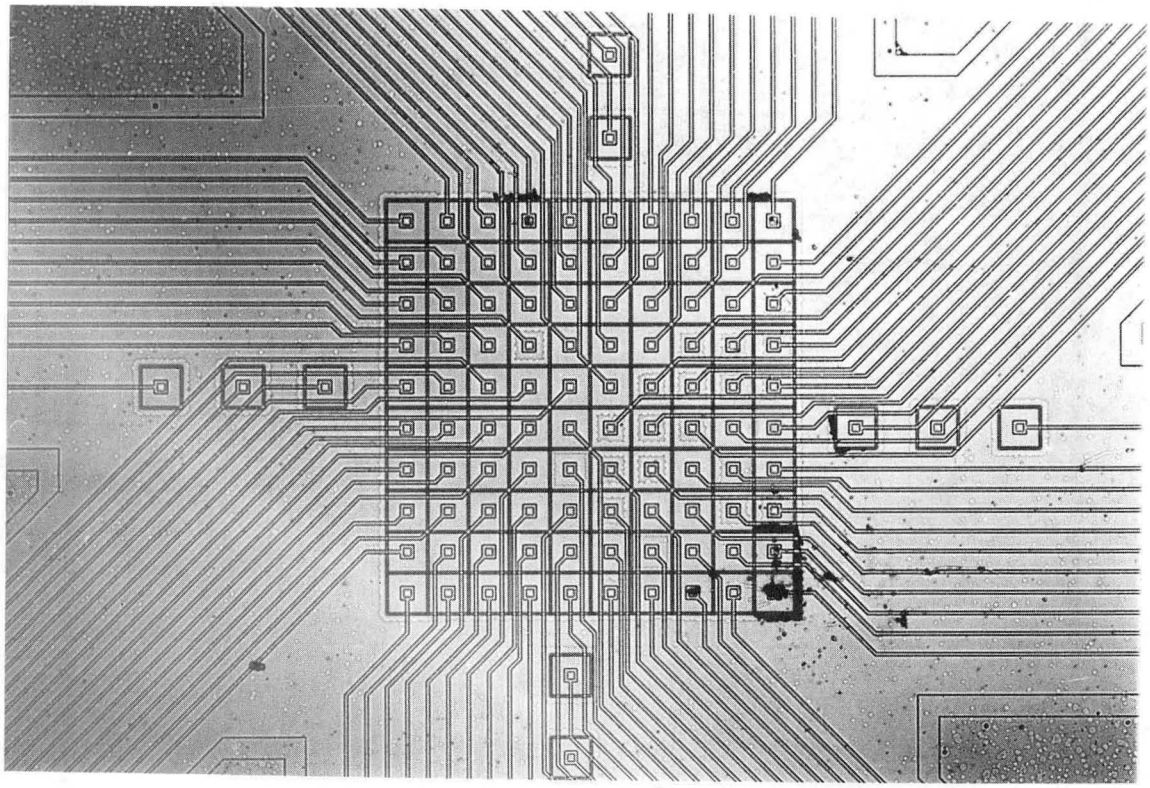

XBB 872-1326

Figure 4. Micro-mosaic electrode #HP01-07 after immersion in $Fe_2(SO_4)_3/H_2SO_4$ electrolyte for approximately five hours.

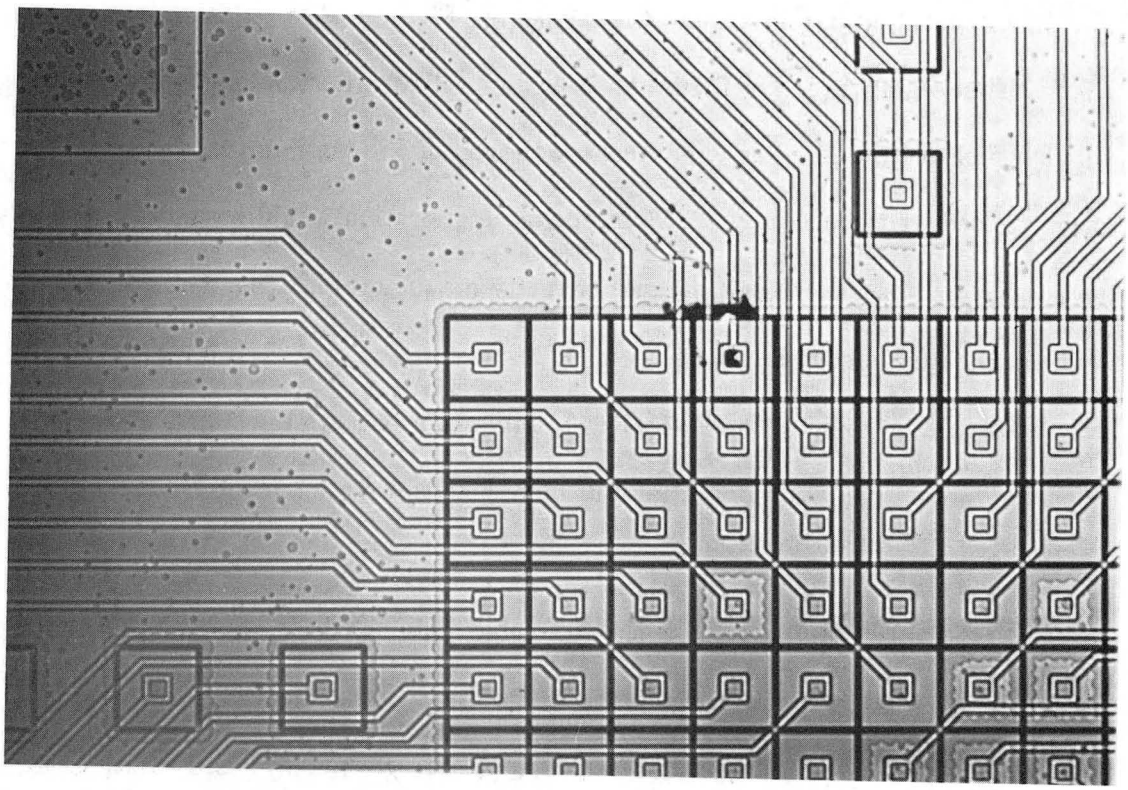

XBB 872-1329

Figure 5. Upper left corner of used micro-mosaic electrode shown in Figure 4, showing scalloped edge.

scalloped border along the outer edge of the 10 × 10 array of segments and along the inner edges of some of the segments. Figure 6 shows the top row of segments at still higher magnification (roughly 220 ×). The dark areas are places where the electrode material has peeled away from the oxide. A similar problem affecting one of the satellite segments of electrode #HP01-07 is shown at 550× magnification in Figure 7. The adhesion of the electrode to the oxide failed only in all areas that look like a scalloped border around the segments. Figure 8 shows this scalloping affect within segment [4,4] in Figure 5. What we believe we are seeing is an area where the chromium, used to enhance the adhesion of the platinum to the oxide, has been oxidized by the electrolyte. This type of deterioration would have been accelerated on a segment that, because of faulty manufacture, was not in contact with the aluminum conductor. In normal operation, the electrode is polarized to about 650 mV cathodic to the Fe^{+2}/Fe^{+3} equilibrium potential, which is still anodic to the chromium oxidation potential, but much less so than if the electrode were at open circuit.

The problem of oxidation of the less noble metal used for adhesion (Cr in the case of the Hewlett-Packard electrodes, and Ti in the Bell Labs electrodes) was foreseen by the researchers who made them, and both groups proposed solutions for future generations of electrodes. The Hewlett-Packard group suggested filling the grooves with silicon nitride as a final processing step. The Bell Labs group proposed using a lift-off metallization technique, which would allow the top electrode layers to cover the sides of the layers beneath, preventing exposure of the less noble metal to the electrolyte.

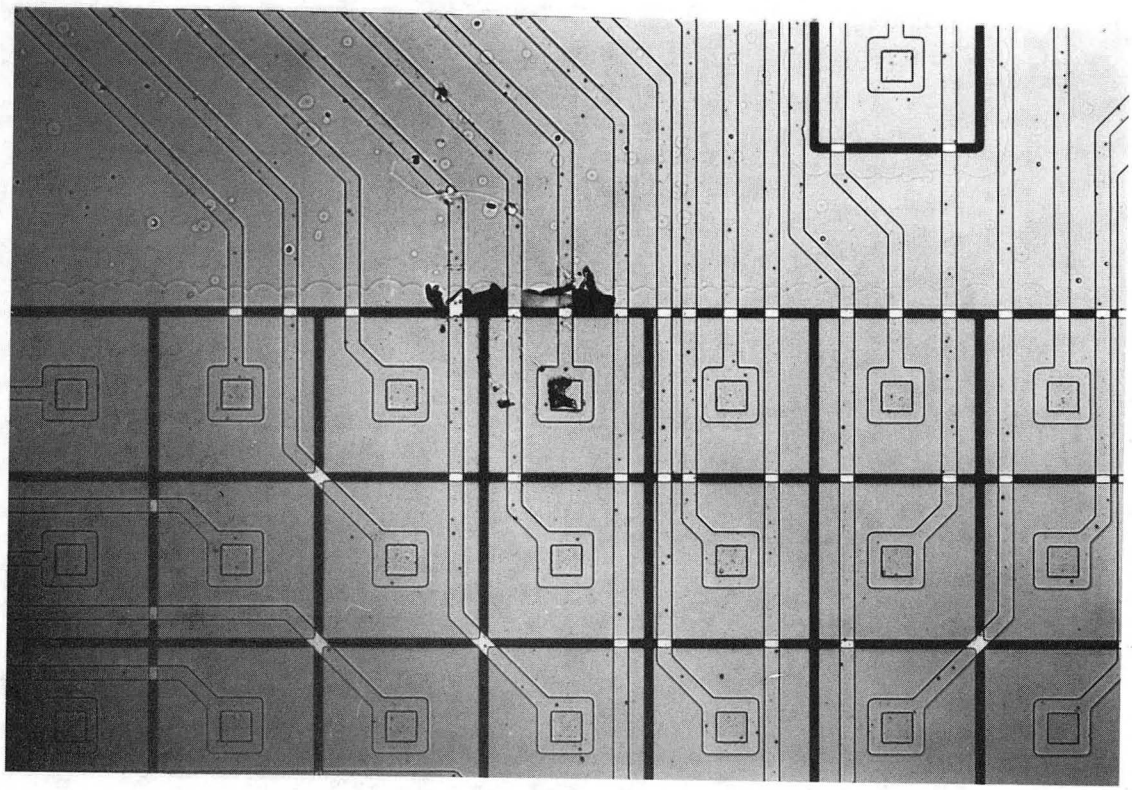

XBB 872-1328

Figure 6. Top row of segments from Figure 4, showing electrode material peeled away from the insulator material.

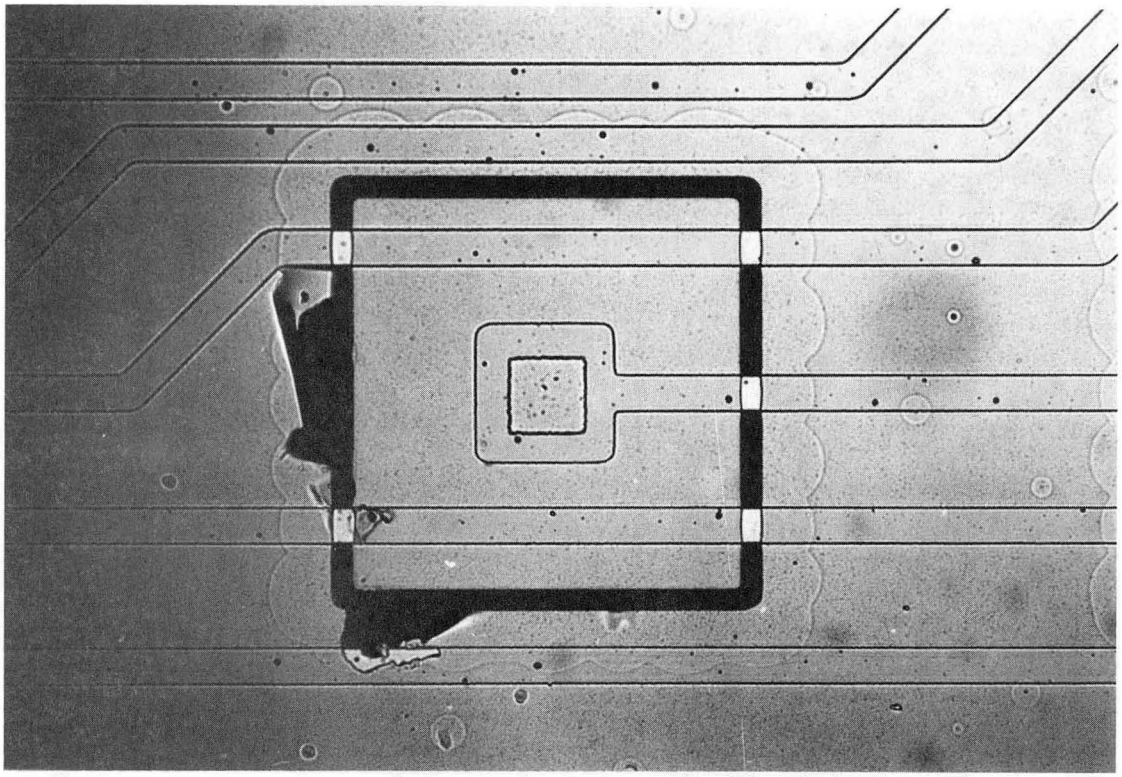

XBB 872-1331

Figure 7. One of the three satellite segments to the right of the 10 × 10 array of micro-electrodes in Figure 4, showing failure of adhesion of the electrode surface, at roughly 550× magnification.

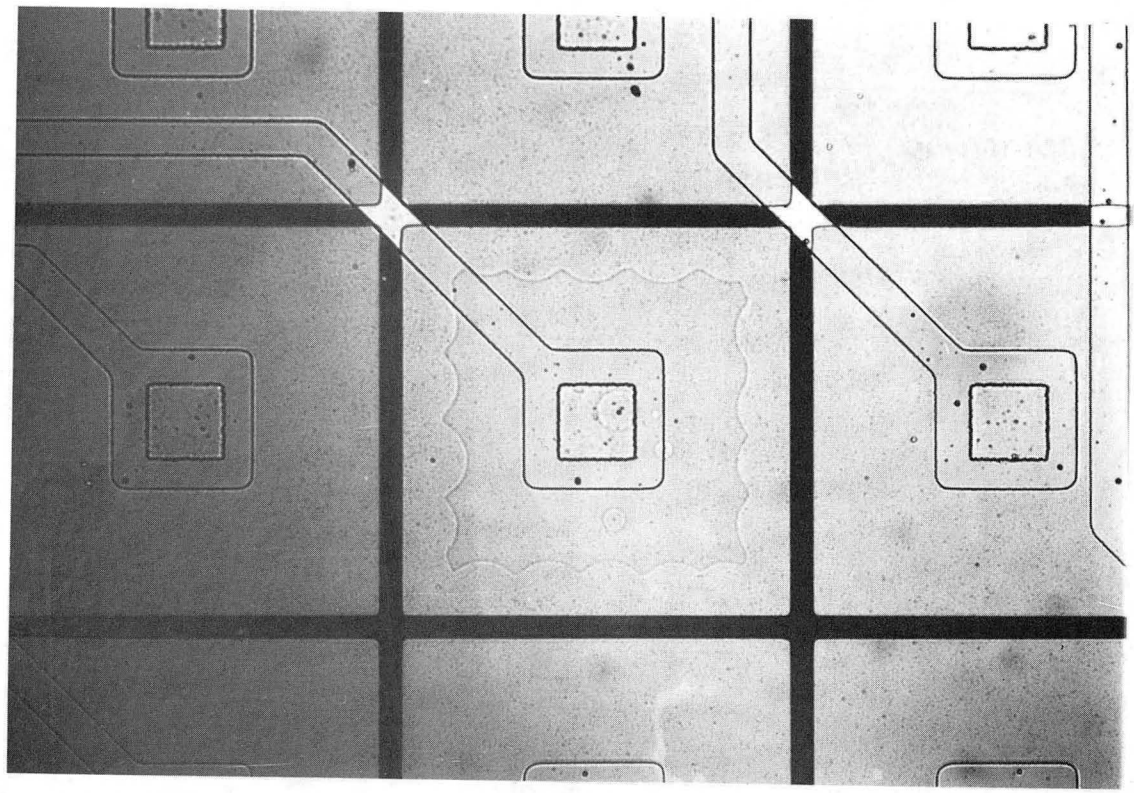

XBB 872-1330

Figure 8. Segment [4,4] in Figure 5, showing edge where the chromium has been oxidized (roughly 550× magnification).

Appendix E. Electrode History

Electrode	Date used	Experiments	Hours in solution	Non-working segments initially	Non-working segments finally
BL01-10	2/21/85	022101-06	6	10	16
BL01-10	2/28/85	022801	2	would not pass current	
HP01-02	3/7/85	030701-04	14	16	29
HP01-03	3/10/85	031001-06	6	24	28
HP01-04	3/12/85	031201-06	5.5	4	5
HP01-05	3/16/85	031601-08	3 in H_2SO_4	15	13
		031609-13	1 in $Fe_2(SO_4)_3$		
HP01-06	10/18/85	101801-04	8	29	25
HP01-07[1]	10/20/85	102001-02	5	would not pass current	
HP01-09	10/21/85	102101-23	10	12	14
HP01-08[2]	3/11/86	031101-09	4	33	40
HP01-10	4/1/86			cell leaked	
BL01-12	6/8/86	060801-04	3	cell leaked	
HP01-11	9/24/86			would not pass current	
HP01-13	10/9/86		3.5	would not pass current	
HP01-04	10/10/86	101001-31	7.5	6	6

[1] Shown in Appendix D, Figures 4-8.

[2] Shown in Appendix D, Figures 1-3.

Appendix F. Chapter 2 Programs

The following programs were used for the calculations in Chapter 2. Program BUBCALC is used to calculate bubble shapes and stability. Program PLOTBUB reads the output files from BUBCALC and creates a plot file that is usable by Tell-a-graph.

Program BUBCALC

```
      Program BUBCAL
      Implicit real*8 (a-h,o-z)

      character*10        outfile

      common  /par/       BetaI, deltB, IND, UI, IPrint, IDraw, Beta
      common  /par2/      IBMax, INDR, IStab, LOUT
      common  /BUB/       Arcl, Cmass, RAR
      common  /BUB2/      RmaxF, Vmax, Theta, Height, Radc, EMax

      LIN =    3
      LOUT = 4

      open (unit=LIN, file='bubcal',
     &           defaultfile='[whitney.bubble].dat', status='old')

      Read (LIN, *) outfile

      open (unit=LOUT, file=outfile,
     &           defaultfile='[whitney.bubble].out', status='new')

      Read (LIN, *) ncase

      Do 100, J = 1, ncase
        Read (LIN, *) IND
        Read (LIN, *) BetaI
        Read (LIN, *)   DeltB
        Read (LIN, *) UI
        Read (LIN, *) IPrint
        Read (LIN, *) IDraw
        Read (LIN, *) IBMax
        Read (LIN, *) INDR
        Read (LIN, *) IStab

        Call BUBSIZ

100   Continue

      Stop
      End

      SUBROUTINE BUBSIZ                                    BUBSIZ
```

```
c           Subroutine BUBSIZ finds maximum bubble size for a
c             given contact angle, Theta, or radius of contact, Rc.
c
c           Input parameters come through blocks param and param2.
c
c           Common par contains:
c             BetaI, deltB, IND, UI, IPrint, IDraw, Beta
c
c           BetaI is an initial guess for Beta ( <0 for bubbles).
c           IND is 0 if final condition is Theta.
c                  1 if final condition is Rc.
c                  2 if final condition is Volume.
c           UI is Theta if IND=0.
c                 Rc if IND=1.
c                 Volume if IND=2.
c           IPrint indicates whether intermediate results should be printed.
c             If IPrint = -1  Prints nothing.
c             If IPrint =  0  Prints Beta, Theta, Rc, Height, Rmax, Volume.
c             If IPrint = +1  Prints above plus Z's and X's FOR
c                    EVERY BUBBLE.
c           IPrint is ususally set at 0.
c
c           IDraw indicates whether Z's and X's should be printed for
c             MAXIMUM SIZE BUBBLE.
c             If IDraw = 0  Prints nothing.
c             If IDraw = 1  Prints Z's and X's.
c           IDraw is usually set at 0.
c
c           Beta is value of Beta for largest bubble meeting condition.
c
c           Common par2 contains:
c             IBMax, INDR, Istab
c
c           IBMax is max number of times beta can be varied.
c
c           INDR is an input indicator
c             If INDR = 0, only first occurences of contact angle are found.
c             If INDR = 1, second occurences are sought.
c
c           Istab=(0,1)  whether or not to print stability results.
c
c     Other indicator variables:
c
c           Global indicators:
```

```
c          IFAIL    = 1 if current beta is too large and condition
c                   can not be met. (Set at direction change if
c                   NDIR = 2.)
c          I4       = Number of times end condition could not be met.
c          IDONE    = 1 if we have found maximum volume beta to three
c                     sig figs.  Going back for previous (best) beta.
c          IBETA    = number of beta values used.
c          INBeta   = number of stored end points.
c
c          Indicators local to value of beta:
c          IDIR     = sign of dx/ds.
c          NDIR     = number of times IDIR has changed.
c          I2       = 0 at start of each beta because first
c                     Runga-Kutta step is different.
c          IREE     = 1 after first beta has been found.
c          INEXT    = 0 at start of each beta, 1 immediately
c                     after finding first theta.  If INEXT
c                     is 1, meeting theta boundary condition
c                     is not checked.
c
c          Other results are returned through common blocks.
c
c
c          Common BUB contains:
c            Arcl   = Arc length of largest bubble,
c            Cmass  = Z-value of center of mass of largest bubble
c                     after release,
c            RAR    = Radius of bubble after release.
c
c          Common BUB2 contains:
c            RmaxF  = Maximum radius of the largest bubble,
c            Vmax   = Volume of largest bubble,
c            Theta  = Contact angle of largest bubble,
c            Height = Height
c            Radc   = Radius of contact.
c
c
c          Program by Gina Whitney, April 15, 1984.
c
c
ccccccccccccccccccccccccccccccccccccccccccccccccccccccccccccccccccccccccccccc
```

Implicit real*8 (a–h,o–z)

dimension F(5), G(5), H(5), W(5), E(5), XK(5,4)

```
      dimension       X(2), Z(2), P(2500), Q(2500), TH(2500), V(2500)
      dimension       Bet(400), Thet(400), CRad(400), Heigh(400)
      dimension       Vo(400), Rma(400), Energ(400), Req7(400)
      dimension       pittsV(400), PittsN(400), PittsR(400)
      dimension       xmu(400), xkappa(400), xlambda(400)

      common  /par/   BetaI, deltB, IND, UI, IPrint, IDraw, Beta
      common  /par2/  IBMax, INDR, IStab, LOUT
      common  /BUB/   Arcl, Cmass, RAR
      common  /BUB2/  RmaxF, Vmax, Theta, Height, Radc, EMax

      data    Sqr2, PI /1.414213562,3.141592654 /


c
c       Calculate constants, initialize Beta and set step size.
c



      A = ( Sqr2 - 1.0 ) / 2.0
      B = ( 2.0 - Sqr2 ) / 2.0
      C =  -Sqr2 / 2.0
      D = 1.0 + Sqr2 / 2.0

      gamma = 72.8
      rho   = 0.997
      gr    = 980.0

      rgog  = rho * gr / gamma
      xLc   = dsqrt (1.d0 / rgog)

      SS = 0.01
      DS = 0.01

      Beta = BetaI
      KMAX = 2500

      Write (LOUT, 901)  IStab, IDraw, IND
901   Format (i5, '    IStab',/,i5,'    IDraw',/,i5,'    IND')

      If (IND . eq . 0) Then
        ThetaC = UI
        U = pi * UI / 180.0
        sinalf = sin ( pi - U )
        U = sinalf
        Write (LOUT, 902)  ThetaC
```

```
  902       Format (f8.3,'    Criterion is contact angle')

            Elseif (IND . eq . 1)  Then
              Rc = UI
              U  = UI
              Write (LOUT, 903)  Rc
  903       Format (f8.5,'    Criterion is Radius of contact')

            Else
              Volc = UI
              U = UI
              Write (LOUT, 904)  Volc
  904       Format (e10.5,'    Criterion is Volume')
            Endif

c
c   Set up headings for output.
c

            If (IPrint . gt . 0)  Then

              Write (LOUT, 910)
  910       Format ( /, 4x,'Beta',6x,'Theta',7x,'Radc',6x,'Height',5x,
     1       'Volume',6x,'Rmax',11x,'Z',12x,'X',//)

            Endif

c
c   Top of loop for first Beta.
c   Initialize indicator variables for finding maximum Beta.
c

    99      IBeta = 1
            NBRC1 = 0
            NBRC2 = 0
            INBeta = 0
            I4 = 0
            IDone = 0
            IFail = 0

c .
c   Top of loop for subsequent Betas.
c   Initialize variables.
c
```

```
c
  100     R0 = sqrt ( abs ( Beta * gamma / ( rho * gr ) ) )

          If ( IBeta . GT . IBMax ) Go to 600

          Energy = 0.0

          Vol    = 0.0
          Arcl   = 0.0
          Cmass  = 0.0

          X(1)   = 0.0
          Z(1)   = 0.0

          F(1)   = 0.0
          G(1)   = 0.0
          H(1)   = 0.0
          W(1)   = 0.0
          E(1)   = 0.0

          P(1)   = 0.0
          Q(1)   = 0.0
          TH(1)  = 180.0
          V(1)   = 0.0

          Kount  = 1
          KTemp  = 1
          KTempd = 1
          IDir   = 1
          NDir   = 0
          I2     = 0
          IREE   = 0
          INEXT  = 0

c
c   Go to 110 to begin Runge-Kutta calculations.
c

          Go to 110

c
c   Changing direction operation.
c

  700     If ( KTempd . ge . 3 ) Go to 720
```

```
c
c   Decrease step size.
c
          DS = 0.1 * DS
          KTempd = KTempd + 1
          Go to 110

c
c   Change direction.
c
  720     IDir = -IDir
          NDir = NDir + 1
          G(1) = 1 - abs (1 - G(1))
          If (NDIR . eq . 1 )  Rmax = X(1)
          DS   = SS
          KTempd = 1

          If (IND . eq . 1 . and . Rmax . lt . U)  IFail = 1
          If (NDir . eq . 2) IFail = 1

          Go to 110


c
c   Meeting condition operation.
c

  750     If ( KTemp . ge . 3)  Go to 770

c
c   Decrease step size.
c
          DS = 0.1 * DS
          KTemp = KTemp + 1
          Go to 110

c
c   Condition met.
c

  770     DS = SS
          KTemp = 1
          Go to 400
```

```
ccccccccccccccccccccccccccccccccccccc
c
c    Runge-Kutta Step
c

  110     Do 230  I = 1, 4

c
c   Check to see if getting time to switch direction.
c

          If ( G(I) . GT . 1 )  Go to 700

c
c   Check to see if getting near stopping condition.
c
          If ( INEXT . EQ . 1 )  Go to 160
          If ( IND . ne . 0 )  Go to 140

c
c   Check Theta.
c

          If ( IDir . EQ . -1 . AND . U . EQ . 1 )  Go to 400
          If ( IDir.EQ.-1 . AND . IREE.EQ.0 . AND . G(I).LT.U )
     &              Go to 750
          If ( IDir.EQ.-1 . AND . IREE.EQ.1 . AND . G(I).GT.U )
     &              Go to 750

          Go to 160

c
c   Check Rc.
c

  140     If ( IND . ne . 1 )  Go to 150
          If ( IREE . eq . 1 )  Go to 145
          If ( IDir . eq .  1 . AND . H(I)*R0 . gt . U )  Go to 750
          Go to 160
  145     If ( IDir . eq . -1 . AND . H(I)*R0 . lt . U )  Go to 750
          Go to 160
c
c   Check Volume.
c
  150     If ( (W(I)*pi*R0**3.0) . gt . U )  Go to 750
```

```
c
c  Proceed with calculation.
c
  160     INEXT = 0

          If ( I2 . ne . 0 )  Go to 180

c
c  First time through.
c

          I2  = 1
          XK(1,I) = DS
          Go to 190

c
c  After first time through.
c

  180     XK(1,I) = DS * IDir * (( 2.0 + Beta * F(I) - G(I) / H(I))
     1       * Sqrt ( 1.0 - G(I) * G(I) ))
  190     XK(2,I) = DS * G(I)
          XK(3,I) = DS * IDir * Sqrt ( 1.0 - G(I) * G(I) )
          XK(4,I) = DS * G(I) * H(I) * H(I)
          XK(5,I) = DS * (2.0 * H(I) + dabs(beta) * H(I) * H(I)
     1       * F(I) * G(I))

  200     If ( I . GT . 1 )  Go to 210

          G(2) = G(1) + XK(1,1) / 2.0
          F(2) = F(1) + XK(2,1) / 2.0
          H(2) = H(1) + XK(3,1) / 2.0
          W(2) = W(1) + XK(4,1) / 2.0
          E(2) = E(1) + XK(5,1) / 2.0
          Go to 230

  210     If ( I . GT . 2 )  Go to 220

          G(3) = G(1) + A * XK(1,1) + B * XK(1,2)
          F(3) = F(1) + A * XK(2,1) + B * XK(2,2)
          H(3) = H(1) + A * XK(3,1) + B * XK(3,2)
          W(3) = W(1) + A * XK(4,1) + B * XK(4,2)
          E(3) = E(1) + A * XK(5,1) + B * XK(5,2)
          Go to 230

  220     If ( I . GT . 3 )  Go to 230
```

```
      G(4) = G(1) + C * XK(1,2) + D * XK(1,3)
      F(4) = F(1) + C * XK(2,2) + D * XK(2,3)
      H(4) = H(1) + C * XK(3,2) + D * XK(3,3)
      W(4) = W(1) + C * XK(4,2) + D * XK(4,3)
      E(4) = E(1) + C * XK(5,2) + D * XK(5,3)

230   Continue

      G(5) = G(1) + (XK(1,1) + XK(1,2))/6.0 + (XK(1,3) + XK(1,4))/3.0
      F(5) = F(1) + (XK(2,1) + XK(2,2))/6.0 + (XK(2,3) + XK(2,4))/3.0
      H(5) = H(1) + (XK(3,1) + XK(3,2))/6.0 + (XK(3,3) + XK(3,4))/3.0
      W(5) = W(1) + (XK(4,1) + XK(4,2))/6.0 + (XK(4,3) + XK(4,4))/3.0
      E(5) = E(1) + (XK(5,1) + XK(5,2))/6.0 + (XK(5,3) + XK(5,4))/3.0

c
c  End of Runge-Kutta.
c

c
c  Update and move things over.
c

      Kount = Kount + 1


      X(2) = H(5) * R0
      Z(2) = F(5) * R0


      CMass = CMass + (pi/2.0) * (Z(2) - Z(1)) * ( Z(1) * X(1) * X(1)
     1      + Z(2) * X(2) * X(2) )

      X(1) = X(2)
      Z(1) = Z(2)

      G(1) = G(5)
      F(1) = F(5)
      H(1) = H(5)
      W(1) = W(5)
      E(1) = E(5)

      Y = Z(1)
      Vol = W(1) * pi * R0**3.0
      Energy = E(1) * pi * gamma * R0 * R0

      If ( IDir . ne . -1 )  Go to 320
```

```
            x5 = 0
            Go to 330

  320       x5 = 180
  330       P(Kount)  = X(1)
            Q(Kount)  = Y
            TH(Kount) = x5 - (180.0/pi) * IDir * Asin(G(1))
            V(Kount)  = Vol

            Arcl  = Arcl + DS * R0

c
c   Check to see if condition not met.
c

  335       If ( IFail . NE . 1 )  Go to 340

            I4 = I4 + 1
            Go to 400

c
c   Condition not yet satisfied.
c

  340       If ( Kount . LT . KMax )  Go to 350
            Write (LOUT, 930)  Kount
  930       Format (10x,'Step size too small ', I5, 'Steps')
            Go to 400

  350       If ( IND . ne . 0 )  Go to 370

c
c   Check theta.
c
            If ( IREE . ne . 0 )  Go to 360

            If ( IDir . eq . 1 . OR . G(1) . gt . U )  Go to 110
            Go to 400

  360       If ( IDir . eq . 1 . OR . G(1) . lt . U )  Go to 110
            Go to 400

c
c   Check Rc.
```

```
c
  370     If ( IND . ne . 1 )  Go to 380
          If ( IREE . eq . 1 )  Go to 375
          If ( IDir . eq .  1 . and . X(1) . lt . U )  Go to 110
          Go to 400
  375     If ( IDir . eq . 1 )  Go to 110
          If ( IDir . eq . -1 . and . X(1) . gt . U )  Go to 110
          Go to 400

c
c  Check volume.
c
  380     If ( Vol . lt . U )  Go to 110

c
c  Met boundary condition.  Print calculations.
c

  400     If ( KTemp . eq . 3 )  Go to 750

          thetarad = TH(KOUNT) * pi / 180.d0

          Energy = Energy - rho * gr * Q(Kount) * Vol  +
     1       gamma * pi * P(Kount) ** 2.0 * cos(thetarad)

          PittsMu = 2.d0 / dsqrt(-Beta)
          PittsVol = Vol / (pi * xLc ** 3.0)
          PittsLam = P(KOUNT) / xLc
          PittsKap = Q(KOUNT) / xLc

          If ( IND . eq . 1 . and . TH(Kount)  . gt . 170. )  IDone = 1
          If ( IND . eq . 2 . and . TH(Kount)  . gt . 120. )  IDone = 1

          If ( IPrint . LT . 0 )  Go to 460

c  Store values

          If (IFail . EQ . 1)  Go to 430
          If (IDone . EQ . 1 . and . IND . eq . 0)  Go to 430
          If (IND . eq . 1 . and . dabs(Beta) . ge . 0.05)  DeltB = 0.01

          INBeta = INBeta + 1
          Bet(INBeta) = Beta
          Thet(INBeta) = TH(KOUNT)
          Crad(INBeta) = P(KOUNT)
          Heigh(INBeta) = Q(KOUNT)
          Vo(INBeta) = Vol
```

```
            Rma(INBeta) = Rmax
            Energ(INBeta) = Energy

            PittsV(INBETA) = PittsVol
            PittsN(INBETA) = -3.0 * PittsVol/tan(thetarad) - PittsLam**3.0
            PittsR(INBETA) = PittsLam*(PittsKap - PittsMu) + sin(thetarad)
            Req7(INBETA) = (PittsVol/PittsLam) - sin(thetarad)
            xMu(INBETA) = PittsMu
            xKappa(INBETA) = PittsKap
            xLambda(INBETA)= PittsLam


  430       If ( IPrint . EQ . 0 )  Go to 460

            If ( IFail . EQ . 1 )  Go to 440

            If ( IREE . EQ . 0 . AND . INDR . EQ . 1 )  Go to 460

  440       Write (LOUT, 940)
  940       Format ()

c   If we're here, IPrint = 1 and we've found reentrant theta or gone to 90.

            Write (LOUT, 960)  Beta, TH(KOUNT), P(KOUNT), Q(KOUNT),
     &                         Vol, RMax, Energy

            Do 450,  I = 1, Kount
  450       Write (LOUT, 950)  TH(I), V(I), Q(I), P(I), -P(I)
  950       Format ( 11x, f11.7, 22x, f11.7, 11x, 3(2x,F11.7) )

  460       If ( IFail . ne . 1 )  Go to 470
            If ( IND . ne . 1 )    Go to 500
            If ( Rmax . lt . U )  Go to 500
c
c   If we're here, (IFAIL=1, IND=1, and IREE=1), we've found first Rc,
c   but not a second.
c
            NBRC1 = NBRC1 + 1
            IFail = 0
            Go to 495

  470       If ( IND . eq . 2 )    Go to 495
            If ( IREE .  eq . INDR  )  Go to 490
```

```
c
c   If we're here we've found first theta or Rc and want to look for
c   second.
c
          Energy = Energy + rho * gr * Q(Kount) * Vol -
     1       gamma * pi * P(Kount)**2.0 * cos(thetarad)

          IREE  = 1
          INEXT = 1

          Go to 110


c
c   Keep track of number of second Rc's found.
c
   490    If ( IND.eq.1 . and . INDR.eq.1 )  NBRC2 = NBRC2 + 1

   495    If ( IDone . EQ . 1 )  Go to 600


c
c   Increase abs ( Beta ) and make a new bubble.
c
          Beta  = Beta - DeltB
          IBeta = IBeta + 1
          Go to 100


c
c   Criterion not met.  Check if first time through.
c
   500    If ( IBeta . ne . 1 )  Go to 520

c
c   First time through.  Adjust abs ( Beta ).
c
          If ( IND . eq . 0 )  Go to 510

c
```

```
c   abs (Beta) too small for Rc or volume condition.
c
            Beta = Beta - DeltB
            Go to 99

c
c   abs (Beta) too large for theta condition.  Decrease abs (Beta).
c
  510       Beta = Beta + DeltB
            Go to 99

c
c   Check if first time condition not met.
c
  520       If ( I4 . ge . 3 )  Go to 540

c
c   First time condition not met. Decrease abs ( Beta ) and DeltB to
c   get more exact value of Beta.
c
            Beta = Beta + 0.9 * DeltB
            DeltB = 0.1 * DeltB
            IBeta = IBeta + 1
            IFail = 0
            Go to 100

c
c   If we got here, we've not met condition for second time
c   so we have Beta to 2 sig figs.
c
c   Decrease Beta one more time to get previous bubble.
c
  540       IDone = 1
            IFail = 0
            Beta  = Beta + DeltB
            IBeta = IBeta + 1
            Go to 100
```

```
c
c  Finally done.  Have largest equilibrium bubble to two sig figs
c  in Beta.  Print results.  Save final values to return.
c
  600     If ( IBeta . le . IBMax )  Go to 605
          Write (LOUT, 955)  IBMax
  955     Format ( I5, ' times — give up and go home' )

  605     Theta  = TH (Kount)
          Height = Q (Kount)
          Radc   = P (Kount)
          RMaxF  = RMax
          VMax   = Vol
          EMax   = Energy

          CMass  = CMass / Vol
          RAR    = (3.0 * Vol / (pi * 4.0) ) ** (1.0/3.0)

c  Print out solutions.


          If (IND . eq . 0)  IABeta = (IBeta - 4) * 2
          If (IND . eq . 1)  IABeta = NBRC2*2 + NBRC1
          If (IND . eq . 2)  IABeta = IBeta

          Write (LOUT, 957)  IABETA
  957     Format (i4,'    number of solutions',/)

          If ( IABeta . eq . INBeta )  Go to 610
          Write (LOUT, 958)  IABeta, INBeta
  958     Format (' Number of Betas does not match, IABeta= ',I3,/
     &      10x,'INBeta = ',I3)
          If (IND . eq . 1)  Write (LOUT, 959)  NBRC2, NBRC1
  959     Format (' NBRC2= ',i3, ' NBRC1= ',i3)
          Go to 655

  610     If (IND . eq . 2 . OR . INDR . eq .0)  Go to 640
          If (IND . eq . 1)  Go to 630


c
c      Print size results for theta case.
c
          Write (LOUT, 900)
  900     Format ( /,x,'Beta',2x,'Theta',6x,'Radc',7x,'Height',6x,
     1      'Volume',7x,'Rmax',7x,'Energy',//)
```

```
          IABeta = IABeta/2
          Do 620  I = 1, IABeta
            J = 2*I -1
  620     Write (LOUT, 960)  Bet(J), Thet(J), Crad(J), Heigh(J),
     &                       Vo(J), Rma(J), Energ(J)
  960     Format (f7.5,x,f6.3,x,e11.5,5(2x,e11.5))

          Do 625  I = 1, IABeta
            J = 2*( IABETA + 1 ) - 2*I
  625     Write (LOUT, 960)  Bet(J), Thet(J), Crad(J), Heigh(J),
     &                       Vo(J),Rma(J),Energ(J)

c
c       Print stability results for theta case.
c

          If (Istab . eq . 1)  Then
            Write (LOUT, 962)
  962       Format ( //, 2x,'Beta',3x,'mu',4x,'kappa',4x,'lambda',
     1         5x,'PittsV',6x,'PittsN',6x,'PittsR',6x,'Eq7R',//)

          Do 626  I = 1, IABeta
              J = 2*I -1
              Write (LOUT, 961)  Bet(J), xMu(J), xKappa(J), xLambda(J),
     &                PittsV(J), PittsN(J), PittsR(J), Req7(J)
  626       Continue
  961       Format (f6.4,x,f6.3,x,f6.4,5(2x,e10.4))

          Do 627  I = 1, IABeta
              J = 2*( IABETA + 1 ) - 2*I
              Write (LOUT, 961)  Bet(J), xMu(J), xKappa(J), xLambda(J),
     &                PittsV(J), PittsN(J), PittsR(J), Req7(J)
  627       Continue

          Endif
          Go to 655

c
c       Print size results for Rc case.
c
  630     Write (LOUT, 900)
          Do 633, I = 2*NBRC2, 2, -2
  633     Write (LOUT, 960)  Bet(I), Thet(I), Crad(I), Heigh(I),
     &                       Vo(I), Rma(I), Energ(I)

          Do 635, I = 1, 2*NBRC2-1, 2
  635     Write (LOUT, 960)  Bet(I), Thet(I), Crad(I), Heigh(I),
```

```
     &                          Vo(I), Rma(I), Energ(I)

           If (IABeta . lt . 2*NBRC2+1)  Go to 655
           Do 637, I = 2*NBRC2+1, IABeta
637        Write (LOUT, 960)  Bet(I), Thet(I), Crad(I), Heigh(I),
     &                          Vo(I), Rma(I), Energ(I)
           Go to 655

c
c  Print results for volume case or first case only for theta or Rc.
c

640        Write (LOUT, 900)
           Do 650, I = 1, IABeta
650        Write (LOUT, 960)  Bet(I), Thet(I), Crad(I), Heigh(I),
     &                          Vo(I), Rma(I), Energ(I)

655        If ( IDraw . EQ . 0 )  Return

           If ( IND . eq . 0 )  Then

             Write (LOUT, 965)  ThetaC, KOUNT
965          Format (//,10x,'Max Bubble for Theta = ',f10.5,
     &             ///,i5,'  number of steps',/)

           Elseif (IND . eq . 1)  Then
             Write (LOUT, 970)  Rc, KOUNT
970          Format (//,10x,'Max Bubble for radius of contact = ',f10.6,
     &             ///,i5,'  number of steps',/)

           Endif

680        Write (LOUT, 980)
980        Format (17x, 'Z',10x, 'X', 10x, '-X', 8x, 'THETA', 9x,
     &             'VOLUME')

           Do 690,  I = 1, Kount
690        Write (LOUT, 990)  I, Q(I), P(I), -P(I), TH(I), V(I)
990        Format (3x, I5, 5(2x,f10.6))

           Return
           End
```

Program PLOTBUB

```
      Program PLOTBUB
      Implicit Real*8 (a-h,o-z)

ccccccccccccccccccccccccccccccccccccccccccccccccccccccccccccccccccccccc
c
c     Program PLOTBUB prepares data files that are ready to plot on
c     Tell-a-graph using the output file of BUBCALC.FOR and user input.
c     User supplies name of bubcalc output file, name of new plot
c     file and chooses from a menu of possible plots.
c
c     Program by Gina Whitney,  May 1, 1987.
c
ccccccccccccccccccccccccccccccccccccccccccccccccccccccccccccccccccccccc

      Dimension       beta(400), Theta(400), Radc(400), Height(400)
      Dimension       Volume(400), Rmax(400), Energy(400)
      Dimension       xp(8,400)
      Dimension       xMu(400), xKap(400), xLam(400), PittsV(400)
      Dimension       PittsN(400), PittsR(400), Eq7R(400)
      Dimension       z(2000), x(2000)
      Character*20    infile, outfile
      Character*40    xlab, ylab

      LIN = 3
      LOUT = 4

  100 Call GetFileName ('What is name of bubcalc.for output file?',
     & infile)

      If (infile . eq . ' ') Then
        Write (*,*) 'Try again'
        Go to 100
      Endif

      Call ChInp ('What is name of the file to contain plot info?',
     & outfile)

      open (unit=LIN, file=infile,
     &      defaultfile='[whitney.bubble]', status='old')

      open (unit=LOUT, file=outfile,
     &      defaultfile='[whitney.bubble]', status='new')

      Read (LIN, *) IStab
```

```
      Read (LIN, *) IDraw
      Read (LIN, *) IND
      Read (LIN, *) criterion
      Read (LIN, *) NBetas

105   Write (*,*) 'What do you want to plot?'

      Write (*,*) 'for Bubble shape parameters  enter 1'
      If (IStab . eq . 1) Then
        Write (*,*) 'for Bubble stability parameters  enter 2'
      Endif
      If (IDraw . eq . 1) Then
        Write (*,*) 'to draw maximum bubble  enter 3'
      Endif
      Read (*, *)  IChoice

      If (IChoice . lt . 3)  Then
        If (IChoice . eq . 1)  Go to 110
        If (IChoice . eq . 2 . and . IStab . eq . 1)  Go to 110
        If (IChoice . eq . 3 . and . IDraw . eq . 1)  Go to 110
        Write (*,*) ' Bad choice, try again'
        Go to 105
      Endif

110   Continue

c
c  Skip the blank lines.

      Do 200, I = 1, IChoice*5 + (IChoice-1)*NBetas
200     Read (LIN, 999)
999   Format ()

      If (IChoice . eq . 1)  Then
        Do 250, J = 1, NBetas
          Read (LIN,*) (xp(i,j), i=1,7)
250     Continue

260     Write (*,*) 'What do you want x to be?'
        Write (*,*) 'For beta      enter 1'
        Write (*,*) 'For theta     enter 2'
        Write (*,*) 'For Radc      enter 3'
        Write (*,*) 'For height    enter 4'
        Write (*,*) 'For volume    enter 5'
        Write (*,*) 'For Rmax      enter 6'
        Write (*,*) 'For energy    enter 7'
        Read (*,*) NX
```

```
      Write (*,*) 'What do you want y to be?'
      Write (*,*) 'For beta      enter 1'
      Write (*,*) 'For theta     enter 2'
      Write (*,*) 'For Radc      enter 3'
      Write (*,*) 'For height    enter 4'
      Write (*,*) 'For volume    enter 5'
      Write (*,*) 'For Rmax      enter 6'
      Write (*,*) 'For energy    enter 7'
      Read (*,*) NY

      If (NX . eq . NY) Then
        Write (*,*) 'X = Y'
        Go to  260
      Endif

      If (NX . gt . 7) Then
        Write (*,*) 'NX cannot be > 7'
        Go to  260
      Endif

      If (NY . gt . 7) Then
        Write (*,*) 'NX cannot be > 7'
        Go to  260
      Endif

      If (NX . eq . 1) xlab = '<l.5m7)b"'
      If (NX . eq . 2) xlab = '<l.5m7)q"'
      If (NX . eq . 3) xlab = '<l.5)Radius of Contact (cm)"'
      If (NX . eq . 4) xlab = '<l.5)Height (cm)"'
      If (NX . eq . 5) xlab = '<l.5)Volume (cm<e.3h.8)3<exhxl.5))"'
      If (NX . eq . 6) xlab = '<l.5)Maximum Radius (cm)"'
      If (NX . eq . 7) xlab = '<l.5)Energy (ergs)"'

      If (NY . eq . 1) ylab = '<m7)b"'
      If (NY . eq . 2) ylab = '<m7)q"'
      If (NY . eq . 3) ylab = 'Radius of Contact (cm)"'
      If (NY . eq . 4) ylab = 'Height (cm)"'
      If (NY . eq . 5) ylab = 'Volume (cm<e.5h.8)3 <exhx) )"'
      If (NY . eq . 6) ylab = 'Maximum Radius (cm)"'
      If (NY . eq . 7) ylab = 'Energy (ergs)"'


    Elseif (IChoice . eq . 2)  Then
      Do 270, J = 1, NBetas
        Read (LIN,*) (xp(i,j), i=1,8)
270   Continue
```

```
280     Write (*,*) 'What do you want x to be?'
        Write (*,*) 'For beta      enter 1'
        Write (*,*) 'For mu         enter 2'
        Write (*,*) 'For kappa     enter 3'
        Write (*,*) 'For lambda    enter 4'
        Write (*,*) 'For PittsV    enter 5'
        Write (*,*) 'For PittsN    enter 6'
        Write (*,*) 'For PittsR    enter 7'
        Write (*,*) 'For Eq7R       enter 8'
        Read (*,*) NX

        Write (*,*) 'What do you want y to be?'
        Write (*,*) 'For beta      enter 1'
        Write (*,*) 'For mu         enter 2'
        Write (*,*) 'For kappa     enter 3'
        Write (*,*) 'For lambda    enter 4'
        Write (*,*) 'For PittsV    enter 5'
        Write (*,*) 'For PittsN    enter 6'
        Write (*,*) 'For PittsR    enter 7'
        Write (*,*) 'For Eq7R       enter 8'
        Read (*,*) NY

        If (NX . eq . NY) Then
          Write (*,*) 'X = Y'
          Go to  280
        Endif

        If (NX . gt . 8) Then
          Write (*,*) 'NX cannot be > 8'
          Go to  280
        Endif

        If (NY . gt . 8) Then
          Write (*,*) 'NX cannot be > 8'
          Go to  280
        Endif

        If (NX . eq . 1) xlab = '<1.5m7)b"'
        If (NX . eq . 2) xlab = '<1.5m7)m"'
        If (NX . eq . 3) xlab = '<1.5m7)k"'
        If (NX . eq . 4) xlab = '<1.5m7)l"'
        If (NX . eq . 5) xlab = '<1.5)Reduced Volume"'
        If (NX . eq . 6) xlab = '<1.5)N"'
        If (NX . eq . 7) xlab = '<1.5)R"'
        If (NX . eq . 8) xlab = '<1.5)R from Eq. 7"'

        If (NY . eq . 1) ylab = '<m7)b"'
```

```
            If (NY . eq . 2) ylab = '<m7)m"'
            If (NY . eq . 3) ylab = '<m7)k"'
            If (NY . eq . 4) ylab = '<m7)l"'
            If (NY . eq . 5) ylab = 'Reduced Volume"'
            If (NY . eq . 6) ylab = 'N"'
            If (NY . eq . 7) ylab = 'R"'
            If (NY . eq . 8) ylab = 'R from Eq. 7"'

          Elseif (IChoice . eq . 3) Then
            Read (LIN, *) NSteps
            Read (LIN, 999)
            Read (LIN, 999)
            Do 300, J = 1, NSteps
              Read (LIN,*) I, Z(J), X(J)
300         Continue

            xlab = '<1.5)x (cm)"'
            ylab = 'z (cm)"'
          Endif

c
c   Find max and min of data to be plotted.

          Xmina = 0.0
          Xmaxa = 0.0
          Ymina = 0.0
          Ymaxa = 0.0

          If (IChoice . lt . 3) Then

            Do 320  J = 1, NBetas
              Xmina = Min (Xmina, xp(NX,J))
              Xmaxa = Max (Xmaxa, xp(NX,J))
              Ymina = Min (Ymina, xp(NY,J))
              Ymaxa = Max (Ymaxa, xp(NY,J))
320         Continue

          Elseif (IChoice . eq . 3) Then
            Do 330  J = 1, NSteps
              Xmaxa = Max (Xmaxa, x(J))
330         Continue

            Ymina = 0.0
            Ymaxa = Z(NSteps)
            Xmina = -Xmaxa
          Endif
```

```
      Write (*,*) 'Minimum y is', Ymina
      Write (*,*) 'What is y min for plot?'
      Read (*,*) Ymin

      Write (*,*) 'Maximum y is', Ymaxa
      Write (*,*) 'What is y max for plot?'
      Read (*,*) Ymax

      Write (*,*) 'What is y step for plot?'
      Read (*,*) Ystep

      Write (*,*) 'Minimum x is', Xmina
      Write (*,*) 'What is x min for plot?'
      Read (*,*) Xmin

      Write (*,*) 'Maximum x is', Xmaxa
      Write (*,*) 'What is x max for plot?'
      Read (*,*) Xmax

      Write (*,*) 'What is x step for plot?'
      Read (*,*) Xstep

c
c  Write Tell-a-graph information.

      Write (LOUT, 930)
  930 Format ('gen plot.',
     &      /,'legend is " ", height 0.2,',
     &      /,'     style swiss light, shade pattern 2,',
     &      /,'     legend frame off,',
     &      /,'     legend box 0.5,2.2,4.0,4.9,',
     &      /,'     units is plot inches.')
      Write (LOUT, 932)
  932 Format ('page border off.',
     &      /,'y room 2.')
      If (IChoice . gt . 0) Write (LOUT, 933)
  933 Format ('legend off.')
      If (IChoice . eq . 1 . or . IChoice . eq . 3) Write (LOUT,934)
  934 Format ('title is "Bubble Shape"')
      If (IChoice . eq . 2) Write (LOUT, 935)
  935 Format ('title is "Bubble Stability"')
      If (IND . eq . 0) Write (LOUT, 936) Criterion
  936 Format ('          "Contact Angle of ',f3.0,' Degrees",',
     &      /,'          height is 0.25,',
     &      /,'          ratio 2,',
     &      /,'          style is swiss light,',
     &      /,'          shade pattern 2.')
```

```
      If (IND . eq . 1)  Write (LOUT, 937) Criterion
937   Format (´          "Radius of Contact of ´,f4.2,´ cm",´,
     &      /,´          height is 0.25,´,
     &      /,´          ratio 2,´,
     &      /,´          style is swiss light,´,
     &      /,´          shade pattern 2.´)
      If (IND . eq . 2)  Write (LOUT, 938) Criterion
938   Format (´          "Volume of ´,f5.3,´ cm<e.5h.7)3<exhx)",´,
     &      /,´          height is 0.25,´,
     &      /,´          ratio 2,´,
     &      /,´          style is swiss light,´,
     &      /,´          shade pattern 2.´)
      Write (LOUT, 941) xlab
941   Format (´x label is "´,a40)
      Write (LOUT, 942)
942   Format (´            height is 0.2,´,
     &      /,´          style is swiss light,´,
     &      /,´          shade pattern 2.´)
      Write (LOUT, 943) ylab
943   Format (´y label is "´,a34)
      Write (LOUT, 942)

      Write (LOUT,944) xmin, xmax, xstep, ymin, ymax, ystep
944   Format (´x min is´,f7.3,´, max´,f7.3,´, step´f7.3,´.´
     &      /,´y min is´,f7.3,´, max´,f7.3,´, step´f7.3,´.´)

      Write (LOUT, 945)
945   Format (´x origin is 2.5.´,
     &      /,´y origin is 3.5.´)

      If (Ichoice . ne . 3)  Write (LOUT, 946)
946   Format (´x length is 4.´,
     &      /,´y length is 5.´)

      If (IChoice . eq . 3)  Write (LOUT, 947)
947   Format (´x length is 4.5.´,
     &      /,´y length is 4.5.´)

      Write (LOUT, 948)
948   Format (´y tick is 2.´,
     &      /,´x tick is 2.´)
      Write (LOUT, 949)
949   Format (´y axis tick marks reversed.´,
     &      /,´x axis tick marks reversed.´)
      If (IChoice . ne . 3)  Then
      Write (LOUT, 950)
950   Format (´curve 1 texture 1.´,
```

```
     &       /,'curve 2 texture 5.',
     &       /,'curve 1 symbol type 8.',
     &       /,'curve 2 symbol type 2.')
          Write (LOUT, 954)
954       Format ('every curve, color is no, thickness 2,',
     &       /,'                  symbol count is 9999.')
          Else
          Write (LOUT, 951)
951       Format ('every curve texture 1.')
          Write (LOUT, 955)
955       Format ('every curve, color is no, thickness 2,',
     &       /,'                  symbol count is 0.')
          Endif

          Write (LOUT, 956)
956       Format ('input data.')
          Write (LOUT, 958)
958       Format ('"upper"')

          If (IChoice . lt . 3)  Then
            Do 400, J = 1, NBetas/2
              Write (LOUT, *) xp(NX,J), xp(NY,J)
400         Continue
            Write (LOUT, 960)
960         Format ('"lower"')
            Do 410, J = NBetas/2 + 1, NBetas
              Write (LOUT, *) xp(NX,J), xp(NY,J)
410         Continue

          Elseif (IChoice . eq .3)  Then
            Do 420, J = 1, NSteps
              Write (LOUT, *) X(J), Z(NSTEPS)-Z(J)
420         Continue
            Write (LOUT, 960)
            Do 430, J = 1, NSteps
              Write (LOUT, *) -X(J), Z(NSTEPS)-Z(J)
430         Continue
          Endif

c
c   Write subplot2 info.

          Write (LOUT, 961)
961       Format ('end of data.',
     &       /,'subplot 1.',
     &       /,'gen plot.')
          Write (LOUT,944) xmin, xmax, xstep, ymin, ymax, ystep
```

```
      Write (LOUT, 945)
      If (Ichoice . ne . 3)  Write (LOUT, 946)
      If (IChoice . eq . 3)  Write (LOUT, 947)
      Write (LOUT, 948)

      If (Ichoice . ne . 3)  Write (LOUT, 963)
963   Format ('x axis offset 5, annotation off.',
     &       /,'y axis offset 4, annotation off.')

      If (Ichoice . eq . 3)  Write (LOUT, 964)
964   Format ('x axis offset 4.5, annotation off.',
     &       /,'y axis offset 4.5, annotation off.')

      Write (LOUT, 965)
965   Format ('y axis mode reversed.',
     &       /,'y axis tick marks reversed.')
      Write (LOUT, 966)
966   Format ('title off.',
     &       /,'every curve symbol count is 0.')
      Write (LOUT, 956)
      Write (LOUT, 958)
      Write (LOUT, 968)
968   Format ('  0  0',
     &       /,'end of data.',
     &       /,'subplot 2.')

      Stop
      End

C Subroutine by Ken Jordan ************************** GetFileName
c Used with permission.

      SUBROUTINE GetFileName(Prompt,FileName)    GetFileName

      INTEGER Length
      CHARACTER*(*) Prompt,FileName
      LOGICAL FileExist

      FileExist=.FALSE.
      DO WHILE (.NOT.FileExist)

         CALL ChInp(Prompt,FileName)

         CALL TrimCh(FileName)
         CALL StringLength(FileName,Length)
         IF (Length.EQ.0) RETURN
```

```
            INQUIRE(FILE=FileName,EXIST=FileExist)
            IF (.NOT.FileExist) WRITE(*,20) FileName
          END DO

          RETURN
20        FORMAT(X,'Warning: Filename ',A<Length>,' doesn''t exist.'
     &           ,/,X,'          Please try again.',/)

          END

c Subroutine by Ken Jordan  ********************************** ChInp
c Used with permission.

          SUBROUTINE ChInp(PROMPT,VAR)                          ChInp

c This subroutine prints the PROMPT and obtains a
c character response in VAR

          COMMON /EDITSUBS/DataEntered

          CHARACTER*(*) PROMPT,VAR
          INTEGER Apostrophe
          LOGICAL DataEntered

          WRITE(*,*) PROMPT(1:LEN(Prompt))
          READ(*,100) VAR
100       FORMAT(A)

          IF (Var.EQ.' ') THEN
            DataEntered=.FALSE.
          ELSE
            DataEntered=.TRUE.
          END IF

200       Apostrophe=INDEX(Var,'''')
          IF (Apostrophe.NE.0) THEN
            Var(Apostrophe:Apostrophe)='`'
            GOTO 200
          END IF

          RETURN
          END

C Subroutine from Ken Jordan ********************************** TrimCh
```

c *Used with permission.*

```
      SUBROUTINE TrimCh(String)                              TrimCh

      CHARACTER*(*) String
      INTEGER Length,I

      Length=LEN(String)

      DO I=1,Length
         IF ((ICHAR(String(I:I)).LT.32)
     & .OR.(ICHAR(String(I:I)).EQ.255)) String(I:I)=' '
      END DO

      IF (String.EQ.' ') RETURN
      IF (Length.LT.2) RETURN

      DO WHILE (String(1:1).EQ.' ')
         String(1:)=String(2:)
      END DO

      RETURN
      END
```

C *Subroutine by Ken Jordan* ********** *StringLength*
c *Used with permission.*

```
      SUBROUTINE StringLength(String,Length)          StringLength

      CHARACTER*(*) String
      INTEGER Length

      Length=LEN(String)
      DO WHILE((String(Length:Length).EQ.' ').OR.
     & (String(Length:Length).EQ.CHAR(0)))
         Length=Length-1
         IF (Length.EQ.0) RETURN
      END DO

      RETURN
      END
```

Appendix G. Chapter 3 Programs

The following programs were used for the calculations in Chapter 3. Program RUNAVG reads a raw data file, usually RUN#.dat, as sent from the HP9825, and averages the current distribution over time. Output is put in RUN#.out. Program CHECK checks RUN#.out for bad segments. Program MICAVG averages over electrode area. Program ACROSS prepares a plot of the average current distribution across the electrode. Program CHANNEL prepares a plot of current to a segment versus time.

Program MICTAL is used to make current distribution plots of the micro-mosaic data using DISSPLA graphics. Program PLOTCYL plots the cuurent distribution due to a rising cylinder.

Program RUNAVG

```
      Program RUNAVG

      implicit real*8(a-h,o-z)

c   This program prepares an electrode plot frame which is the
c   average for an entire run or portion thereof.  Two data files
c   are required.  The first data file is RUNAVG.DAT in
c   directory [whitney.runstat].  It contains:
c
c       Line #   # of record          variable
c
c            1           1          RUN, run #
c            2           1          IPAR = 0, entire run used
c                                        = 1, setting time window
c                                        = 2, setting scan limits
c            3           1          if IPAR=1, TBegin, TEnd
c                                   if IPAR=2, MBegin, MEnd
c
c   The second data file is 'Run #'.DAT in directory [whitney.bubdat].
c   It contains:
c
c       Line #   # of record          variable
c
c            1           1          M,       total # scans
c            2           1          TperP, time per point
c            3           M          (T(I), I=1,M), time at start of scan
c
c            4           100        (D(I), I=1,100), channel asssignments
c            5           M*100      V(M,I), voltage data
c
c
c    Program by Gina Whitney, August 20, 1985.
c
c
ccccccccccccccccccccccccccccccccccccccccccccccccccccccccccccccccccccccccc

      character*6       RUN
      real*8            T(1000), V(1000,100), Pot(100)
      integer           D(100)
```

```
c
c  Read in data for averaging.

      open (unit=3, file='runavg',
     &     defaultfile='[whitney.runstat].dat', status='old')

      Read (3,900) RUN
900   Format (A6)
      Read (3,901) IPAR
901   Format(i3)
      If (IPAR . eq . 1)  Read (3,902) TBegin, TEnd
902   Format (2f10.5)
      If (IPAR . eq . 2)  Read (3,903) MBegin, MEnd
903   Format (2i5)

c
c  Now get the data for the run.

      open (unit=4, file=RUN,
     &     defaultfile='[whitney.bubdat].dat', status='old')
      open (unit=19, file=RUN,
     &     defaultfile='[whitney.runstat].out', status='new')

      Read (4,*) M
      Read (4,*) TperP
      Do 100,  I = 1, M
        Read (4,*) T(I)
100   Continue

      Do 120, I = 1, 100
        Read (4,*) D(I)
120   Continue


c
c  Check input times.

      If (IPAR . eq . 0)  Go to 200
      If (IPAR . eq . 1 . and . TBegin . ge . T(1) . and .
     &                  TEnd . le . T(M))  Go to 200
      If (IPAR . eq . 2 . and . MBegin . ge . 1 . and .
     &                  MEnd . le . M )  Go to 200
      Write (19,910) T(1), T(M), M
910   Format (' Bad start or stop conditions',/
     &        ' T(1) =  ',f10.5,' T(M) = ',f10.5,' M = ',i5)
      Stop
```

```
c
c  Find region of interest.

  200     If (IPAR . eq . 0)  Go to 300
          If (IPAR . eq . 2)  Go to 400
c
c  Figure MBegin and MEnd for time-specified case.
c
          Do 220, I = 1, M
            If (T(I) . ge . TBegin)  Go to 240
  220     Continue
  240     MBegin = I - 1

          Do 260, I = MBegin, M
            If (T(I) . gt . TEnd)  Go to 280
  260     Continue
  280     MEnd = I
          Go to 400


  300     X = 1.0
          MBegin = 1
          MEnd = M

  400     If (MBegin . eq . 1)  Go to 450

c
c  Skip irrelevant info.

          Do 420, I = 1, MBegin - 1
            Do 420, L = 1, 100
            Read (4,999)
  420     Continue
  999     Format ()

  450     Do 470, L = 1, 100
            Pot(L) = 0.0
  470     Continue

c
c  Read relevant info.

          Do 500, I = MBegin, MEnd
            Do 500  L = 1, 100
              Read (4,930) V(I,L)
              Pot(L) = Pot(L) + V(I,L)
  500     Continue
```

```
  930     Format (6x,f10.5)

c
c   Write average current distribution.

          Write(19,940) RUN, MBegin, MEnd
  940     Format (' Run Number ',A6,' Average current dist for scans ',
     &            i5,' through ',i5)

          Do 520, L = 1, 100
            Pot(L) = Pot(L) / float( MEnd + 1 - MBegin )
            Write (19,950)  Pot(L)
  520     Continue
  950     Format (f10.5)

          Stop
          End
```

Program CHECK

```
          PROGRAM CHECK

          implicit real*8(a-h,o-z)


c   This program skims a current distribution file and determines
c   how many of the electrode segments are anodic or not passing
c   current.  Two data files are required.  The first data file
c   is CHECK.DAT in directory [whitney.runstat].  It contains
c   the run number of the data file to check, RUN.
c
c   The second data file is 'RUN'.out in directory [whitney.runstat].
c   It contains:
c
c        Line #      # of record          variable
c
c           1            1                  comment line
c           2            100                V(I,J), voltage data
c
c
c    Program by Gina Whitney, March 20, 1986.
c
```

```
c
ccccccccccccccccccccccccccccccccccccccccccccccccccccccccccccccccccccccccc

      character*6       RUN
      real*8            VAN(100), VZIP(100), VMAX(100)
      integer           IAN(100,2), IZIP(100,2), IMAX(100,2)

      LIN = 3
      LRUN = 4
      LOUT = 9
c
c  Read in data for what run to check.

      open (unit=LIN, file='check',
     &     defaultfile='[whitney.runstat].dat', status='old')

      Read (LIN,900) RUN
  900 Format (A6)

c
c  Now get the data for the run.

      open (unit=LRUN, file=RUN,
     &   defaultfile='[whitney.runstat].out', status='old')

      open (unit=LOUT, file=RUN,
     &   defaultfile='[whitney.runstat].check', status='new')

      Read (LRUN,999)
  999 Format ()

      Write (LOUT,910) RUN
  910 Format (5x,'Electrode check for run number  ',A6)

      KAN = 0
      KZIP = 0
      Do 100 I = 1, 10
        Do 100  J = 1, 10
          Read (LRUN,*) V
          If (V . lt . -0.01)  Then
            KAN = KAN + 1
            IAN(KAN,1) = I
            IAN(KAN,2) = J
            VAN(KAN) = V
          Elseif (abs(V) . le . 0.01)  Then
            KZIP = KZIP + 1
            IZIP(KZIP,1) = I
```

```
            IZIP(KZIP,2) = J
            VZIP(KZIP) = V
          Elseif (V . ge . 1.25) Then
            KMAX = KMAX + 1
            IMAX(KMAX,1) = I
            IMAX(KMAX,2) = J
            VMAX(KMAX) = V
          Endif
100     Continue

        Write (LOUT,920) KAN
920     Format (5x,i5,' segments are anodic.')
        If (KAN . gt . 0) Then
          Do 200 K = 1, KAN
            Write (LOUT,*) IAN(K,1), IAN(K,2), VAN(K)
200       Continue
        Endif

        Write (LOUT,930) KZIP
930     Format (5x,i5,' segments do not pass current.')
        If (KZIP . gt . 0) Then
          Do 300 K = 1, KZIP
            Write (LOUT,*) IZIP(K,1), IZIP(K,2), VZIP(K)
300       Continue
        Endif

        Write (LOUT,940) KMAX
940     Format (5x,i5,' segments pass maximum current.')
        If (KMAX . gt . 0) Then
          Do 400 K = 1, KMAX
            Write (LOUT,*) IMAX(K,1), IMAX(K,2), VMAX(K)
400       Continue
        Endif

        Stop
        End
```

Program MICAVG

```
        PROGRAM MICAVG
c
c       This program computes the average current distribution for an
```

```
c       electrode plot.  It requires two input files, both in directory
c       [whitney.runstat].  The first is MICAVG.DAT.  It includes:
c
c       Card #      # of cards          Variable
c
c           1           1          RUN,   run number
c           2           1          NNot, # segments not averaged
c           3          NNot        I,J    segments not averaged
c
c       The second data file is RUN.out, the output file from the
c       program RUNAVG.FOR.


            Integer             LRUN,   LIN
            Real                ZZ(10,10)
            Character*6         RUN

            LRUN = 3
            LIN = 7
            LOUT = 8

c       ***** OPEN INPUT AND OUTPUT FILES.

            open (unit=LIN, file='micavg',
        &     defaultfile='[whitney.runstat].dat', status='old')
            Read (LIN, 900) RUN
    900     Format (A6)

            open (unit=LRUN, file=RUN,
        &     defaultfile='[whitney.runstat].out', status='old')

            Read (LRUN, 905)
    905     Format ()

            open (unit=LOUT, file=RUN,
        &     defaultfile='[whitney.runstat].avg', status='new')

            Write (LOUT, 906) RUN
    906     Format ('Run number  ',A6)

            Do 30  I = 1, 10
              Do 30  J = 1, 10
                Read (LRUN, 910) ZZ(I,J)
                If ( ZZ(I,J) . lt . 0)  ZZ(I,J) = 0
     30     Continue

    910     Format (f10.4)
```

```
      Read (LIN, 920) NNot
920   Format (i3)
      Write (LOUT, 930) NNot
930   Format (i3, ' Segments not averaged')
      Sum = 0.0
      Do 100 I = 1,10
        Do 50 J = 1, 10
          Sum = Sum + ZZ(I,J)
 50     Continue
100   Continue
      If (NNot.eq.0) Go to 300

      Do 200 K = 1, NNot
        Read (LIN, 950) I,J
        Sum = Sum - ZZ(I,J)
        Write (LOUT, 940) I,J
200   Continue

300   CurDen = Sum*10.0/(100.0-float(NNot))

      Write (LOUT,960) CurDen

940   Format ('Segment #',2i3)
950   Format (2i3)
960   Format ('Average Current Density = ',f10.6,' mA/cm2')

      Stop
      End
```

Program ACROSS

```
      PROGRAM ACROSS

      Real            ZZ(10,10), X(3) ,Z(10)
      Character*6     RUN


c     This program requires two data files.  The first is across.dat
c     in directory [whitney.runstat].  It contains:
c
c     # of cards      Variable
c
```

```
c           1          RUN
c           1          imess, whether or not to write I bub
c           1          bubcur
c
c       The second data file is RUN.save in directory [whitney.runstat].
c
c           1          NNot,  # segments not averaged
c           NNot       I,J    segments not averaged
c           10         JCol,  Column number of separate column
c           10         NRNot, Number of segments in JCol
c                               to exclude
c           10xNRNot           IRow,JCol  Segment to exclude
c
c       The third data file is RUN.out in directory [whitney.runstat].
c
          LIN1  = 10
          LIN   = 3
          LRUN  = 4
          LPLOT = 9

          open (unit=LIN1, file='across',
     &      defaultfile='[whitney.runstat].dat', status='old')
          Read (LIN1, 900) RUN
          Read (LIN1, *) imess
          Read (LIN1, *) bubcur
  900     Format (A6)

          open (unit=LRUN, file=RUN,
     &      defaultfile='[whitney.runstat].out', status='old')

          open (unit=LIN, file=RUN,
     &      defaultfile='[whitney.runstat].save', status='old')

          open (unit=LPLOT, file=RUN,
     &      defaultfile='[whitney.runstat].across', status='new')

          NX = 10
          NY = 10

c
c       Write Tell-a-graph information.
c

          Write (LPLOT, 911)
  911     Format ('gen plot.',
     &        /,'legend is "Legend", height 0.2,',
```

```
     &       /,'      style swiss light, shade pattern 2,',
     &       /,'      legend frame off,',
     &       /,'      legend box 1.5,3.5,0.5,2.5,',
     &       /,'      units is plot inches.')
          Write (LPLOT, 912)
912       Format ('page border off.')
          Write (LPLOT, 913)
913       Format ('y room 2.')
          Write (LPLOT, 914) RUN
914       Format ('title is "Run # ',A6,'"',
     &       /,'           "Current Distribution Across Electrode",',
     &       /,'          ratio 2,',
     &       /,'          height is 0.35,',
     &       /,'          style is swiss light,',
     &       /,'          shade pattern 2.',
     &       /,'title off.')
          Write (LPLOT, 915)

915       Format ('y label is "Current Density,',
     &         ' i ( mA/cm<e.8h.8)2<hxex) )",',
     &       /,'          height is 0.2,',
     &       /,'          style is swiss light,',
     &       /,'          shade pattern 2.')
          Write (LPLOT, 916)
916       Format ('x label is "<l.5)Horizontal Position (<m7)m<mx)m)",',
     &       /,'          height is 0.2,',
     &       /,'          style is swiss light,',
     &       /,'          shade pattern 2.')
          Write (LPLOT,917)
917       Format ('y min is 0, max 6, step 1.',
     &       /,'x min is -500, max 500, step 500.',
     &       /,'cross off.')

          Write (LPLOT, 918)
918       Format ('x origin is 2.5.',
     &       /,'y origin is 3.5.')
          Write (LPLOT, 919)
919       Format ('x length is 4.',
     &       /,'y length is 5.')
          Write (LPLOT, 920)
920       Format ('y tick is 5.',
     &       /,'x tick is 5.')
          Write (LPLOT, 921)
921       Format ('y axis tick marks reversed.',
     &       /,'x axis tick marks reversed.')
          Write (LPLOT, 922)
922       Format ('curve 1 texture 1.',
```

```
     &       /,'curve 2 texture 2.',
     &       /,'curve 3 texture 5.',
     &       /,'curve 4 texture 14.')
          If (imess . eq . 1 )  then
          Write (LPLOT, 923) bubcur
923       Format ('msg 1 txt is "I<l.7h.7)bub <lxhx)= ',f4.1,
     &          '<m7)m<mx)A",',
     &       /,'      style is swiss light,',
     &       /,'      shade pattern 2,',
     &       /,'      height 0.2.')
          Write (LPLOT, 924)
924       Format ('msg 1 connect LC, x = -450.0   y = 5.0',
     &       /,'      units coordinate.')
          Endif

          Write (LPLOT, 926)
926       Format ('every curve, color is no, thickness 2.',
     &       /,'                  symbol count is 0.')
          Write (LPLOT, 928)
928       Format ('input data.')
          Write (LPLOT, 929)
929       Format ('"curve 1"')


          Read (LRUN, 999)
999       Format ()
          Read (LRUN, 935) ((ZZ(I,J), J=1,NY), I=1,NX)
935       Format (f10.4)


          Do 50  J = 1, 10
            Do 50  I = 1, 10
              If (ZZ(I,J) . lt . 0)  ZZ(I,J) = 0.0
 50       Continue

          Read (LIN, *) NNot
          Sum = 0.0
          Do 100 I = 1,10
            Do 75 J = 1, 10
              Sum = Sum + ZZ(I,J)
 75         Continue
100       Continue
          If (NNot.eq.0) Go to 300

          Do 200 K = 1, NNot
            Read (LIN, *) I,J
            Sum = Sum - ZZ(I,J)
```

```
200     Continue

300     CurDen = Sum*10.0/(100.0-float(NNot))

c**** Now begin column calculations.

        NTCNot = 0
        SumTC = 0.0

        Do 500 K = 1, 10
          Read (LIN, *) JCol
          Read (LIN, *) NRNot

          NTCNot = NTCNot + NRNot

          Sum2 = 0.0
          Do 400 I = 1,10
            Sum2 = Sum2 + ZZ(I,JCol)
400       Continue

          If (NRNot.eq.0) Go to 490

          Do 450 KK = 1, NRNot
            Read (LIN, *) IRow
            Sum2 = Sum2 - ZZ(IRow,JCol)
450       Continue


490       SUMTC = SUMTC + Sum2
          Sum2 = Sum2*10.0/(10.0-float(NRNot))
          Z(Jcol) = Sum2
500     Continue


        X(1) = 500.0
        X(2) = 0.0
        Write (LPLOT, 995) -X(1), X(2)
        Do 600 J = 1, 10
          Do 590 II = 1,3
            X(II) = 100.0 * float(J) - 50. + float(II-2)*49. - 500.0
            Write (LPLOT, 995) X(II), Z(J)
590       Continue
600     Continue

        X(1) = 500.
        X(2) = 0.
```

```
      Write (LPLOT, 995) X(1), X(2)
995   Format (2f10.4)

c
c  Write subplot2 info.

      Write (LPLOT, 961)
961   Format ('end of data.',
     &       /,'subplot 1.',
     &       /,'gen plot.')
      Write (LPLOT, 917)
      Write (LPLOT, 918)
      Write (LPLOT, 919)
      Write (LPLOT, 920)
      Write (LPLOT, 962)
962   Format ('x axis offset 5, annotation off.',
     &       /,'y axis offset 4, annotation off.')
      Write (LPLOT, 964)
964   Format ('y axis mode reversed.')
      Write (LPLOT, 965)
965   Format ('y axis tick marks reversed.')
      Write (LPLOT, 966)
966   Format ('title off.',
     &       /,'every curve symbol count is 0.')
      Write (LPLOT, 928)
      Write (LPLOT, 929)
      Write (LPLOT, 968)
968   Format ('  0  0',
     &       /,'end of data.',
     &       /,'subplot 2.')

      Stop
      End
```

Program CHANNEL

```
      PROGRAM CHANNEL

      implicit real*8(a-h,o-z)
```

```
c   This program prepares a channel plot for an electrode segment
c   vs time or 1 / sqrt(time) and calculates the Cottrell slope
c   from the file of raw data for the run.  It is a simplified
c   version of POTSTEP.FOR.  It does not require preRUN.dat
c   for potential step info.  Two data files are required.
c
c   The first is CHANNEL.DAT in directory [whitney.runstat].
c   It contains:
c
c        Line #      # of record          variable
c
c           1            1                RUN, run #
c           2            1                TPBegin, Time to begin plotting
c           3            1                TPEnd, Time to end plotting
c           4            1                I J  = segment of interest
c
c
c   The second data file is 'Run #'.DAT in directory [whitney.bubdat].
c   It contains:
c
c        Line #      # of record          variable
c
c           1            1                M,       total # scans
c           2            1                TperP, time per point
c           3            M                (T(I), I=1,M), time at
c                                                 start of scan
c           4            100              (D(I), I=1,100), channel
c                                                 asssignments
c           5            M*100            V(M,I), voltage data
c
c    Output files are RUN.chan in directory [whitney.runstat] for
c    slope info and RUN.chanIJ in directory [whitney.semtag] for
c    plot file.
c
c    Program by Gina Whitney, October 23, 1985.
c
c
ccccccccccccccccccccccccccccccccccccccccccccccccccccccccccccccccccccccc

      character*6       RUN
      character*25      DFILE
      real*8            T(1000), V(1000)
      integer           D(100)

      LIN = 3
      LRUN = 4
      LOUT = 8
```

```
          LPLOT = 9
c
c  Read in data for the run.

          open (unit=LIN, file='channel',
     &      defaultfile='[whitney.runstat].dat', status='old')

          Read (LIN, 900) RUN
  900     Format (A6)

          open (unit=LOUT, file=RUN,
     &      defaultfile='[whitney.runstat].chan', status='new')

          Read (LIN, *) TPBegin
          Read (LIN, *) TPEnd

          Read (LIN, *) I, J
  903     Format (2i3)
          ICHAN = 10*I + J


c
c  Now get the data for the run.

          open (unit=LRUN, file=RUN,
     &      defaultfile='[whitney.bubdat].dat', status='old')

          Encode (30, 907, DFILE) ICHAN
  907     Format ('[whitney.runstat].chan',i3)


          ICHAN = ICHAN - 10

  908     Format (A25)
          Read (LRUN, *) M
  905     Format (i5)
          Read (LRUN, *) TperP
  906     Format (f15.9)
          Do 100, II = 1, M
            Read (LRUN, *) T(II)
  100     Continue

          Do 120, II = 1, 100
            Read (LRUN, *) D(II)
  120     Continue
  902     Format (i3)
```

```
c
c   Check input times.

          If (TPEnd . gt . T(M))  Go to 150
          If (TPBegin. lt . T(1))  Go to 150
          Go to 200

  150     Write (LOUT,910) T(1), T(M), TPBegin, TPEnd
  910     Format (' Bad start or stop time',/
     &            '  T(1) =    ',f10.5,'  T(M) = ',f10.5,/
     &            '  TPBegin = ',f10.5,'  TPend = ',f10.5)
          Stop

c
c       Write Tell-a-graph information
c

  200     open (unit=LPLOT, file=RUN,
     &          defaultfile=DFILE, status='new')
          Write (LPLOT, 911)
  911     Format ('gen plot.',
     &         /,'legend is "Legend", height 0.2,',
     &         /,'     style swiss light, shade pattern 2,',
     &         /,'     legend frame off,',
     &         /,'     legend box 1.5,3.5,0.5,2.5,',
     &         /,'     units is plot inches.')
          Write (LPLOT, 912)
  912     Format ('page border off.')
          Write (LPLOT, 913)
  913     Format ('y room 2.')
          Write (LPLOT, 914) RUN, I, J
  914     Format ('title is "Run # ',A6,'"',
     &         /,'          "Segment # [',i2,',',i2,']",',
     &         /,'          height is 0.35,',
     &         /,'          style is swiss light,',
     &         /,'          shade pattern 2.')
          Write (LPLOT, 915)
  915     Format ('y label is "Cathodic Current (<m7)m<mx)A)",',
     &         /,'          height is 0.2,',
     &         /,'          style is swiss light,',
     &         /,'          shade pattern 2.')
          Write (LPLOT, 916)
  916     Format ('x label is "Time (Seconds)",',
     &         /,'          height is 0.2,',
     &         /,'          style is swiss light,',
     &         /,'          shade pattern 2.')
          Write (LPLOT,917)
```

```
 917      Format ('y min is 0, max 0.5, step 0.1.',
     &         /,'x min is 0, max 20, step 5.')
          Write (LPLOT, 918)
 918      Format ('x origin is 2.5.',
     &         /,'y origin is 3.5.')
          Write (LPLOT, 919)
 919      Format ('x length is 4.',
     &         /,'y length is 5.')
          Write (LPLOT, 920)
 920      Format ('y tick is 5.',
     &         /,'x tick is 5.')
          Write (LPLOT, 921)
 921      Format ('y axis tick marks reversed.',
     &         /,'x axis tick marks reversed.')
          Write (LPLOT, 922)
 922      Format ('curve 1 texture 1.')
          Write (LPLOT, 923)
 923      Format ('curve 2 texture 2.')
          Write (LPLOT, 924)
 924      Format ('curve 3 texture 5.')
          Write (LPLOT, 925)
 925      Format ('curve 4 texture 14.')
          Write (LPLOT, 926)
 926      Format ('every curve, color is no, thickness 2.',
     &         /,'                  symbol count is 0.')
          Write (LPLOT, 928)
 928      Format ('input data.')
          Write (LPLOT, 929)
 929      Format ('"curve 1"')

c
c  Read potential info.

 210      Do 290, MM = 1, M
            Do 290  I = 1, 100
              If (I . eq . ICHAN)  Then
                Read (LRUN, 933) V(MM)
              Else
                Read (LRUN, 999)
              Endif
 290      Continue
 933      Format (6x,f10.5)
 999      Format ()
```

```
c
c   Initialize summations.

          N = 0
          sumx  = 0.d0
          sumy  = 0.d0
          sumxy = 0.d0
          sumx2 = 0.d0
          sumy2 = 0.d0

c
c   Begin calculations.

          Do 350, MM = 1, M
            Time = T(MM) + TperP * float(D(ICHAN)-1)
            If (Time . ge . TPBegin . and . Time . le . TPEnd)  Then
              Write (LPLOT, 935) Time, V(MM)
            Else
              Endif
  935       Format (2f10.6)

  300       If (Time . lt . TPBegin . or . Time . gt . TPEnd)
     &      Go to 350
              sumx  = sumx + Time
              sumy  = sumy + V(MM)
              sumxy = sumxy + Time * V(MM)
              sumx2 = sumx2 + Time * Time
              sumy2 = sumy2 + V(MM) * V(MM)
              N = N +1
  350       Continue

c
c   Calculate slope and y-intercept.

          yavg = sumy / float(N)
          xnum = float(N) * sumxy - sumx * sumy
          slope = xnum / (float(N) * sumx2 - sumx * sumx)
          yint = sumy / float(N) - slope * sumx / float(N)
          denom = (float(N) * sumx2 - sumx * sumx) *
     &            (float(N) * sumy2 - sumy * sumy)
          if (denom . gt . 0)  then
            r = xnum / sqrt(denom)
          else
            r = 0.0
          endif

          Write (LOUT, 940) yavg, slope
```

```
  940     Format ('       yavg = ',e15.9,/,'       slope = ',e15.9)
          Write (LOUT, 945) yint
  945     Format ('       y intercept = ',e15.9,'  microamps')
          Write (LOUT, 950) r
  950     Format ('       correlation coefficient = ',e15.9)

c
c  Write subplot2 info.

          Write (LPLOT, 960)
  960     Format ('end of data.',
     &         /,'subplot 1.',
     &         /,'gen plot.')
          Write (LPLOT, 917)
          Write (LPLOT, 918)
          Write (LPLOT, 919)
          Write (LPLOT, 920)
          Write (LPLOT, 962)
  962     Format ('x axis offset 5, annotation off.',
     &         /,'y axis offset 4, annotation off.')
          Write (LPLOT, 964)
  964     Format ('y axis mode reversed.')
          Write (LPLOT, 965)
  965     Format ('y axis tick marks reversed.')
          Write (LPLOT, 966)
  966     Format ('title off.',
     &         /,'every curve symbol count is 0.')
          Write (LPLOT, 928)
          Write (LPLOT, 929)
          Write (LPLOT, 968)
  968     Format ('  0  0',
     &         /,'end of data.',
     &         /,'subplot 2.')

          Stop
          End
```

Program MICTAL

```
          PROGRAM MICTAL

c         ***** Program for plotting micromosaic data using DISSPLA
```

```
c       ***** on the talars printer.
c       First data file is mictal.dat in directory [whitney.disspla].
c       It contains:
c
c       line              variable
c
c            1          infile
c
c       infile.dat contains:
c
c            1          RUN, run #
c            1          iarrow, =1 draw arrow showing bubble motion
c            1          imess, =1 write time at bottom
c            1          nlines, number of lines of message
c            nlines     LmessN(10), nth lines message
c            1          irotate, rotates view (90 deg x irotate)
c                                  counterclockwise by rotating
c                                  data block 90 deg clockwise
c            1          nkill,  number of segments to kill
c            nkill      i, j,  coordinates of segments to kill
c
c   The third data file is 'Run #'.OUT in directory [whitney.bubdat].
c   It contains:
c
c     # of lines          variable
c
c            M*100      V(M,I), voltage data
c
c
c   Program by Gina Whitney, November, 1986.  Revised March, 1987.
c
c
ccccccccccccccccccccccccccccccccccccccccccccccccccccccccccccccccccccccccc

            dimension          ZMAT(22,22)
            character*10       infile
            character*6        RUN
            character*32       dummy1, dummy2
            dimension          ikill(10)
            dimension          Lmess1(8), Lmess2(8), IPKRAY(100)
            equivalence        (Lmess1,dummy1)
            equivalence        (Lmess2,dummy2)

            data   IXPTS /1/
            data   IYPTS /1/

            LIN = 3
```

```
      LDAT = 4
      LGRID = 7
      LOUT = 8

      open (unit=LIN, file='mictal',
     &   defaultfile='[whitney.dissplа].dat', status='old')
      Read (LIN, *) infile

      open (unit=LDAT, file=infile,
     &   defaultfile='[whitney.dissplа].dat', status='old')

      Read (LDAT, *) RUN
      Read (LDAT, *) Iarrow
      Read (LDAT, *) Imess
      Read (LDAT, *) nlines
      If (Nlines . gt . 0) Then
        Read (LDAT,*) dummy1
      Endif
      If (Nlines . gt . 1) Then
        Read (LDAT,*) dummy2
      Endif
      Read (LDAT, *) Irotate
      Read (LDAT, *) Nkill
      if (Nkill . gt . 0) Then
        Do 50 N = 1, Nkill
          Read (LDAT, *) I, J
          Ichan = 10*(I-1) + J
          Ikill(N) = Ichan
50    Continue
      Endif

c     Now get the data from the run.

      open (unit=LGRID, file=RUN,
     &   defaultfile='[whitney.runstat].out', status='old')

c     ***** Read in data to contour.
c     ***** Transform 10 * 10 grid to 22 * 22
c     ***** for use with unequal grid spacing.

c     ***** First do the interior node values.

      Read (LGRID,999)
999   Format ()

      Do 200 I = 1, 10
        Do 200 J = 1, 10
```

```
            Read (LGRID, 900) ZVAL
            If (ZVAL . LT . 0.) ZVAL = 0.
            If (Nkill . gt .0) Then
              Ichan = 10*(I-1) + J
              Do 90 NN = 1, Nkill
                If (Ichan . eq . Ikill(NN)) ZVAL = 0.0
90            Continue
            Endif

            Do 100 II = 2*I, 2*I+1
              Do 100 JJ = 2*J, 2*J+1
                If (Irotate . eq . 0) ZMAT(II,JJ) = ZVAL
                If (Irotate . eq . 1) ZMAT(JJ,23-II) = ZVAL
                If (Irotate . eq . 2) ZMAT(23-II,23-JJ) = ZVAL
                If (Irotate . eq . 3) ZMAT(23-JJ,II) = ZVAL
100           Continue
200       Continue
900       Format (E10.5)

c       ***** Now zero the boundaries to obtain skirt effect.

          Do 300 I = 1, 22
            ZMAT(1,I) = 0.0
            ZMAT(22,I) = 0.0
            ZMAT(I,1) = 0.0
            ZMAT(I,22) = 0.0
300       Continue

c       ***** Begin DISSPLA.

          Call TALARS
          Call NOBRDR
          Call PAGE (8.5, 11.0)
          Call PHYSOR (2.4,2.0)
          Call AREA2D (5.2,7.)
          Len = LINEST (IPKRAY, 100, 40)


          Call HEIGHT (0.2)
          CALL LINESP (2.0)
          CALL SWISSL
          Call MX1ALF ('STANDARD','%')
          Call MX2ALF ('MATHE','*')
          Call MX3ALF ('GREEK','@')
          Call MX4ALF ('INSTRUCTION','!')
          Call NUMODE ('EQUAL')
          CALL SHDCHR (90., 1, .01, 1)
```

```
      If (imess . eq . 1)  Then
        CALL LINES (Lmess1,IPKRAY,1)
        if (Nlines . gt . 1)  CALL LINES (Lmess2,IPKRAY,2)

        XW = XSTORY(IPKRAY,Nlines)
        YW = YSTORY(IPKRAY,Nlines)
        XL = 4.5 - XW
        YL = 6.5 - YW

        CALL STORY (IPKRAY, Nlines, XL, YL)

      Endif

c     ***** Set up workbox area.

      Call VOLM3D (10.0, 10.0, 5.0)

      Call SETSPC (2.0, 2.0, 0.03)
      Call HEIGHT (0.25)
      Call X3NAME ('!L1.0A3%Vertical Dimension&',100)
      Call Y3NAME ('Horizontal Dimension&',100)
      Call Z3NAME ('Current ( @m%A )&',100)

      Call VUABS  (55.0, -25.0, 35.0)
      Call ZAXANG (90.0)
      Call INTAXS

c     ***** Switch to virtual coordinates.

      Call XAXCTR
      Call YAXCTR
      Call YAXEND ('ENDS')
      Call GRAF3D (1., 1., 11., 1., 1., 11., 0., .1, .5)
      Call RESET ('SETSPC')

c     ***** Calculate grid values for ZMAT(IXROW,IYCOL).

      Call SURTRN ('BOTH')

c     ***** Draw surface.

      Call SURMAT (ZMAT, IXPTS, 22, IYPTS, 22, 0)
      If (Iarrow . eq . 1)  then
        Call VECTR3 (-10, 6.5, 0.15, -5, 6.5, 0.15, 1001)
      Endif
      Call SURMAT (ZMAT, IXPTS, 22, IYPTS, 22, 0)
      Call ENDPL(0)
```

```
      Call DONEPL

      Stop
      End


      Function X3DMAT(IXROW)                                    X3DMAT
      Dimension XTABLE(22)
      data XTABLE / 1.00, 1.01, 1.99, 2.01, 2.99, 3.01, 3.99, 4.01,
     &              4.99, 5.01, 5.99, 6.01, 6.99, 7.01, 7.99, 8.01,
     &              8.99, 9.01, 9.99, 10.01, 10.99, 11.00 /
      X3DMAT = XTABLE(IXROW)
      Return
      End

      Function Y3DMAT(IYCOL)                                    Y3DMAT
      Dimension XTABLE(22)
      data XTABLE / 1.00, 1.01, 1.99, 2.01, 2.99, 3.01, 3.99, 4.01,
     &              4.99, 5.01, 5.99, 6.01, 6.99, 7.01, 7.99, 8.01,
     &              8.99, 9.01, 9.99, 10.01, 10.99, 11.00 /
      Y3DMAT = XTABLE(IYCOL)
      Return
      End
```

Program PLOTCYL

```
      Program PLOTCYL
      Character*64      outfile, geofile
c
c   This program plots the theoretical current distribution
c   due to a rising cylinder.
c
c   It requires two data files.  The first is plotcyl.dat in
c   directory [whitney.cylin].  It has:
c
c         outfile,              name of output file for average value
c         geofile,              name of input file for geometric data
c         Dif,        diffusion coefficient of reactant
c         Cinf,       concentration of reactant in the bulk
c         dist,       distance of cylinder from electrode
c         rad,        radius of cylinder
c         mode,       = 1 equal volume (no liquid entrained)
```

```
c                    = 2 equivalent drag
c                    = 3 max liquid entrained
c          bubcur    bubble current in microamps
c          iarrow, =1 draw arrow showing bubble motion
c          imess, =1 write time at bottom
c          nlines, number of lines of message
c          LmessN(10), nth lines message
c
c
c  The second data file is geofile.dat.  It contains the geometric
c  information for the calculation.
c
c  This program must be linked by using the command 'linkdis plotcyl'
c  on this account.
c
ccccccccccccccccccccccccccccccccccccccccccccccccccccccccccccccccc

          dimension          ZMAT(22,22)
          dimension          Lmess1(8), Lmess2(8), IPKRAY(100)
          character*32       dummy1, dummy2
          equivalence        (Lmess1,dummy1)
          equivalence        (Lmess2,dummy2)

          DATA  F      /96486.7d0/
          DATA  gamma  /0.892979511d0/
          DATA  pi     /3.141592653d0/
          RToP = 82.055d0 * 298.15d0 / 1.d0
          IXPTS = 1
          IYPTS = 1

c
c  Open input files

          LIN1 = 3
          LIN2 = 4
          LOUT = 7

          open (unit=LIN1,file='plotcyl',
     &      defaultfile='[whitney.cylin].dat', status='old')
          read (LIN1, *) outfile
          read (LIN1, *) geofile
          open (unit=LIN2,file=geofile,
     &      defaultfile='[whitney.cylin].dat', status='old')
          open (unit=LOUT,file=outfile,
     &      defaultfile='[whitney.cylin].dat', status='new')

          read (LIN1,*) Dif
```

```
      read (LIN1,*) Cinf
      read (LIN1,*) dist
      read (LIN1,*) rad
      read (LIN1,*) mode
      read (LIN1,*) bubcur
      Read (LIN1,*) Iarrow
      Read (LIN1,*) Imess
      Read (LIN1,*) nlines
      If (Nlines . gt . 0)  Then
        Read (LIN1,*) dummy1
      Endif
      If (Nlines . gt . 1)  Then
        Read (LIN1,*) dummy2
      Endif

      a = sqrt (dist*dist - rad*rad)
      eta = alog ( ( dist + a ) / rad )
c
c  Calculate Vc based on mode.
c
      Vdot = bubcur * RToP * 1.d-6 / ( 2.d0 * F)

      if (mode . eq . 1) then
        Vc = Vdot / (pi * rad * rad)
      elseif (mode . eq . 2) then
        Vc = Vdot / (pi * rad * rad) * 6.d0 *eta/(4.d0*fun(rad/dist))
      elseif (mode . eq . 3) then
        Vc = 2.d0 * rad * rad * 980.d0 / (9.d0 * 0.01d0)
      else
        write (LOUT,990)
  990   format ('bad mode')
        stop
      endif

      group = (2.d0 * a * Vc / (9.d0 * Dif * eta)) ** ( 1.d0/3.d0 )
      factor = F*Dif * Cinf *(3.d0/2.d0) * group / ( gamma * 10.d0 )
      write (LOUT,920) factor
  920 format ('factor = ',3x,d15.9)

c  Read in geometry file and transform 10 * 10 grid to 22 * 22
c  for use with unequal grid spacing


c     ***** FIRST DO THE INTERIOR NODE VALUES

      sum = 0.d0
      DO 200  I = 1, 10
```

```
            DO 200  J = 1, 10
              READ (LIN2, *)  ZVAL
              ZVAL = ZVAL * factor
              write (LOUT,*) ZVAL
              sum = sum + ZVAL
              DO 100 II = 2*I, 2*I + 1
                DO 100 JJ = 2*J, 2*J + 1
                  ZMAT(II,JJ) = ZVAL
  100       CONTINUE
  200       CONTINUE

            sum = sum / 100.d0
            write (LOUT,930) sum
  930       format (' averge current is ',d15.9,3x,'microamps')

c       ***** Now zero the boundaries to obtain skirt effect.

            DO 300  I = 1, 22
              ZMAT(1,I)  = 0.0
              ZMAT(22,I) = 0.0
              ZMAT(I,1)  = 0.0
              ZMAT(I,22) = 0.0
  300       CONTINUE
C
C       ***** BEGIN DISSPLA
C
            Call VT240
            Call NOBRDR
            Call PAGE(8.5, 11.0)
            Call PHYSOR (2.4, 2.0)
            Call AREA2D (5.2, 7.0)
            Len = LINEST (IPKRAY, 100, 40)

            Call HEIGHT (0.2)
            CALL LINESP (2.0)
            CALL SWISSL
            Call MX1ALF ('STANDARD','+')
            Call MX2ALF ('MATHE','*')
            Call MX3ALF ('GREEK','@')
            Call MX4ALF ('INSTRUCTION','!')
            Call NUMODE ('EQUAL')
            CALL SHDCHR (90., 1, .1, 1)

            If (imess . eq . 1)  Then
              CALL LINES (Lmess1,IPKRAY,1)
              if (Nlines . gt . 1)  CALL LINES (Lmess2,IPKRAY,2)
```

```
            XW = XSTORY(IPKRAY,Nlines)
            YW = YSTORY(IPKRAY,Nlines)
            XL = 4.5 - XW
            YL = 6.5 - YW

            CALL STORY (IPKRAY, Nlines, XL, YL)

          Endif

C       ***** SET UP WORKBOX AREA

          Call VOLM3D (10.0, 10.0, 5.0)

          Call SETSPC (2.0, 2.0, 0.03)
          Call HEIGHT (0.25)
          Call X3NAME ('!L1.0A3+Vertical Dimension&',100)
          Call Y3NAME ('Horizontal Dimension&',100)
          Call Z3NAME ('Current ( @m+A )&',100)

          Call VUABS  (55.0, -25.0, 35.0)
          Call ZAXANG (90.0)
          Call INTAXS

C       ***** SWITCH TO VIRTUAL COORDINATES

          Call XAXCTR
          Call YAXCTR
          Call YAXEND ('ENDS')
          Call GRAF3D (1., 1., 11., 1., 1., 11., 0., .1, .5)
          Call RESET ('SETSPC')

C       ***** CALCULATE GRID VALUES FOR ZMAT(IXROW,IYCOL)

          Call SURTRN ('BOTH')

C       ***** DRAW SURFACE

          Call SURMAT (ZMAT, IXPTS, 22, IYPTS, 22, 0)
          If (Iarrow . eq . 1)  then
            Call VECTR3 (-15, 7.5, 1.1, -10, 7.5, 1.1, 1001)
          Endif
          Call SURMAT (ZMAT, IXPTS, 22, IYPTS, 22, 0)
          Call ENDPL(0)
          Call DONEPL

          Stop
          End
```

```
      Function Fun(x)                                          Fun
      real*8    x

      fun = 1.d0 - 9.d0*x/16.d0 + x**3.d0/8.d0 -
     &          x**4.d0*45.d0/256.d0 - x**5.d0/16.d0
      Return
      End

      FUNCTION X3DMAT(IXROW)                                   X3DMAT
      Dimension XTABLE(22)
      data XTABLE / 1.00, 1.01, 1.99, 2.01, 2.99, 3.01, 3.99, 4.01,
     &              4.99, 5.01, 5.99, 6.01, 6.99, 7.01, 7.99, 8.01,
     &              8.99, 9.01, 9.99, 10.01, 10.99, 11.00 /
      X3DMAT = XTABLE(IXROW)
      Return
      End

      FUNCTION Y3DMAT(IYCOL)                                   Y3DMAT
      Dimension XTABLE(22)
      data XTABLE / 1.00, 1.01, 1.99, 2.01, 2.99, 3.01, 3.99, 4.01,
     &              4.99, 5.01, 5.99, 6.01, 6.99, 7.01, 7.99, 8.01,
     &              8.99, 9.01, 9.99, 10.01, 10.99, 11.00 /
      Y3DMAT = XTABLE(IYCOL)
      Return
      End
```

Program GEOM

```
      Program GEOM

      Implicit Real*8 (a-h,o-z)
      External fun
      Character*64       outfile
      Real*8    zfact(10), yfact(10)

c
c     This program prepares a file containg the geometric portion
c     of the current function due to a rising cylinder for use
c     with the program plotcyl.  This program must be linked with
c     yint.

      LIN  = 3
      LOUT = 4

      Open (unit=LIN, file='geom',
```

```
     &        defaultfile='[whitney.cylin].dat', status='old')

          Read (LIN,*) outfile

          Open (unit=LOUT, file=outfile,
     &      defaultfile='[whitney.cylin].dat', status='new')

          Read (LIN,*) dist
          Read (LIN,*) rad
          a = dsqrt( dist * dist    - rad * rad )

          Do 100  i = 1, 10
            z1 = 0.2d0 + dfloat(i-1)*0.01d0
            z2 = z1 + 0.01d0
            zfact(i) = (z2**(2.d0/3.d0) - z1**(2.d0/3.d0)) / (z2 - z1)

            y1 = -0.05d0 + dfloat(i-1)*0.01d0
            y2 = y1 + 0.01d0

          Call yint (y1, y2, a, fun, yfact(i) )

100       Continue

          Do 200  i = 1, 10
            Do 200  j = 1, 10
              fact = zfact(i) * yfact(j)
              Write (LOUT, *) fact
200       Continue

          Stop
          End

          SUBROUTINE yint( b1, b2, par, fun, val)                yint
          Implicit Real*8 (a-h, o-z)
          External fun

c
c   Uses Simpson's rule to integrate 'fun' from lower limit b1
c   to upper limit b2.  Par is a parameter (optionally) used
c   in 'fun'.  Val is the returned value.


          m = 10
          xm = dfloat(m)
          h  = (b2 - b1) / (2.d0 * xm)
          sum4 = 0.d0
          sum2 = 0.d0
```

```
      Do 100  i = 1, m-1
        xi = b1 + (2.d0 * dfloat(i) - 1.d0) * (b2 - b1)/(2.d0 * xm)
        xip = xi + h
        sum4 = sum4 + fun(xi,par)
        sum2 = sum2 + fun(xip,par)
100   Continue

      xm = b2 - h
      sum4 = sum4 + fun(xm,par)
      val = h/3.d0 * (fun(b1,par) + 4.d0*sum4 + 2.d0*sum2
     &            + fun(b2,par)) / (b2 - b1)

      Return
      End


      Function fun(x,p1)                                        fun
      Implicit real*8 (a-h, o-z)

      fun = 1.d0 / (x*x + p1*p1) ** (1.d0/3.d0)
      End
```

Appendix H. Chapter 4 Programs

The following programs were used for the calculations in Chapter 4. Program FITRHO is used to fit the density of sulfuric acid to the concentration, while accounting for the incomplete dissociation of the bisulfate ion. Program SIMPFIT, a simplified version of FITRHO, is used to fit $FeSO_4$ and $Fe_2(SO_4)_3$ density information and is not listed here. Program NATFEM is a finite element code used to solve the coupled equations of ionic species transport and solution electroneutrality. The equations are given in the appendix of Chapter 4.

Program FITRHO

```
      PROGRAM FITRHO
      Implicit Double Precision (a-h,o-z)

c
c
c     Program FITRHO reduces density information for sulfuric
c     acid to obtain the constants in the equation
c
c          rho  = a + b(cH+) + c(cHSO4-) + d(cSO4=)
c
c     User input file, FITRHO.dat, reads as follows:
c
c  # OF LINES      VARIABLE
c
c     1          infile
c     1          outfile
c
c     Second input file is 'infile.dat'.  It contains:
c
c  # OF LINES      VARIABLE
c
c     1          TITLE  (A70)
c     1          N
c     1          Mode     = 0, solve for all alphas
c                         = 1, set alpha SO4= to 0
c                         = 2, set alpha SO4= and alpha HSO4- to 0
c     1           iplot   = 1, plot density info
c     1           plotf   = name of plot file
c     1           corr    = correction for density to convert from
c                           sp.g. to density
c     1          indw     = 1 if data is in wt%, 0 if in M.
c     N          Cacid(i), rho(i)
c
c     TITLE is a comment up to 70 letters.
c     N is the number of conc, rho data points.
c
c     In order that the output specify the concentration range
c       covered by the density data, the user should
c       input the lowest concentration data point first and the
c       highest last.  However, the order of the data has no
c       effect on the computation.
```

```
c
c          Program FITRHO solves for a, b, c, d directly by minimizing
c            the sum of squares of the differences between the calculated
c            and experimental densities.
c
c          Program by Gina Whitney, September 7, 1986
c
c
ccccccccccccccccccccccccccccccccccccccccccccccccccccccccccccccccccccccccc

      Common / MAT /A(4,4), B(4)
      real*8          Cacid(100), rho(100), c(3,100)
      Character*70    TITLE
      Character*12    plotf, infile, outfile

      LIN1  = 3
      LIN   = 4
      LOUT  = 7
      LPLOT = 9

      open (unit=LIN1, file='FITRHO',
     &   defaultfile='[whitney.natcon].dat', status='old')

      Read (LIN1, *)  infile
      Read (LIN1, *)  outfile

      open (unit=LIN, file=infile,
     &   defaultfile='[whitney.natcon].dat', status='old')

      open (unit=LOUT, file=outfile,
     &   defaultfile='[whitney.natcon].out', status='new')


   50 Read (LIN, 900) TITLE
  900 Format (A70)

      write (LOUT, 905) TITLE
  905 Format (10x,A70)

      Read (LIN, *) N

      If (N.gt.100) then
      Write (LOUT, 915) N
  915 Format (5x,'N = ',i3,' N cannot be greater than 100',/,
     &   'change dimension statement for Cacid and rho')
      Stop
      Endif
```

```
      Read (LIN, *) Mode
      Read (LIN, *) iplot
      Read (LIN, *) plotf
      Read (LIN, *) corr
      Read (LIN, *) indw
      Do 100  i = 1, N
        Read (LIN, *) Cacid(i), rho(i)
100   Continue

c
c  Correct density info for density of water (rho info in CRC
c  is in sp.g.)

      Do 110  i = 1, N
        rho(i) = rho(i) * corr
110   Continue

      corrc = 98.08d0
      if (indw . eq . 1)  then
        Do 120  i = 1, N
          Cacid(i) = Cacid(i) * rho(i) * 1000.d0 / corrc
120     Continue
      endif

      Write (LOUT, 920)
920   format (' Cacid    Kount      CH      CHSO4-     CSO4=',
     &                '          ion str      xKp')

c
c  Calculate dissociation of Bisulphate at each concentration.

      Do 150  i = 1, N

      ct = Cacid(i)
      if (ct . lt . 1.e-10)  then
        c1 = ct
        c2 = ct
        c3 = ct
        go to 140
      endif

      cFe = 0.d0
      CALL DISSOC(ct, cFe, c1, c2, c3, ierr, LOUT)
      if (ierr . eq . 1)  then
        Write (LOUT, 930) i
930     Format (' DISSOC did not converge, data point #', i5)
        stop
```

```
            endif

  140       c(1,i) = c1
            c(2,i) = c2
            c(3,i) = c3
  150       Continue

c
c   Initialize summations.
c

            sum1   = 0.0d0
            sum2   = 0.0d0
            sum3   = 0.0d0
            sum11  = 0.0d0
            sum12  = 0.0d0
            sum13  = 0.0d0
            sum22  = 0.0d0
            sum23  = 0.0d0
            sum33  = 0.0d0
            sumr   = 0.0d0
            sumr1  = 0.0d0
            sumr2  = 0.0d0
            sumr3  = 0.0d0

            Do 200  i = 1,N
              sum1  = sum1  + c(1,i)
              sum2  = sum2  + c(2,i)
              sum3  = sum3  + c(3,i)
              sum11 = sum11 + c(1,i) * c(1,i)
              sum12 = sum12 + c(1,i) * c(2,i)
              sum13 = sum13 + c(1,i) * c(3,i)
              sum22 = sum22 + c(2,i) * c(2,i)
              sum23 = sum23 + c(2,i) * c(3,i)
              sum33 = sum33 + c(3,i) * c(3,i)
              sumr  = sumr  + rho(i)
              sumr1 = sumr1 + rho(i) * c(1,i)
              sumr2 = sumr2 + rho(i) * c(2,i)
              sumr3 = sumr3 + rho(i) * c(3,i)
  200       Continue

            A(1,1) = dfloat(N)
            A(1,2) = sum1
            A(2,1) = sum1
            A(1,3) = sum2
            A(3,1) = sum2
            A(2,2) = sum11
```

```
          A(2,3) = sum12
          A(3,2) = sum12
          A(3,3) = sum22
          A(1,4) = sum3
          A(4,1) = sum3
          A(2,4) = sum13
          A(4,2) = sum13
          A(3,4) = sum23
          A(4,3) = sum23
          A(4,4) = sum33

          B(1) = sumr
          B(2) = sumr1
          B(3) = sumr2
          B(4) = sumr3

          nm = 4 - mode

          CALL MATINV(nm, Determ)

          if (determ . eq . 0)  write (LOUT, 940)
  940     format ( ' determ = 0')

          cons     = B(1)
          alphH    = B(2)
          alphBI   = B(3)
          alphSO4  = B(4)
          if (mode . eq . 1)  alphSO4 = 0.d0
          if (mode . eq . 2)  then
            alphSO4 = 0.d0
            alphBI  = 0.d0
          endif

          if (iplot . eq . 1)  open (unit=LPLOT, file=plotf,
      &     defaultfile='[whitney.natcon].dat', status='new')

c
c       Write Tell-a-graph information
c

          Write (LPLOT, 911)
  911     Format ('gen plot.',
      &         /'legend is " ", frame legend,',
      &         /'legend box 1.5,3.0,0.5,3, units plot inches,'
      &         /'legend off.')
          Write (LPLOT, 912)
  912     Format ('page border off.')
```

```
      Write (LPLOT, 913)
913   Format ('title is "Sulfuric Acid Density",',
     &      /,'      style is swiss light,',
     &      /,'      shade pattern 2,',
     &      /,'      height 0.35.')
      Write (LPLOT, 914)
914   Format ('y room 2.')
      Write (LPLOT, 916)
916   Format ('y label is "Density (g/cm<e.8)3<ex) )",',
     &      /,'      style is swiss light,',
     &      /,'      shade pattern 2,',
     &      /,'      height 0.2.')
      Write (LPLOT, 917)
917   Format ('x label is "<l.5)<h1.2)[<hx)H<l1.1)2<l.5)SO<l1.1)',
     &     '4<l.5)<h1.2)]<hx) (M)",',
     &      /,'      style is swiss light,',
     &      /,'      shade pattern 2,',
     &      /,'      height 0.2.')
      Write (LPLOT,918)
918   Format ('y min is 0.98, max is 1.08, step 0.02.',
     &       /'x min is 0, max 1.2, step 0.2.')
      Write (LPLOT, 919)
919   Format ('x origin is 2.5.',/,'y origin is 3.5.',
     &      /,'x length is 4.0.',/,'y length is 5.0.')
      Write (LPLOT, 921)
921   Format ('x tick is 2.',/,'y tick is 2.')
      Write (LPLOT, 922)
922   Format ('x tick marks mode reversed.',
     &      /,'y tick marks mode reversed.')
      Write (LPLOT, 923)
923   Format ('curve 1 scattered.')
      Write (LPLOT, 924)
924   Format ('curve 2 texture 1.',
     &      /,'curve 3 texture 2.'
     &      /,'curve 4 texture 5.',
     &      /,'curve 5 texture 14.')
      Write (LPLOT, 925)
925   Format ('every curve, color is no, thickness 2,symbol count 0.',
     &      /,'curve 1 symbol count 1.')
      Write (LPLOT, 926) 3-mode
926   Format ('comment is "Fitting',i3,' coefficient(s)".')
      Write (LPLOT, 927)
927   Format ('input data.')
      Write (LPLOT, 928)
928   Format ('"data"')
```

```
          Do 252  i = 1, N
            Write (LPLOT, *)  Cacid(i), rho(i)
  252     Continue

          Write (LPLOT, 942)
  942     Format (' "fit"')

c
c  Check accuracy of fit.
c

          Emax = 0.0
          sumE = 0.0

          Do 300  i = 1, N
            rhoc = cons + alphH*c(1,i) + alphBI*c(2,i) + alphSO4*c(3,i)
            Write (LPLOT, *)  Cacid(i), rhoc
            E = rho(i) - rhoc
            sumE = sumE + abs(E)
            if (abs(E).ge.Emax)  then
              Emax = abs(E)
              Nmax = i
            endif
  300     Continue

          sumE = sumE * 100.0 / dfloat(N)
          Emax = Emax * 100.0

          Write (LPLOT, 944)
  944     Format (' end of data.')

c
c  Print results
c

          Write (LOUT, 950) N
          Write (LOUT, 960) Cacid(1), Cacid(N)
          Write (LOUT, 970) cons, alphH, alphBI, alphSO4
          Write (LOUT, 980) sumE
          Write (LOUT, 990) Emax, Cacid(Nmax)

  950     Format (5x,'Result of density fit for',I3,' points')
  960     Format (5x,'from Cacid = ',f10.4,'  to Cacid = ',f10.4)
  970     Format (10x,' const = ',e15.7, /10x,' alpha H = ',e15.7,
     &      /10x,' Alpha bi = ',f15.7, /10x,' alpha SO4=  =',e15.7)
  980     Format (5x,'Average percent deviation = ',f15.8)
  990     Format (5x,'Max percent deviation =',f15.8,' at Cacid =',f10.4)
```

```
      stop
      End

      SUBROUTINE DISSOC(a, b, CH, CHSO4, CSO4,          DISSOC
     &                  ierr, LOUT)

ccccccccccccccccccccccccccccccccccccccccccccccccccccccccccccccccccccc
c
c     This subroutine calculates solution composition based on the
c     equilibrium dissociation of bisulfate ion.
c
c     Input parameters are
c
c        a          concentration of H2SO4,                  M
c        b          concentration of Fe2(SO4)3,              M
c
c     Output parameters are
c
c        CH         concentration of H+
c        CHSO4      concentration of HSO4-
c        CSO4       concentration of SO4=
c
c     Program by Gina Whitney,  September 4, 1986
c
ccccccccccccccccccccccccccccccccccccccccccccccccccccccccccccccccccccc

      implicit real*8 (a-h,o-z)

      xK = 0.0104d0
      err = 1.d-15
      Kmax = 20
      ierr = 0

      CFe = 2.d0*b

      if (a . le . 0) then
        write (LOUT,910) a
        stop
      endif
  910 format (' a cannot be less than 0,  a = ', e15.6)

      alph = ( -(3.d0*b + a + xK) + dsqrt((3.d0*b + a +
     &           xK)**2.d0 - 4.d0*a*(3.d0*b-xK)) ) / (2.d0*a)

      CH = a * (1.d0 + alph)
      CSO4 = 3.d0*b + a*alph
      CHSO4 = a * (1.d0 - alph)
```

```
      Kount = 1

100   str = 0.5d0 * (CH + 4.d0*CSO4 + CHSO4 + 9.d0*CFe)
      sstr = dsqrt(str)
      xKp = xK * dexp( 5.29d0*sstr / (1.d0 + 0.56d0*sstr) )

      CoH = CH
      CoSO4 = CSO4
      CoHSO4 = CHSO4

      alph = ( -(3.d0*b + a + xKp) + dsqrt((3.d0*b + a +
     &          xKp)**2.d0 - 4.d0*a*(3.d0*b-xKp)) ) / (2.d0*a)

      CH = a * (1.d0 + alph)
      CSO4 = 3.d0*b + a*alph
      CHSO4 = a * (1.d0 - alph)

      sum = ((CH-CoH)/CH)**2.d0 + ((CSO4-CoSO4)/CSO4)**2.d0
     &          + ((CHSO4-CoHSO4)/CHSO4)**2.d0

      Kount = Kount + 1

      if (sum.gt.err) then
        if (Kount . le . Kmax) go to 100
      endif

      if (Kount . gt . Kmax) then
        ierr = 1
        write (LOUT, 930) Kmax
      endif
930   format (/,'  No convergence,    Kmax = ',i5)

      write (LOUT,940) a, Kount, CH, CHSO4, CSO4, str, xKp
940   format (f7.4,2x,i5,5(2x,e11.5))

      Return
      End


      Subroutine MATINV(N,DETERM)                    MATINV
      Implicit Double Precision (a-h,o-z)

c
c  Matrix inversion routine by John Newman.
```

```
c   Used with permission.
c
          Common / MAT / B(4,4), D(4)

          dimension  ID(4)

          determ = 1.0

          Do 1  I = 1, N
    1       ID(I) = 0

          Do 18  NN = 1, N
            Rmin = 1.1

c
c   Find the row which has the smallest ratio of the
c     2nd largest element in the row to the largest element.
c
          Do 6 I = 1, N
            If (ID(I). NE. 0)  Go to 6
            Bnext = 0.0
            Bmax  = 0.0

            Do 5 J = 1, N
              If (ID(J). NE. 0)  Go to 5
              If (DABS(B(I,J)). LE. Bnext)  Go to 5
              Bnext = DABS(B(I,J))
              If (Bnext. LT. Bmax)  Go to 5
              Bnext = Bmax
              Bmax  = DABS(B(I,J))
              JC = J
    5         Continue

          If (Bnext. GE. Rmin*Bmax)  Go to 6
            Rmin = Bnext/Bmax
            Irow = I
            Jcol = JC
    6     Continue

          If (ID(JC). EQ. 0)  Go to 8
          Determ = 0.0
          Return

    8     ID(Jcol) = 1
          If (Jcol. EQ. Irow)  Go to 12
```

```
      Do 10  J = 1, N
        Save        = B(Irow, J)
        B(Irow,J) = B(Jcol,J)
        B(Jcol,J) = Save
10    Continue

      Save      = D(Irow)
      D(Irow) = D(Jcol)
      D(Jcol) = Save

12    F = 1.0 / B(Jcol,J) * F
      Do 13  J = 1, N
13      B(Jcol,J) = B(Jcol,J) * F

      D(Jcol) = D(Jcol) * F

      Do 17  I = 1, N
        If (I. EQ.Jcol)  Go to 17
        F = B(I,Jcol)

        Do 16  J = 1, N
16        B(I,J) = B(I,J) - F * B(Jcol,J)

        D(I) = D(I) - F * D(Jcol)
17    Continue

18    Continue

      Return
      End
```

FITRHO Data File

```
Fitting H2SO4 density data from 0.4 to 1 M
12      data points
1       don't fit alphSO4
1       make plot file
0.998203d0
1
0.045d0          1.0302d0
0.050d0          1.0336d0
0.055d0          1.0370d0
0.060d0          1.0404d0
0.065d0          1.0438d0
0.070d0          1.0472d0
```

```
0.075d0          1.0506d0
0.080d0          1.0541d0
0.085d0          1.0575d0
0.090d0          1.0610d0
0.095d0          1.0645d0
0.100d0          1.0680d0
```

FITRHO Output File

```
                Fitting H2SO4 density data from 0.4 to 1 M
Cacid  Kount      cH          cHSO4-       cSO4=        ion str      xKp
0.4718  14  0.59848E+00   0.34515E+00  0.12667E+00  0.72515E+00  0.21964E+00
0.5260  14  0.66771E+00   0.38422E+00  0.14174E+00  0.80946E+00  0.24633E+00
0.5805  14  0.73768E+00   0.42326E+00  0.15721E+00  0.89489E+00  0.27399E+00
0.6353  15  0.80837E+00   0.46226E+00  0.17305E+00  0.98142E+00  0.30262E+00
0.6905  15  0.87977E+00   0.50124E+00  0.18927E+00  0.10690E+01  0.33220E+00
0.7460  15  0.95189E+00   0.54021E+00  0.20584E+00  0.11577E+01  0.36271E+00
0.8019  15  0.10247E+01   0.57916E+00  0.22277E+00  0.12475E+01  0.39414E+00
0.8582  15  0.10983E+01   0.61818E+00  0.24007E+00  0.13384E+01  0.42652E+00
0.9148  15  0.11725E+01   0.65715E+00  0.25768E+00  0.14302E+01  0.45975E+00
0.9718  15  0.12475E+01   0.69620E+00  0.27564E+00  0.15231E+01  0.49391E+00
1.0292  15  0.13231E+01   0.73529E+00  0.29393E+00  0.16171E+01  0.52893E+00
1.0870  15  0.13995E+01   0.77442E+00  0.31253E+00  0.17120E+01  0.56480E+00
      Result of density fit for 12 points
      from Cacid =       0.4718   to Cacid =       1.0870
            const =     0.9988335E+00
            alpha H =     0.1698817E-01
            Alpha bi =          0.0561220
            alpha SO4=  =     0.0000000E+00
      Average percent deviation =          0.00160619
      Max percent deviation =        0.00329005 at Cacid =       0.9148
```

Program NATFEM

```
      PROGRAM NATFEM

c           Program NATFEM solves the diffusion and migration
c           problem for concentration and potential profiles in a
c           stagnant diffusion layer, or at a growing mercury drop
```

```
c       or in unsteady stagnant diffusion, or at a rotating
c       disk.
c       This program uses the finite element technique to
c       solve the coupled equations.  This version uses a banded
c       solver in the IMSL math library, and must be linked with
c               link natfem,sys_imsls/lib
c       (which is included in forlinkb.com, on this account.)
c
c       My case is the reduction of Fe+3 ion in H2SO4/Fe2(SO4)3
c       solution for a potential step into limiting current.
c       The variables in this computation are:
c       C(k) where k refers to both species number (i) and
c               dimensionless position or similarity variable.
c               i = 1 is H+
c                   2 is SO4=
c                   3 is Fe+2
c                   4 is Fe+3, the reactant
c       The above variables are made dimensionless with C(Fe+3, bulk).
c       i = 5 is dimensionless potential, PHI = phi*F/RT.
c
c       The program solves for values of the above variables
c       as functions of the similarity variable,
c               eta = x / sqrt(4Dif(R)t),
c       in this case.
c
c       The program uses the finite element method to solve
c       Ficks second law for one-dimensional migration and
c       diffusion in a stagnant medium and the equation of
c       electroneutrality.  Finally, it calculates the
c       dimensionless current,
c           i / { nFDif(R)CB(R) / [1000*S(R)*sqrt(4Dif(R)*t)] }
c       and [ rho-rho(bulk) ] / rho(bulk), the density
c       difference and delta, the boundary layer thickness.
c
c       The program requires one data file, NATFEM.dat in
c       directory [whitney.natcon].  It contains:
c
c       Number
c         of
c       lines       variable
c
c       1           Mode        = 1 for Nernst stagnant diffusion
c                               = 2 for growing Hg drop or
c                                   unsteady stagnant diffusion
```

```
c                                   = 3 for rotating disk
c          1          Neq           = Number of unknowns  (5 for this case)
c          1          CR0           = Concentration of reactant at electrode
c          1          IPLOTC        = 0 don't print concentration profile
c                                      1 print dimensionless conc profile
c          1          IPLOTR        = 0 don't print density profile
c                                      1 print density profile
c          1          * blank*
c
c          Nvar-1     Name(I), Dif(I), zv(I), s(I), CB(I), alphap(I)
c
c  Mesh info:
c
c          1          ntype         = 1 for linear
c                                   = 2 for quadratic
c                                   = 3 for Hermite cubics.
c          1          nreg          the number of mesh regions (<=9)
c          nreg       nel(i)        # of elements in region i
c          nreg+1     xmesh(i)                region boundaries
c
c  i/o info:
c
c          1          resfile       name of restart file
c          1          iopt          indicator to print restart calculations
c          1          outres        name of new restart file
c
c
c  Newton-Raphson info:
c
c          1          err           convergence tolerence
c          1          Kmax          max number of Newton-Raphson iterations
c          1          iNR           print Newton-Raphson iterations
c
c  Calculation info:
c
c          1          Ntime         = Number of points at which to calculate
c                                     current, boundary layer thickness
c                                     and Rayleigh number
c          1          htime         = time interval for above calculation
c
c
c
c  Program by Gina Whitney, May 5, 1986.
c
```

```
ccccccccccccccccccccccccccccccccccccccccccccccccccccccccccccccccc

      implicit real*8 (a-h, o-z)
      character*20      resfile, outres
      character*6       Name(5)
      real*8            xlm(2)
      integer           R


      common / mesh   / ntype, nreg, xmesh(6), nel(5)
      common / nodes  / ne, nnodes, x(1001)
      common / soln   / c(5005)
      common / meshpar          / ku, nnpe, nvpn, nfac
      common / bc     / nveq(10), nBC(10), iBC(10), valBC(10),
     &                  neqv
      common / param  / neq, Dif(5), zv(5), s(5), CB(5), alphap(5)
      common / param2 / const, mode, nm1, nm2, R
      common / tfun   / phi(3,4), dphidz(3,4)
      common / gauss  / w(3), z(3)

c
c   Set values for Gauss points and weights (3 point adjusted for 0 to 1)

      z(1) = 0.5d0
      z(2) = ( 0.774596669241483 + 1.d0) / 2.d0
      z(3) = (-0.774596669241483 + 1.d0) / 2.d0
      w(1) = 4.d0 / 9.d0
      w(2) = 5.d0 / (9.d0 * 2.d0)
      w(3) = w(2)

      LIN   = 3
      LOUT  = 4
      LPLOTC = 7
      LPLOTR = 9
      LRES   = 10
      LOUTRES = 11
      F      = 96486.7d0
      FoRT = F / (8.314*298.15)

      open (unit=LIN, file='NATFEM',
     &      defaultfile='[WHITNEY.NATCON].dat', status='old')

      Read (LIN, *) MODE
      Read (LIN, *) Neq
      Read (LIN, *) CR0
      Read (LIN, *) IPLOTC
      Read (LIN, *) IPLOTR
```

```
      Nvar = Neq
      nm2 = Nvar-2
      nm1 = Nvar-1
      R   = nm1

      Read (LIN, 999)
999   Format ()
      Read (LIN, *) (Name(I),Dif(I), zv(I), s(I), CB(I), alphap(I),
     &                        I = 1, nm1)

      Read (LIN, *) ntype
      Read (LIN, *) nreg
      Do 110  j = 1, nreg
        Read (LIN, *) nel(j)
110   Continue

      Do 120  j = 1, nreg+1
        Read (LIN, *) xmesh(j)
120   Continue

      Read (LIN,*) resfile
      Read (LIN,*) iopt
      Read (LIN,*) outres
      Read (LIN,*) err
      Read (LIN,*) Kmax
      Read (LIN,*) iNR

      Read (LIN, *) Ntime
      Read (LIN, *) htime

      Name(Nvar) = ' Phi  '
      CB(Nvar) = 0.d0

      open (unit=LOUT, file='NATFEM',
     &   defaultfile='[WHITNEY.NATCON].out', status='new')

      open (unit=LRES, file=resfile,
     &   defaultfile='[WHITNEY.NATCON].dat', status='old')

c
c  Calculate boundary conditions from input information.

      neqv = 2*Nvar - 2
c
```

```
c   Program bulk concentrations at infinity.

          Do 130   i = 1, Nvar
            nveq(i) = i
            nBC(i)  = 1
            iBC(i)  = 1
            valBC(i) = CB(i)/CB(R)
  130     Continue
c
c   Program concentration of reactant at electrode.

          nveq(Nvar+1) = R
          nBC(Nvar+1)  = 0
          iBC(Nvar+1)  = 1
          valBC(Nvar+1)  = CR0/CB(R)
c
c   Program flux of non-reacting ions.

          Do 140   i = Nvar+2, 2*Nvar-2
            nveq(i) = i - (Nvar+1)
            nBC(i)  = 0
            iBC(i)  = 2
            valBC(i) = 0.d0
  140     Continue

c
c   Define differences in problem types.

          if (MODE . eq . 1)  then
            Write (LOUT, 900)
            Const = 0.d0
            if (xmesh(nreg+1) . gt . 1.d0)  Then
              Do 150   i = 1, nreg+1
                xmesh(i) = xmesh(i)/xmesh(nreg+1)
  150         Continue
            endif
          elseif (MODE . eq . 2)  then
            Write (LOUT, 901)
            Const = 2.d0
          elseif (MODE . eq . 3)  then
            Write (LOUT, 902)
            Const = 3.d0
          else
            Write (LOUT, 903) MODE
            Stop
          endif
  900     Format (' Nernst diffusion layer')
```

```
  901     Format (' Planar diffusion or growing mercury drop')
  902     Format (' Rotating disk')
  903     Format (' Invalid mode,  mode = ', i3)

c
cc  Calculate transference number of reacting ion.

        sum = 0.d0
        Do 160  i = 1, nm1
          sum = sum + zv(i) * zv(i) * CB(i) * Dif(i)
  160   Continue
        tran = zv(R) * zv(R) * CB(R) * Dif(R) / sum
        Write (LOUT, 905) tran
  905   Format (/,'  Transference number of reacting ion =  ',f15.9)

c
cc  Write input information.

        Write (LOUT, 906)
  906   Format (/'   Name          Diff          Cbulk '
     &  '          alpha')
        Write (LOUT, *) (Name(I),Dif(I), CB(I), alphap(I),
     &                   I = 1, Neq)
        Write (LOUT, 907) ntype
  907   Format (/'   Type of basis functions : ', i3)
        Write (LOUT, 908) nreg
  908   Format (3x, i3, ' region(s)')
        Write (LOUT, 909)
  909   Format ('      Node structure')

        Do 170  j = 1, nreg
          Write (LOUT, *) nel(j)
  170   Continue

        Do 180  j = 1, nreg+1
          Write (LOUT, *) xmesh(j)
  180   Continue

        Write (LOUT, 910)
  910   Format (/,'      Boundary condition info',
     &       /,'          nveq        nBC       iBC       valBC')
        Do 190  j = 1, neqv
          Write (LOUT, *) nveq(j), nBC(j), iBC(j), valBC(j)
  190   Continue

        Write (LOUT, 912) err
  912   Format (/'    Err = ',e15.8)
```

```
      Write (LOUT, 914) Kmax
914   Format (' Kmax = ', i4)


c
c  Define differences in mesh types.

      if (ntype . eq . 1)  Then
        ku = 2
        nnpe = 1
        nvpn = 1
      elseif (ntype . eq . 2)  Then
        ku = 3
        nnpe = 2
        nvpn = 1
      elseif (ntype . eq . 3)  Then
        ku = 4
        nnpe = 1
        nvpn = 2
      else
        Write (LOUT, 916) ntype
916     Format (' Bad value for ntype, ',i5)
        Stop
      endif
      nfac = neq * nnpe * nvpn

c
c  Generate mesh points.

      Call GENMESH(LOUT)
      nvart = neq * nvpn * (1 + nnpe*ne)
c
c  Calculate initial guesses from restart file info.

      Call RESTART (LRES, iopt, LOUT, neq)

c
c  Calculate local phi's and dphidz's.

      Call TFUNCT (ntype)

c
```

```
c   Call finite element routine.

          Call FINEL(nvart, err, Kmax, iNR, Kountnr, iconv, LOUT)

          Write (LOUT, 917)  Kountnr
  917     Format (/,'  Newton-Raphson Iterations: ',i5)

          If (iconv . eq . 0)  Then
            Write (LOUT, 918) Kountnr, err, Kmax
  918       Format (/,'  Newton-Raphson did not converge.',
     &        /,'  Kountnr =',i5,'  err =',e15.9,'  Kmax =',i5)
            Stop
          Endif


          amp = ( c(neq*nvpn+R)-c(R) ) / (x(2)-x(1))

c
cc Convergence!

c
c   Write to output restart file.


          open (unit=LOUTRES, file=outres,
     &        defaultfile='[WHITNEY.NATCON].dat', status='new')

          Write (LOUTRES, *) nnodes
          Do 200  j = 1, nnodes
            Write (LOUTRES,919) x(j), (c(neq*nvpn*(j-1)+i), i=1, neq)
  200     Continue
  919     Format (2x,f7.4,5(x,e11.4))
c
c   Write dimensionless concentration profile.
c
          Ibeenhere = 0
          Ibeenhere95 = 0

c
c   Open plot files.

          If (IPLOTC . eq . 1)  open (unit=LPLOTC, file='plotconf',
     &      defaultfile='[WHITNEY.NATCON].dat', status='new')

          If (IPLOTR . eq . 1)  open (unit=LPLOTR, file='plotrhof',
     &      defaultfile='[WHITNEY.NATCON].dat', status='new')
```

```
c
c   Write Tell-a-graph information.

          If (IPLOTR . eq . 1) Then
            Write (LPLOTR, 921)
  921       Format (' page border off.')
            Write (LPLOTR, 922)
  922       Format (' title is "Density Profile Following a"')
            Write (LPLOTR, 923)
  923       Format ('        "Potential Step into Limiting Current",',
     &           /,'          height 0.35,',
     &           /,'          style is swiss light, shade pattern 2.')
            Write (LPLOTR, 925)
  925       Format (' y label is "Density (g/cm<e.8)3<ex) )",',
     &           /,'          height 0.2,',
     &           /,'          style is swiss light, shade pattern 2.')
            Write (LPLOTR, 927)
  927       Format (' x label is "Dimensionless Distance, <m7)c",',
     &           /,'          height 0.2,',
     &           /,'          style is swiss light, shade pattern 2.')
            Write (LPLOTR, 929)
  929       Format (' x origin is 2.3.')
            Write (LPLOTR, 930)
  930       Format (' y tick is 2.')
            Write (LPLOTR, 931)
  931       Format (' x tick is 2.',/,' frame axis.',/,' frame legend.')
            Write (LPLOTR, 932)
  932       Format (' curve 1 texture 1.',
     &           /,' curve 2 texture 2.')
            Write (LPLOTR, 936)
  936       Format (' every curve, color is no, thickness 2,'
     &           /,'                    symbol count is 0.')

            Write (LPLOTR, 939)
  939       Format (' comment is "Linear profile based on equiv force".')
            Write (LPLOTR, 941)
  941       Format (' input data.')
            Write (LPLOTR, 942)
  942       Format (' "Calc"')
          Endif

          If (IPLOTC . eq . 1) Then
            Write (LPLOTC, 921)
            Write (LPLOTC, 924)
  924       Format ('title is "Concentration Profile Following a"')
            Write (LPLOTC, 923)
            Write (LPLOTC, 926)
```

```
926       Format (' y label is "Concentration x 10<e.8)3<ex)',
     &            ' ( gmol/cm<e.8)3<ex) )"',
     &          /,'          height 0.2,',
     &          /,'          style is swiss light, shade pattern 2.')
          Write (LPLOTC, 927)
          Write (LPLOTC, 928)
928       Format (' y min is 0.')
          Write (LPLOTC, 929)
          Write (LPLOTC, 930)
          Write (LPLOTC, 931)
          Write (LPLOTC, 932)
          Write (LPLOTC, 936)
          Write (LPLOTC, 940)
940       Format (' comment is "Linear profile based on equiv area".')
         Write (LPLOTC, 941)
         Write (LPLOTC, 942)
        Endif

c
c   Initialize variables for integral calculation.

        rhoinf  = 1.0465d0

        sume = 0.d0
        sumf = 0.d0
        sumc = 0.d0
        summ = 0.0d0
        eta1 = x(nnodes)
        etam = eta1
        c1 = c(nfac*ne+R)
        ifirst = 0
        rho1 = rhoinf
        rhom = rhoinf
        If (IPLOTC.eq.1) Write (LPLOTC,947) eta1,c(nfac*ne+R)*CB(R)
        If (IPLOTR.eq.1) Write (LPLOTR,947) eta1, rho1

        Do 410  j = nnodes-1, 1, -1
          eta = x(j)
          If (IPLOTC . eq . 1)
     &    Write (LPLOTC, 947) eta, c(neq*nvpn*(j-1)+R) * CB(R)
          drho = 0.d0
          Do 405  i = 1,nm1
            drho  = drho  + alphap(i) * (c(neq*nvpn*(j-1)+i) -
     &      c(nfac*ne+i) ) * CB(R)
405       Continue
          rho = rhoinf * (1.d0 + drho)
```

```
c
c   Looking for rhomax.

            If (rho . ge . rhom) Then
              Ifirst = 1
              rhom = rho
              etam = eta
              jm = j
            Endif

c
c   Integral calculation.

          eta2 = eta
          rho2 = rho
          v2   = (rho2 - rhoinf) * eta2
          v1   = (rho1 - rhoinf) * eta1
          sume = sume + (v1 + v2)/2.d0 * (x(j+1)-x(j))
          sumf = sumf + ((rho1 + rho2)/2.d0 - rhoinf) * (x(j+1)-x(j))
          sumc = sumc + ((c(neq*nvpn*(j)+R) + c(neq*nvpn*(j-1)+R))/2.d0
     &                 - c(nfac*ne+R)) *  (x(j+1)-x(j))
          if (rho . lt . rhom . and . ifirst . gt . 0)  Then
            summ = summ + ((rho1 + rho2)/2.d0 - rhom) * (x(j+1)-x(j))
          endif

          eta1 = eta2
          rho1 = rho2
c
c   Plotting.

          If (IPLOTR . eq . 1)  Write (LPLOTR, 947) eta, rho

          if ( c(neq*nvpn*(j-1)+R) . lt . 0.9 )  Then
            if (Ibeenhere . eq . 0)  Then
              c1 = c(neq*nvpn*(j-1)+R)
              e1 = eta
              Ibeenhere = 1
            endif
          endif

          if ( c(neq*nvpn*(j-1)+R) . lt . 0.95 )  Then
            if (Ibeenhere95 . eq . 0)  Then
              c195 = c(neq*nvpn*(j-1)+R)
              e195 = eta
              Ibeenhere95 = 1
            endif
          endif
```

```
      if (Ibeenhere . eq . 0)  Then
        c2 = c(neq*nvpn*(j-1)+R)
        e2 = eta
      endif

      if (Ibeenhere95 . eq . 0)  Then
        c295 = c(neq*nvpn*(j-1)+R)
        e295 = eta
      endif
410   Continue
947   Format (2(2x,e15.9))

      if (Ibeenhere . eq . 0)  Then
        Write (LOUT, 950)
950     Format (' No crossing of conc = 0.9, check profile stuff')
        Go to 420
      endif

      if (Ibeenhere95 . eq . 0)  Then
        Write (LOUT, 952)
952     Format (' No crossing of conc = 0.95, check profile stuff')
        Go to 420
      endif

      eta9 = e1 + (0.9 - c1) * (e2 - e1) / (c2 - c1)
      deltrat = eta9 * amp
      Write (LOUT, 955) eta9, deltrat
955   Format (/,' eta at (c = 0.9*Cb) = ',f15.9,/
     &        ' ratio of delta.9 to deltcur = ', f15.9,/)

      eta95 = e195 + (0.95 - c195) * (e295 - e195) / (c295 - c195)
      deltrat = eta95 * amp
      Write (LOUT, 958) eta95, deltrat
958   Format (/,' eta at (c = 0.95*Cb) = ',f15.9,/
     &        ' ratio of delta.95 to deltcur = ', f15.9,/)


420   Write (LOUT, 960)
960   Format (' Species  CBulk  CZero  Amp')

      potinf = c(nfac*ne+Nvar)/FoRT
      potelec = c(Nvar)/FoRT

      Write (LOUT, 962) amp, (Name(i), c(nfac*ne+i)*CB(R),
     &          c(i)*CB(R),  I=1,nm1)
      Write (LOUT, 963) Name(NVar), potinf, potelec
962   Format (45x,e15.9,/(5x,A6,3x,e12.6,3x,e12.6))
```

```
963     Format (5x,A6,3x,e12.6,3x,e12.6)


        drhoelec = 0.d0

        Do 500  i = 1,nm1
          drhoelec = drhoelec + alphap(i) * (c(i) - c(nfac*ne+i))
     &                        * CB(R)
500     Continue
        rhoelec = rhoinf * (1.d0 + drhoelec)

        xint = sume * 6.d0 / (rhoelec - rhoinf)
        If (xint . lt . 0)  Then
          Write (LOUT, 966)
966     Format (' Cannot calculate etaint.  Check solution')
        Else
          etaint = dsqrt( xint )
          Write (LOUT, 965) etaint
965     Format (/,' Equivalent bouyant energy eta = ',e15.8)
        Endif

        etaintf =  sumf * 2.d0 / (rhoelec - rhoinf)
        Write (LOUT, 968) etaintf
968     Format (/,' Equivalent force eta = ',e15.8)

        etaintm =  summ * 2.d0 / (rhoelec - rhom)
        Write (LOUT, 969) etaintm
969     Format (/,' Equivalent eta based on max density = ',e15.8)

        etaintlm =  summ * 2.d0 / (rhoelec - rhoinf)
        Write (LOUT, 971) etaintlm
971     Format (/,'       Equivalent eta l sub m = ',e15.8)

        etaintc = - sumc * 2.d0 / (C(nfac*ne+R) - C(R))
        Write (LOUT, 970) etaintc
970     Format (/,'       Equivalent conc eta = ',e15.8)

        rhomd = rhom / rhoinf
        Write (LOUT, 972) rhom, rhomd, etam
972     Format (/,'       Max density = ',e15.8,
     &          /,'      over rhoinf = ',e15.8,
     &          /,'      at eta      = ',e15.8)


        Rast = 980.d0 * (rhoelec-rhoinf)/(rhoinf*0.01d0*Dif(R))
        Rastm = 980.d0 * (rhoelec-rhom)/(rhom*0.01d0*Dif(R))
        Write (LOUT,975)  rhoinf, rhoelec, Rast, Rastm
```

```
975     Format (/,15x,'rhoinf = ',f15.9,/,15x,'rhoelec =',f15.9,
    &           /,15x,'Rast = ',e15.9,/,15x,'Rastm = ',e15.9)

        Write (LOUT, 980)
980     Format (/,x,'Time',5x,'Current',7x,'delta',9x,'Ra',9x,'Ra max',
    &           8x,'Ra c')


        Do 550, i = 1, Ntime
          time = htime * dfloat(i)
          cur  = F*Dif(R)*CB(R)*amp / (s(R)*dsqrt(4.d0*Dif(R)*time))
          delta = dsqrt(4.d0*Dif(R)*time)
          Ra = Rast * delta ** 3.d0
          deltam = etam * dsqrt(4.d0*Dif(R)*time)
          Ram = Rastm * deltam ** 3.d0
          deltac = etaintc * dsqrt(4.d0*Dif(R)*time)
          Rac = Rast * deltac ** 3.d0
          Write (LOUT, 982) time, cur, delta, Ra, Ram, Rac
982       Format (f5.1,5(2x,e11.5))
550     Continue

        If (IPLOTR . eq . 1) Then
          Write (LPLOTR, 983)
          xx = 0.d0
          Write (LPLOTR, 947) xx, rhoelec
          Write (LPLOTR, 947) etaintlm, rhoinf
          xx = xmesh(nreg+1)
          Write (LPLOTR, 947) xx, rhoinf
          Write (LPLOTR, 984)
        Endif
983     Format (' "linear eq"')
984     Format (' end of data.')

        If (IPLOTC . eq . 1) Then
          Write (LPLOTC, 983)
          xx = 0.d0
          Write (LPLOTC, 947) xx, c(R) * CB(R)
          Write (LPLOTC, 947) etaintc, c(nfac*ne+R) * CB(R)
          xx = xmesh(nreg+1)
          Write (LPLOTC, 947) xx, c(nfac*ne+R) * CB(R)
          Write (LPLOTC, 984)
        Endif

        Stop
        End
```

```
ccccccccccccccccccccccccccccccccccccccccccccccccccccccccccccccccccccc
```

Subroutine GENMESH(LOUT) *GENMESH*

```
      implicit real*8    (a-h, o-z)

      common / mesh      / ntype, nreg, xmesh(6), nel(5)
      common / nodes     / ne, nnodes, x(1001)
      common / meshpar / ku, nnpe, nvpn, nfac

      ne = 0
      x(1) = xmesh(1)
      k = 1

      Do 200  i = 1, nreg
        ne = ne + nel(i)
        Do 150  ii = 1, nel(i)
          dx = (xmesh(i+1) - xmesh(i)) / dfloat(nel(i)*nnpe)

          Do 100  j = 1, nnpe
            k = k + 1
            x(k) = x(k-1) + dx
100       Continue
150     Continue
200   Continue

      nshouldbe = ne*nnpe + 1
      nnodes = k

      If (nnodes . ne . nshouldbe)  Then
        Write (LOUT, 920)  nnodes, nshouldbe
920     Format (/,' Genmesh did not work, nodes =',i5,
     &          ' should be',i5)
        Stop
      Endif

      Return
      End
```

```
ccccccccccccccccccccccccccccccccccccccccccccccccccccccccccccccccccccc
```

Subroutine RESTART(LRES, iopt, LOUT, neqr) *RESTART*

```
      implicit real*8 (a-h, o-z)

      common / mesh      / ntype, nreg, xmesh(6), nel(5)
      common / nodes     / ne, nnodes, x(1001)
```

```
      common / soln      / c(5005)
      common / meshpar / ku, nnpe, nvpn, nfac

      real*8    c1(5), c2(5)
      Read (LRES, *)  nnodeso
      Read (LRES, *) x1, (c1(i), i = 1, neqr)
      Read (LRES, *) x2, (c2(i), i = 1, neqr)
      k = 2
      slop = 1.d-6

      Do 100  j = 1, nnodes
50      If (x(j) . le . x2+slop)  Then
          Do 75  i = 1, neqr
            c(neqr*nvpn*(j-1)+i) = c1(i) +
     &                  (x(j)-x1) * (c2(i)-c1(i)) / (x2-x1)
75        Continue
          If (ntype . eq . 3) Then
            Do 80  i = 1, neqr
              c(neqr*nvpn*(j-1)+neqr+i) = 0.d0
80        Continue
        Endif
        Go to 100

        Else
          x1 = x2
          Do 90  i = 1, neqr
            c1(i) = c2(i)
90        Continue
          k = k+1
          If (k . gt . nnodeso)  Then
            Write (LOUT, 900) k, nnodes, nnodeso
900         Format (/,'   Restart did not work   ',
     &        /,'    k =',i5,'  nnodes =',i5,' old nnodes =',i5)
            Stop
          Else
            Read (LRES, *) x2, (c2(i), i = 1, neqr)
            If (neqr . eq . 2)  Read (LRES, *) x2, c2, T2
            Go to 50
          Endif
        Endif

100   Continue

      If (iopt . eq . 1)  Then
        Write (LOUT, 910)
910     Format (/,'   Restart information')
        Do 200  j = 1, nnodes
```

```
            Write (LOUT,919) j, x(j), (c(neqr*nvpn*(j-1)+i),
     &           i=1, neqr)
            If (ntype . eq . 3) Then
              Write (LOUT,919) j,x(j),(c(neqr*nvpn*(j-1)+neqr+i),
     &           i=1,neqr)
            Endif
  200     Continue
        Endif
  919   Format (2x,i3,2x,f7.4,5(x,e11.4))

        Return
        End

cccccccccccccccccccccccccccccccccccccccccccccccccccccccccccccccccccccccc

        Subroutine FINEL(nvarf, errf, Kmaxf, iNRf, Kountnrf,    FINEL
     &           iconvf, LOUT)

        implicit real*8    (a-h, o-z)
        real*8              sk(5005,19), sf(5005), xl(2), con(4), dcdx(4)
        real*8              xwrk(50050)
        integer             R, isld(5005)

        common / mesh    / ntype, nreg, xmesh(6), nel(5)
        common / nodes   / ne, nnodes, x(1001)
        common / soln    / c(5005)
        common / meshpar / ku, nnpe, nvpn, nfac
        common / bc      / nveq(10), nBC(10), iBC(10), valBC(10), neqv
        common / param   / neq, Dif(5), zv(5), s(5), CB(5), alphap(5)
        common / param2  / const, mode, nm1, nm2, R
        common / tfun    / phi(3,4), dphidz(3,4)
        common / gauss   / w(3), z(3)

c
c   Calculate bandwidth and set up isld.

        nbw = neq*4 -1
        nc = (nbw-1)/2
        j = -nc
        Do 50  n = 1, nvarf
          isld(n) = j
          j = j + 1
   50   Continue
```

```
c
c   Initialize Newton-Raphson variables.

          Kountnrf = 0
          If (iNRf . eq . 1)  Write (LOUT, 910)
  910     Format (/,'         Newton-Raphson Convergence',
     &          /,'  KountNR      Norm. of Res.',/)

c
c   Top of loop for Newton-Raphson.

  100     Kountnrf = Kountnrf + 1
c
c   Zero matrices.

          Do 150  i = 1, nvarf
            sf(i)  = 0.d0
              Do 150  j = 1, nbw
                sk(i,j)  = 0.d0
  150     Continue

c
c   Begin element by element construction.

          Do 300  i = 1, ne
            xl(1) = x(nnpe*(i-1)+1)
            xl(2) = x(nnpe*(i) + 1)
            dx = xl(2) - xl(1)
            eta0 = xl(1)

            Do 300  j = 1, 3
              eta = eta0 + z(j) * dx
cc  Zero local solution.

            Do 175  ii = 1, nm1
              con(ii) = 0.d0
              dcdx(ii) = 0.d0
  175       Continue
            pot  = 0.d0
            dpotdx = 0.d0

c
c   Calculate local solution.

            Do 200  k = 1, ku
              index = nfac * (i-1) + neq * (k-1)
              Do 190  ii = 1, nm1
```

```
                con(ii) = con(ii) + phi(j,k) * c(index+ii)
                dcdx(ii) = dcdx(ii) + dphidz(j,k) * c(index+ii) / dx
  190         Continue
              pot = pot + phi(j,k) * c(index+neq)
              dpotdx = dpotdx + dphidz(j,k) * c(index+neq) / dx
  200         Continue

c
c  Loop over local rows.

              Do 300  l = 1, ku
                l1 = nfac * (i-1) + neq * (l-1)
                Do 230  ii = 1, nm1
                sf(l1+ii) = sf(l1+ii) - w(j) * dx *
     &            ( - Dif(ii) / Dif(R) * dcdx(ii) *dphidz(j,l)/dx
     &            + const * eta**dfloat(Mode-1) * dcdx(ii) * phi(j,l)
     &            - zv(ii) * Dif(ii) / Dif(R) * con(ii) * dpotdx
     &             * dphidz(j,l) / dx )
                sf(l1+neq) = sf(l1+neq) - w(j) * dx *
     &            zv(ii)*con(ii) * phi(j,l)
  230           Continue

c
c  Loop over local columns.  Shifted column = full column - isld(row).

              Do 300  m = 1, ku
                m1 = nfac * (i-1) + neq * (m-1)
                Do 250  ii = 1, nm1

          sk(l1+ii,m1+ii-isld(l1+ii)) = sk(l1+ii,m1+ii-isld(l1+ii))
     &            + w(j) * dx *
     &            ( -Dif(ii)/Dif(R) * dphidz(j,m) *dphidz(j,l)/(dx*dx)
     &            + const*eta**dfloat(Mode-1) * dphidz(j,m) * phi(j,l)/dx
     &            - zv(ii) * Dif(ii)/Dif(R) * phi(j,m) * dpotdx
     &             * dphidz(j,l) / dx )
          sk(l1+ii,m1+neq-isld(l1+ii)) = sk(l1+ii,m1+neq-isld(l1+ii))
     &            + w(j) * dx *
     &            (- zv(ii) * Dif(ii) / Dif(R) * con(ii) * dphidz(j,m)
     &             * dphidz(j,l) / (dx*dx) )
          sk(l1+neq,m1+ii-isld(l1+neq)) = sk(l1+neq,m1+ii-isld(l1+neq))
     &            + w(j) * dx * zv(ii) * phi(j,m) * phi(j,l)
  250           Continue
  300 Continue
```

```
c
c   Adjust equations for boundary conditions.

          Do 400   j = 1, neqv

c
c   Calculate equation number as if BC were an essential BC.

          nneq = nBC(j) * nfac * ne + nveq(j)

c   First program essential condition or natural for Hermite.

          if (iBC(j) . eq . 1 . or . ntype . eq . 3)  Then

c   Adjust equation number if doing derivative condition
c   with Hermite.

            if (iBC(j) . eq . 2)  nneq = nneq + neq
            sf(nneq) = -c(nneq) + valBC(j)
            Do 350   i = 1, nbw
              sk(nneq,i) = 0.d0
  350       Continue
            sk(nneq,nneq-isld(nneq)) = 1.d0

c   Now natural condition.

            elseif (iBC(j) . eq . 2 . and . ntype . ne . 3)  Then
              sf(nneq) = sf(nneq) + dfloat(1-2*nBC(j)) *  valBC(j)
            else
              Write (LOUT, 920) j, iBC(j)
  920       Format (' Bad BC # ', i4, '  Type  ',i4)
            endif
  400       Continue

c
c   Now flux-matching condition for product.

          sf(nm2) = sf(nm2) + s(nm2)/s(R)
     &                      * (c(neq*nvpn+R)-c(R))/(x(2)-x(1))
          sk(nm2,neq*nvpn+R-isld(nm2)) = sk(nm2,neq*nvpn+R-isld(nm2))
     &                      - s(nm2)/s(R) /(x(2)-x(1))
          sk(nm2,R-isld(nm2)) = sk(nm2,R-isld(nm2))
     &                      + s(nm2)/s(R) /(x(2)-x(1))
```

```
c
c   Solve for delta node values using library banded solver.

          Call LEQT1B (sk, nvarf, nc, nc, 5005, sf, 1, 5005, 0,
     &                              xwrk, ier)
          if (ier . eq . 129)  Write (LOUT, 930) Kountnrf
  930     Format (' error in LEQT1B, Kountnr = ', i5)

c
c   Check convergence and make corrections to c(i).

          sum = 0.d0
          Do 480  i = 1, nvarf
            sum = sum + sf(i) * sf(i)
            c(i) = c(i) + sf(i)
  480     Continue

          sum = dsqrt( sum / dfloat(nvarf) )

          If (iNRf . eq . 1)  Write (LOUT, 940)  Kountnrf, sum
  940     Format (2x,i5,3x,e15.9)

          if (sum . le . errf)  Then
            iconvf = 1

c   Convergence!
            Return
          endif

          if (Kountnrf . lt . Kmaxf)  Go to 100

c
c   (Damn).

          iconvf = 0
          Return

          End

ccccccccccccccccccccccccccccccccccccccccccccccccccccccccccccccccccccccccccccc

          Subroutine TFUNCT(nt)                              TFUNCT
          implicit real*8 (a-h, o-z)

          common / tfun      / phi(3,4), dphidz(3,4)
          common / gauss     / w(3), z(3)
```

```
      If (nt . eq . 1)  Then

        Do 100  j = 1, 3
          phi(j,1) = 1.d0 - z(j)
          phi(j,2) = z(j)
          dphidz(j,1) = -1.d0
          dphidz(j,2) =  1.d0
100     Continue

      Elseif (nt . eq . 2)  Then

        Do 200  j = 1, 3
          phi(j,1) = 1.d0 - 3.d0*z(j) + 2.d0*z(j)*z(j)
          phi(j,2) = 4.d0*z(j) * (1.d0 - z(j))
          phi(j,3) = z(j) * (-1.d0 + 2.d0*z(j))
          dphidz(j,1) = -3.d0 + 4.d0*z(j)
          dphidz(j,2) =  4.d0 - 8.d0*z(j)
          dphidz(j,3) = -1.d0 + 4.d0*z(j)
200     Continue

      Elseif (nt . eq . 3)  Then

        Do 300  j = 1, 3
          phi(j,1) = 1.d0 - 3.d0*z(j)*z(j) + 2.d0*z(j)**3.d0
          phi(j,2) = z(j) - 2.d0*z(j)*z(j) + 1.d0*z(j)**3.d0
          phi(j,3) = 3.d0*z(j)*z(j) - 2.d0*z(j)**3.d0
          phi(j,4) = - 1.d0*z(j)*z(j) + 1.d0*z(j)**3.d0
          dphidz(j,1) = - 6.d0*z(j) + 6.d0*z(j)*z(j)
          dphidz(j,2) = 1.d0 - 4.d0*z(j) + 3.d0*z(j)*z(j)
          dphidz(j,3) = 6.d0*z(j) - 6.d0*z(j)*z(j)
          dphidz(j,4) = - 2.d0*z(j) + 3.d0*z(j)*z(j)
300     Continue

      Endif

      Return
      End
```

LAWRENCE BERKELEY LABORATORY
TECHNICAL INFORMATION DEPARTMENT
UNIVERSITY OF CALIFORNIA
BERKELEY, CALIFORNIA 94720